

Chapter 4

Results and Discussion

4.1 Yield Strength Models

4.1.1 Response graphs of Input variables and Yield Strength of Ferritic Steel Welds using committee model of Bayesian Neural Network

The Trends of the Input Variables (Independent Variables) and Yield Strength of Ferritic Steel Welds are given below in form of the graphs.

Trends of Yield Strength Model

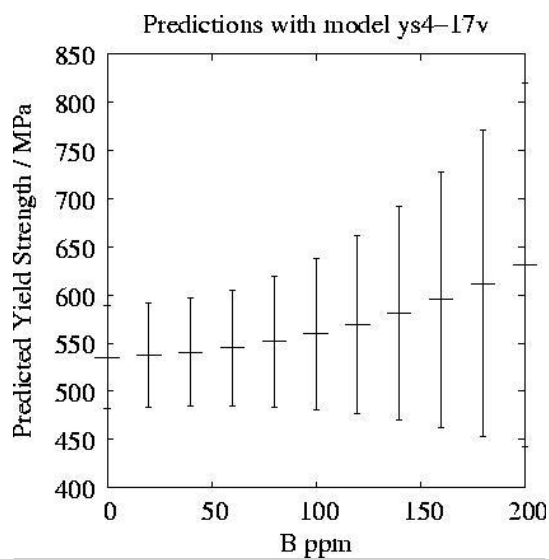


Fig a. Predicted variations in Yield Strength with Boron variation.

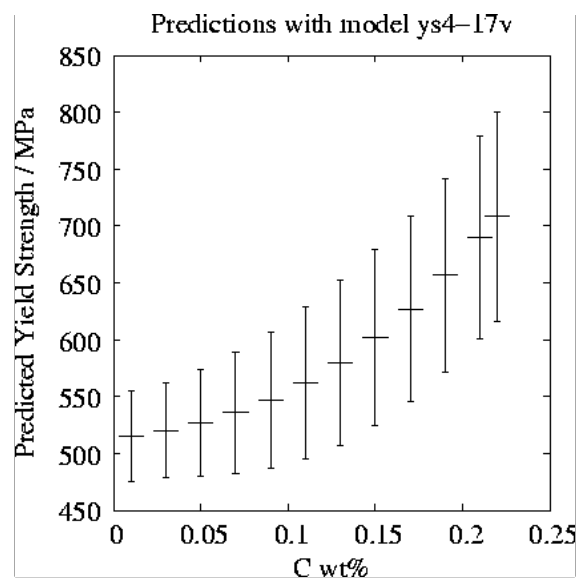


Fig b. Predicted variations in Yield Strength with Carbon variation.

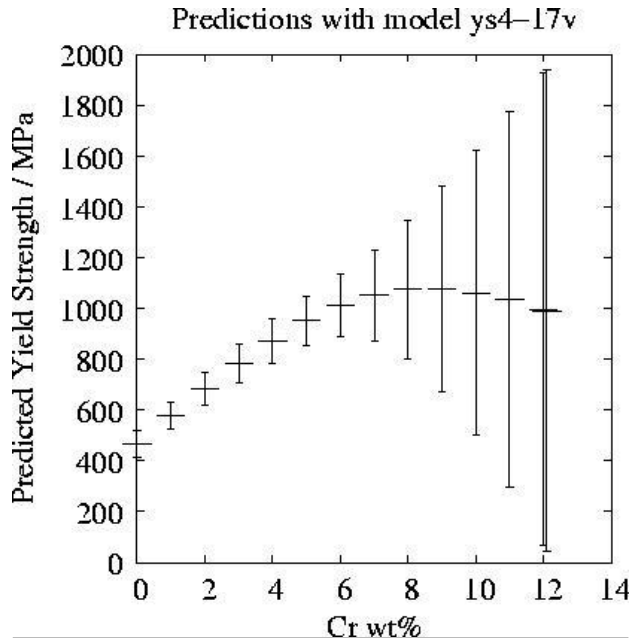


Fig c. Predicted variations in Yield Strength with Chromium variation.

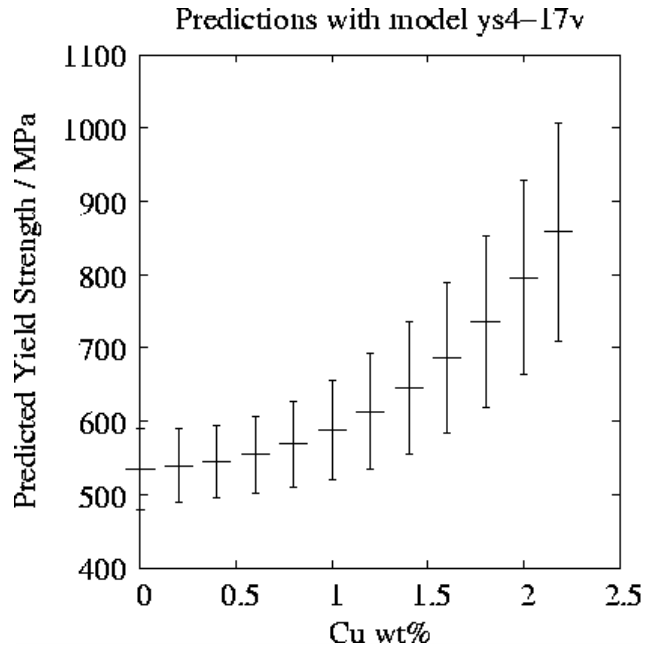


Fig d. Predicted variations in Yield Strength with Copper variation.

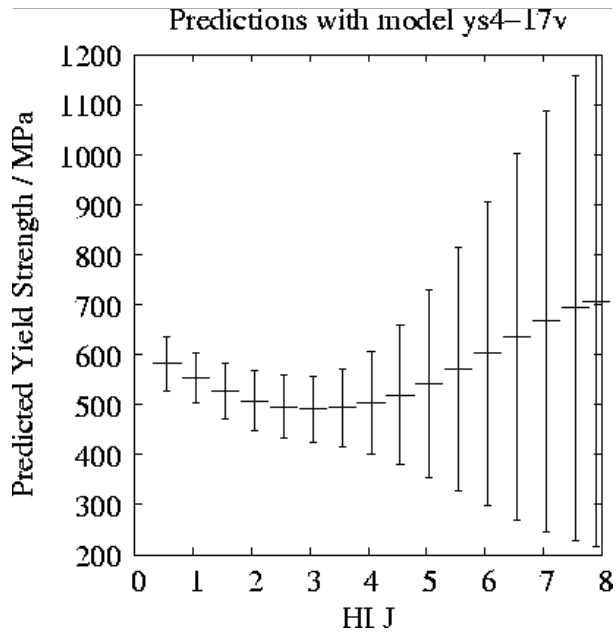


Fig e. Predicted variations in Yield Strength with Heat input variation.

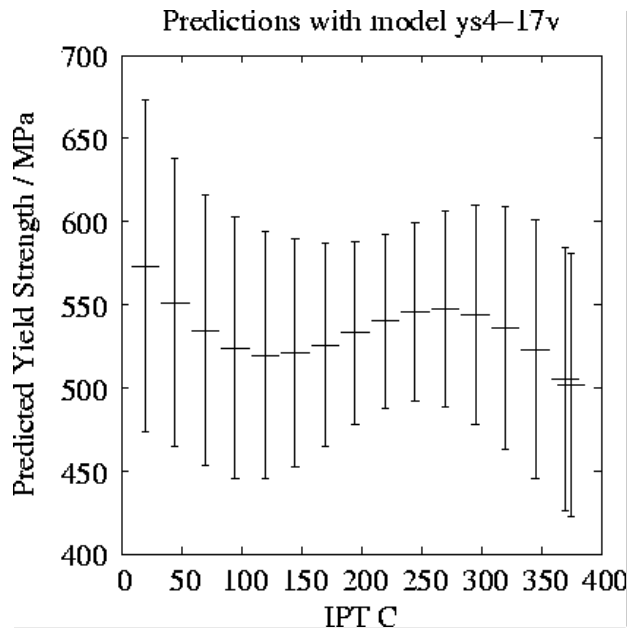


Fig f. Predicted variations in Yield Strength with Interpass Temperature variation.

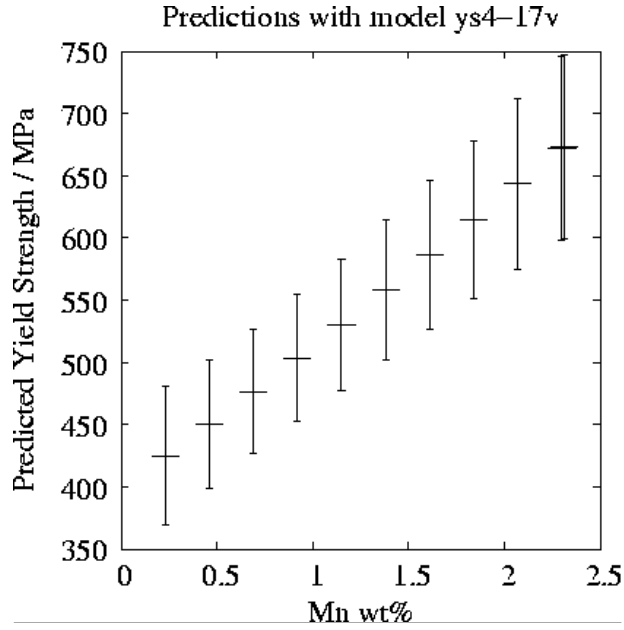


Fig g. Predicted variations in Yield Strength with Manganese variation.

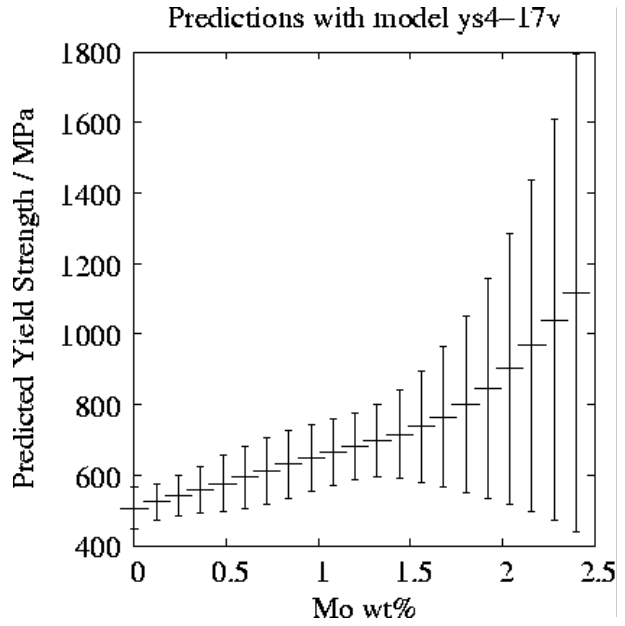


Fig h. Predicted variations in Yield Strength with Molybdenum variation.

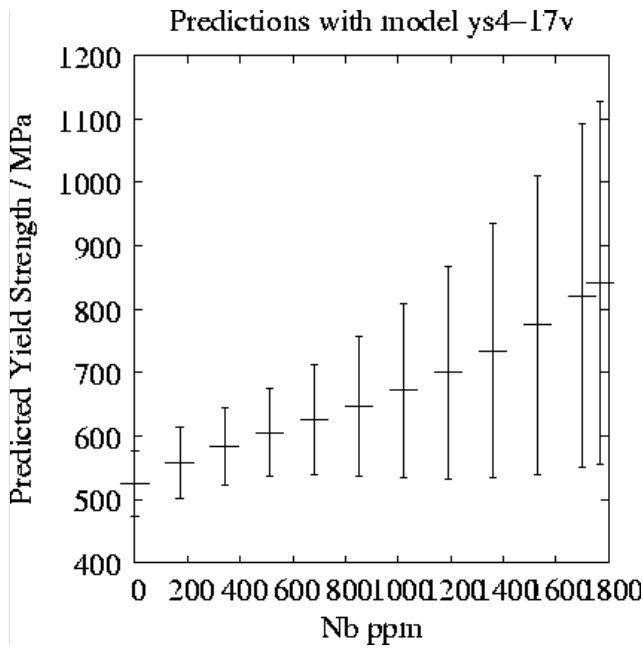


Fig i. Predicted variations in Yield Strength with Niobium variation.

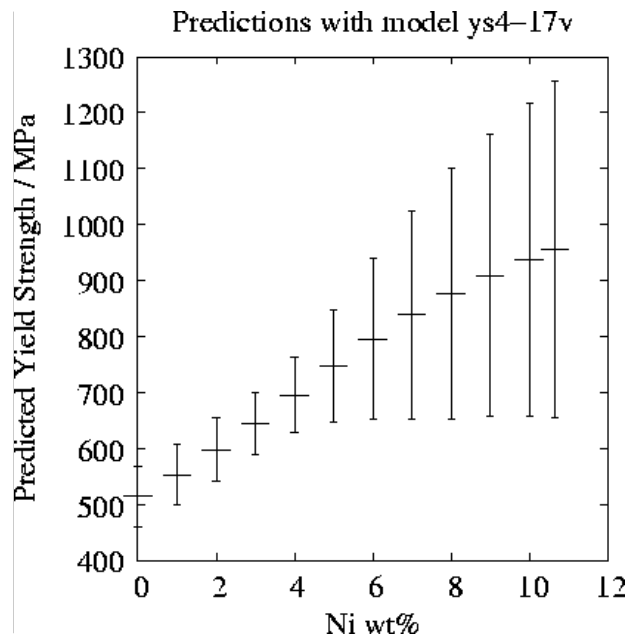


Fig j. Predicted variations in Yield Strength with Nickel variation.

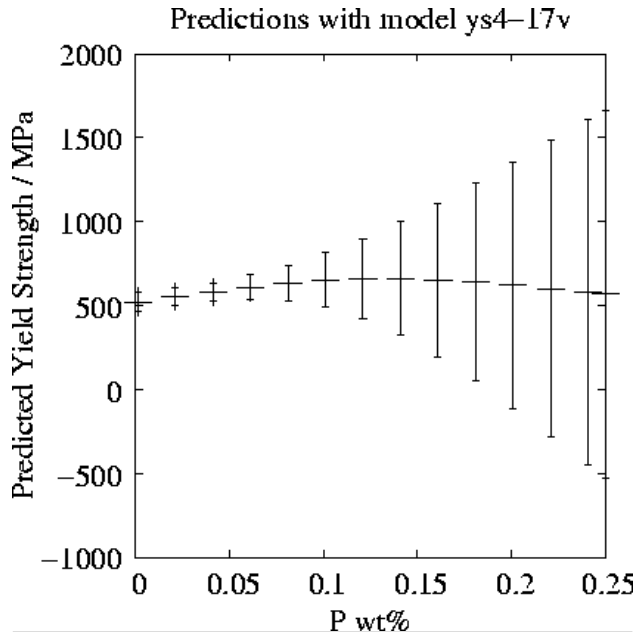


Fig k. Predicted variations in Yield Strength with Phosphorus variation.

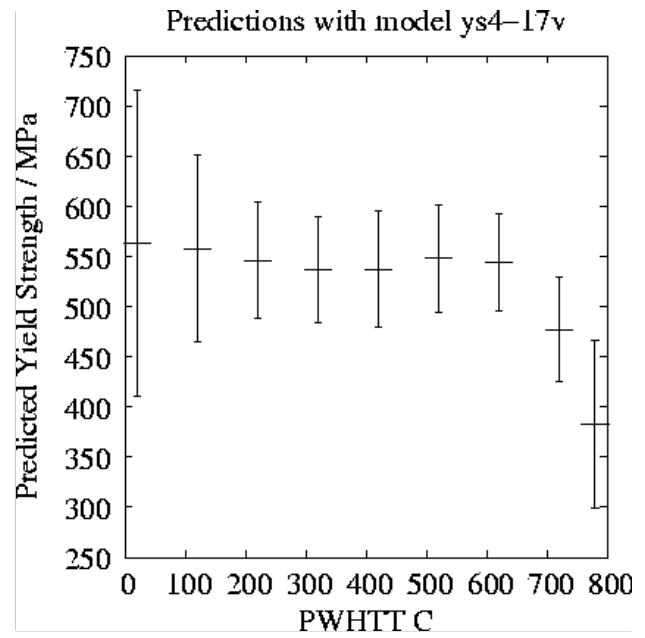


Fig l. Predicted variations in Yield Strength with Post Weld Heat Treatment Temperature variation.

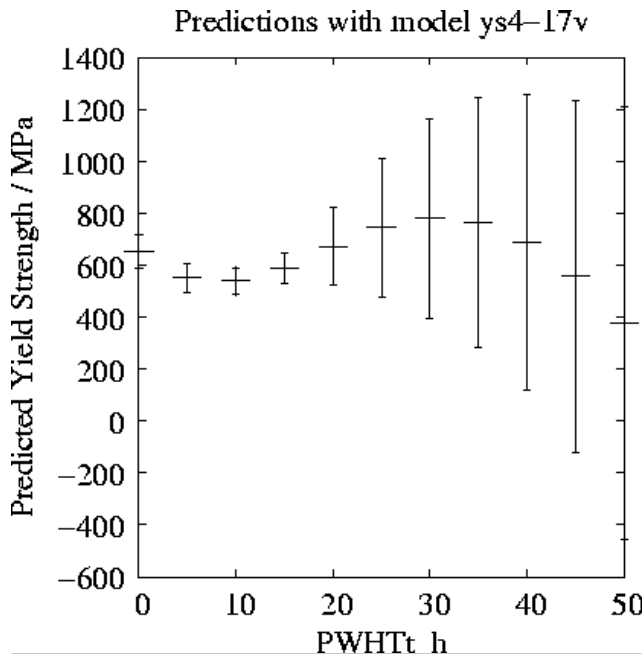


Fig m. Predicted variations in Yield Strength with Post Weld Heat Treatment Time variation.

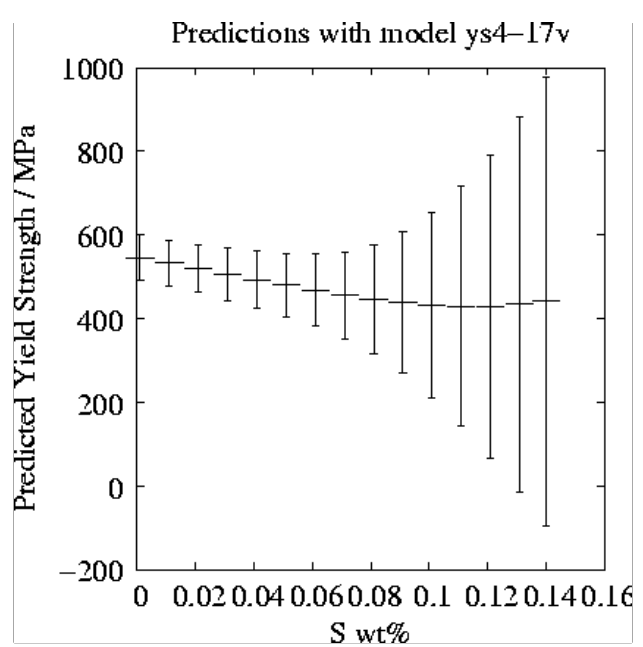


Fig n. Predicted variations in Yield Strength with Sulphur variation.

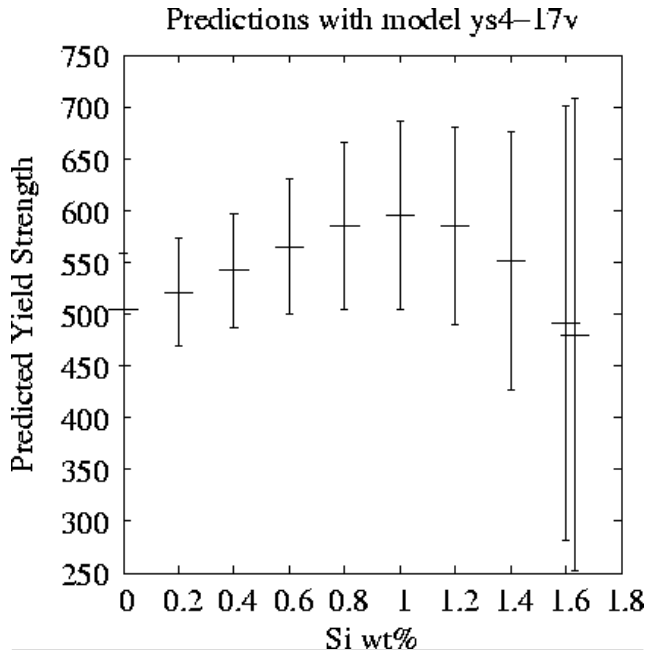


Fig o. Predicted variations in Yield Strength with Silicon variation.

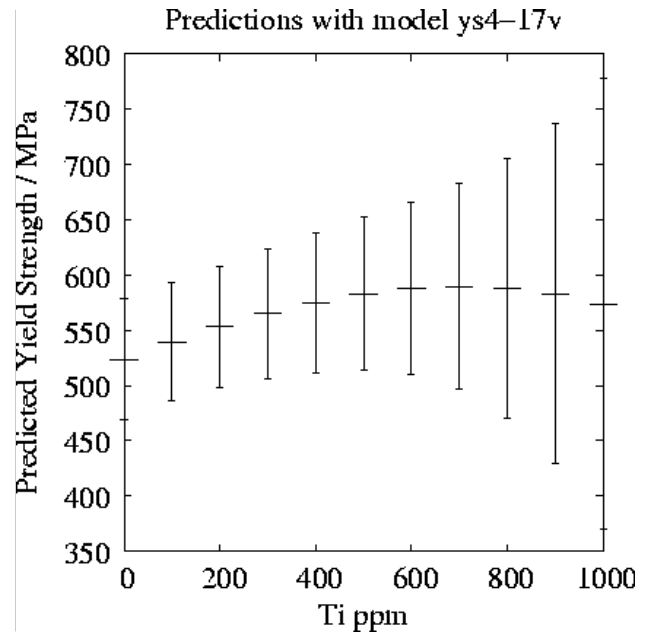


Fig p. Predicted variations in Yield Strength with Titanium variation.

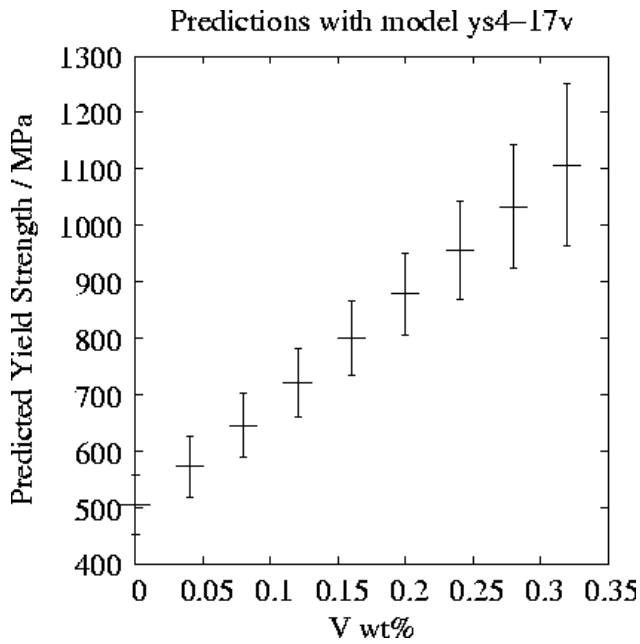


Fig q. Predicted variations in Yield Strength with Vanadium variation.

Figure 4.1 (a to q) Response graphs (a to q) of Input variables and Yield Strength of Ferritic Steel Welds using committee model of Bayesian Neural Network

These trends are confirmed in the present analysis as illustrated in Figure 4.1 (a to q). It is emphasized that these calculations are done without permitting any of the other variables to change. They are impossible to reproduce in practice.

All the graphs show the error bars. The error bars are uniform in size indicate that the uniformity of data, like the graph the prediction of the Yield Strength as a function of Manganese. The error bars are large in size indicate non-uniformity of data, like the graph the prediction of the Yield Strength as a function of Chromium.

In this case, when the concentration of Nickel and Chromium is respectively below 6 and 8 wt%, the prediction can be reliable But above those limits (6 wt% for Ni and 8 wt% for Cr), the model can no more be trusted and this is inferred by the large error bars. Similarly it is applicable to other graphs where larger error bars are present. More experiments with concentrations in this range of values need to be carried out to improve the model. Uncertainty because of a lack of data is one of the limitations of a neural network. The error bars and output variable (Yield Strength) sometimes showing unphysical (negative) values, this is because of the empirical equation in Neural Network modelling.[29].

The input variables like Boron, Carbon, Copper, Manganese, Molybdenum, Niobium, Nickel, and Vanadium are increasing in concentration, increase the Yield Strength of ferritic Steel welds.

The input variables like Post Weld Heat Treatment Temperature and Sulphur increase quantitatively decrease the Yield Strength of ferritic Steel welds. The Phosphorus has shown little effect on the Yield Strength.

The input variables like Chromium, Heat Input, Interpass Temperature, Post Weld Heat Treatment Time, Silicon, and Titanium indicate their non linear behavior with the Yield Strength.

The trends of the graphs by Bayesian Neural network model are useful to design the Yield Strength of Ferritic Steel welds efficiently.

In summary, a reasonable committee model has been obtained for Yield Strength. It appears that these input variables are affected on the Yield Strength of Ferritic Steel Welds, as could be expected from a metallurgical point of view.

4.1.2 Response Graphs of the Yield Strength GRNN model

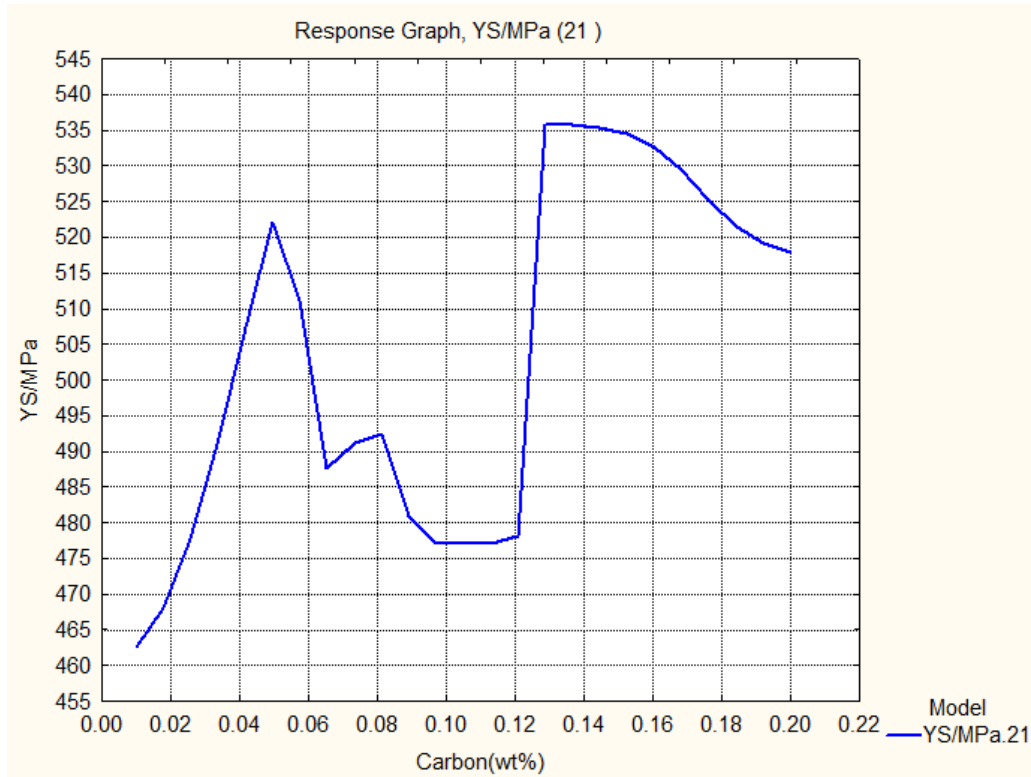


Fig. a Response Graph of Yield Strength MPa and Carbon(wt%)

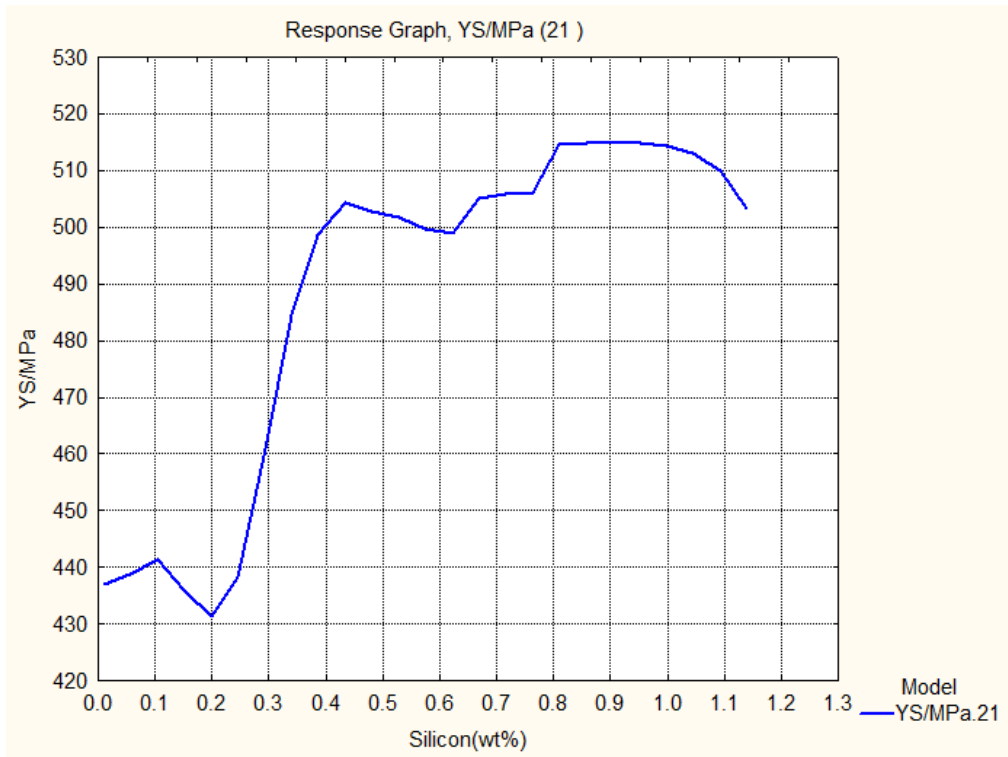


Fig. b Response Graph of Yield Strength MPa and Silicon(wt%)

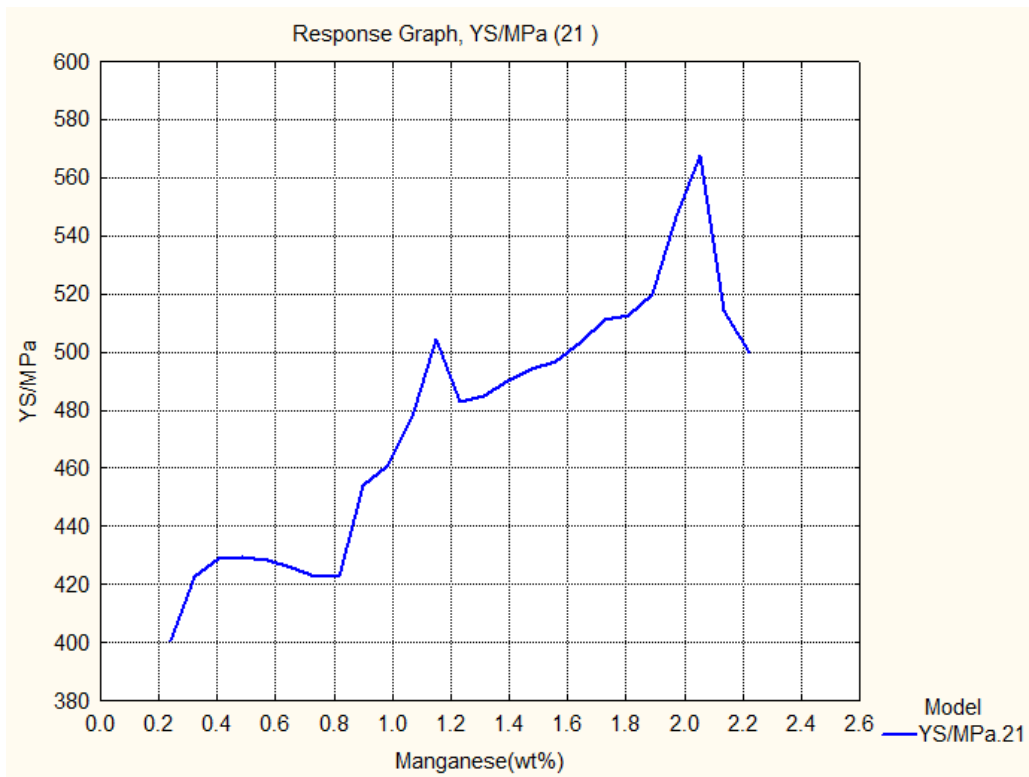


Fig. c Response Graph of Yield Strength MPa and Manganese(wt%)

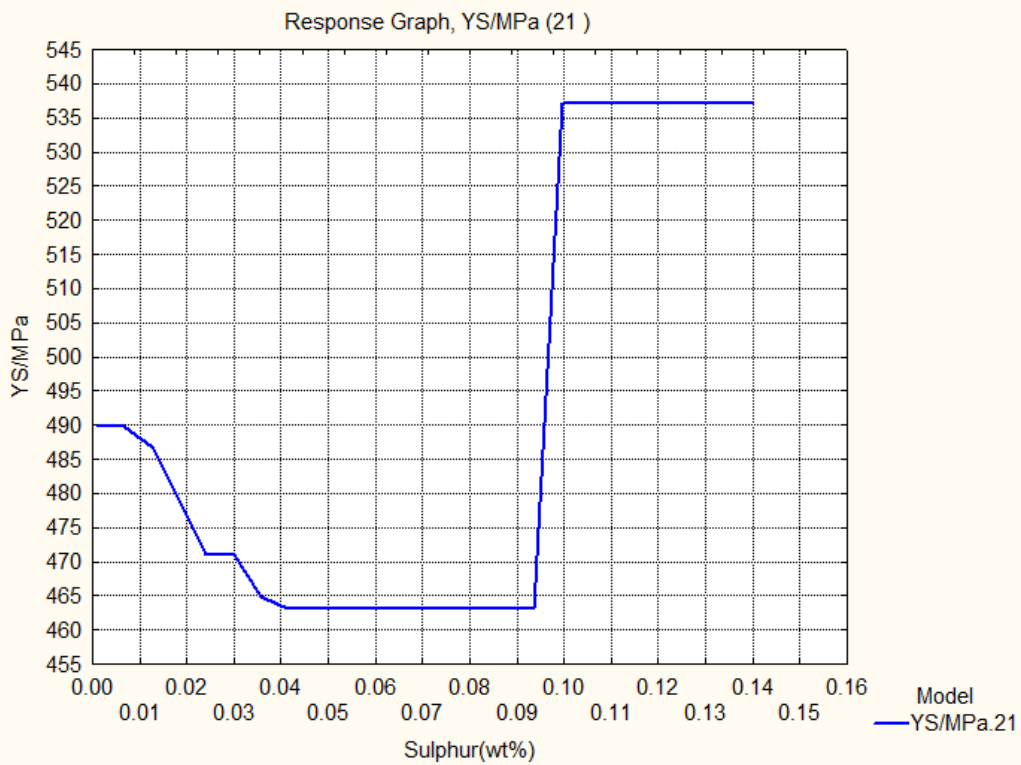


Fig. d Response Graph of Yield Strength MPa and Sulphur(wt%)

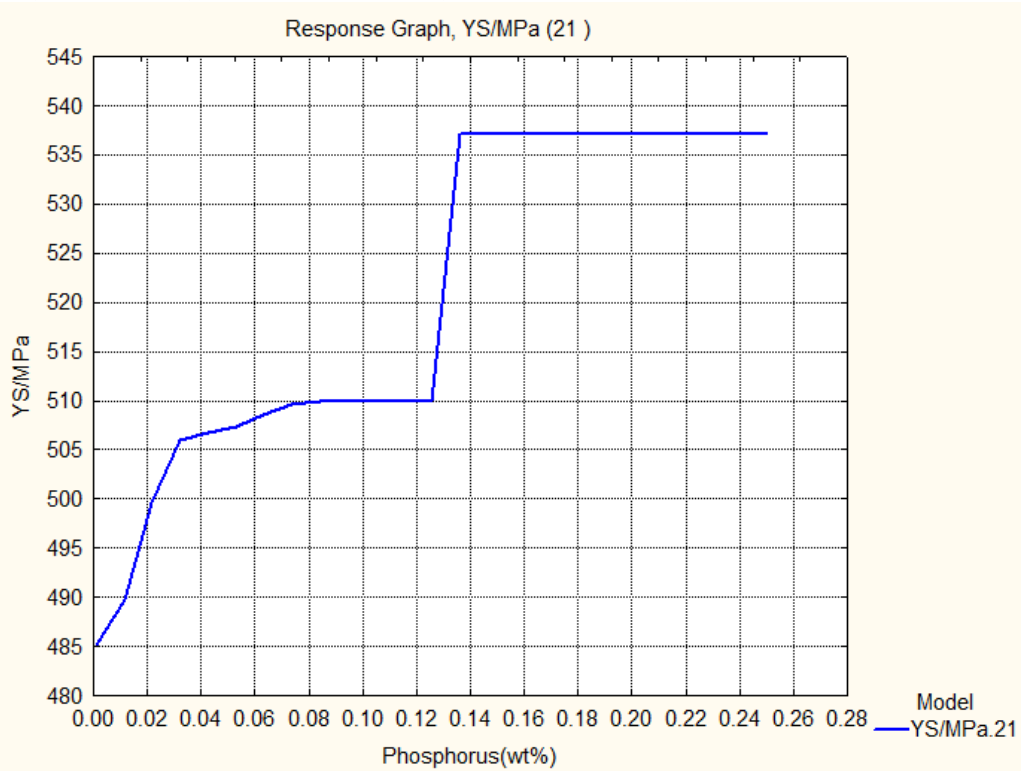


Fig. e Response Graph of Yield Strength MPa and Phosphorus(wt%)

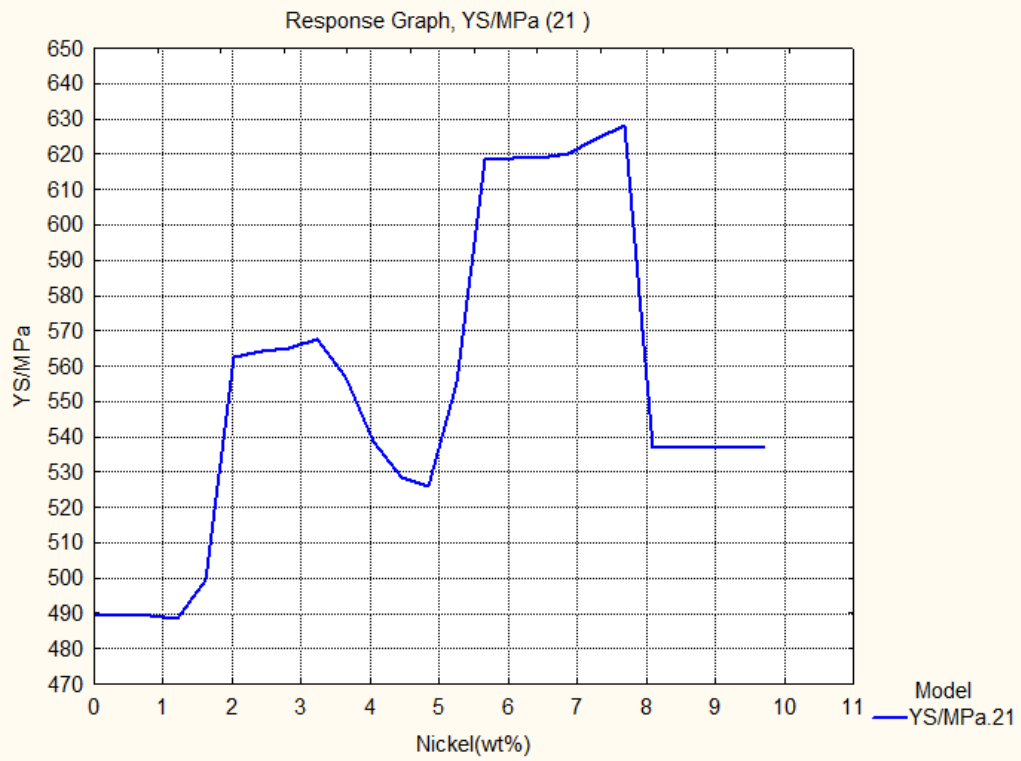


Fig. f Response Graph of Yield Strength MPa and Nickel(wt%)

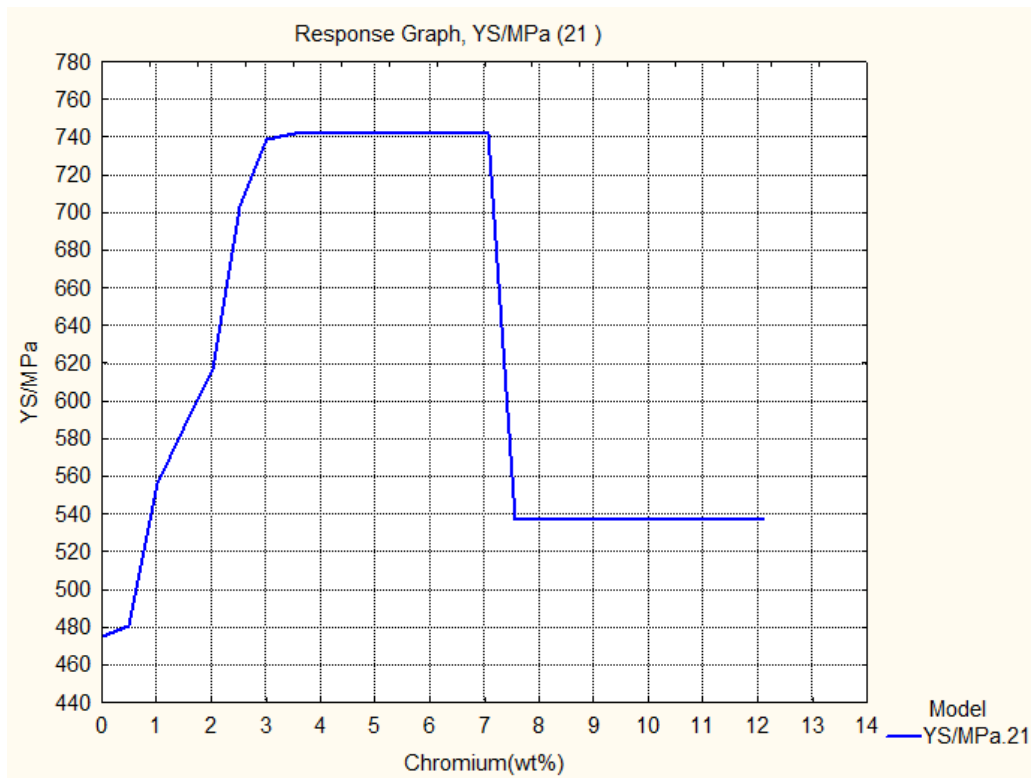


Fig. g Response Graph of Yield Strength MPa and Chromium(wt%)

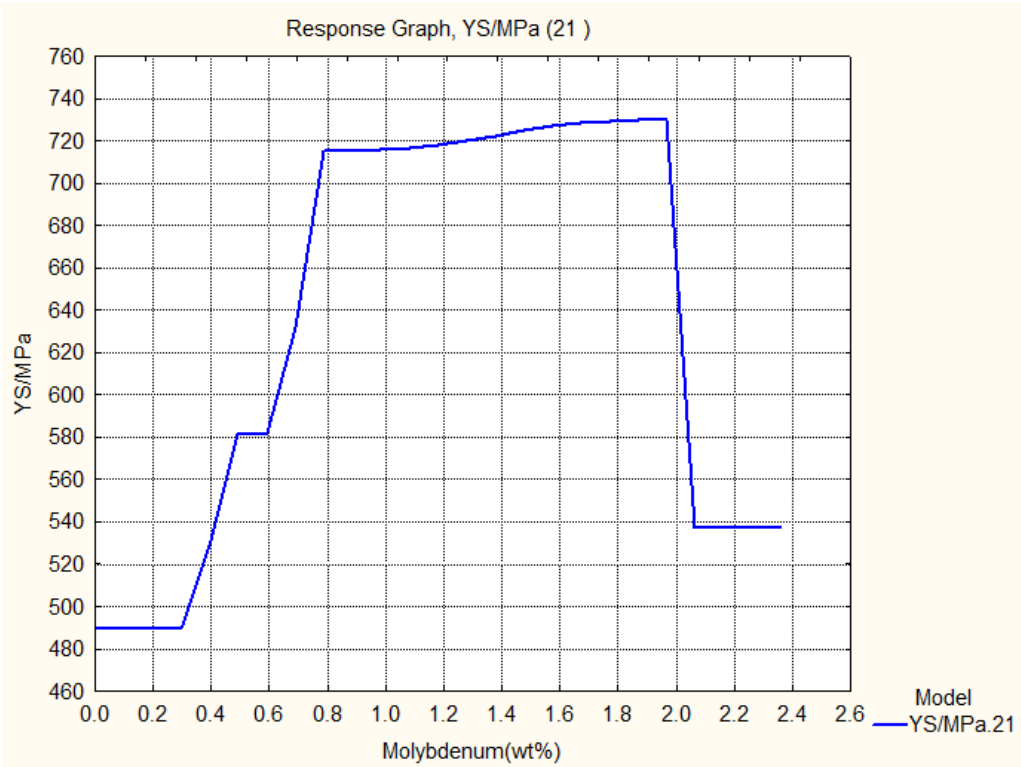


Fig. h Response Graph of Yield Strength MPa and Molybdenum(wt%)

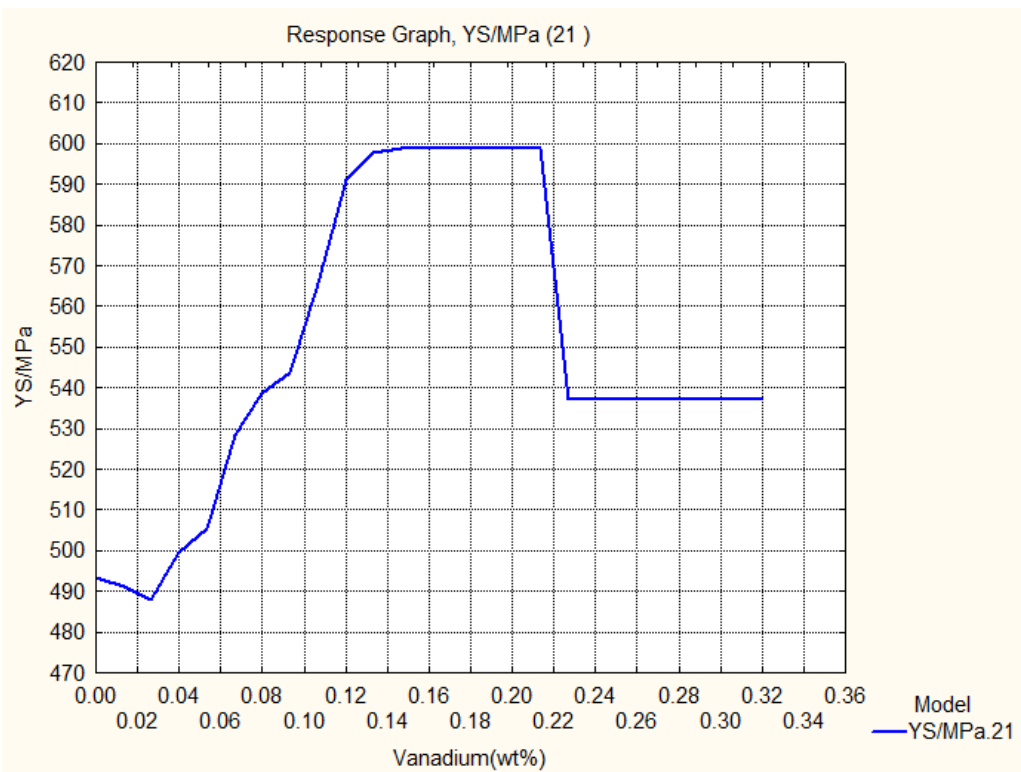


Fig. i Response Graph of Yield Strength MPa and Vanadium(wt%)

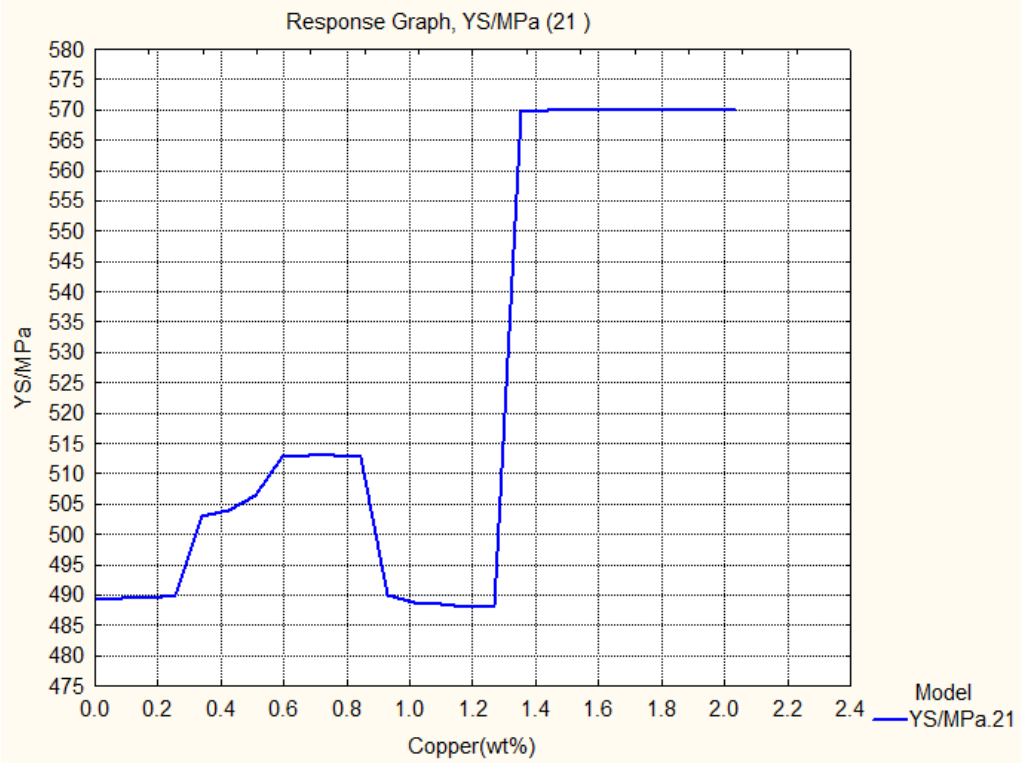


Fig. j Response Graph of Yield Strength MPa and Copper(wt%)

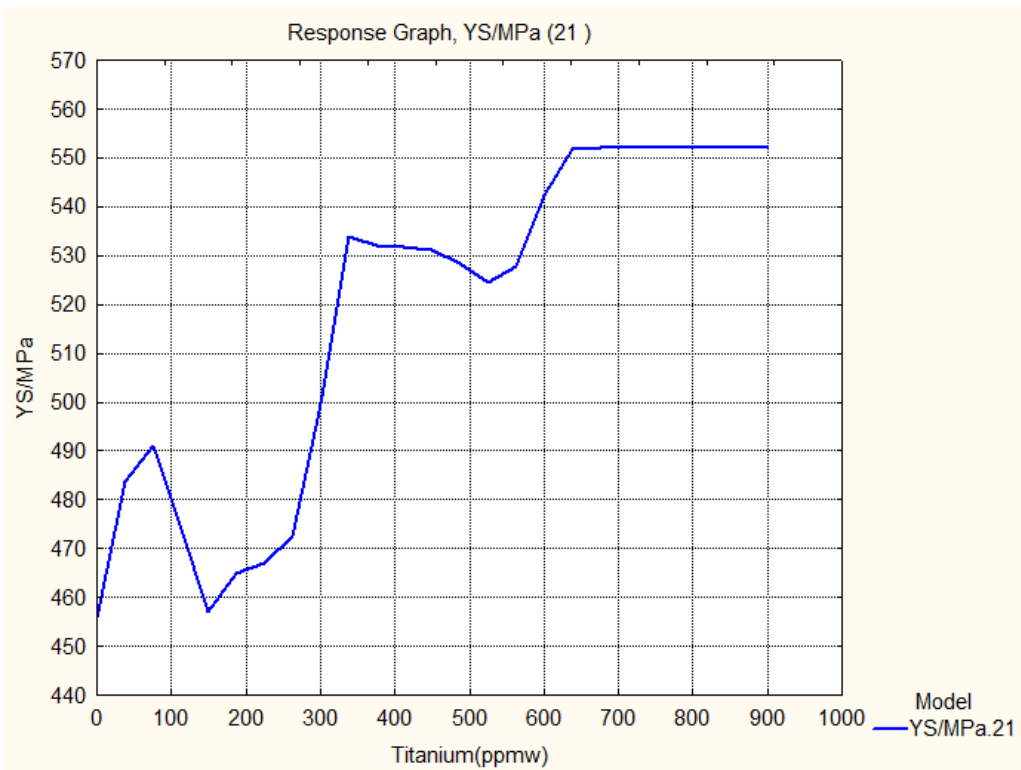


Fig. k Response Graph of Yield Strength MPa and Titanium(ppmw)

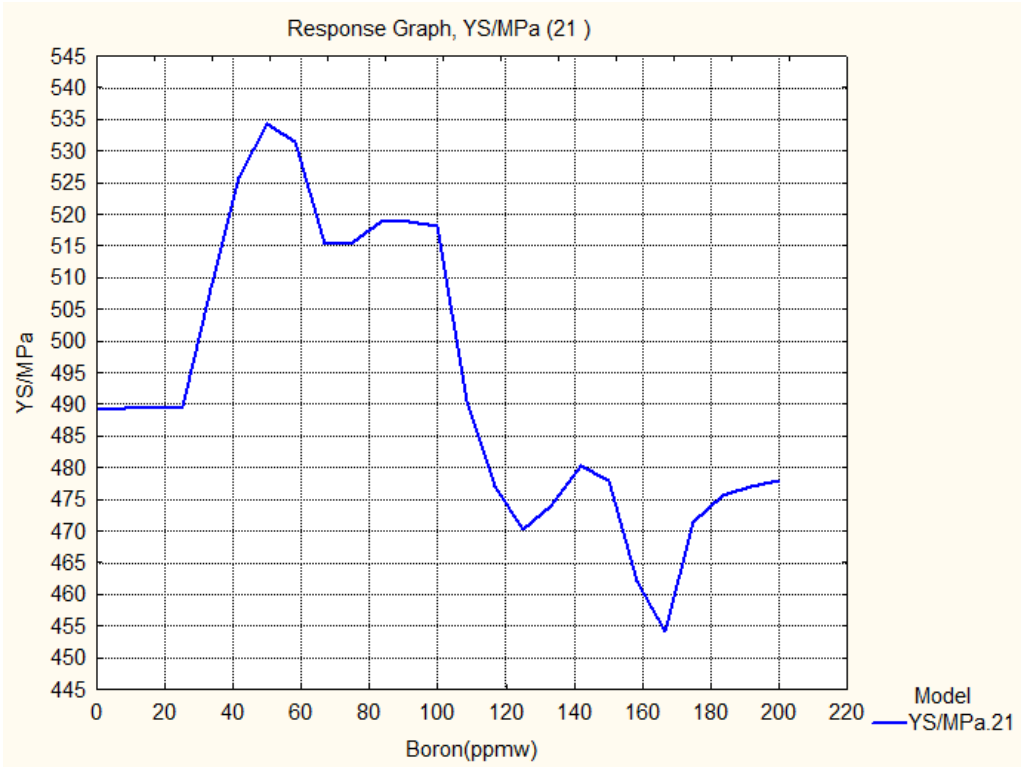


Fig. l Response Graph of Yield Strength MPa and Boron(ppmw)

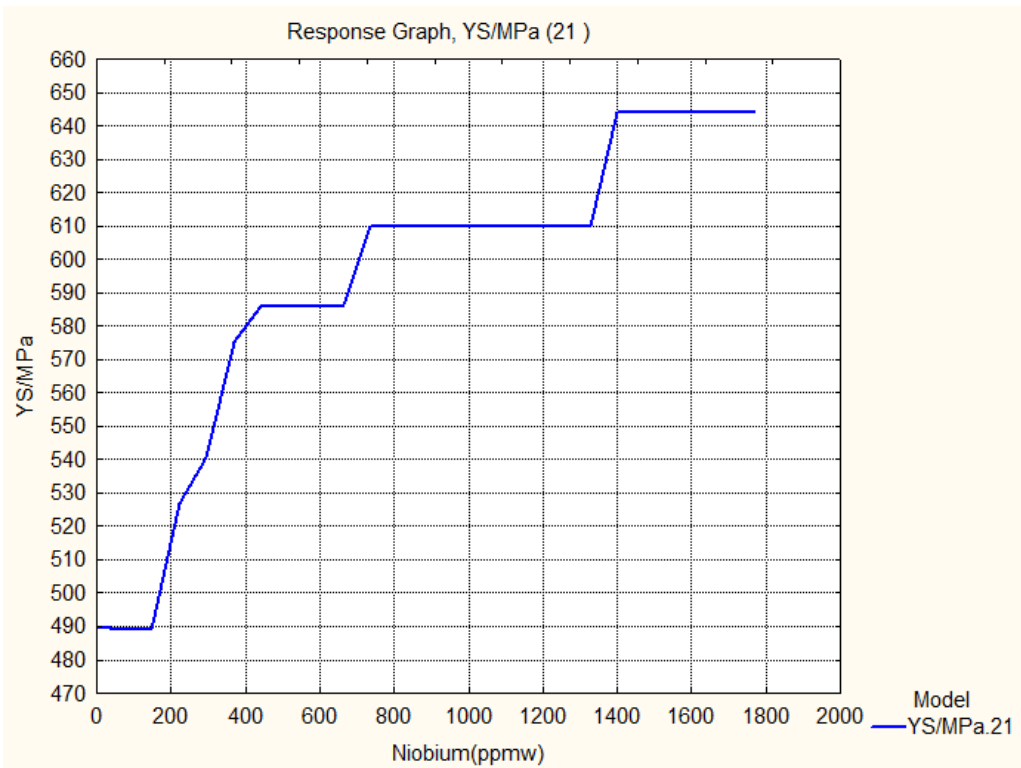


Fig. m Response Graph of Yield Strength MPa and Niobium(ppmw)

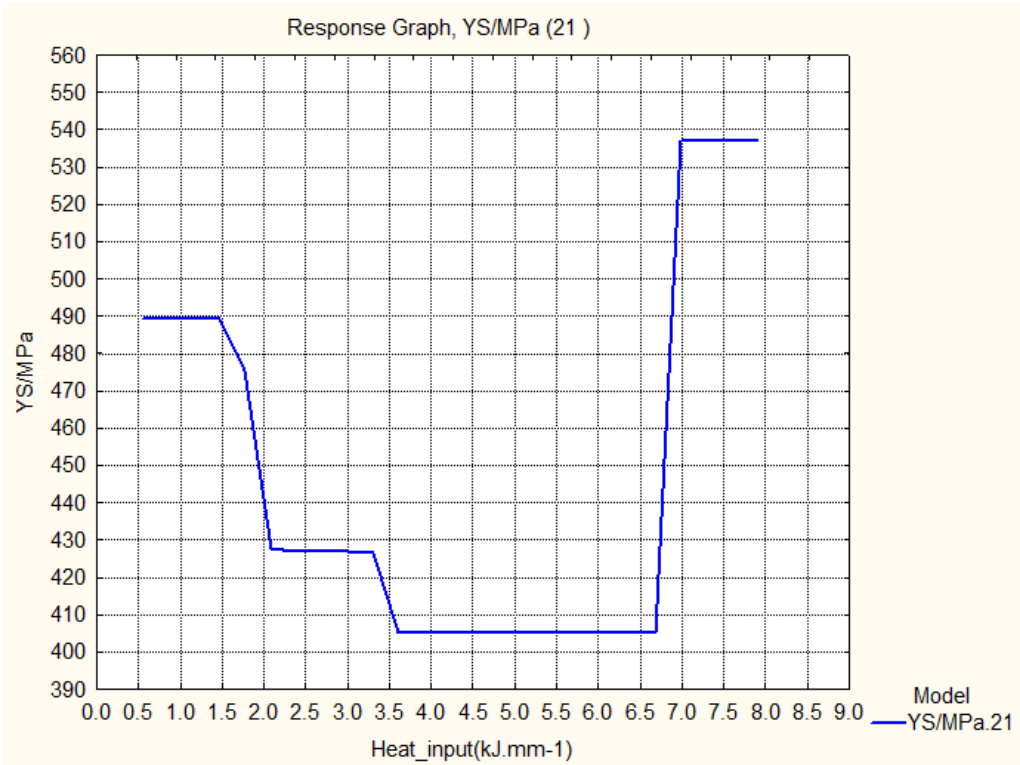


Fig. n Response Graph of Yield Strength MPa and Heat input(kj mm-1)

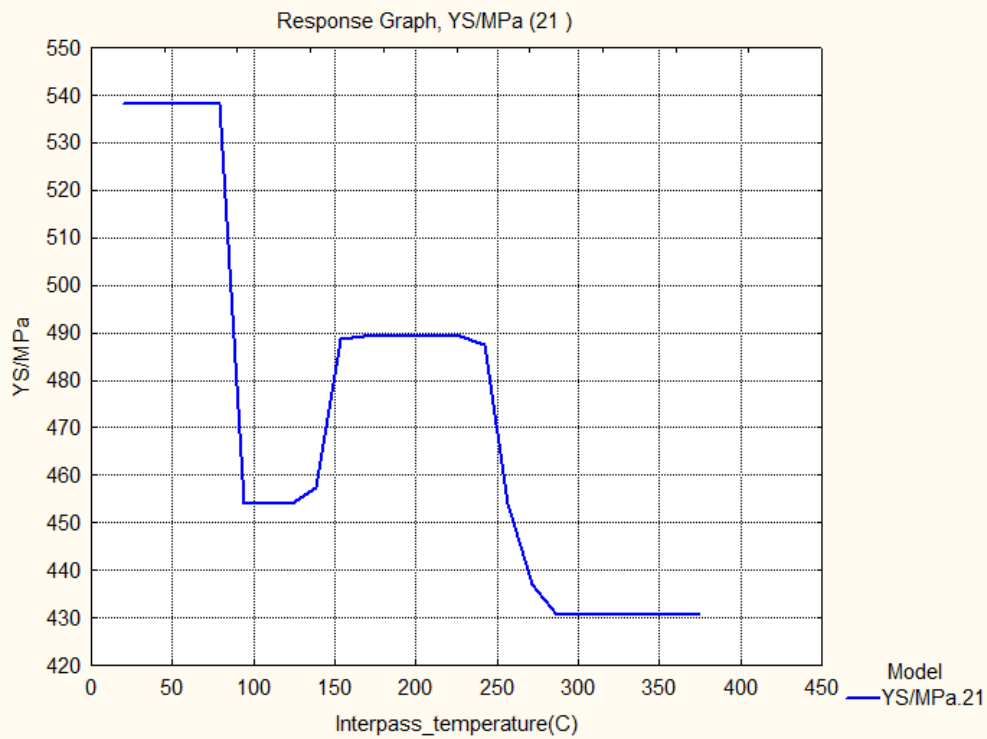


Fig. o Response Graph of Yield Strength MPa and Interpass temperature(C)

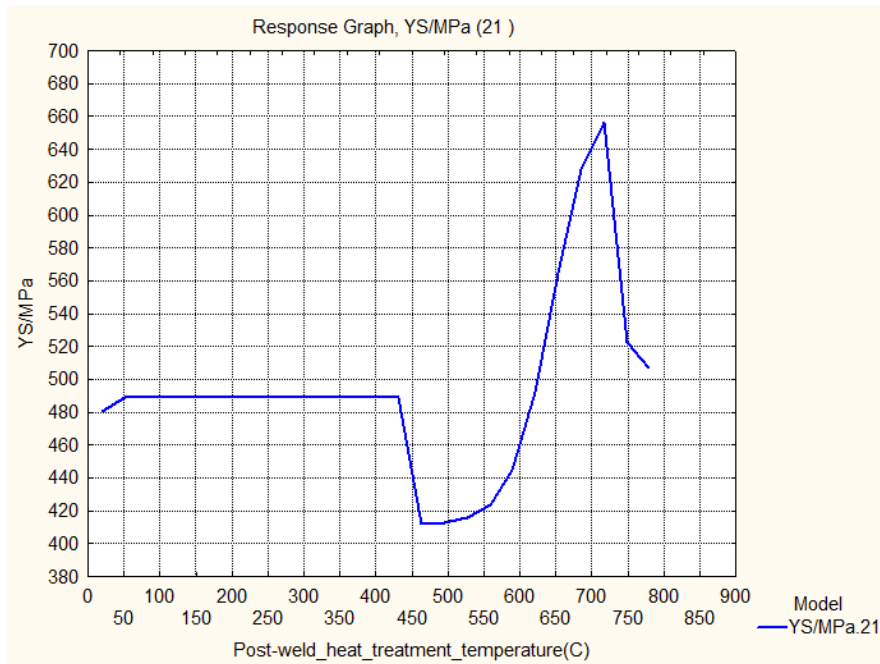


Fig. p Response Graph of Yield Strength MPa and Post-weld heat treatment temperature(C)

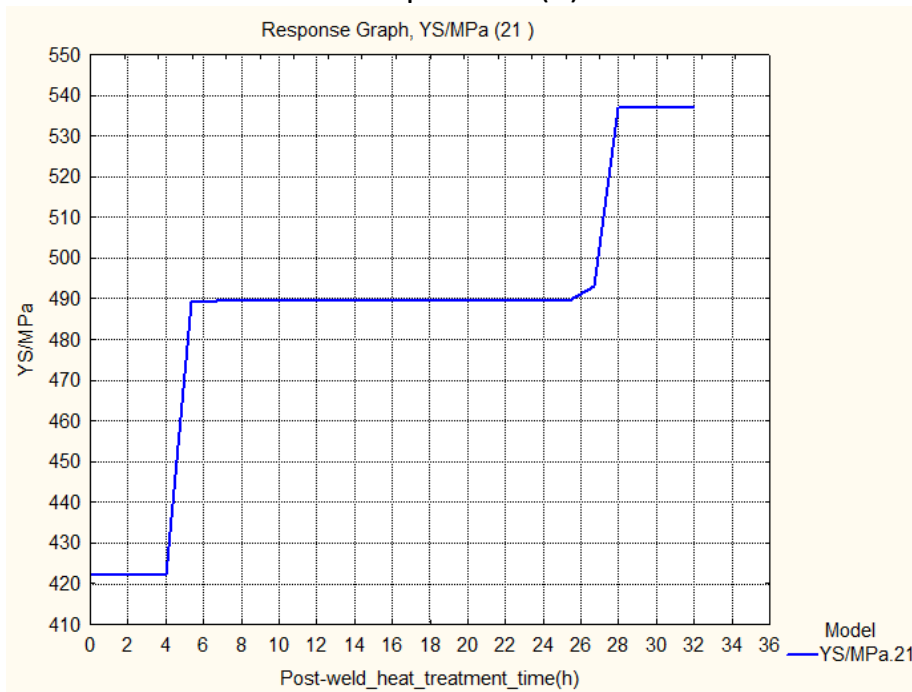


Fig. q Response Graph of Yield Strength MPa and Post-weld heat treatment time(h)

Figure 4.2 (a to q) Response graphs of Input variables and Yield Strength of Ferritic Steel Welds (GRNN)

The influence of each of the variables on the yield strength of welding alloys which is discussed here. The carbon increases the yield strength up to 522 MPa with 0.05% then drop to 477 MPa at 0.1%. After 0.15% C, yield strength increases to 536 MPa than decrease to 519 MPa at 0.2% C. In the case of silicon between 0.1% to 0.2%, there is a drop of the 440 MPa to 431 MPa in yield strength and then increases to 505 MPa at 0.45%. At 0.8%, yield strength is 515 MPa and decreases between 1.0% to 1.2% from 515 MPa to 504 MPa. The trend of manganese shows the increase in the Mn% the value of the yield strength is also increased from 400 MPa to 563 MPa. At various points, 0.8%, 1.1%, 2.1% the decrease in yield strength is observed. The sulphur shows the first decrease in the yield strength from 490 MPa to 464 MPa. At slightly more than 0.09%, it is increased from 464 MPa to 537 MPa. The Phosphorus gives the increase in yield strength from 485 MPa to 537 MPa. The nickel has the maximum yield strength of 629 MPa at 7.8% and minimum 490 MPa at 1%. In figure. It shows at 4.9% the yield strength value drop to 528 MPa. More than 7.8 %i Ni gives a further drop in yield strength 539 MPa. The Chromium has a maximum yield strength of 740 MPa between 3% to 7%. More than 7% Cr reduces the yield strength to 539 MPa. Increase in the yield strength from 479 MPa to 740 MPa only by the gradual addition of chromium up to 3%. Molybdenum increases the yield strength from 490 MPa to 730 MPa at 1.98%. At 0.8% Mo gives yield strength 719 MPa. More than 1.98% Mo decreases yield strength from 730 MPa to 539 MPa. Vanadium increases the yield strength from 492 MPa to 600 MPa at 0.15%. At 0.22% V, yield strength decreases to 538 MPa. Copper increases the yield strength from 490 MPa to 513 MPa at 0.6%. At 1.2% Cu, yield strength decreases to 488 MPa. Cu gives maximum yield strength of 570 MPa when it is more than 1.27%. Titanium gives a minimum yield strength of 457 MPa to maximum 553 MPa. At 700 ppm yield strength is the highest. In between some range of Titanium from 90 ppm to 630 ppm, up and down in yield strength. Boron shows maximum yield strength of 535 MPa at 50 ppm. More than 50 ppm decreases the yield strength to 454 MPa. Niobium has a trend of increase in yield strength from 490 to 644 MPa with an increase from 180 to 1400 ppm.

Heat Input has stated of the yield strength of 490 MPa, then drops in between 1.5 to 6.6 kJ mm⁻¹ to 406 MPa. The highest value of yield strength 537 MPa is obtained at and more than 6.7 kJ mm⁻¹. When the Interpass temperature is less than 70 C, the yield strength is 538 MPa. More

than 70 C decrease in yield strength is observed to 470 MPa and further increase to 490 MPa at 150 C. Minimum yield strength is 430 MPa at 270 C. Post weld heat treatment temperature increases up to 425 C shows yield strength 480 MPa and 490 MPa. More than 455 C, the yield strength increases to maximum 655 MPa at 710 C then drop to 510MPa. Post weld heat treatment time has a trend of increase in yield strength from 420 to 490 MPa between 4 to 5 hours. More than 25 hours, it increases maximum yield strength to 538 MPa.

The relationship between the input variables and yield strength is a nonlinear as seen above in response graphs(Figure 4.2 (a to q)).

The GRNN model has good accuracy in prediction of yield strength of ferritic steel welds on unseen data which is excellent for the design of welds.(Table.3.5) The predicted yield strength for the unseen data of three weld alloys are compared with measured values of yield strength shows the prediction capacity of the GRNN model. This GRNN model can be used for practical applications, research and development of ferritic steel alloys.

4.1.3 3D Contour plots of the Yield Strength GRNN model

The effect in combination of any two input variables (Independent variables) from Carbon, Silicon, Manganese, Sulphur, Phosphorus, Nickel, Chromium, Molybdenum, Vanadium, Copper, Titanium, Boron, Niobium, Heat_input, Interpass_temperature, Post- weld heat treatment temperature and Post-weld heat treatment time on the Yield Strength of Ferritic Steel Welds are given in form of 3D contour plots.(Figure.4.3.1 to4.3.18)

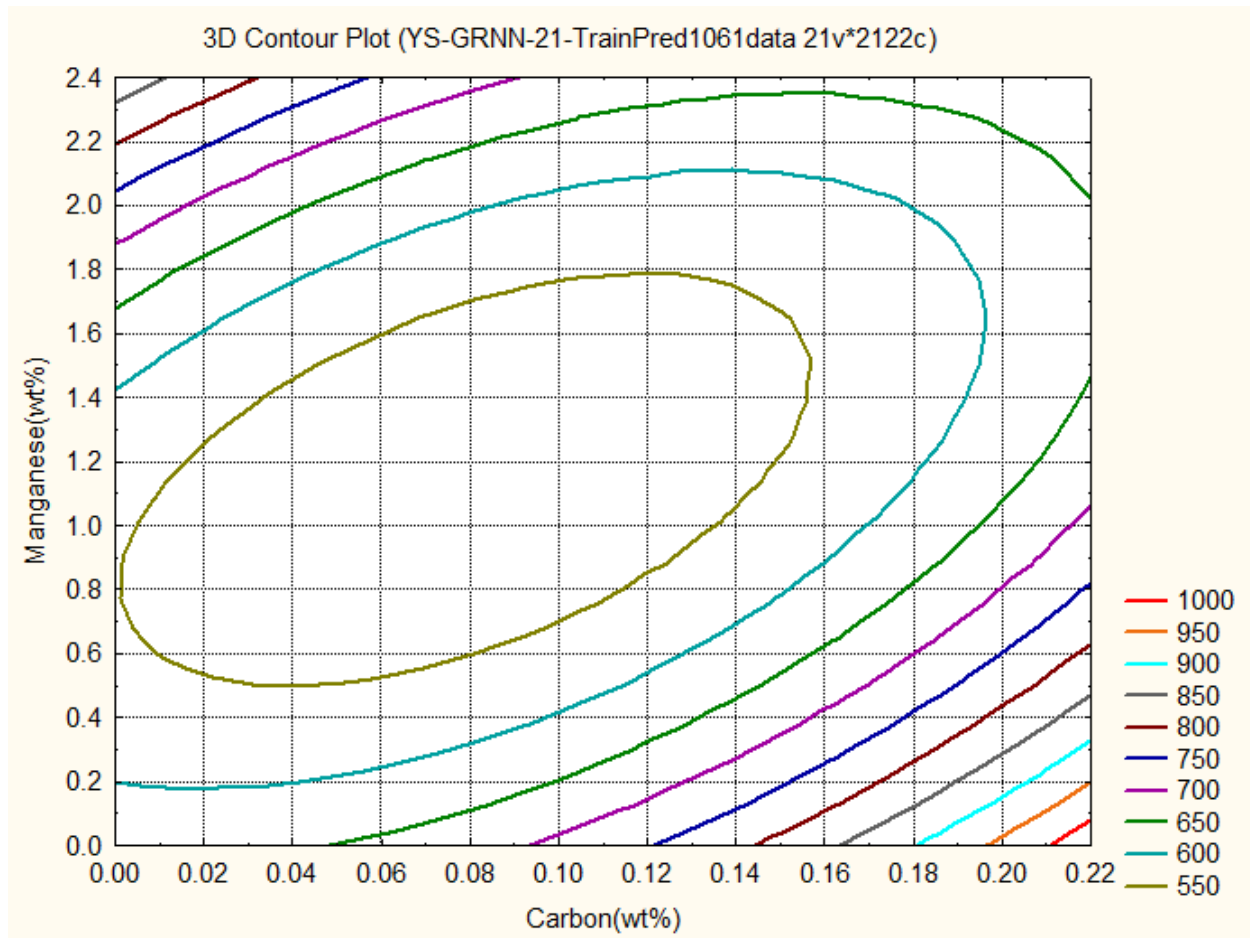


Figure.4.3.1 Predicted variations in Yield Strength (MPa) as a function of the Carbon and Manganese concentrations

3D contour Plot gives the relations between the **two input variables** and **one output variable**. **Figure. 4.3.1** shows the relations between Carbon, Manganese and Yield Strength by GRNN. The graph gives the information about how these two, Carbon and Manganese control the Yield Strength from 550MPa to 1000MPa.. Traditionally in alloy design it is known that increase the Carbon decrease the Yield Strength. In **Figure. 4.3.1**, it is very critical to maintain the Yield Strength with Carbon and Manganese. Higher Yield Strength is maintained by the Carbon and Manganese with lower concentrations in weld deposits. Higher Yield Strength can achieve with very low carbon less than 0.03 wt% and higher amount of Manganese more than 2 wt% in ferritic steel weld deposits. To achieve a **950 MPa and more**, the compositions of Carbon must be maintained below 0.20 wt% and Manganese must be maintained maximum **0.2 wt%**.

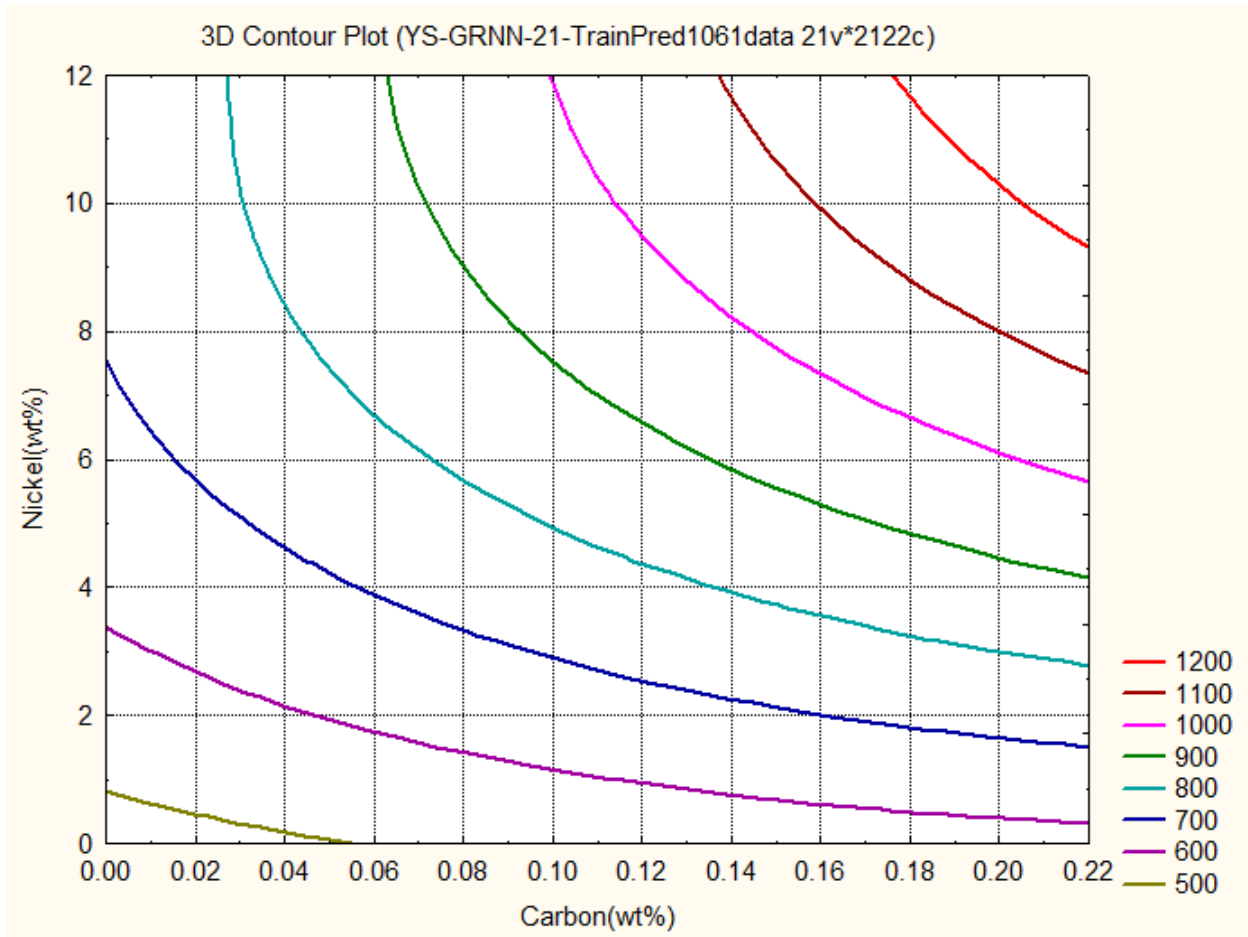


Figure.4.3.2 Predicted variations in Yield Strength (MPa) as a function of the Carbon and Nickel concentrations

3D contour Plot gives the relations between the **two input variables** and **one output variable**. **Figure. 4.3.2** shows the relations between Carbon, Nickel and Yield Strength by GRNN. The graph gives the information about how these two, Carbon **and** Nickel control the Yield Strength from 500MPa to 1200MPa. Both alloying elements, Carbon **0.21 wt%** and Nickel **11 wt%** increase the Yield strength more than 1100 MPa in ferritic steel welds (fsw). Reduction in the concentrations of Carbon and Nickel, lowering the Yield Strength to 500 MPa.

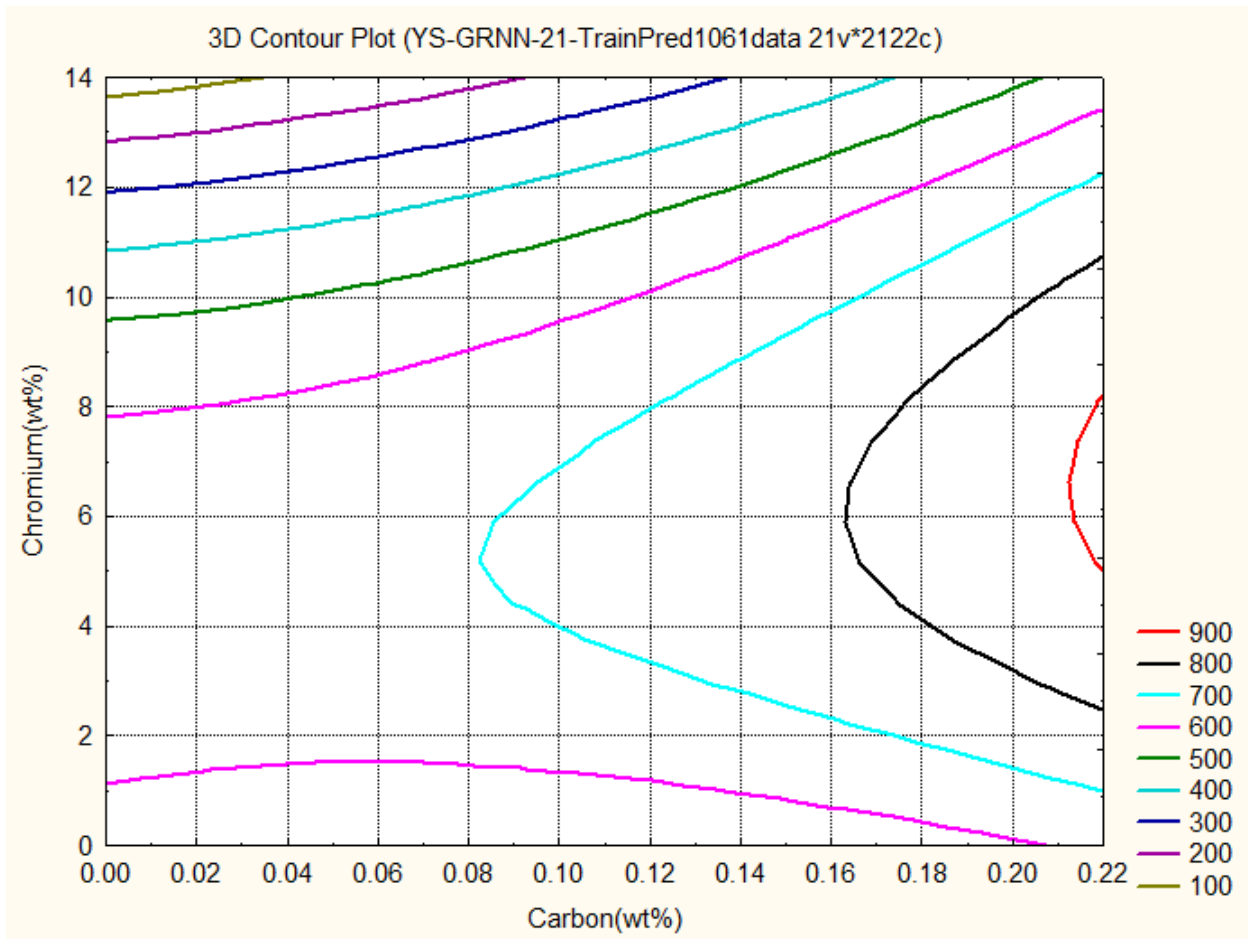


Figure.4.3.3 Predicted variations in Yield Strength (MPa) as a function of the Carbon and Chromium concentrations

3D contour Plot gives the relations between the **two input variables** and **one output variable**. **Figure. 4.3.3** shows the relations between Carbon, Chromium and Yield Strength by **GRNN**. The graph gives the information about how these two, Carbon **and** Chromium control the Yield Strength from 100MPa to **900MPa**.

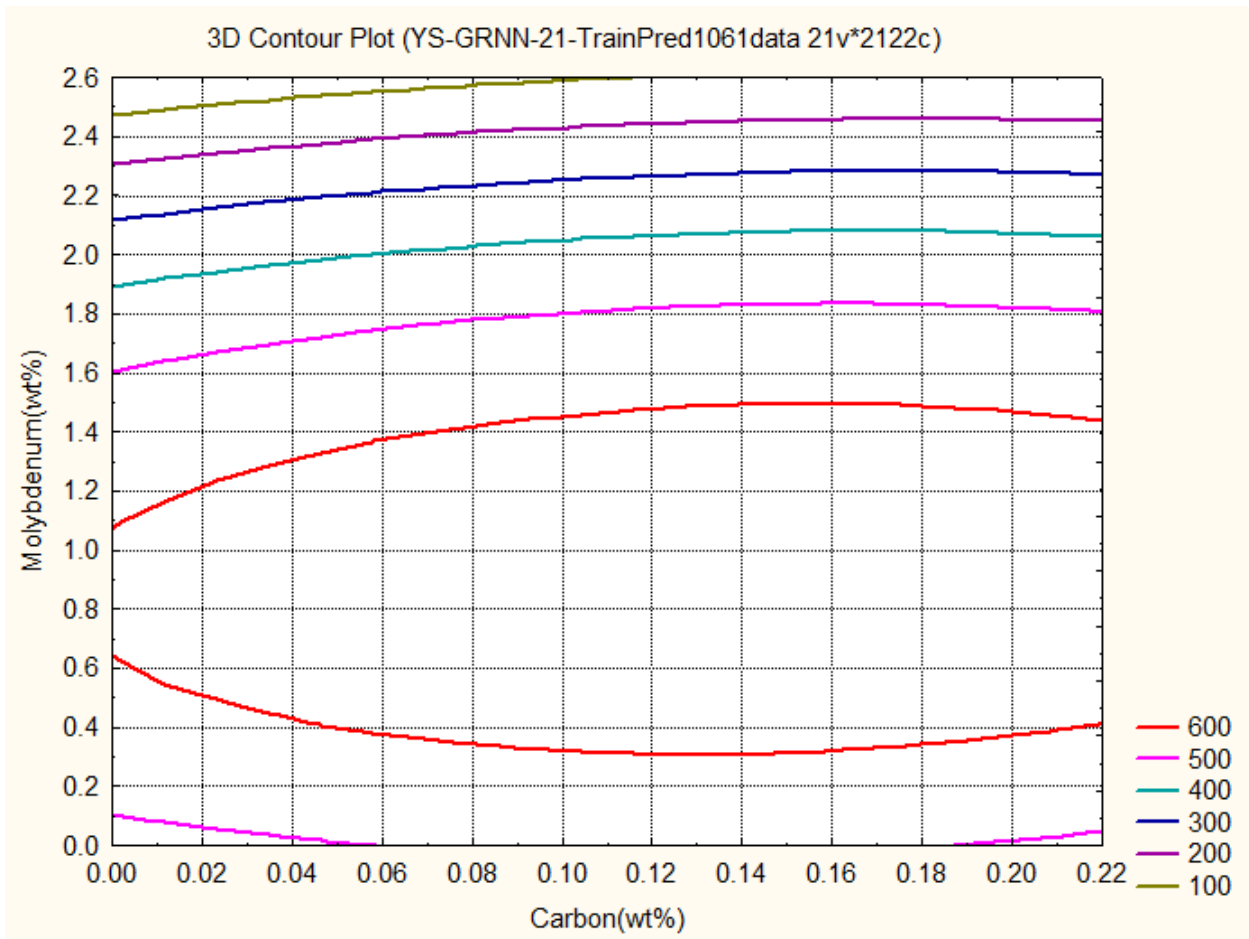


Figure. 4.3.4 Predicted variations in Yield Strength (MPa) as a function of the Carbon and Molybdenum concentrations

3D contour Plot gives the relations between the **two input variables** and **one output variable**. **Figure. 4.3.4** shows the relations between Carbon, Molybdenum and Yield Strength by **GRNN**. The graph gives the information about how these two, Carbon **and** Molybdenum control the Yield Strength from **100MPa to 600MPa**.

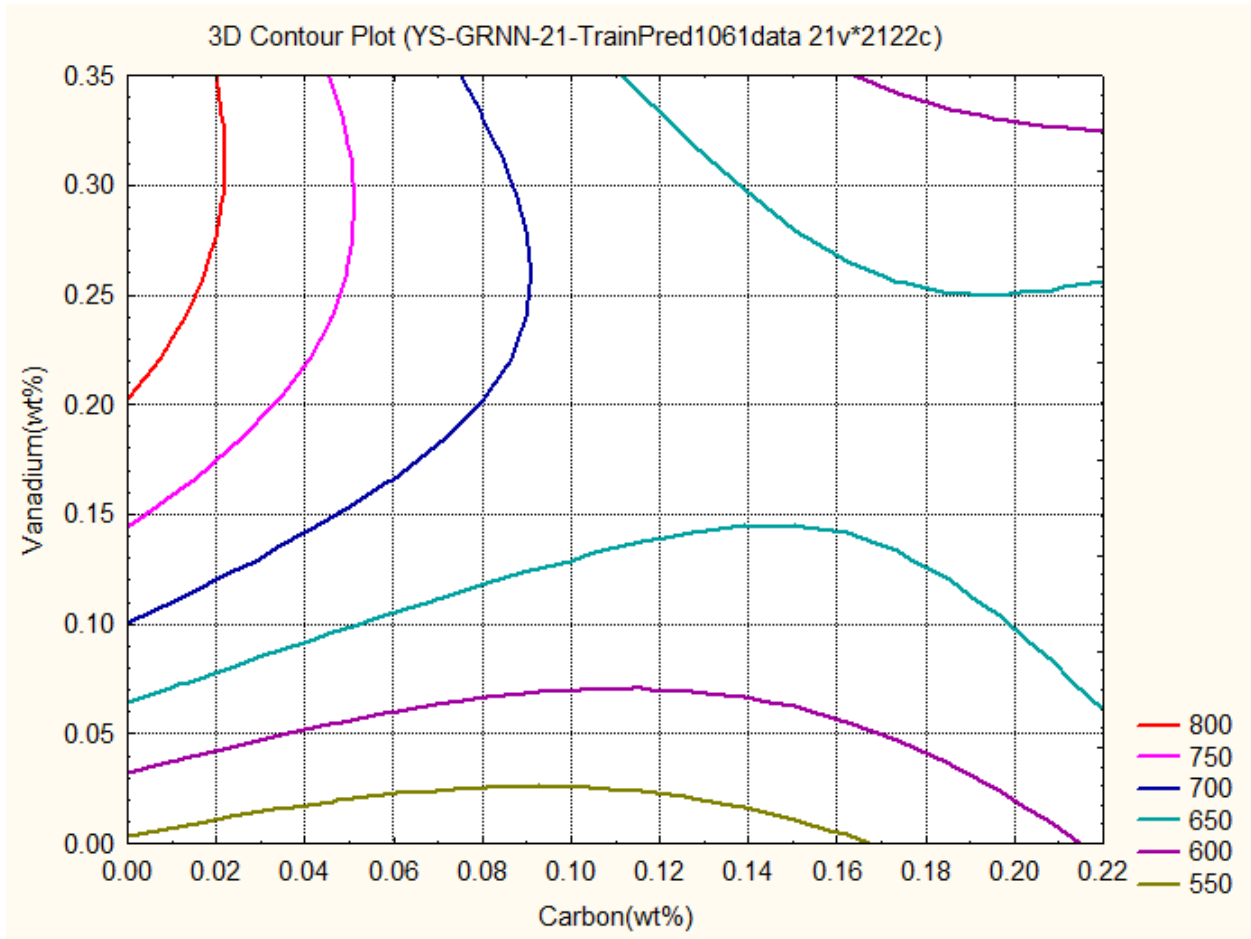


Figure. 4.3.5 Predicted variations in Yield Strength (MPa) as a function of the Carbon and Vanadium concentrations

3D contour Plot gives the relations between the **two input variables** and **one output variable**. **Figure. 4.3.5** shows the relations between Carbon, Vanadium and Yield Strength by **GRNN**. The graph gives the information about how these two, Carbon **and** Vanadium control the Yield Strength from 550MPa to 800MPa.

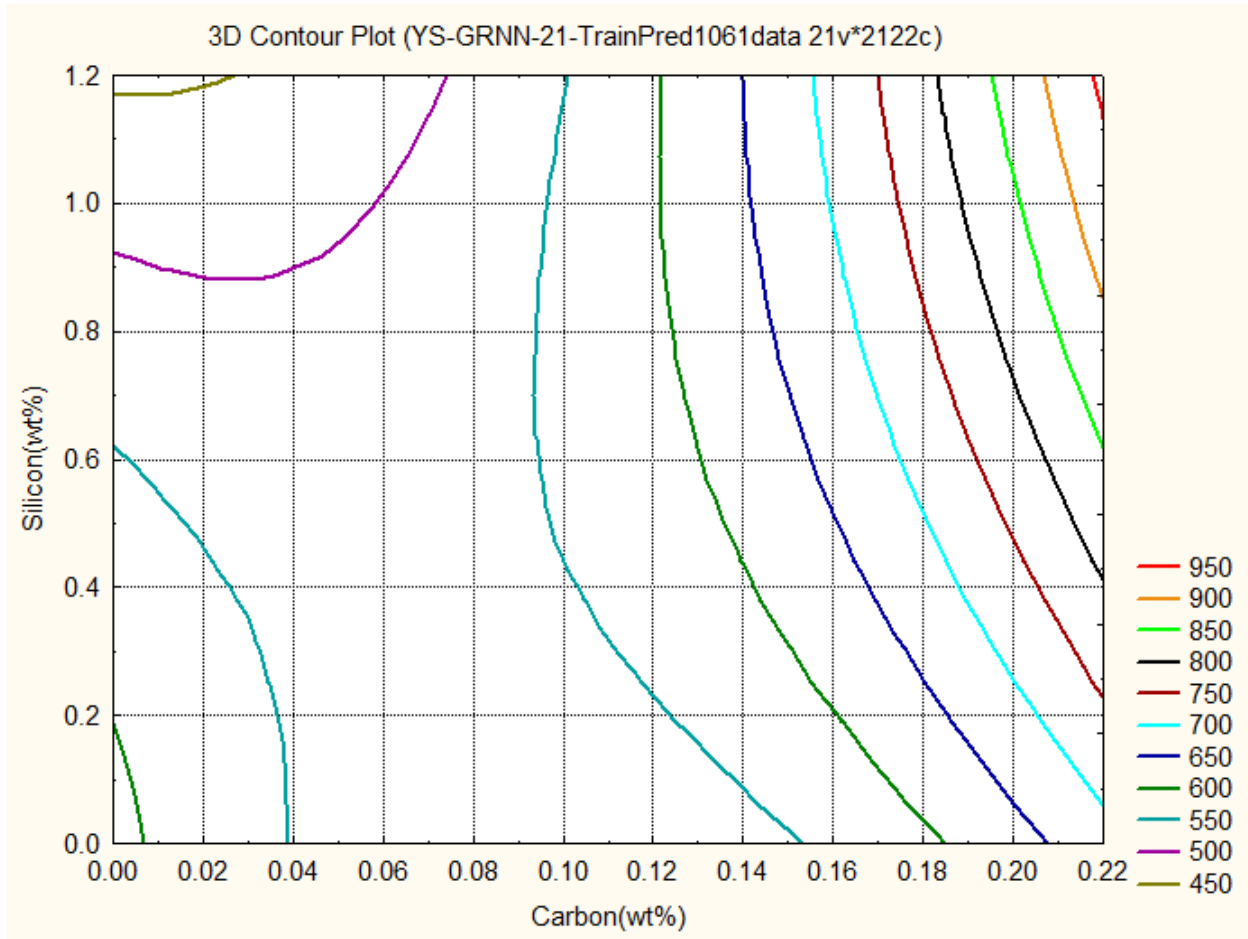


Figure. 4.3.6 Predicted variations in Yield Strength (MPa) as a function of the Carbon and Silicon concentrations

3D contour Plot gives the relations between the **two input variables** and **one output variable**. **Figure. 4.3.6** shows the relations between Carbon, Silicon and Yield Strength by **GRNN**. The graph gives the information about how these two, Carbon **and** Silicon control the Yield Strength from 450 MPa to 950 MPa.

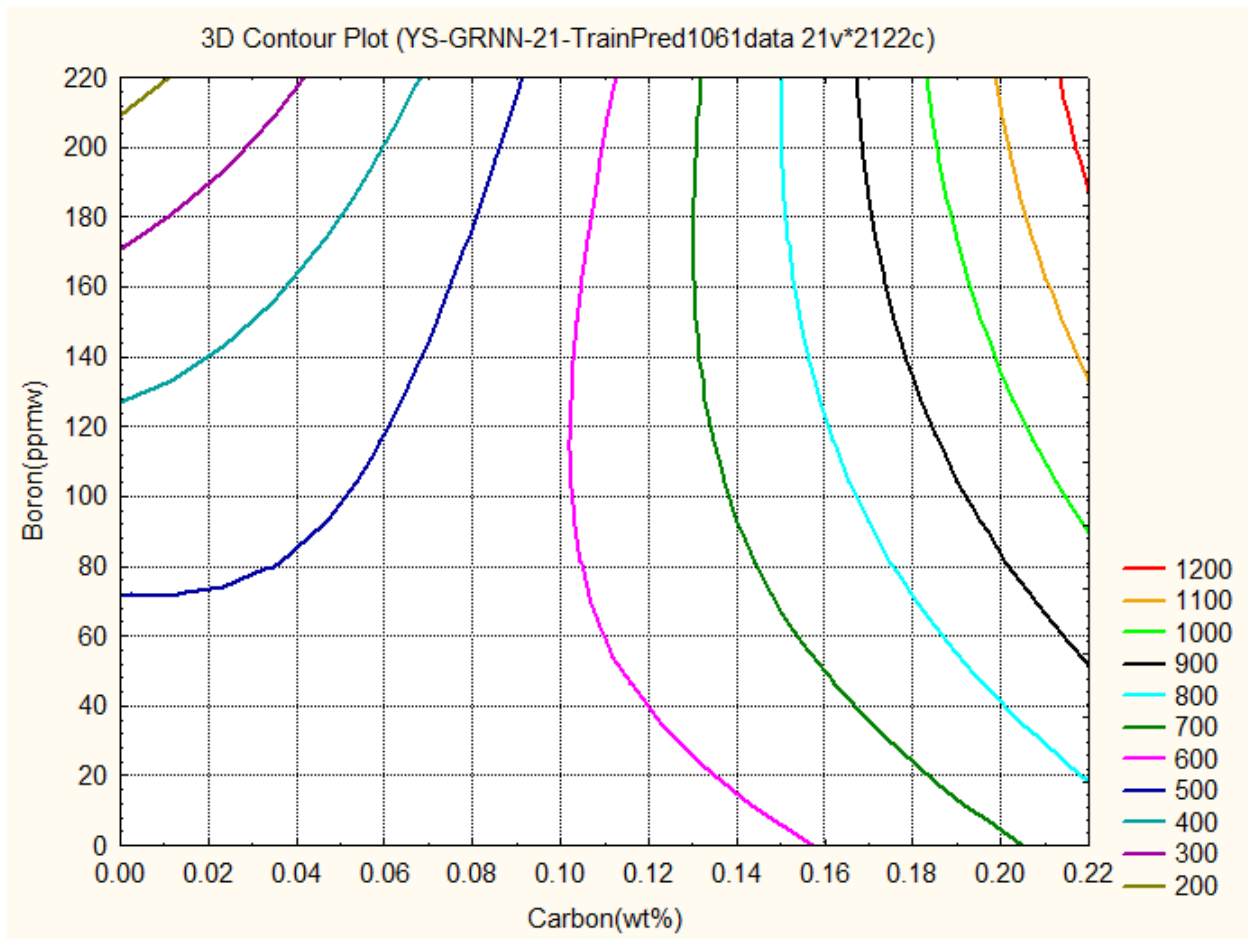


Figure. 4.3.7 Predicted variations in Yield Strength (MPa) as a function of the Carbon and Boron concentrations

3D contour Plot gives the relations between the **two input variables** and **one output variable**. **Figure. 4.3.7** shows the relations between Carbon, Boron and Yield Strength by **GRNN**. The graph gives the information about how these two, Carbon **and** Boron control the Yield Strength from 200MPa to 1200MPa.

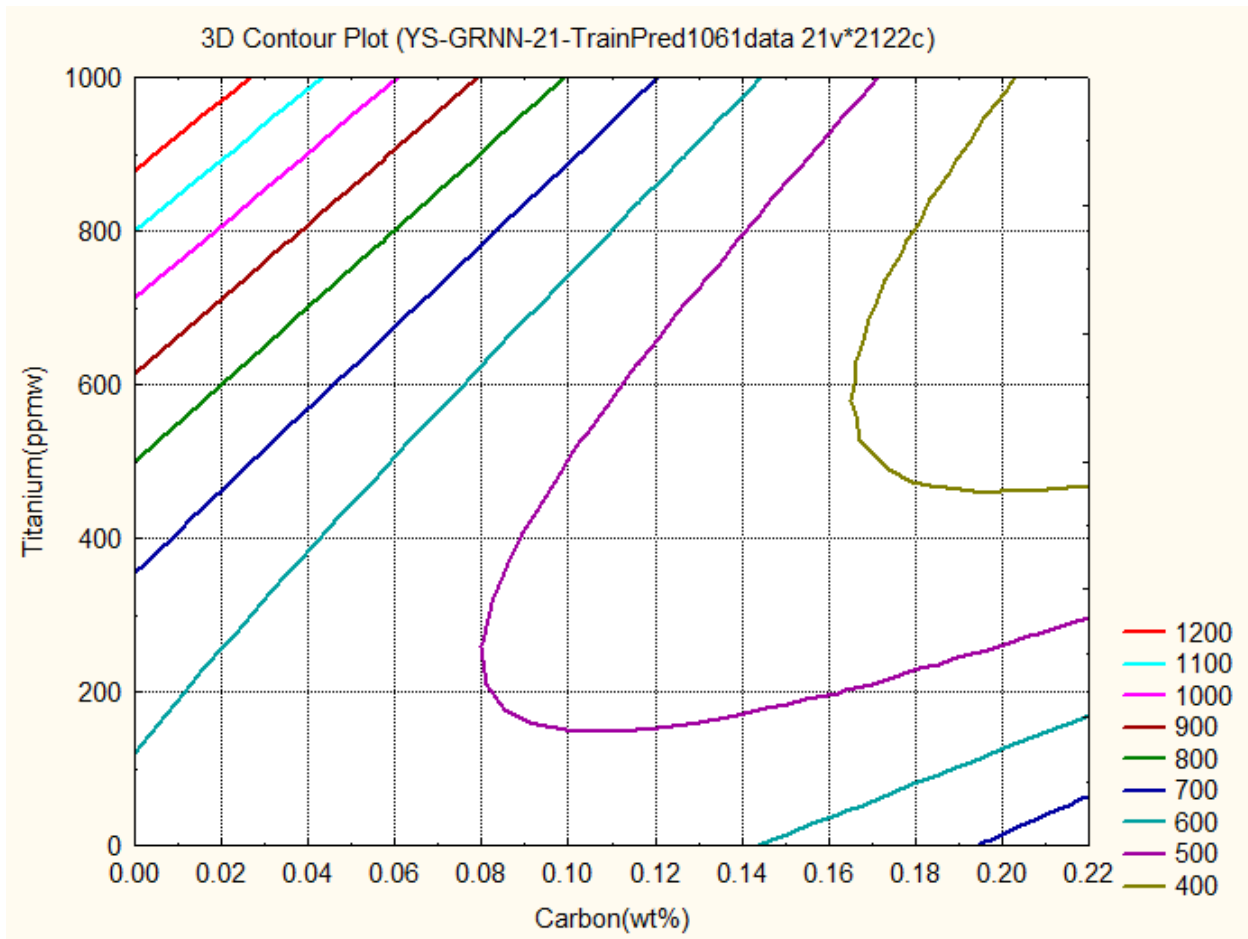


Figure. 4.3.8 Predicted variations in Yield Strength (MPa) as a function of the Carbon and Titanium concentrations

3D contour Plot gives the relations between the **two input variables** and **one output variable**. **Figure. 4.3.8** shows the relations between Carbon, Titanium and Yield Strength by **GRNN**. The graph gives the information about how these two, Carbon **and** Titanium control the Yield Strength from 400MPa to 1200MPa.

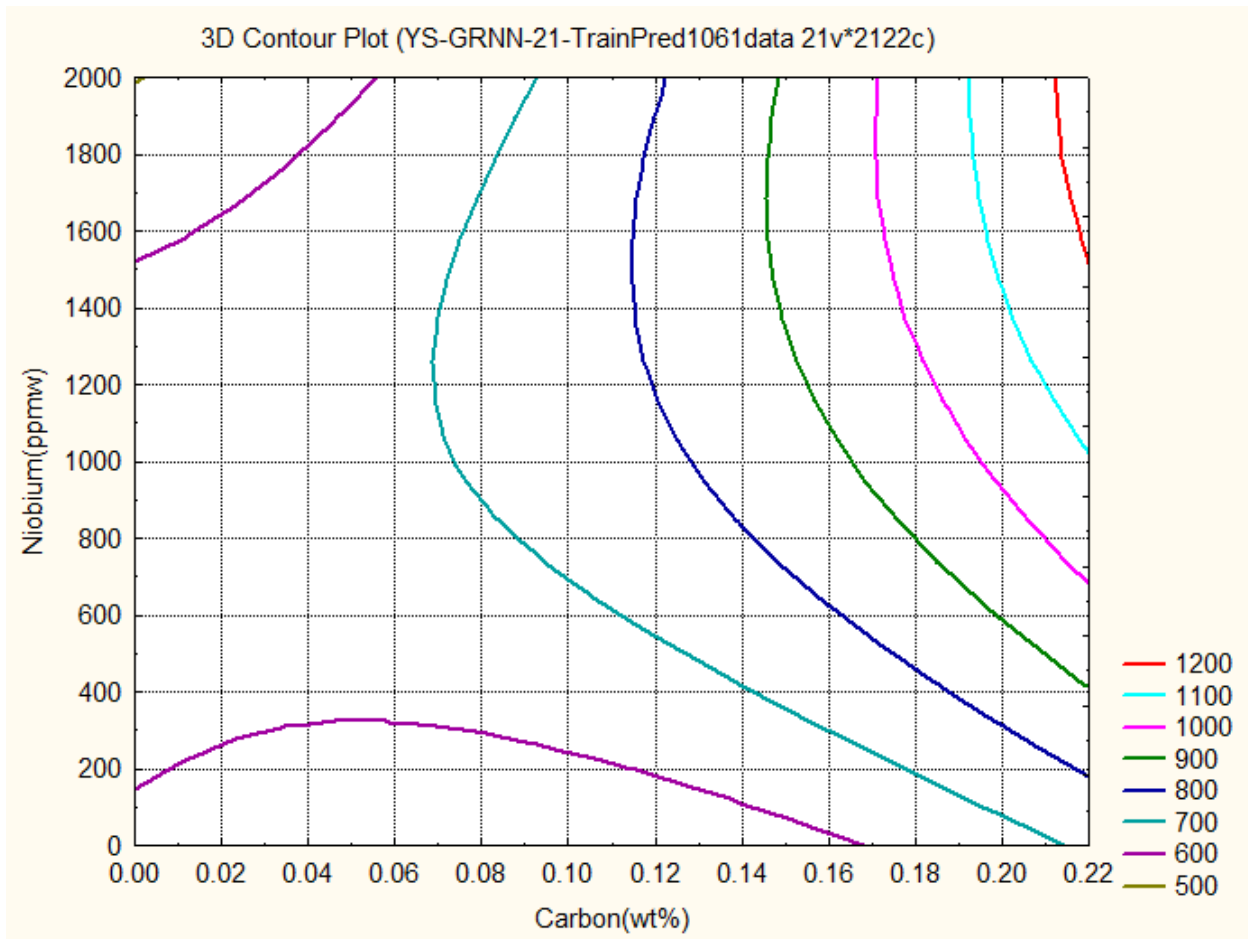


Figure. 4.3.9 Predicted variations in Yield Strength (MPa) as a function of the Carbon and Niobium concentrations

3D contour Plot gives the relations between the **two input variables** and **one output variable**. **Figure. 4.3.9** shows the relations between Carbon, Niobium and Yield Strength by **GRNN**. The graph gives the information about how these two, Carbon **and** Niobium control the Yield Strength from 500MPa to 1200MPa.

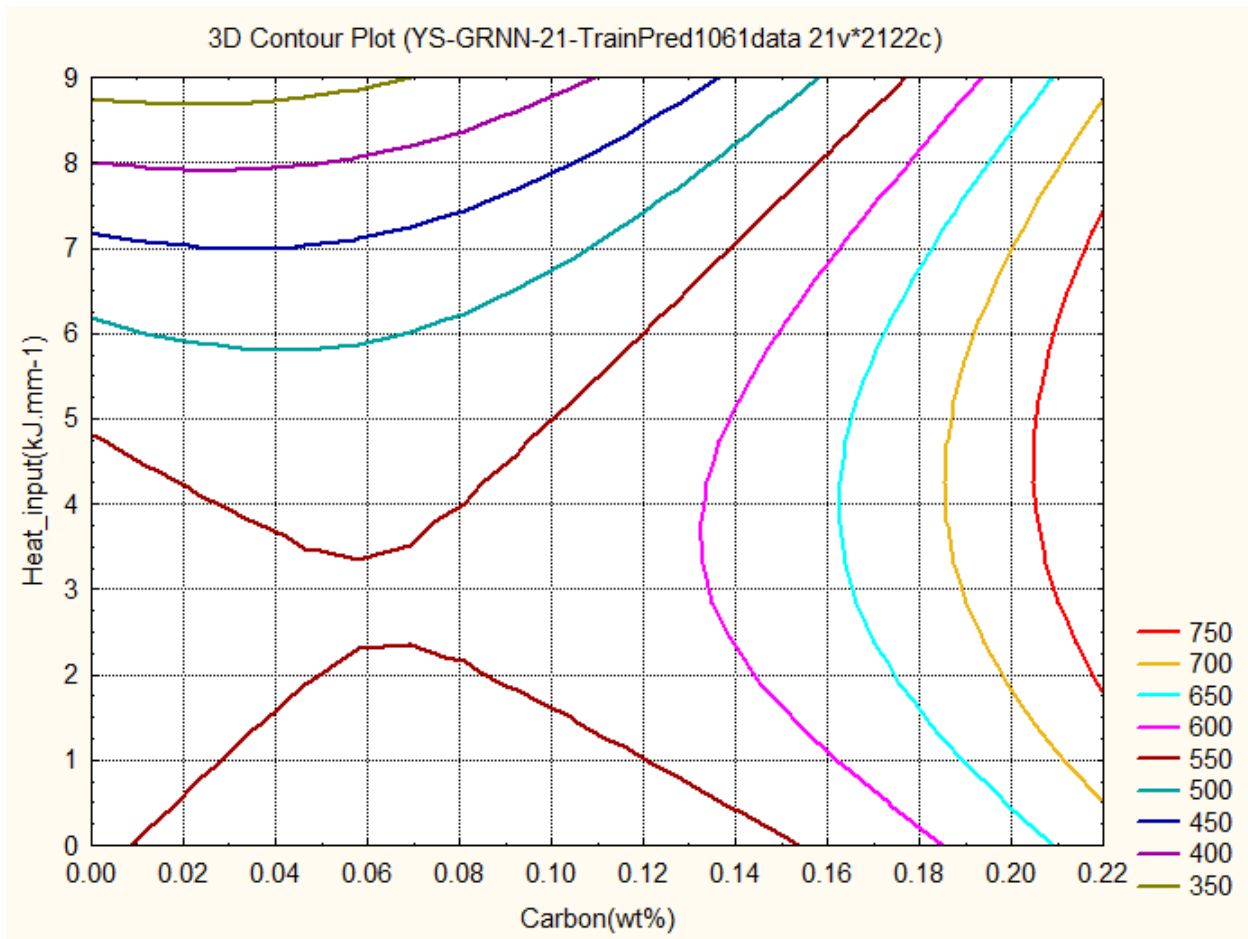


Figure. 4.3.10 Predicted variations in Yield Strength (MPa) as a function of the Carbon concentration and Heat input

3D contour Plot gives the relations between the **two input variables** and **one output variable**. **Figure. 4.3.10** shows the relations between Carbon, Heat input and Yield Strength by **GRNN**. The graph gives the information about how these two, Carbon **and** Heat input control the Yield Strength from 350MPa to 750MPa.

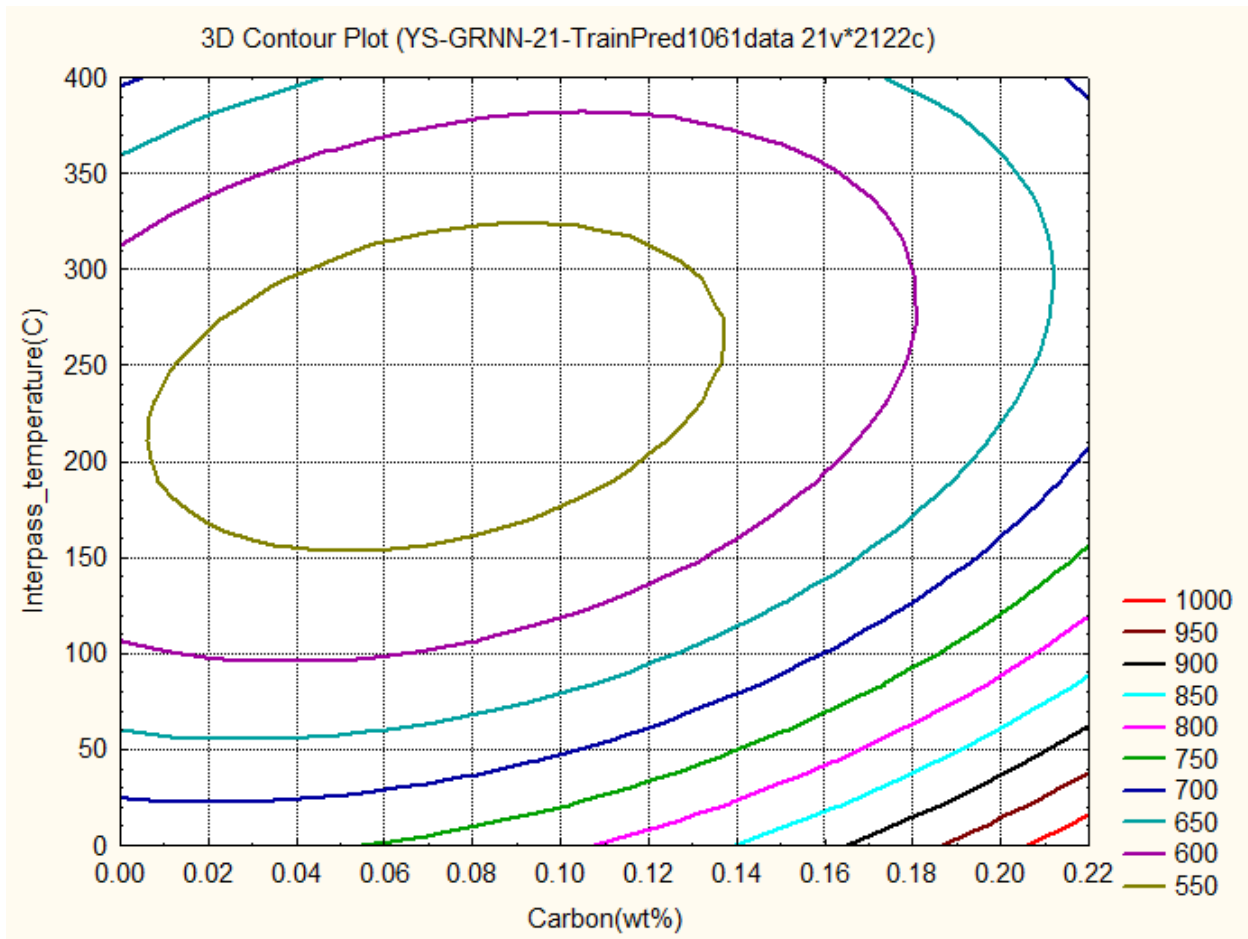


Figure. 4.3.11 Predicted variations in Yield Strength (MPa) as a function of the Carbon concentration and Interpass temperature

3D contour Plot gives the relations between the **two input variables** and **one output variable**. **Figure. 4.3.11** shows the relations between Carbon, Interpass temperature and Yield Strength by **GRNN**. The graph gives the information about how these two, Carbon **and** Interpass temperature control the Yield Strength from 550MPa to 1000MPa.

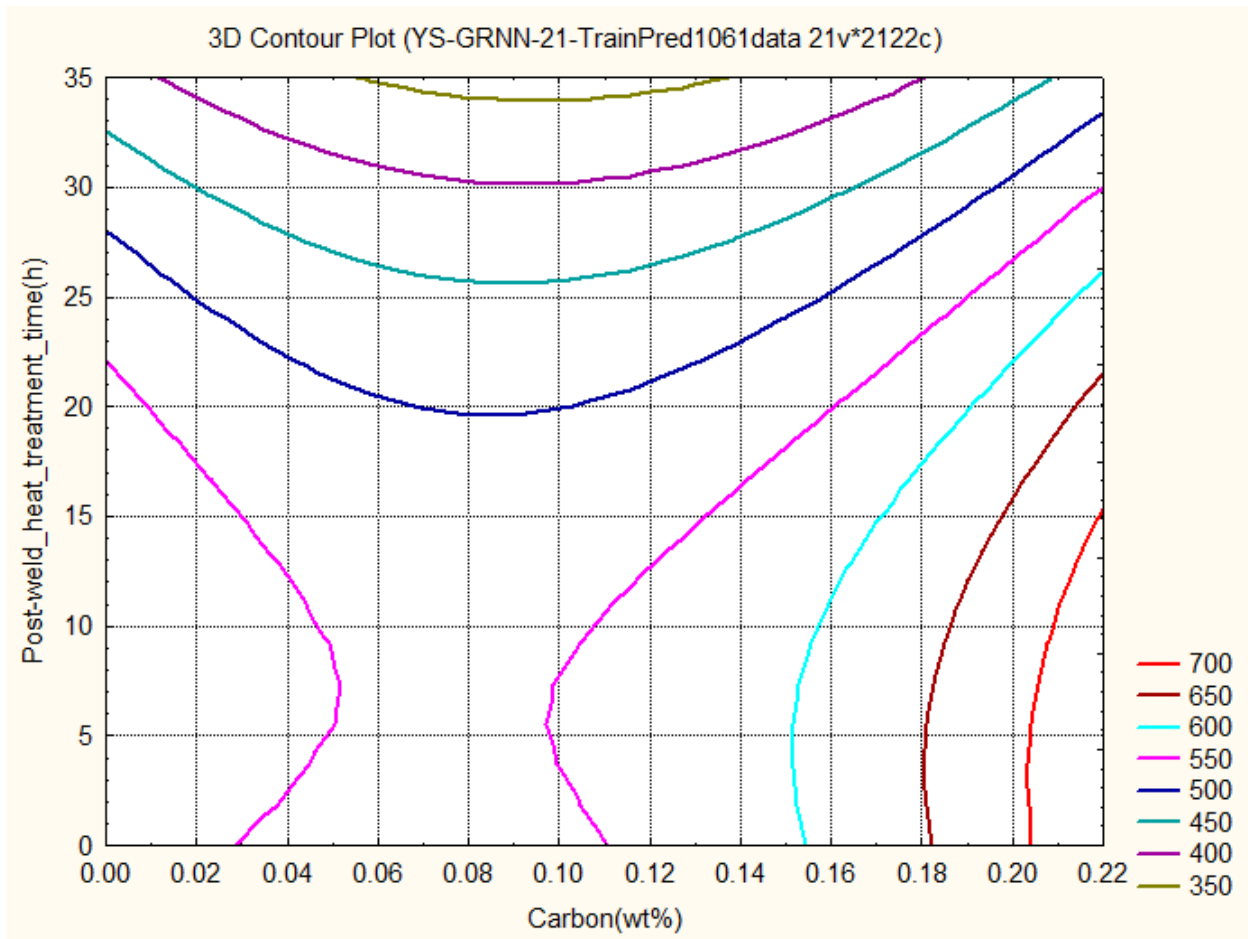


Figure. 4.3.12 Predicted variations in Yield Strength (MPa) as a function of the Carbon concentration and Post-weld heat treatment time

3D contour Plot gives the relations between the **two input variables** and **one output variable**. **Figure. 4.3.12** shows the relations between Carbon, Post-weld heat treatment time and Yield Strength by **GRNN**. The graph gives the information about how these two, Carbon **and** Post-weld heat treatment time control the Yield Strength from 350MPa to 700MPa.

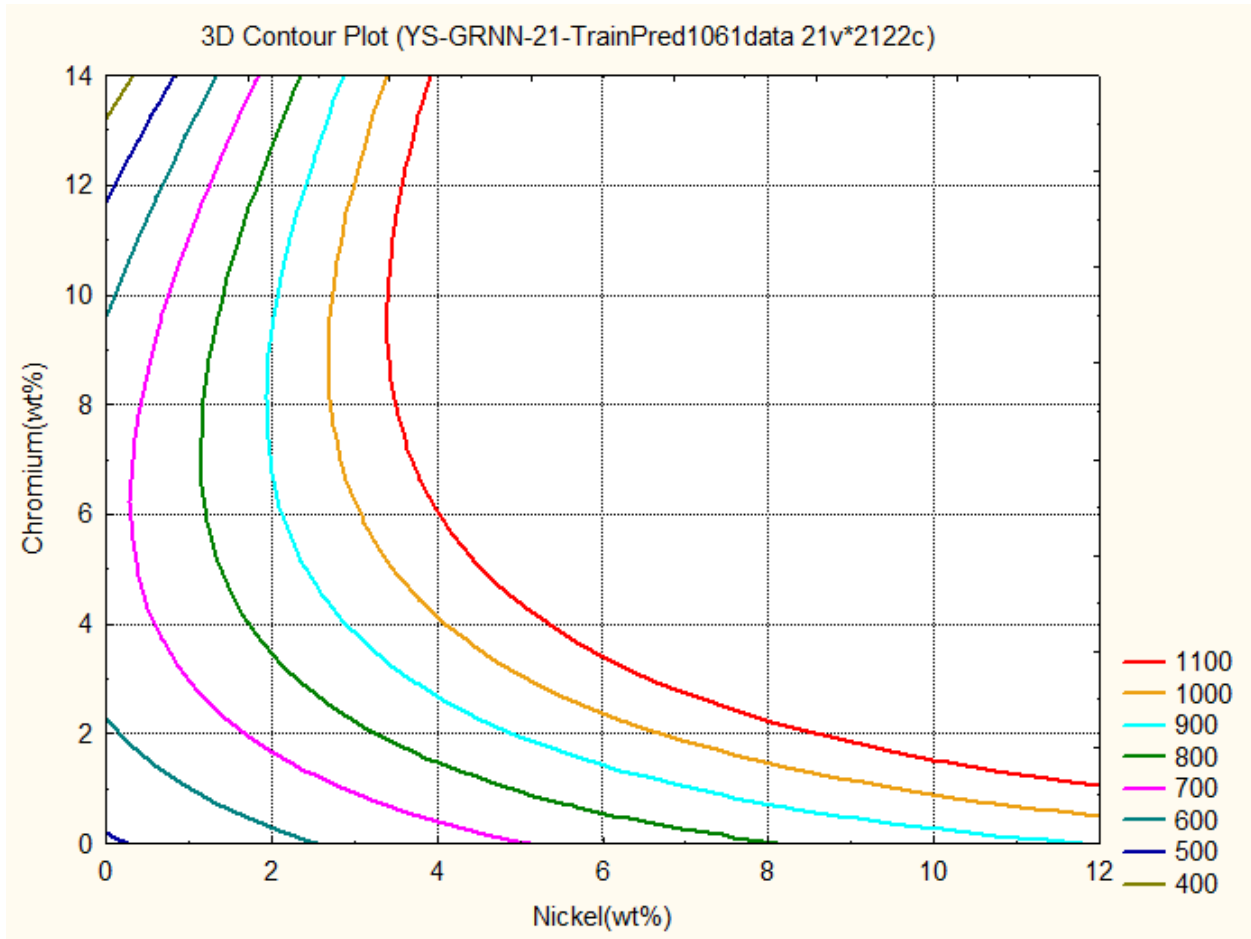


Figure. 4.3.13 Predicted variations in Yield Strength (MPa) as a function of the Nickel and Chromium concentrations

3D contour Plot gives the relations between the **two input variables** and **one output variable**. **Figure. 4.3.13** shows the relations between Nickel, Chromium and Yield Strength by **GRNN**. The graph gives the information about how these two, Nickel **and** Chromium control the Yield Strength from 400MPa to 1100MPa.

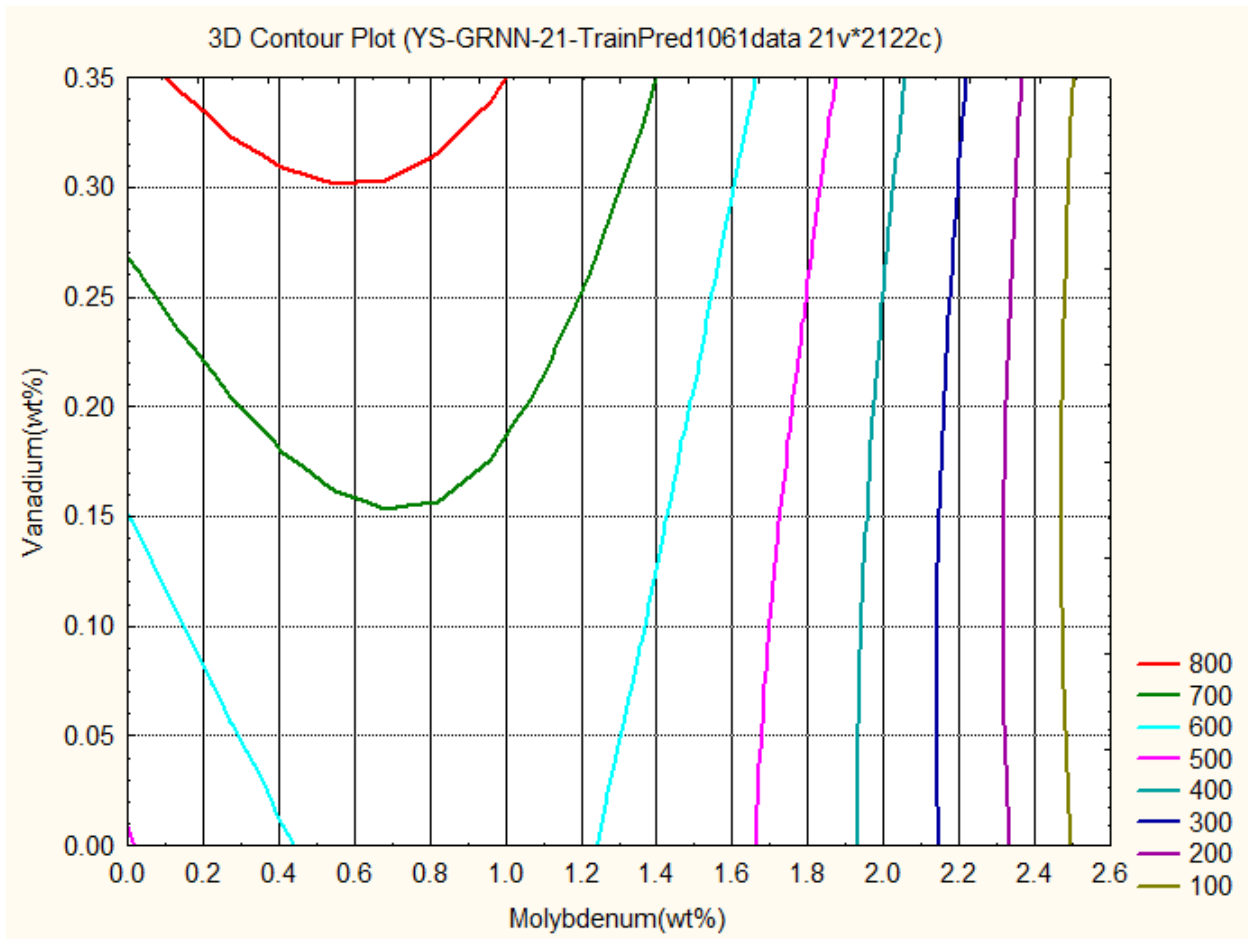


Figure. 4.3.14 Predicted variations in Yield Strength (MPa) as a function of the Molybdenum and Vanadium concentrations

3D contour Plot gives the relations between the **two input variables** and **one output variable**. **Figure. 4.3.14** shows the relations between Molybdenum, Vanadium and Yield Strength by **GRNN**. The graph gives the information about how these two, Molybdenum **and** Vanadium control the Yield Strength from 100MPa to 800MPa.

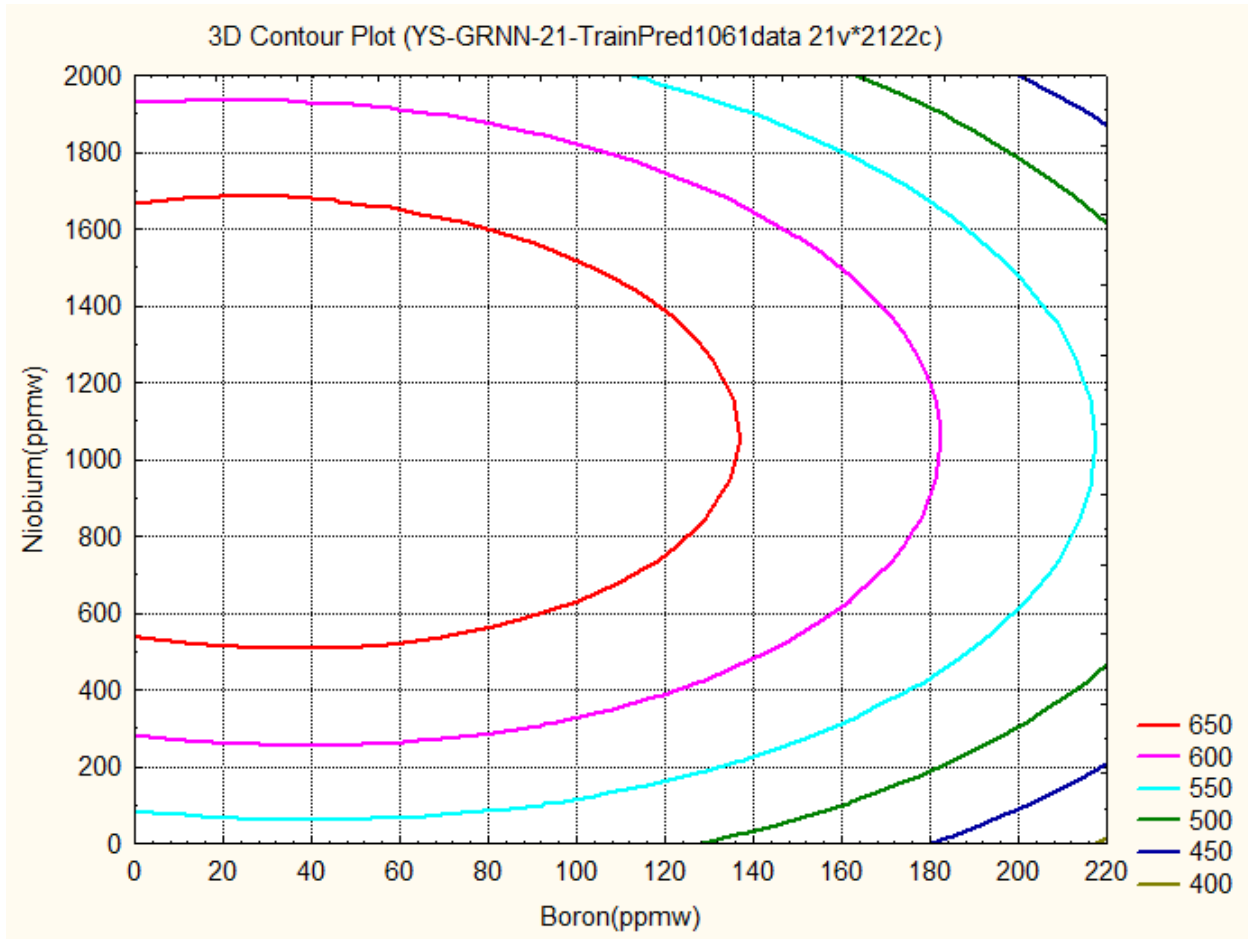


Figure 4.3.15. Predicted variations in Yield Strength (MPa) as a function of the Boron and Niobium concentrations

3D contour Plot gives the relations between the **two input variables** and **one output variable**. **Figure. 4.3.15** shows the relations between Boron, Niobium and Yield Strength by **GRNN**. The graph gives the information about how these two, Boron **and** Niobium control the Yield Strength from 400MPa to 650MPa.

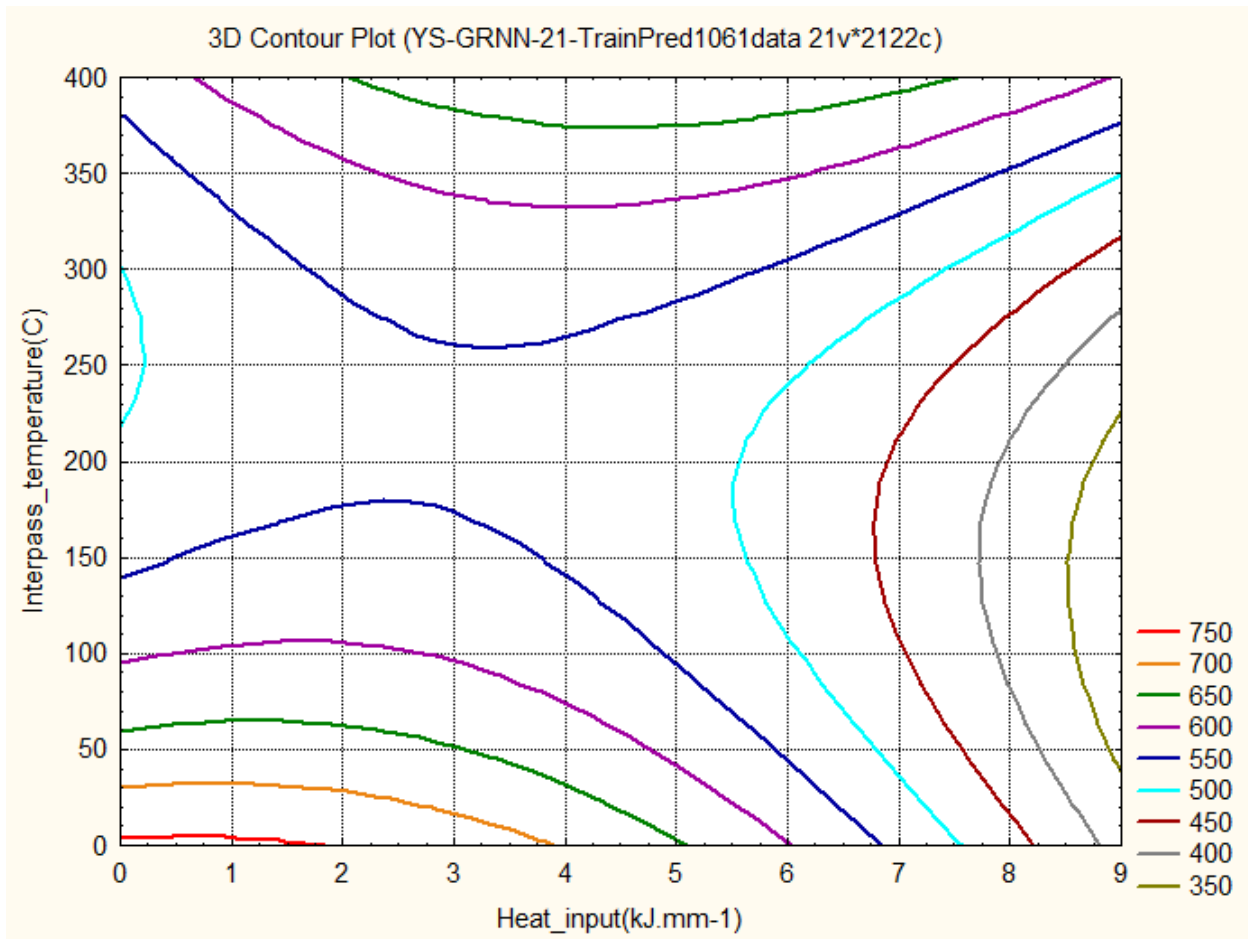


Figure. 4.3.16 Predicted variations in Yield Strength (MPa) as a function of the Heat input and Interpass temperature

3D contour Plot gives the relations between the **two input variables** and **one output variable**. **Figure. 4.3.16** shows the relations between Heat input, Interpass temperature and Yield Strength by **GRNN**. The graph gives the information about how these two, Heat input **and** Interpass temperature control the Yield Strength from 350MPa to 750MPa.

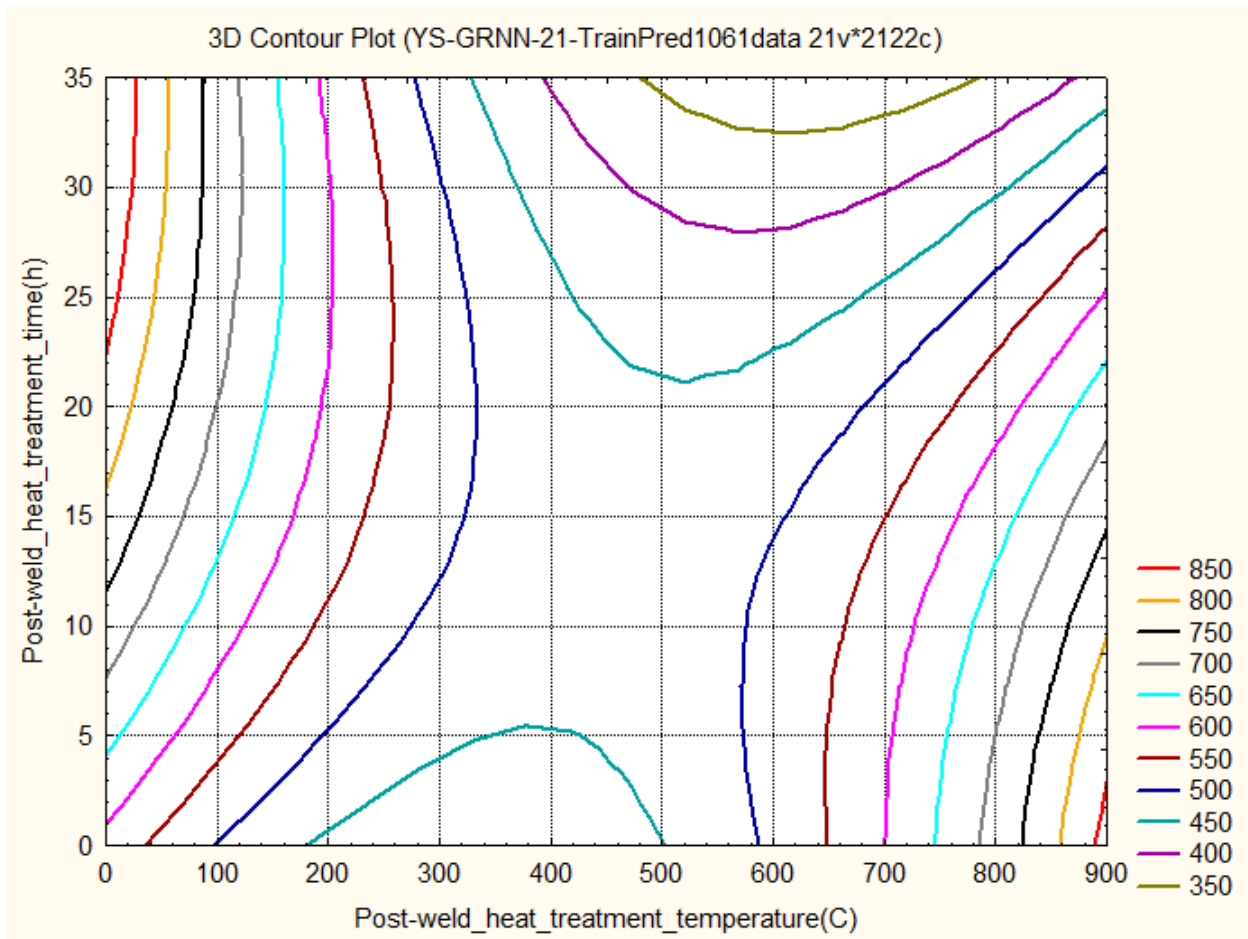


Figure. 4.3.17 Predicted variations in Yield Strength (MPa) as a function of the Post-weld heat treatment temperature and Post-weld heat treatment time

3D contour Plot gives the relations between the **two input variables** and **one output variable**. **Figure. 4.3.17** shows the relations between the Post-weld heat treatment temperature, Post-weld heat treatment time and Yield Strength by **GRNN**. The graph gives the information about how these two, the Post-weld heat treatment temperature **and** Post-weld heat treatment time control the Yield Strength from 350MPa to **850MPa**.

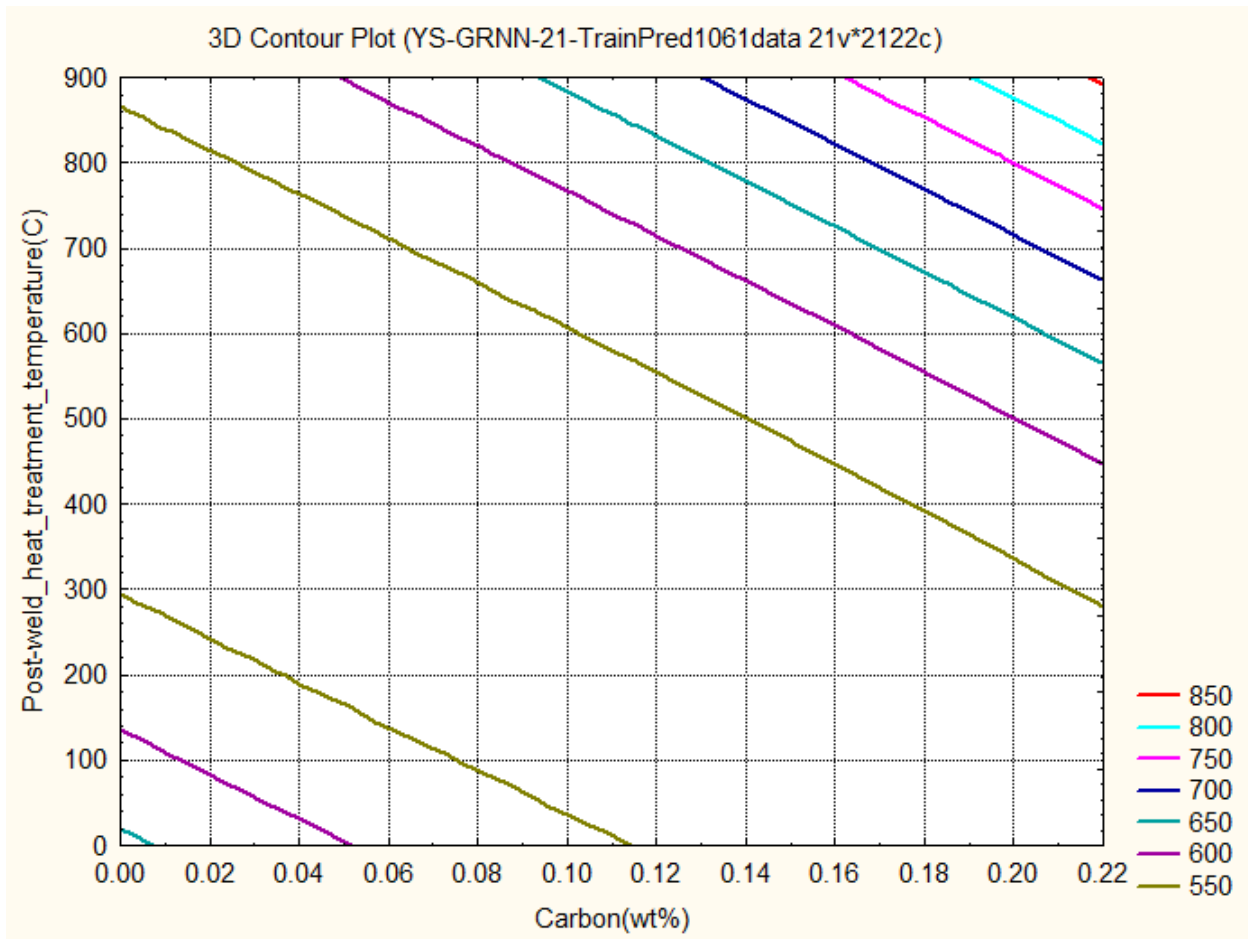


Figure. 4.3.18 Predicted variations in Yield Strength (MPa) as a function of the Carbon and Post-weld heat treatment temperature

3D contour Plot gives the relations between the **two input variables** and **one output variable**. **Figure.4.3.18** shows the relations between the Carbon, Post-weld heat treatment temperature and Yield Strength by **GRNN**. The graph gives the information about how these two, the Carbon **and** Post-weld heat treatment temperature control the Yield Strength from 550MPa to 850MPa.

Figure 4.3.1. YS (z) - Mn (y) - C (x) 3D plot.

Figure 4.3.1. shows the contour of Yield Strength 550 MPa with the Carbon in the range from 0.02% to 0.158% and the Manganese in the range from 0.5% to 1.78%. The increase in the Yield Strength is achieved outside the 550 MPa contour by keeping Manganese constant and Carbon concentration varies and vice versa. The concentration of %C and %Mn give the Yield Strength in wide range from less than 550 MPa to 1000 MPa. The trends of both the independent variables are less complex and flexible for designing the Yield Strength.

Figure 4.3.2. YS (z) - Ni (y) - C (x) 3D plot.

Figure 4.3.2. shows the increase in the Yield Strength from 500 MPa to 1200 MPa with an increase in the concentrations of both Carbon and Nickel. The increase in the Yield Strength is also achieved by keeping Carbon constant and Nickel concentration varies and vice versa. The higher value of Yield Strength 1200 MPa is obtained with %wt C in the range from 0.176% to 0.22% and % wt Ni in the range from 9.4% to 12%. The trends of both the independent variables are less complex and flexible for designing the Yield Strength.

Figure 4.3.3. YS (z) - Cr (y) - C (x) 3D plot.

Figure 4.3.3. shows the increase in the Yield Strength from 700 MPa to more than 900 MPa with the increase and decrease in the concentrations Chromium from 1% to 12.2% and the increase in concentrations of Carbon from 0.084% to 0.22%. The Chromium in the range from 7.8% to 14% and Carbon in the range from 0% to 0.22% decrease the Yield Strength from 600MPa to less than 100 MPa. The Yield Strength 700MPa is obtained with %wt C in the range from 0.084% to 0.22% and % wt Cr in the range from 1% to 12.2%. The Yield Strength 900 MPa and higher are obtained with % wt C in the range from 0.21% to 0.22% and % wt Cr in the range from 5.2% to 8.2%. The independent variables Carbon and Chromium both have a wide range for designing the Yield Strength between 600 MPa to 700 MPa. The trends of both the independent variables are complex for designing the Yield Strength 900 MPa and higher.

Figure 4.3.4. YS (z) - Mo (y) - C (x) 3D plot.

Figure 4.3.4. shows the Yield Strength 600 MPa is obtained with %wt C in the range from 0% to 0.22% and %wt Mo in the range from 0.32% to 1.5%. The content of %wt Mo more than 1.5% and %wt C in the range from 0% to 0.22% decrease the Yield Strength from 600 MPa to less

than 100 MPa. The content of %wt Mo less than 0.32% and %wt C in the range from 0% to 0.22% decrease the Yield Strength from 600 MPa to less than 500 MPa. The trends of both the independent variables are complex for designing the Yield Strength with a wide range of combinations available.

Figure 4.3.5. YS (z) - V (y) - C (x) 3D plot.

Figure 4.3.5. shows the Yield Strength values 700 MPa and more than 800MPa are observed in the left side of the graph. Left side of the graph has a range of the Vanadium from 0.1% to 0.35% and the Carbon from 0% to 0.092%. The Yield Strength 800MPa and higher are obtained with the range of % wt V from 0.202% to 0.35% and by maintaining the Carbon, in the range from 0% to 0.024%. The Upper side right corner of the plot show the contours of the decrease in the Yield Strength from 650 MPa and less than 600 MPa with %wt V in the range from 0.25% to 0.35% and %wt C in the range from 0.112% to 0.22%. The bottom side of the plot show the contours of the decrease in the Yield Strength from 650 MPa and less than 550 MPa with %wt V in the range from 0% to 0.14% and %wt C in the range from 0% to 0.22%.. Both the independent variables have a complex relationship with the Yield Strength. The trends of the independent variables is significant for designing the Yield Strength.

Figure 4.3.6. YS (z) - Si (y) - C (x) 3D plot.

Figure 4.3.6. shows the increase in the Yield Strength from 550 MPa to 950 MPa with an increase in the concentration of both Carbon and Silicon. The Yield Strength 550 MPa and more than 950 MPa are obtained with %wt C in the range from 0.092% to 0.22% C and wt% Silicon in the range from 0% to 1.2%. The Yield Strength in this range from 550 MPa to 950 MPa are obtained by keeping the wt% Si constant and varying the wt% of Carbon. The Yield Strength in this range from 600 MPa to 950 MPa are obtained by keeping the wt% C constant in between the 0.14% to 0.22% and varying the wt% of Si in the range from 0% to 1.2%. The decrease in the Yield Strength from less than 550 MPa to 450 MPa is obtained with %wt C less than 0.074% and Silicon in the range from 0.88% to 1.2% at the left upper side corner of the graph. The increase in the Yield Strength from 550 MPa to more than 660 MPa is obtained with %wt C less than 0.038% and Silicon in the range from 0% to 0.62% at the left bottom side corner of the graph. Both the independent variables have a complex relationship with the Yield Strength. The trends of the independent variables are significant for designing the Yield Strength.

Figure 4.3.7. YS (z) - B (y) - C (x) 3D plot.

Figure 4.3.7. shows the contours of the Yield Strength increase from 200 MPa to 1200 MPa with an increase in wt% C in the range from 0% to 0.22% and Boron ppm in the range from 0 ppm to 220 ppm. The increase in the Yield Strength is achieved by keeping Boron ppm constant and Carbon concentration varies in the range from 0% to 0.22%. The increase in Yield Strength is obtained by maintaining the higher wt% C, more than 0.14% and the constant Boron ppm and vice versa. The decrease in the Yield Strength from 500 MPa to less than 200MPa is observed with wt% C in the range from 0% to 0.09% and Boron ppm from 72 ppm to 220 ppm at the left upper side corner of the graph. The trends of both the independent variables are not complex for designing the Yield Strength.

Figure 4.3.8. YS (z) - Ti (y) - C (x) 3D plot.

Figure 4.3.8. shows the decrease in the Yield Strength from 500 MPa to less than 400 MPa with an increase in the concentration of both Carbon and Titanium. The Yield Strength 600 MPa and more than 1200 MPa are obtained with %wt C in the range from 0% to 0.144% and Titanium ppm in the range from 130 ppm to 1000 ppm. The Yield Strength 600 MPa and more than 700 MPa are also achieved with %wt C in the range from 0.144% to 0.22% and Titanium ppm in the range from 0 ppm to 160 ppm. Selection of these two independent variables is very important for the design of the Yield Strength. Because both the independent variables have a nonlinear complex relationship with the Yield Strength.

Figure 4.3.9. YS (z) - Nb (y) - C (x) 3D plot.

Figure 4.3.9. shows the increase in the Yield Strength from 700 MPa to 1200 MPa with an increase in the concentration of both Carbon and Niobium. The Yield Strength 700 MPa and more than 1200 MPa are obtained with %wt C in the range from 0.068% to 0.22%C and Niobium ppm in the range from 0 ppm to 2000 ppm. In this range 700 MPa to 1200 MPa is obtained by keeping the Nb ppm constant and varying the wt% of Carbon. The decrease in the Yield Strength from 600 MPa to less than 600 MPa is obtained with %wt C less than 0.056% and Niobium ppm in the range from 1520 ppm to 2000 ppm at the upper left corner of the graph. The decrease in the Yield Strength from 600 MPa to less than 600 MPa is obtained with %wt C less than 0.166% and Niobium ppm in the range from 0 ppm to 340 ppm at the bottom side

contour of 600MPa. Both the independent variables have a complex relationship with the Yield Strength. The trends of the independent variables are significant for designing the Yield Strength.

Figure 4.3.10. YS (z) - HI (y) - C (x) 3D plot.

Figure 4.3.10. shows the increase in the Yield Strength from 600 MPa to 750 MPa with an increase in the concentration of Carbon and changing Heat input lower value to higher value. The Yield Strength 600 MPa and more than 750 MPa are obtained with % wt C in the range from 0.132% to 0.22%C and Heat input kJmm-1 in the range from 0 kJmm-1 to 9 kJmm-1. In this range 700 MPa to 1000 MPa is obtained by keeping the Heat input constant and varying the wt% of Carbon. But for the Yield Strength 750 MPa and higher is obtained with the Heat input in the range from 1.8 kJmm-1 to 7.4 kJmm-1 and the wt% C in the range from 0.2065 to 0.22%. The decrease in the Yield Strength from less than 550 MPa to less than 350 MPa is obtained with %wt C less than 0.132% and the Heat input in the range from 0 kJmm-1 to 9 kJmm-1. Both the independent variables have a complex relationship with the Yield Strength. The trends of the independent variables are significant for designing the Yield Strength.

Figure 4.3.11. YS (z) - IPT (y) - C (x) 3D plot.

Figure 4.3.11. shows the contour of Yield Strength 550 MPa with the Carbon in the range from 0.006% to 0.138% and the Interpass temperature in the range from 155 C to 320 C. The increase in the Yield Strength is achieved outside the 550 MPa contour by keeping Interpass temperature constant and increasing Carbon concentration. The decrease in the Yield Strength is achieved outside the 700 MPa contour by keeping Carbon concentration constant and increasing the Interpass temperature. The concentration of the Carbon and the Interpass temperature combinations give the Yield Strength in wide range from less than 550 MPa to 1000 MPa. The trends of both the independent variables are a complex and flexible for designing the Yield Strength. The trends of the independent variables are significant for designing the Yield Strength.

Figure 4.3.12. YS (z) – PWHTt (y) - C (x) 3D plot.

Figure 4.3.12. shows the increase in the Yield Strength from 550 MPa to 700 MPa with an increase in the concentration of Carbon and Post Weld Heat Treatment time. The Yield Strength 550 MPa and more than 700 MPa are obtained with %wt C in the range from 0.096% to 0.22%C and Post Weld Heat Treatment time in the range from 0 h to 30 h. The Yield Strength in this range from 550 MPa to 700 MPa are obtained by keeping the Post Weld Heat Treatment time constant and varying the wt% of Carbon. The decrease in the Yield Strength from less than 500 MPa to 350 MPa is obtained with %wt C in the range from 0% to 0.22% and Post Weld Heat Treatment time in the range from 19.5 h to 35 h at the upper side of the graph. The increase in the Yield Strength from 550 MPa to more than 550 MPa is obtained with %wt C less than 0.052% and Post Weld Heat Treatment time in the range from 0 h to 22 h at the left bottom side corner of the graph. Both the independent variables have a complex relationship with the Yield Strength. The trends of the independent variables are significant for designing the Yield Strength.

Figure 4.3.13. YS (z) – Cr (y) - Ni (x) 3D plot.

Figure 4.3.13 shows the increase in the Yield Strength from 500 MPa to 1000 MPa with equally increase in wt% Chromium from 0% to 4.6% and wt% Nickel from 0% to 4.6%. The increase in the Yield Strength is also achieved by keeping Chromium constant and Nickel concentration varies and vice versa. Both independent variables show complexity and uniqueness in their trends. The independent variables are significant for designing the Yield Strength.

Figure 4.3.14. YS (z) – V (y) - Mo (x) 3D plot.

Figure 4.3.14. shows the contour of Yield Strength 700 MPa with the Molybdenum in the range from 0% to 1.4% and the Vanadium in the range from 0.16% to 0.35%. The 800 MPa and more than 800 MPa Yield Strength are obtained with wt% Mo in the range from 0.1% to 1% and wt% V in the range from 0.305% to 0.35%. The decrease in the Yield Strength from 600 MPa to 100 MPa are obtained by keeping Vanadium concentration constant and increasing Molybdenum concentration. The Molybdenum less than 0.44% and more than 1.24% decreases the Yield

Strength. Both independent variables show complexity in their trends. The independent variables are significant for designing the Yield Strength.

Figure 4.3.15. YS (z) – Nb (y) - B (x) 3D plot.

Figure 4.3.15. shows the contour of Yield Strength 650 MPa with the Boron in the range from 0 ppm to 136 ppm and the Niobium in the range from 540 ppm to 1660 ppm. The decrease in the Yield Strength is achieved outside the 650 MPa contour by keeping Niobium constant and increasing Boron concentration. The concentration of the Boron and the Niobium combinations give the Yield Strength in wide range from less than less than 450 MPa to more than 650 MPa. The trends of both the independent variables are a complex and flexible for designing the Yield Strength. The trends of the independent variables are significant for designing the Yield Strength.

Figure 4.3.16. YS (z) – IPT (y) - HI (x) 3D plot.

Figure 4.3.16. shows the Yield Strength values 550 MPa and more than 550MPa are observed in the upper side and bottom side of the graph. Right side of the graph has the range of the Interpass Temperature from 0 C to 350 C and the Heat Input from 5.5 kJmm⁻¹ to 9 kJmm⁻¹. Left side of the graph has the range of the Interpass Temperature from 220 C to 300 C and the Heat Input from 0 kJmm⁻¹ to 0.3 kJmm⁻¹. The Yield Strength 650 MPa and higher are obtained with the range of the Interpass Temperature from 375 C to 400 C and by maintaining the Heat Input, in the range from 2.1 kJmm⁻¹ to 7.4 kJmm⁻¹ at the upper side of the plot. The Yield Strength 700MPa and higher are obtained with the range of the Interpass Temperature from 0 C to 25 C and by maintaining the Heat Input, in the range from 0 kJmm⁻¹ to 3.8 kJmm⁻¹ at the bottom side of the plot. The Upper side and bottom side of the plot show the contours of the increase in the Yield Strength from 550 MPa and more than 550 MPa. Both the independent variables have a complex relationship with the Yield Strength. The trends of the independent variables are significant for designing the Yield Strength.

Figure 4.3.17. YS (z) – PWHTt (y) – PWHTT (x) 3D plot.

Figure 4.3.17. shows the Yield Strength values 450 MPa and less than 450MPa are observed in the upper side and bottom side of the graph. Right side of the graph has the range of the Post Weld Heat Treatment Time from 0 h to 35 h and the Post Weld Heat Treatment temperature from 0 C to 330 C. Left side of the graph has the range of the Post Weld Heat Treatment Time from 0 h to 31.5 h and the Post Weld Heat Treatment temperature from 570 C to 900 C. The Yield Strength 500 MPa and higher are obtained with the range of the Post Weld Heat Treatment temperature from 0 C to 330 C and by maintaining the Post Weld Heat Treatment Time, in the range from 0 h to 35 h at the left side of the plot. The Yield Strength 500 MPa and higher are obtained with the range of the Post Weld Heat Treatment temperature from 570 C to 900 C and by maintaining the Post Weld Heat Treatment Time, in the range from 0 h to 31.5 h at the right side of the plot. The Upper side and bottom side of the plot show the contours of the decrease in the Yield Strength from 450 MPa and less than 350 MPa. The Right side and left side of the plot show the contours of the increase in the Yield Strength from 500 MPa and more than 8500 MPa Both the independent variables have a complex relationship with the Yield Strength. The trends of the independent variables are significant for designing the Yield Strength.

Figure 4.3.18. YS (z) – PWHTT (y) - C (x) 3D plot.

Figure 4.3.18. shows the increase in the Yield Strength from 550 MPa to 850 MPa with the increase in the Post Weld Heat Treatment Temperature in the range from 280 C to 900 C and the increase in the Carbon in the range from 0% to 0.22% at the upper side of the graph. The increase in the Yield Strength from 550 MPa to 650 MPa with the decrease in the Post Weld Heat Treatment Temperature in the range from 0 C to 290 C and the increase in the Carbon in the range from 0% to 0.114% at the bottom left corner of the graph. Both the independent variables have a complex relationship with the Yield Strength. The trends of the independent variables are significant for designing the Yield Strength.

4.1.4 Application of Trained Best Neural Network Models

4.1.4.1 Prediction of The Yield Strength on unseen data by BNN Model

The BNN model has good accuracy in prediction of yield strength of ferritic steel welds on unseen data which is excellent for the design of welds.(Table 4.1) The predicted yield strength for the unseen data of three weld alloys are compared with measured values of yield strength shows the prediction capacity of the BNN model. This BNN model can be used for practical applications, research and development of ferritic steel alloys.

Table 4.1 Predicted yield strength by BNN model for unseen data of three ferritic weld deposits

Variable	Weld alloy 1	Weld alloy 2	Weld alloy 3
Carbon(wt%)	0.041	0.049	0.081
Silicon(wt%)	0.30	0.35	0.24
Manganese(wt%)	0.62	1.37	0.59
Sulphur(wt%)	0.007	0.007	0.009
Phosphorus(wt%)	0.010	0.013	0.012
Nickel(wt%)	2.38	1.06	10.8
Chromium(wt%)	0.03	0.03	1.17
Molybdenum(wt%)	0.005	0.005	0.300
Vanadium(wt%)	0.012	0.012	0.006
Copper(wt%)	0.03	0.03	0.30
Titanium(ppm)	55	55	00
Boron(ppm)	2	2	1
Niobium(ppm)	20	20	10
Heat_input(kJ.mm-1)	1.0	1.0	1.2
Interpass_temperature(C)	200	200	150
Postweld_heat_treatment_temperature(C)	250	250	250
Post-weld_heat_treatment_time(h)	14	14	14
Measured YS/MPa	466	498	896
Predicted YS/MPa	456.22	509.9	895.03

4.1.4.2 Prediction of The Yield Strength on unseen data by GRNN Model

The GRNN model has good accuracy in prediction of yield strength of ferritic steel welds on unseen data which is excellent for the design of welds.(Table.4.2) The predicted yield strength for the unseen data of three weld alloys are compared with measured values of yield strength shows the prediction capacity of the GRNN model. This GRNN model can be used for practical applications, research and development of ferritic steel alloys.

Table 4.2 Predicted yield strength by GRNN model for unseen data of three ferritic weld deposits

Variable	Weld alloy 1	Weld alloy 2	Weld alloy 3
Carbon(wt%)	0.041	0.049	0.081
Silicon(wt%)	0.30	0.35	0.24
Manganese(wt%)	0.62	1.37	0.59
Sulphur(wt%)	0.007	0.007	0.009
Phosphorus(wt%)	0.010	0.013	0.012
Nickel(wt%)	2.38	1.06	10.8
Chromium(wt%)	0.03	0.03	1.17
Molybdenum(wt%)	0.005	0.005	0.300
Vanadium(wt%)	0.012	0.012	0.006
Copper(wt%)	0.03	0.03	0.30
Titanium(ppm)	55	55	00
Boron(ppm)	2	2	1
Niobium(ppm)	20	20	10
Heat_input(kJ.mm-1)	1.0	1.0	1.2
Interpass_temperature(C)	200	200	150
Postweld_heat_treatment_temperature(C)	250	250	250
Post-weld_heat_treatment_time(h)	14	14	14
Measured YS/Mpa	466	498	896
Predicted YS/Mpa	466	497	913

Prediction of The Yield Strength for new data of input variables can be achieved accurately with best trained models by BNN and GRNN as given in above Tables 4.1 and 4.2. These Models have capacity for changing any individual input variable, any combination of more than one input variables or all input variables to predict the Yield Strength of Ferritic Steel Welds. These are only possible with the BNN and GRNN Models which are impossible practically. By simply running these Models the various design of the Ferritic Steel Welds are possible which save money, time and labour during Research and Development of the Ferritic Steel Welds.

4.1.5 Genetic Algorithms and applications to the yield strength of Ferritic Steel Welds

4.1.5.1 Target yield strength of 466 MPa and High value of yield strength 1200 MPa

The first simulation is made to check the behaviour of the genetic algorithm. The target value of yield strength is set to -0.7. which correspond to an unnormalised value of 466 MPa. The dataset provides such values of yield strength and the aim of this simulation is to check the results of the genetic algorithm.. The 17 parameters(input variables) are allowed to vary, in between **-1** and **+ 1** during the genetic algorithm process. After 3000 generations, the best results obtained is shown Table 4.3.

The second simulation is made to check the genetic algorithm for high value of the Yield Strength. The target value of yield strength is set to 0.2 which correspond to an unnormalised value of 1200 MPa. The dataset does not provide such value of yield strength and the aim of this simulation is to check the results of the genetic algorithm.. The 17 parameters (input variables) are allowed to vary, in between **-1** and **+ 1** during the genetic algorithm process. After 3000 generations, the best results obtained is shown Table 4.3.

According to Table 4.3, the genetic algorithm has managed to reach the target after 3000 generations. Moreover, the associated error obtained is very reasonable.

To check if the given compositions correspond to Ferritic Steel Weld, compare with the actual data of Yield Strength.

Table 4.3 Predicted Input variables by NN-GA model for two targeted Yield Strength of ferritic weld deposits

Variable	Weld 1	Weld 1	Weld 2
	Result GA	Data	Result GA
Carbon(wt%)	0.039	0.041	0.22
Silicon(wt%)	0.28	0.30	1.58
Manganese(wt%)	0.7	0.62	2.01
Sulphur(wt%)	0.004	0.007	0.006
Phosphorus(wt%)	0.010	0.010	0.01
Nickel(wt%)	1.98	2.38	11.2
Chromium(wt%)	0.02	0.03	13.1
Molybdenum(wt%)	0.005	0.005	2.4
Vanadium(wt%)	0.012	0.012	0.32
Copper(wt%)	0.01	0.03	1.78
Titanium(ppm)	51	55	980
Boron(ppm)	0	2	210
Niobium(ppm)	19	20	1760
Heat_input(kJ.mm-1)	1.2	1.0	7.4
Interpass_temperature(C)	190	200	365
Postweld_heat_treatment_temperature(C)	249	250	680
Post-weld_heat_treatment_time(h)	14	14	48
GA calculated YS/MPa	463	---	1184
Target Value YS/MPa	466	---	1200
Error YS/MPa	22	---	43
Measured YS/MPa	---	466	---

The NNGA models have good accuracy in predicting 18 input variables of the Yield Strength of ferritic steel welds, which is excellent for weld design.(Table.4.3). The predicted results of the targeted values of the two weld deposits are very close. The results of Genetic Algorithms are match with trends of measured data and fundamental of metallurgy. The output results show the predictive capacity of the NN-GA model. This NN

GA model can be used in practical applications, research and development of ferritic steel alloys.

[Appendix-B]

4.1.6 Summary

The Neural Network and Genetic algorithms Methods have been used for efficient design of the Yield strength of Ferritic Steel Welds. From the Modelling works and Results and Discussion of this Chapter some useful conclusions can be drawn:

The distribution of the Data of the Yield Strength of Ferritic Steel Welds is uniform for some Input variables and non-uniform for some Input variables. The distribution is clearly observed in Scatter plots.

In the case of Bayesian Neural Network method, all the response graphs show error bars when the concentration of Nickel and Chromium is respectively below 6 and 8 wt%, the prediction can be reliable. But above those limits (6 wt% for Ni and 8 wt% for Cr), the model can no more be trusted and this is inferred by the large error bars. Similarly it is applicable to other graphs where larger error bars are present. More experiments with concentrations in this range of values need to be carried out to improve the model. Uncertainty because of a lack of data is one of the limitations of a neural network. The error bars and output variable (Yield Strength) sometimes showing unphysical (negative) values, this is because of the empirical equation in Neural Network modelling. This error bars feature of Bayesian Neural Network is an excellent guideline for research and Development.

In the case of General Regression Neural Network method, there is no problems of noisy data. It can handle noises in the Inputs. The Response graphs of the GRNN show more define about the non linearity or complexity between the Input variables and the Yield Strength of Ferritic Steel Welds.

The Response Graphs show about the individual relationship between the input variables and Output variable (Yield Strength). The 3D contour plots show the relationship between the two Input variables with Output variable (Yield Strength).

These trends are confirmed in the present analysis as illustrated in both the types of the Graphs Figure 4.1 (a to q) and Figure 4.2 (a to q). They are impossible to reproduce in practice. They give a clear understanding of the relationship between the Input variables and the Yield Strength of Ferritic Steel Welds. These pieces of information are very valuable for design, as well

as understanding the existing theory and also guiding about new research and new finding for the Ferritic steel Welds.

The 3D contour plots show the relationship between the two Input variables with Yield Strength. There is a total combination of 136 3D contour plots formed by 17 Input variables with the Yield Strength. In the present work, 18 3D contour plots are given with their important relationship with the Yield Strength. These 3D contour plots show some hidden complex behaviour of the input variables with the Yield Strength which is not available and not well understood. Some innovative theoretical relations can be established by the proper interpretation of these 3D contour plots which become the new knowledge base for the future work on Ferritic Steel Welds. The Input variables show complex trends because during welding, there are formation of various types of the microstructures in Ferritic Steel Welds, qualitatively and quantitatively.

The trained BNN and GRNN models give the accurate predictions of unseen data which is useful in designing the Ferritic Steel Welds for the welding electrodes industries. With simply change the quantity of Input variables in model and run it, the predicted Yield Strength is obtained in the seconds.

The Genetic Algorithms method gives the prediction of the Input Variables for the Targeted Yield Strength value. It also predicted Input variables for the Targeted Yield Strength value which is beyond the range of data. The results are excellent.

4.2 Ultimate Tensile Strength Models

4.2.1 Response graphs of Input variables and Ultimate Tensile Strength of Ferritic Steel Welds using committee model of Bayesian Neural Network

The Trends of the Input Variables (Independent Variables) and Ultimate Tensile Strength of Ferritic Steel Welds are given below in the form of the graphs.

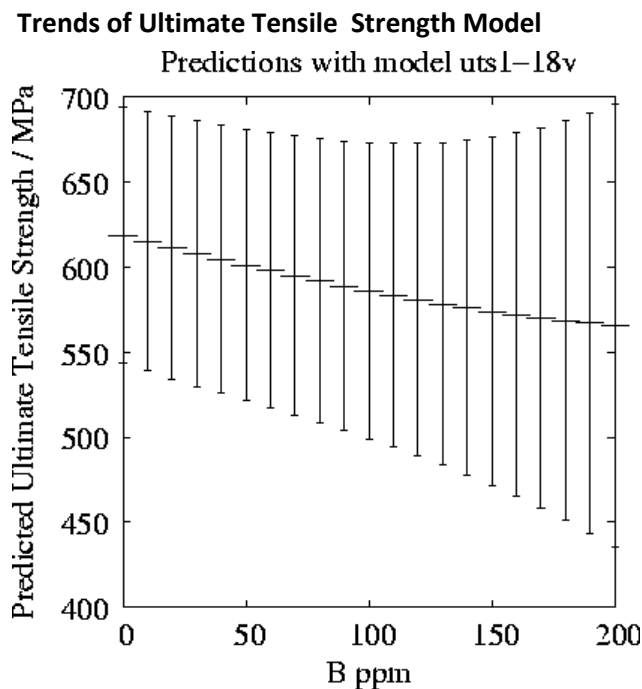


Fig a. Predicted variations in Ultimate Tensile Strength with Boron variation.

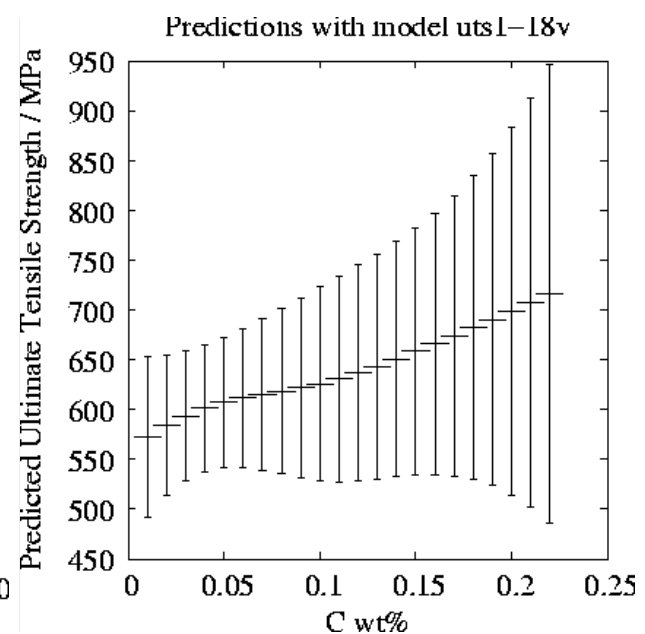


Fig b. Predicted variations in Ultimate Tensile Strength with Carbon variation.

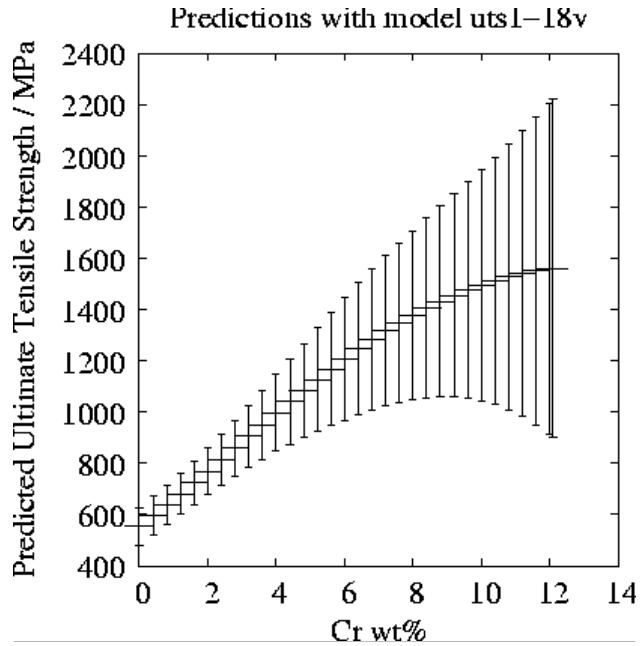


Fig c. Predicted variations in in Ultimate Tensile Strength with Chromium variation.

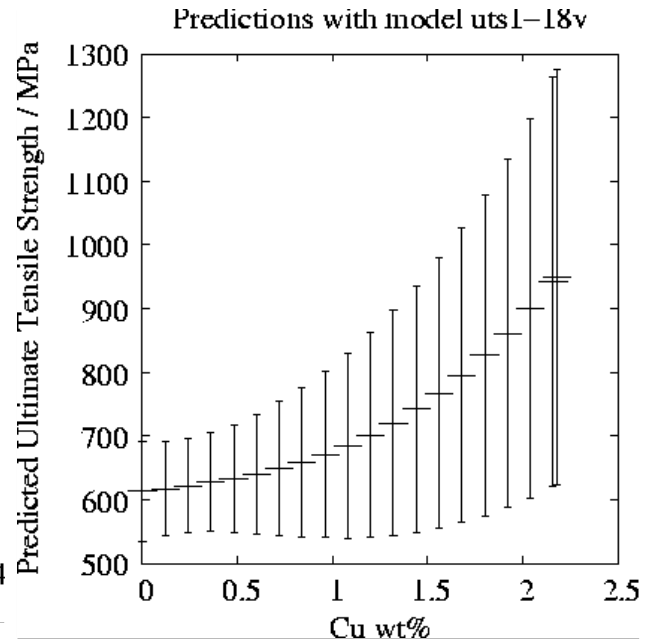


Fig d. Predicted variations in in Ultimate Tensile Strength with Copper variation.

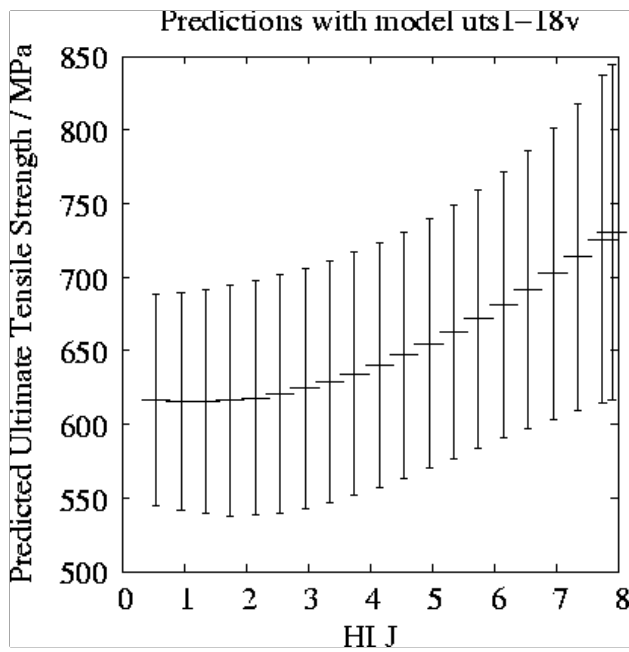


Fig e. Predicted variations in in Ultimate Tensile Strength with Heat input variation.

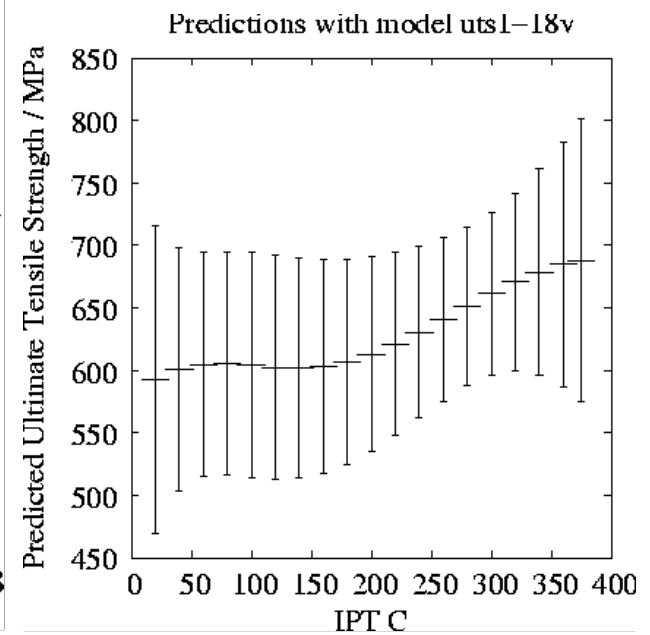


Fig f. Predicted variations in in Ultimate Tensile Strength with Interpass Temperature variation.

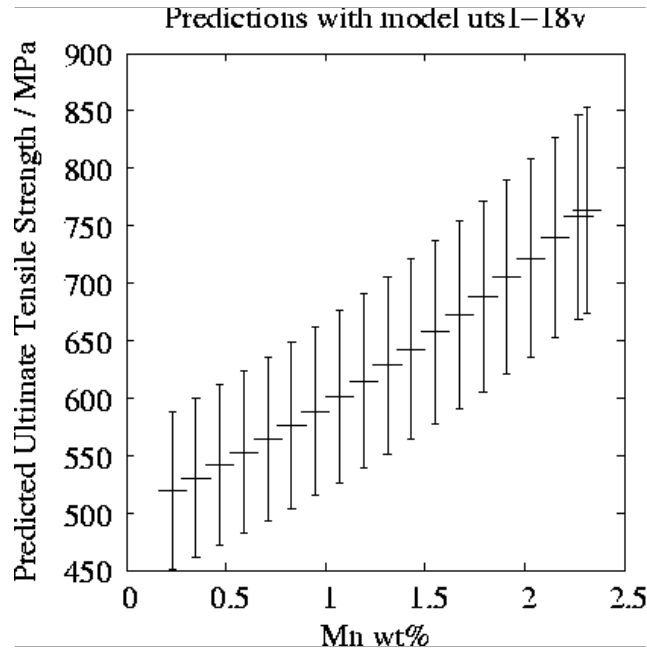


Fig g. Predicted variations in in Ultimate Tensile Strength with Manganese variation.

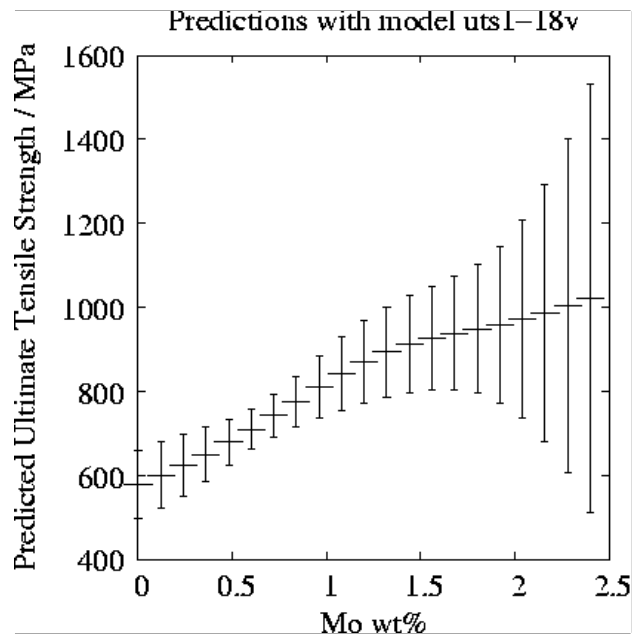


Fig h. Predicted variations in in Ultimate Tensile Strength with Molybdenum variation.

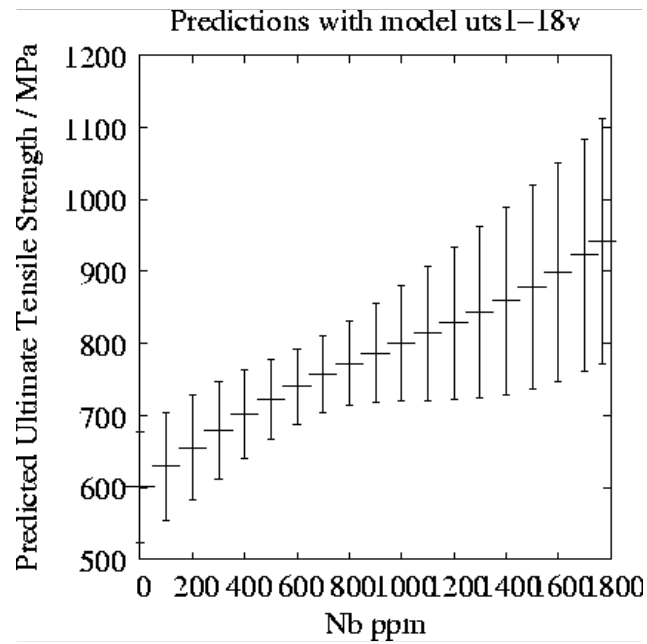


Fig i. Predicted variations in in Ultimate Tensile Strength with Niobium variation.

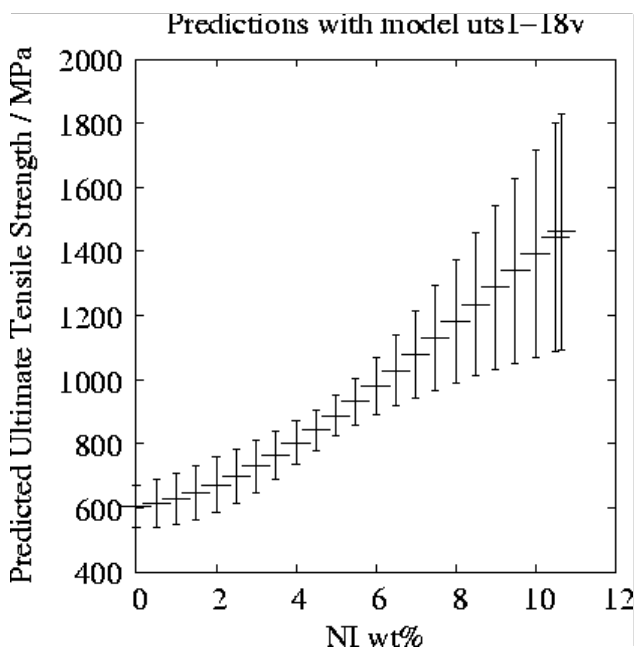


Fig j. Predicted variations in in Ultimate Tensile Strength with Nickel variation.

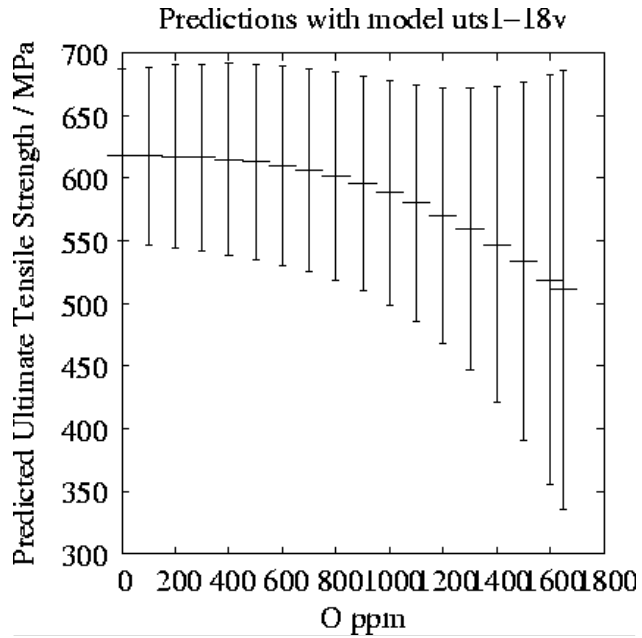


Fig k. Predicted variations in in Ultimate Tensile Strength with Oxygen variation.

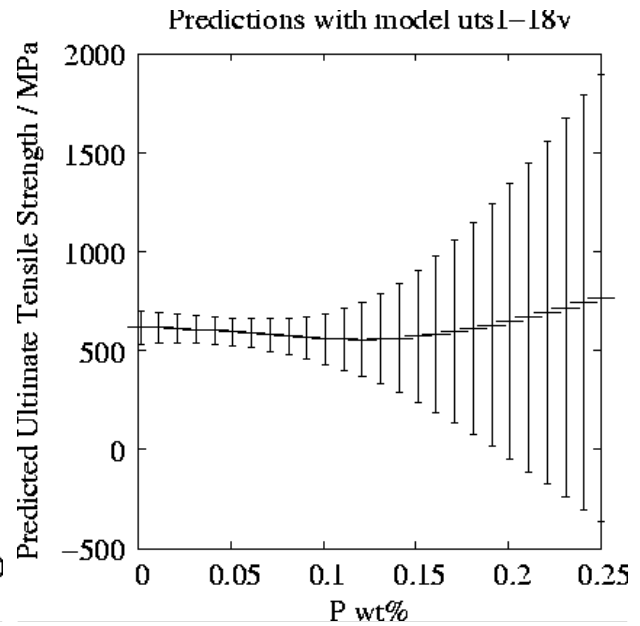


Fig l. Predicted variations in in Ultimate Tensile Strength with Phosphorus variation.

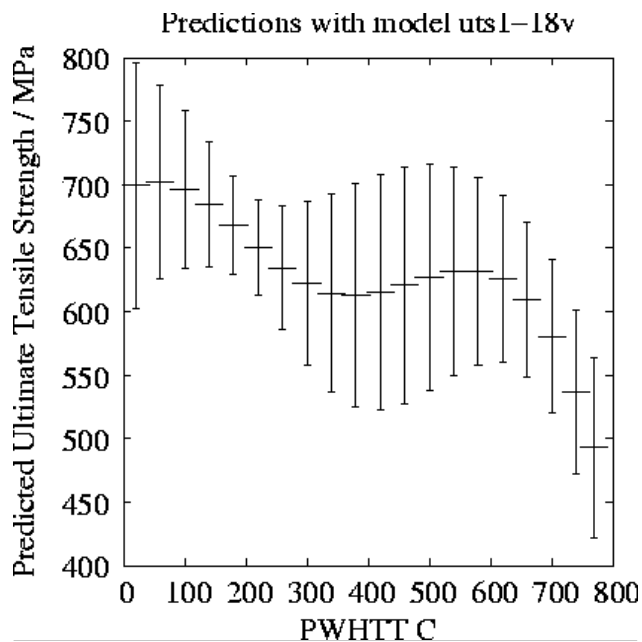


Fig m. Predicted variations in in Ultimate Tensile Strength with Post Weld Heat Treatment Temperature variation.

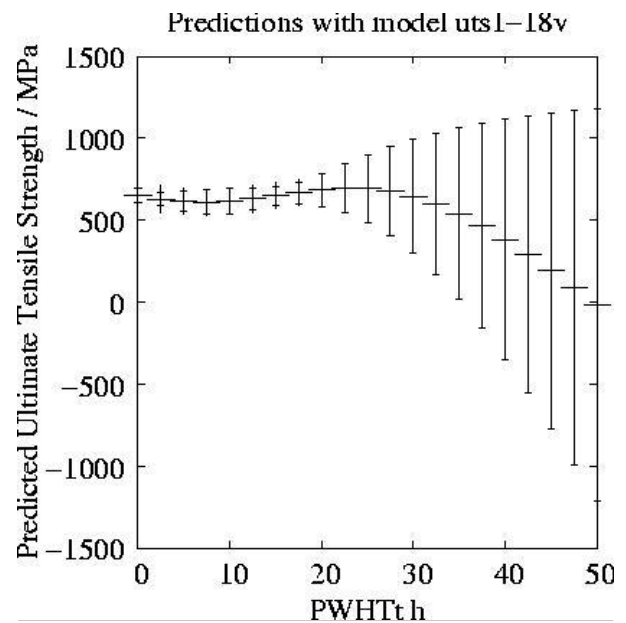


Fig n. Predicted variations in in Ultimate Tensile Strength with Post Weld Heat Treatment Time variation.

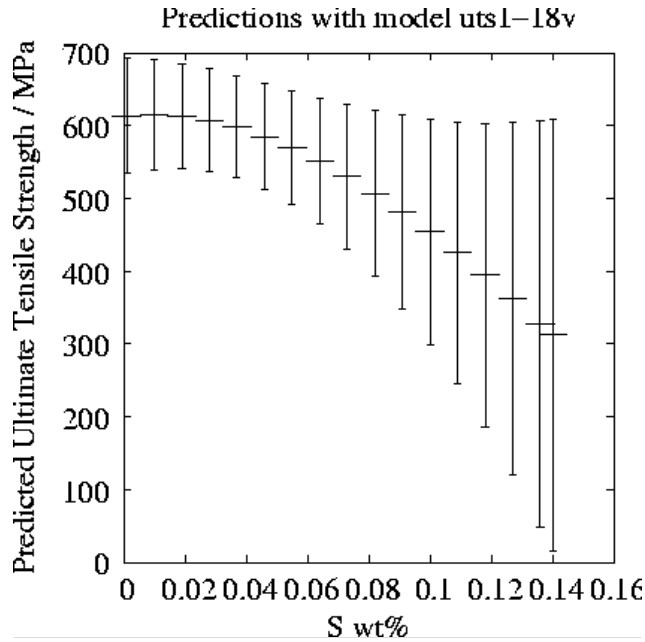


Fig o. Predicted variations in in Ultimate Tensile Strength with Sulphur variation.

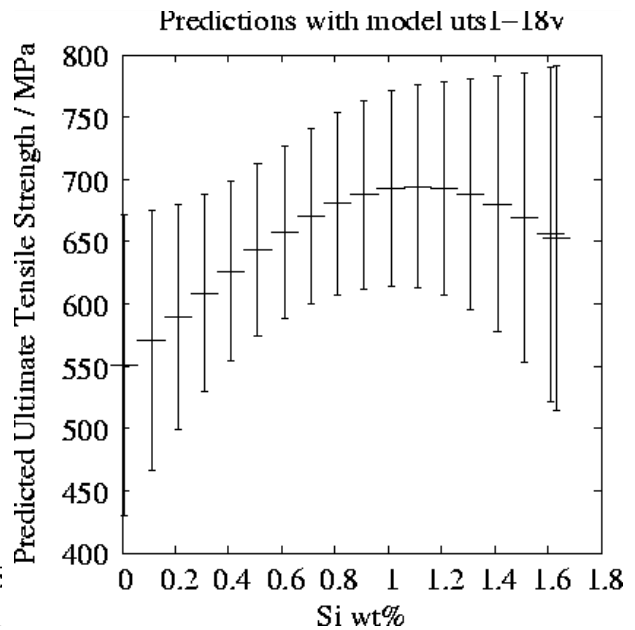


Fig p. Predicted variations in in Ultimate Tensile Strength with Silicon variation.

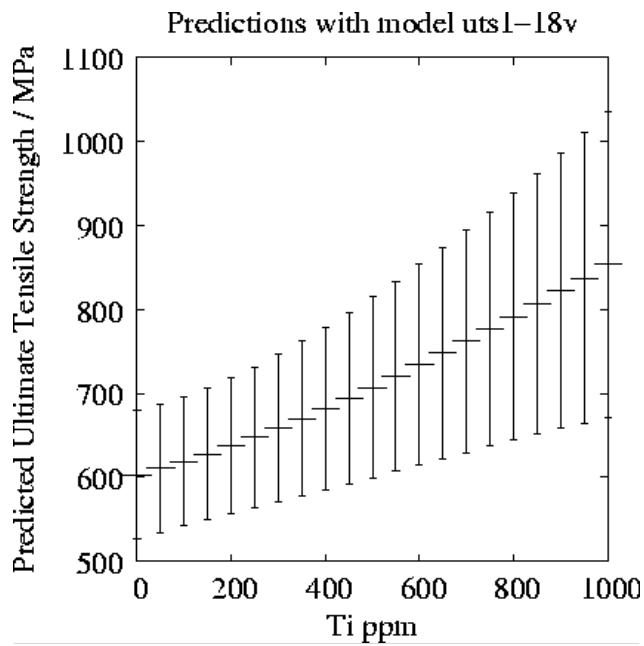


Fig q. Predicted variations in in Ultimate Tensile Strength with Titanium variation.

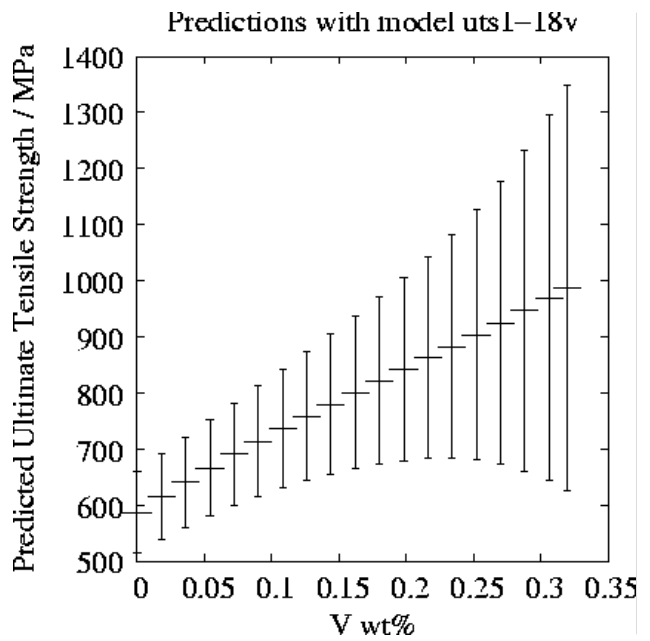


Fig r. Predicted variations in in Ultimate Tensile Strength with Vanadium variation.

Figure 4.4 Response graphs (a to r) of Input variables and Ultimate Tensile Strength of Ferritic Steel Welds using committee model of Bayesian Neural Network

These trends are confirmed in the present analysis as illustrated in Figure 4.4 (a to r). It is emphasised that these calculations are done without permitting any of the other variables to change. They are impossible to reproduce in practice.

All the graphs show the error bars. The error bars are uniform in size indicate that the uniformity of data, like the graph the prediction of the Ultimate Tensile Strength as a function of Manganese. The error bars are large in size indicate non-uniformity of data, like the graph the prediction of the Ultimate Tensile Strength as a function of Chromium.

In this case, when the concentration of Nickel and Chromium is respectively below 8 and 6 wt%, the prediction can be reliable but above those limits (8 wt% for Ni and 6 wt% for Cr), the model can no more be trusted and this is inferred by the large error bars. Similarly it is applicable to other graphs where larger error bars are present. More experiments with concentrations in this range of values need to be carried out to improve the model. Uncertainty because of a lack of data is one of the limitations of a neural network. The error bars and output variable (Ultimate Tensile Strength) sometimes showing unphysical (negative) values, this is because of the empirical equation in Neural Network modelling. [Ref. Jun Hak, Pak]

The input variables like Carbon, Chromium, Copper, Heat Input, Interpass Temperature, Manganese, Molybdenum, Niobium, Nickel, Titanium and Vanadium are increasing in concentration or in amount, increase the Ultimate Tensile Strength of ferritic Steel welds.

The input variables like Boron, Oxygen, Post Weld Heat Treatment Time, and Sulphur increase quantitatively, decrease the Ultimate Tensile Strength of ferritic Steel welds. The Phosphorus has shown little effect on the Ultimate Tensile Strength.

The input variable like Post Weld Heat Treatment Temperature, and Silicon indicate their non linear behaviour with the Ultimate Tensile Strength.

The trends of the graphs of Bayesian Neural network model are useful to design the Ultimate Tensile Strength of Ferritic Steel welds efficiently.

In summary, a reasonable committee model has been obtained for Ultimate Tensile Strength. It appears that these input variables are affected on the Ultimate Tensile Strength of Ferritic Steel Welds, as could be expected from a metallurgical point of view.

4.2.2 Response Graphs of the Ultimate Tensile Strength GRNN model

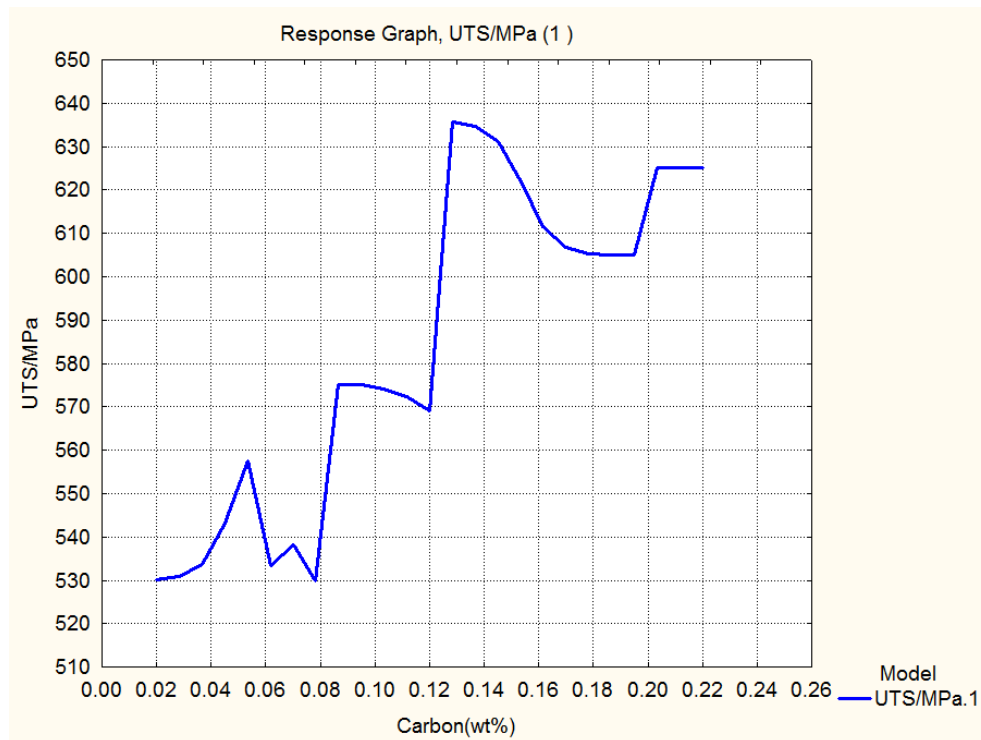


Fig. a Response Graph of Ultimate Tensile Strength MPa and Carbon(wt%)

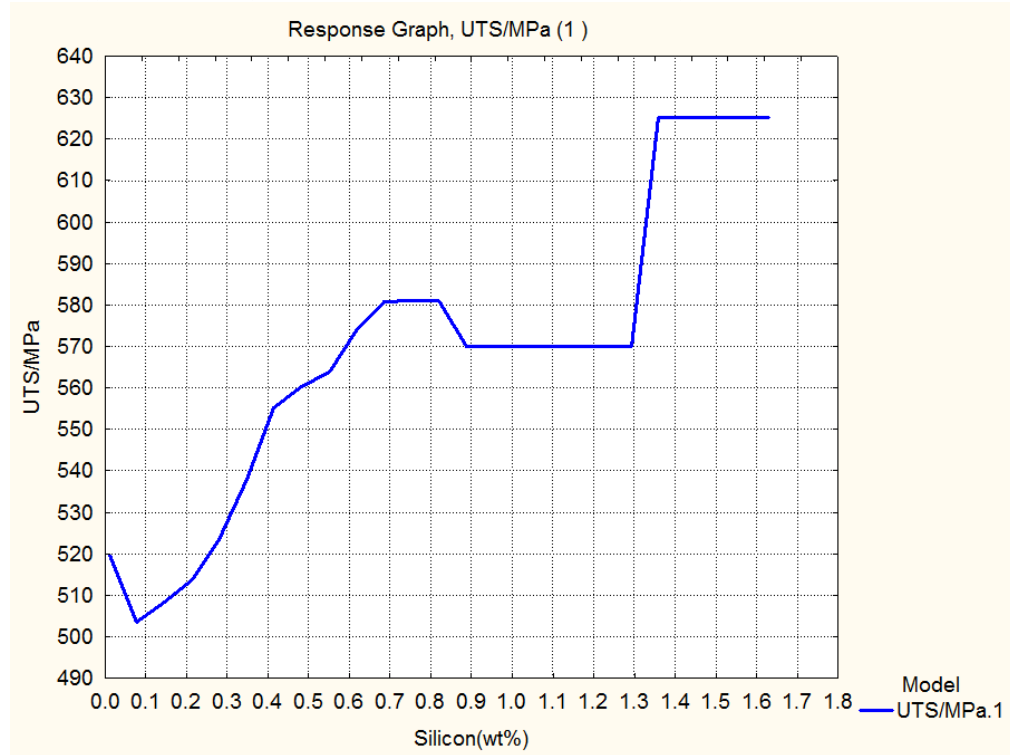


Fig. b Response Graph of Ultimate Tensile Strength MPa and Silicon(wt%)

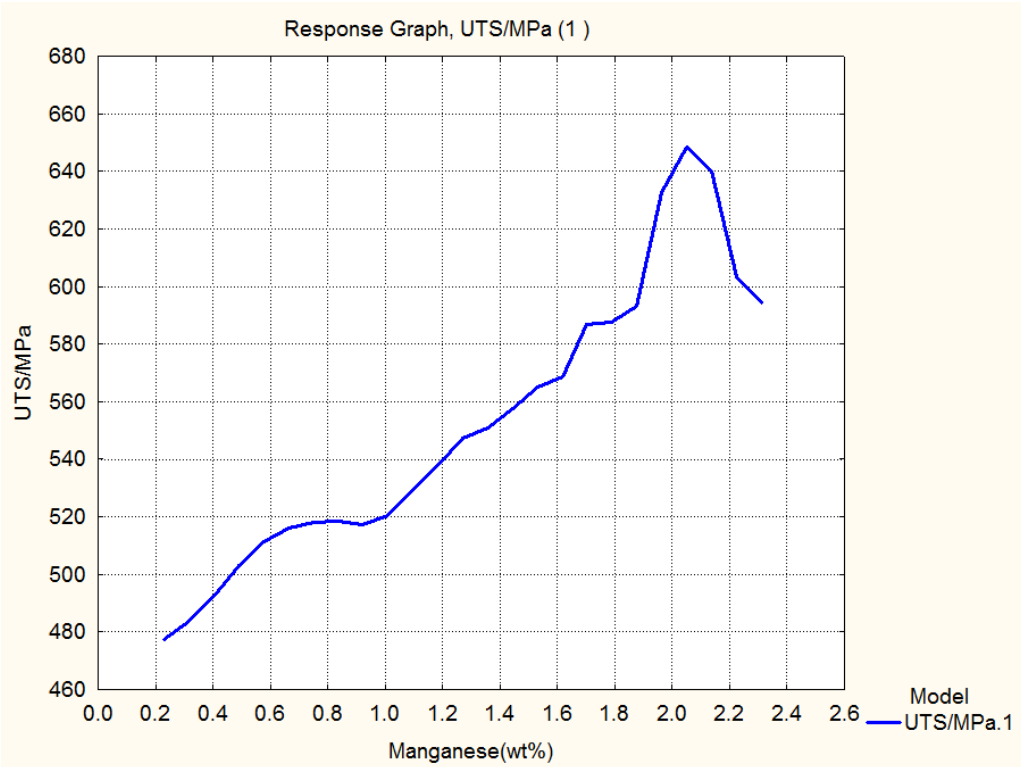


Fig. c Response Graph of Ultimate Tensile Strength MPa and Manganese(wt%)

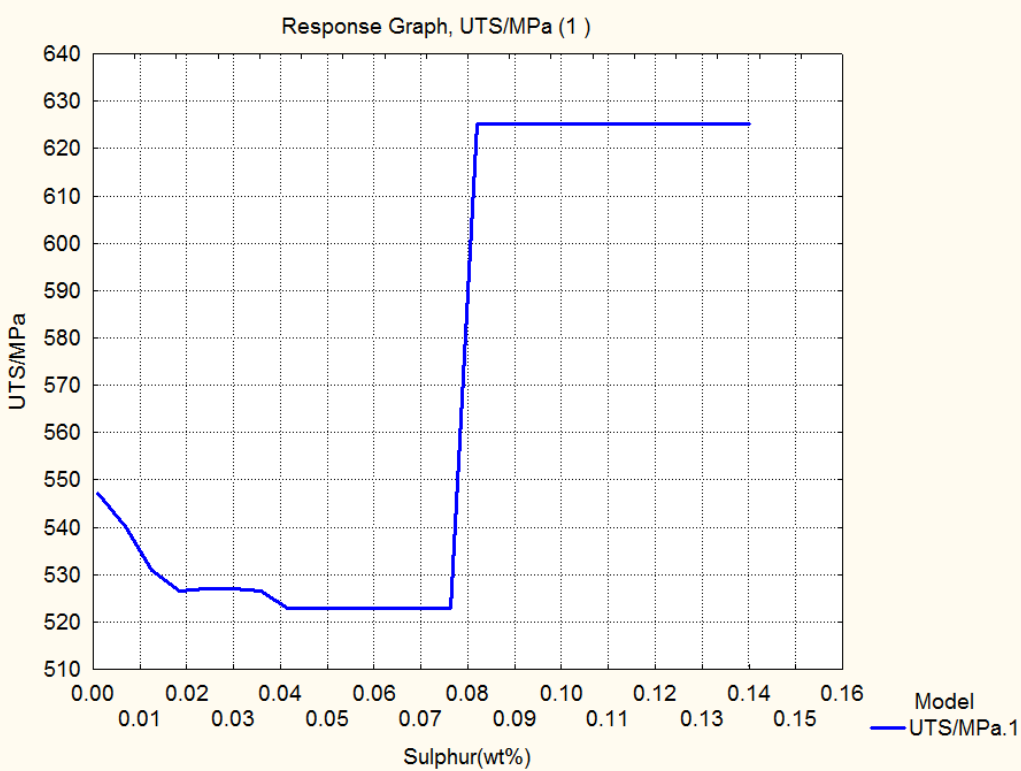


Fig. d Response Graph of Ultimate Tensile Strength MPa and Sulphur(wt%)

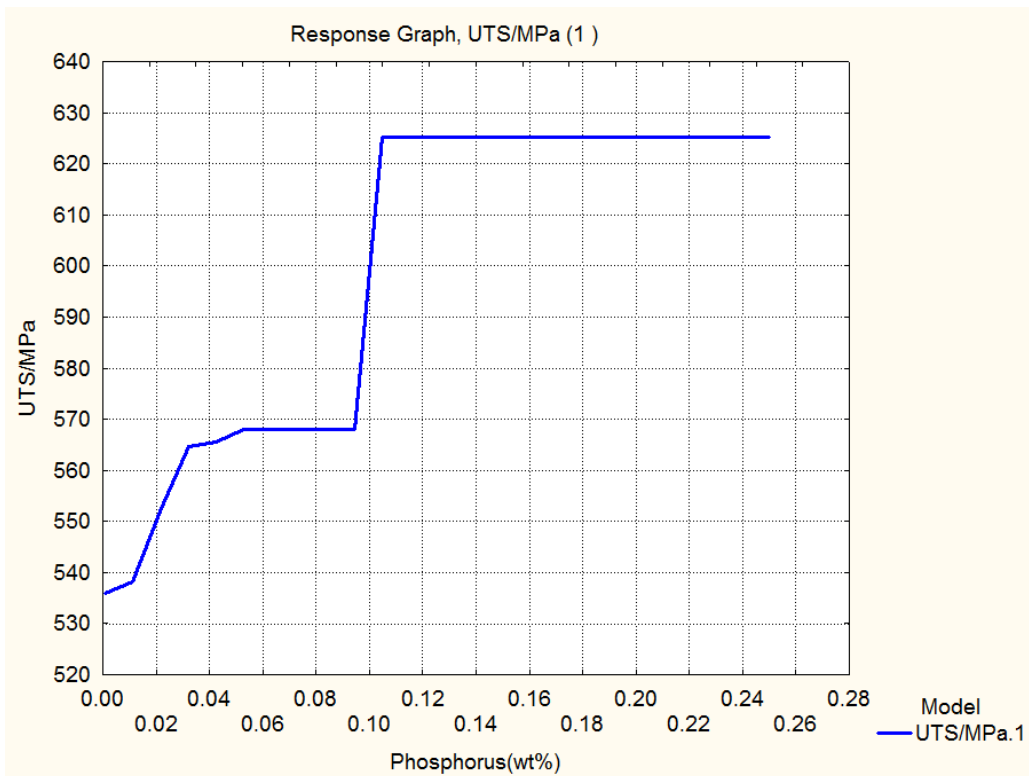


Fig. e Response Graph of Ultimate Tensile Strength MPa and Phosphorus(wt%)

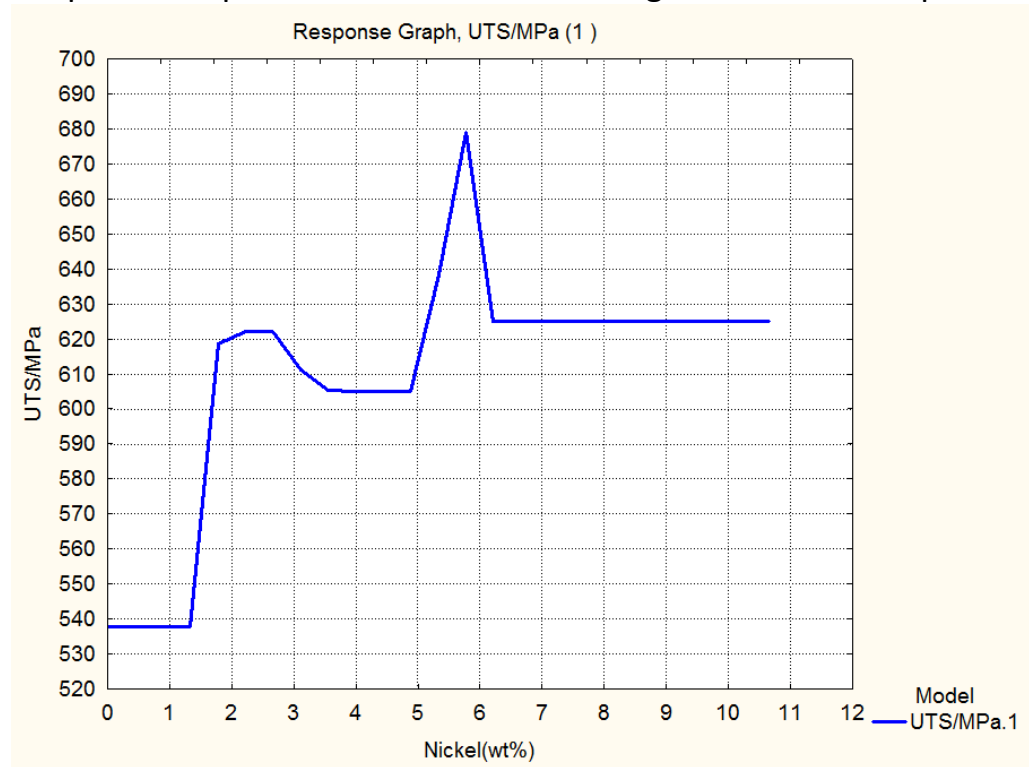


Fig. f Response Graph of Ultimate Tensile Strength MPa and Nickel(wt%)

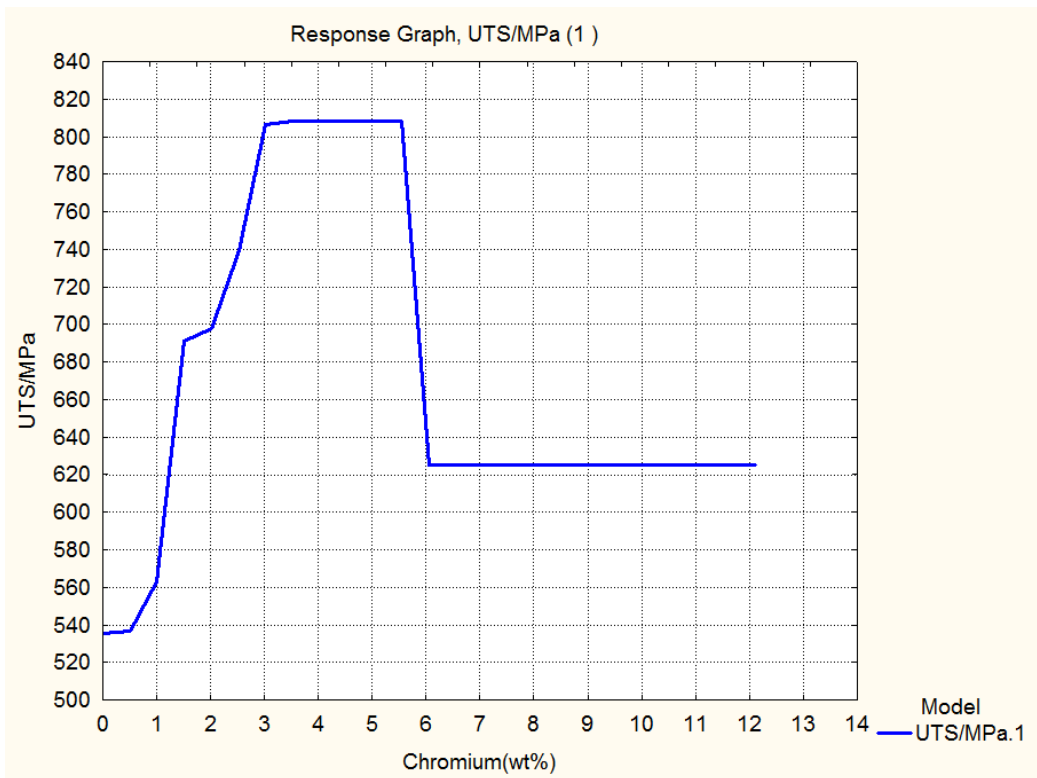


Fig. g Response Graph of Ultimate Tensile Strength MPa and Chromium(wt%)

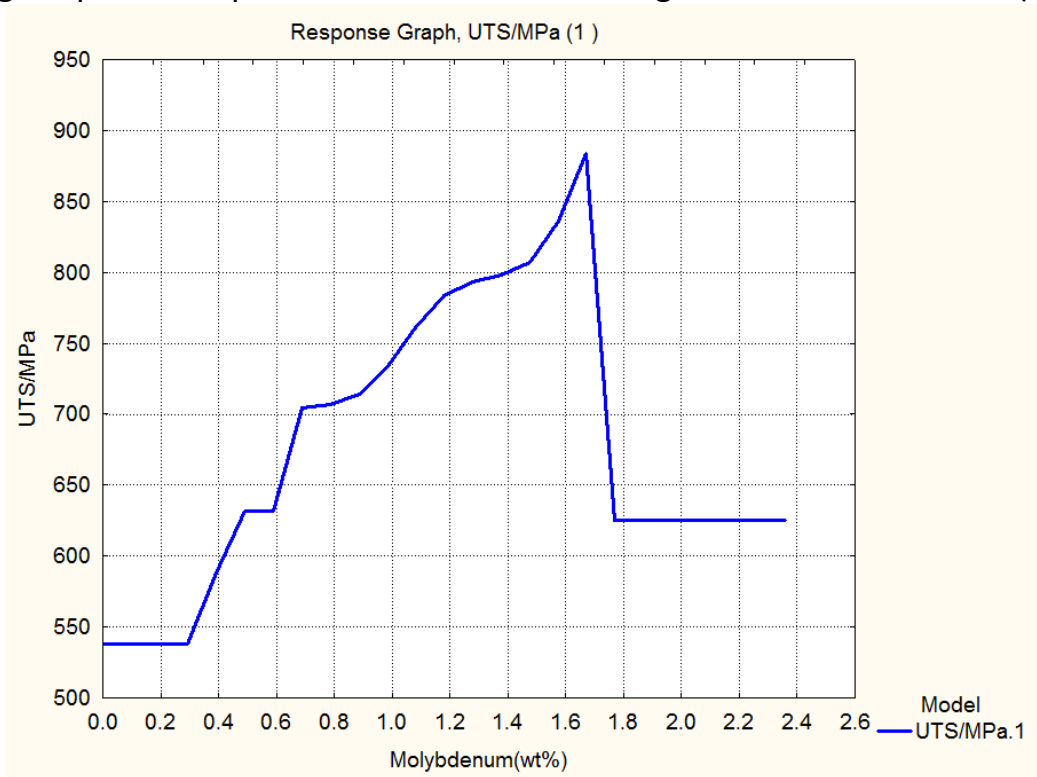


Fig. h Response Graph of Ultimate Tensile Strength MPa and Molubdenum(wt%)

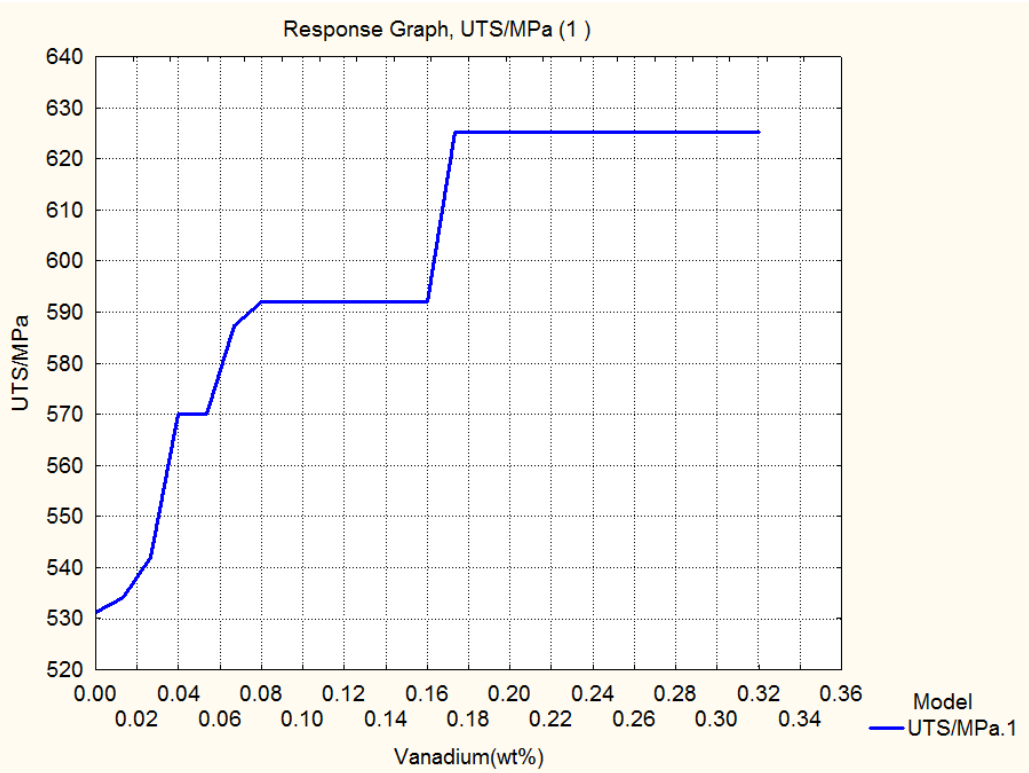


Fig. i Response Graph of Ultimate Tensile Strength MPa and Vanadium(wt%)

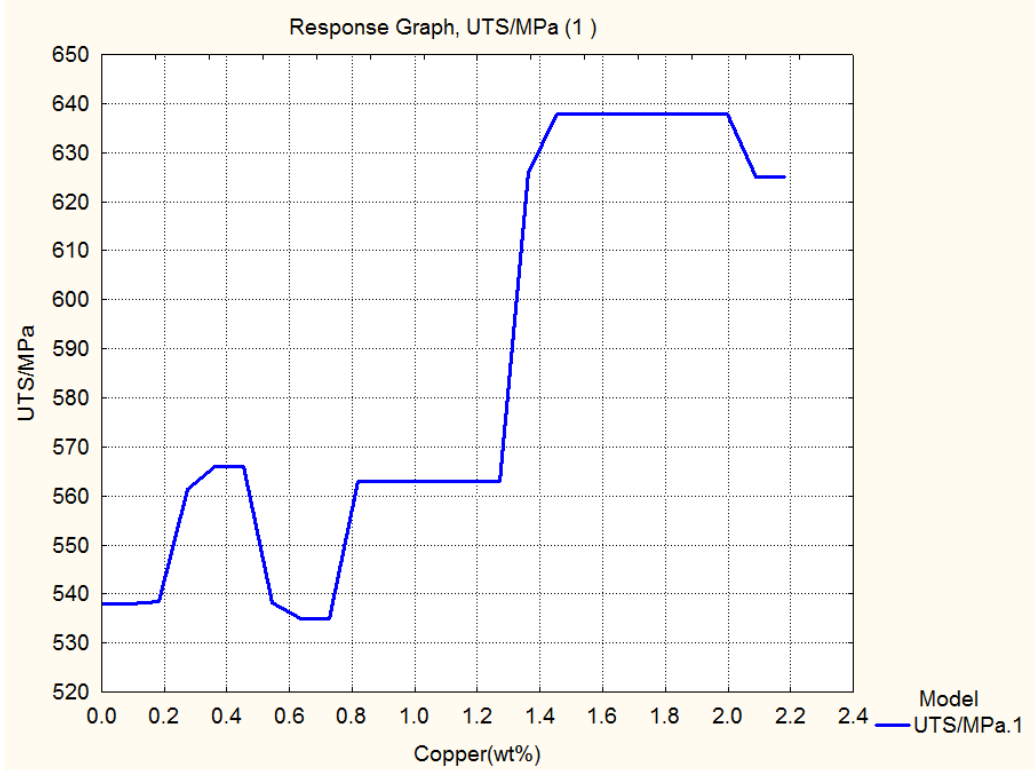


Fig. j Response Graph of Ultimate Tensile Strength MPa and Copper(wt%)

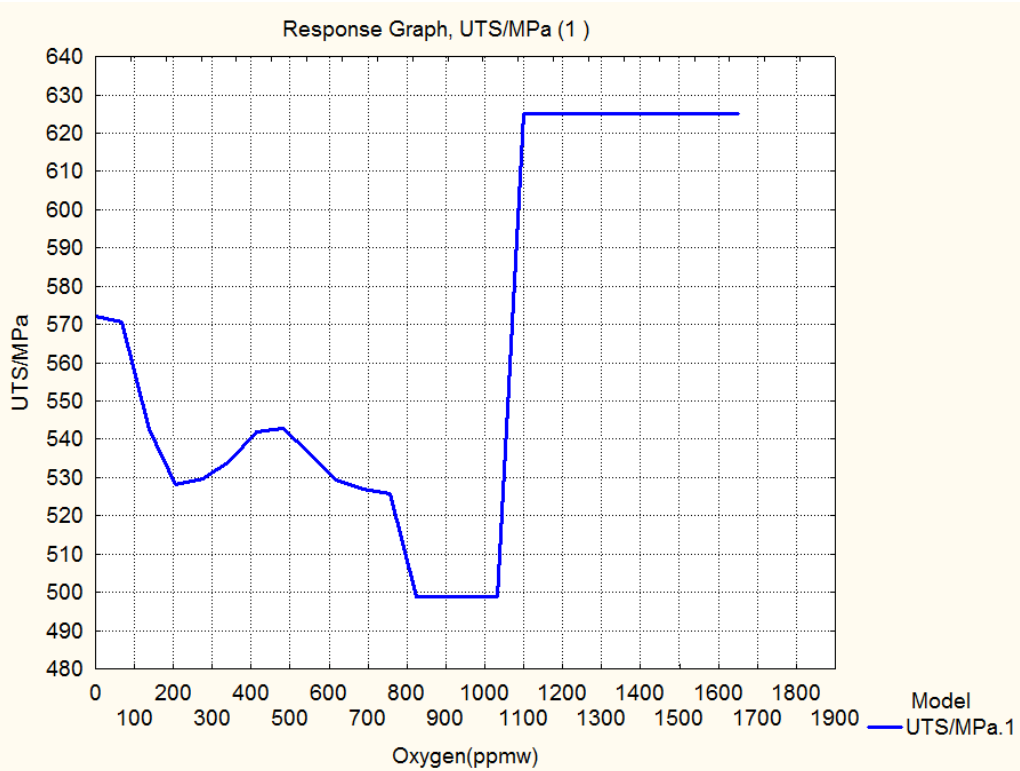


Fig. k Response Graph of Ultimate Tensile Strength MPa and Oxygen(ppmw)

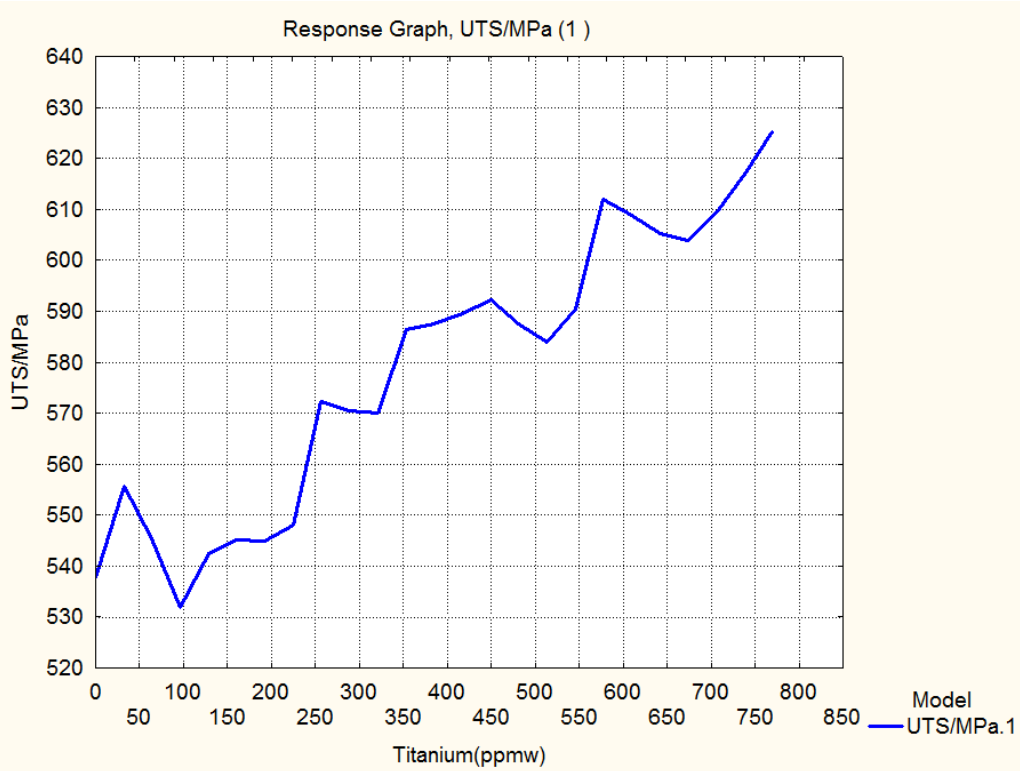


Fig. l Response Graph of Ultimate Tensile Strength MPa and Titanium (ppm)

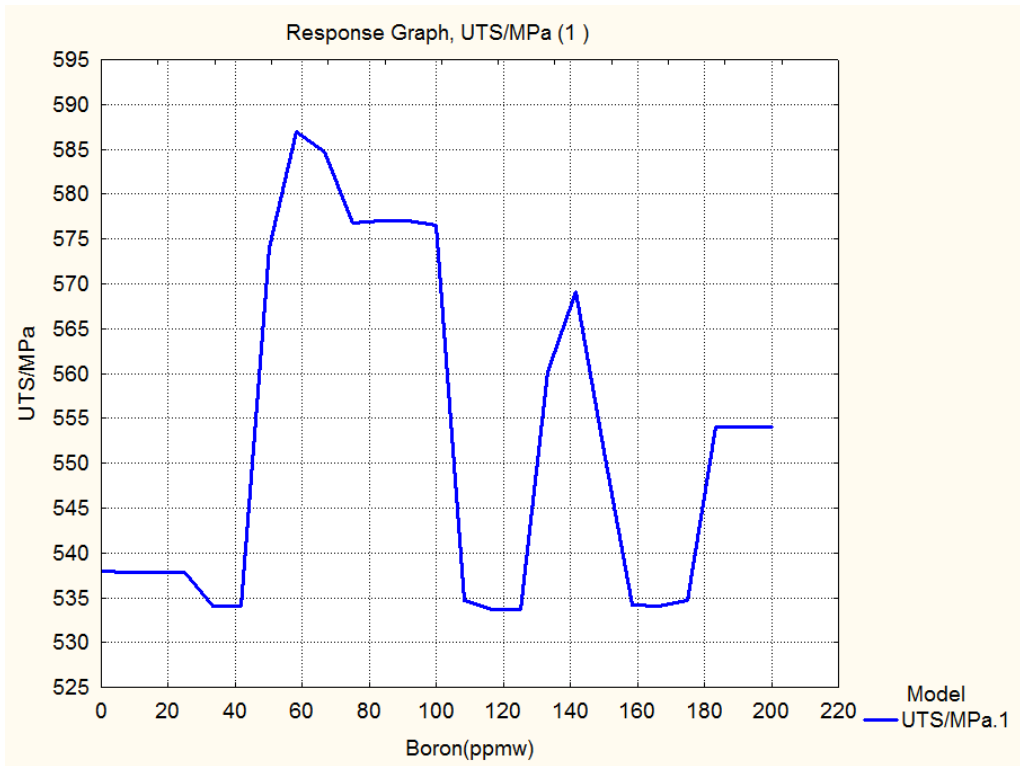


Fig. m Response Graph of Ultimate Tensile Strength MPa and Boron(ppmw)

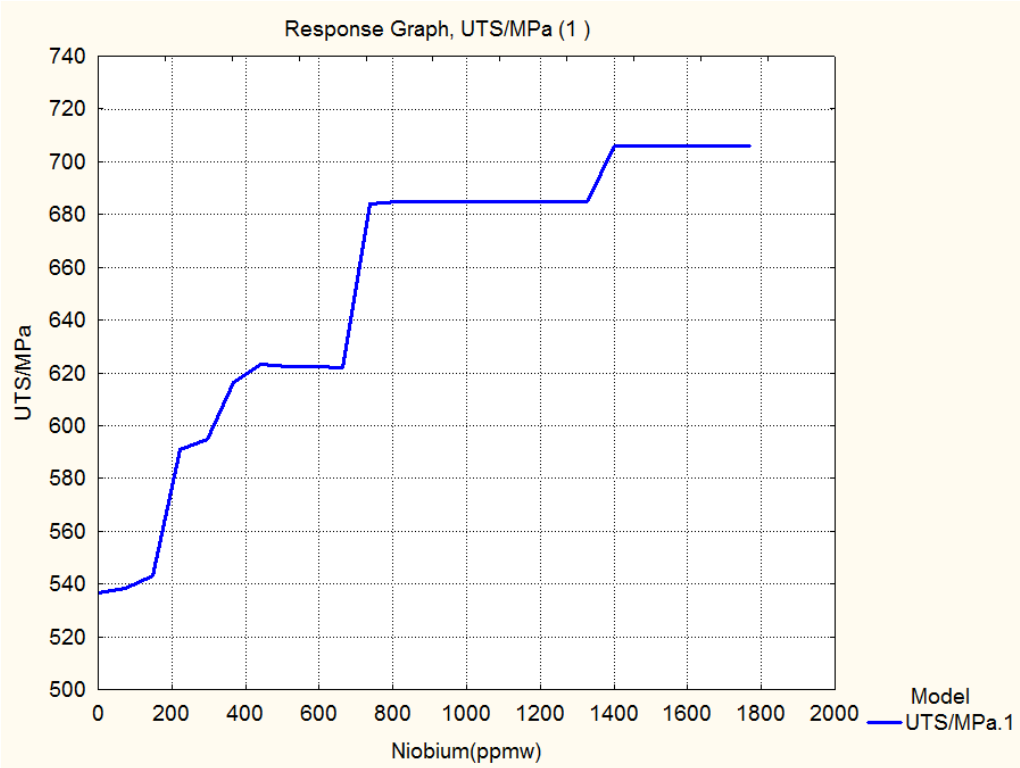


Fig. n Response Graph of Ultimate Tensile Strength MPa and Niobium(ppmw)

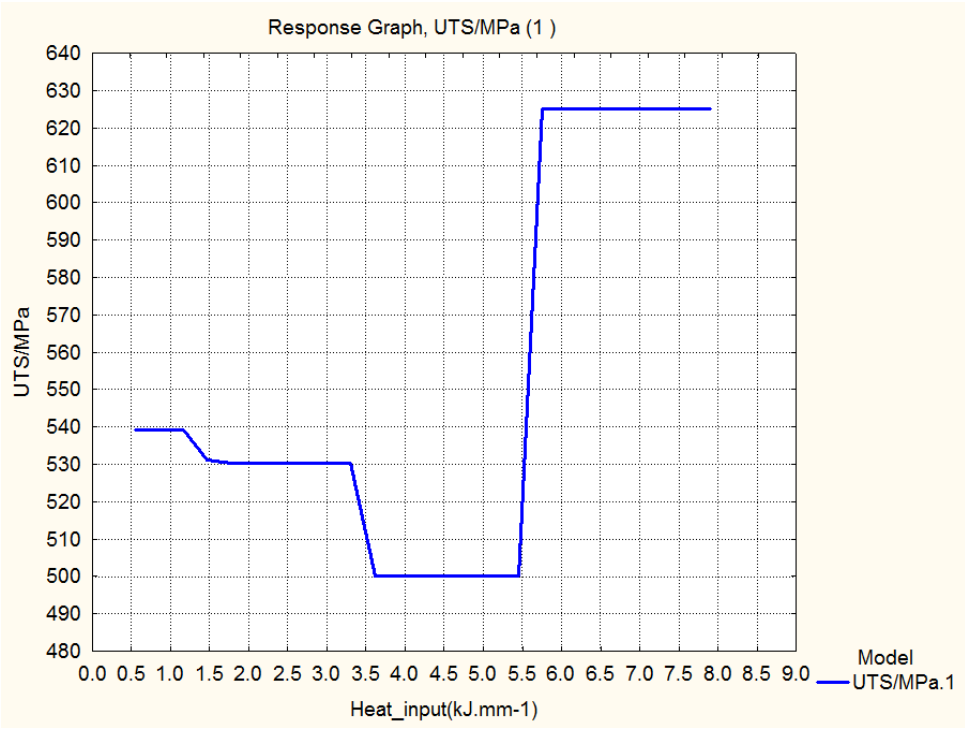


Fig. o Response Graph of Ultimate Tensile Strength MPa and Heat input (kJ mm-1)

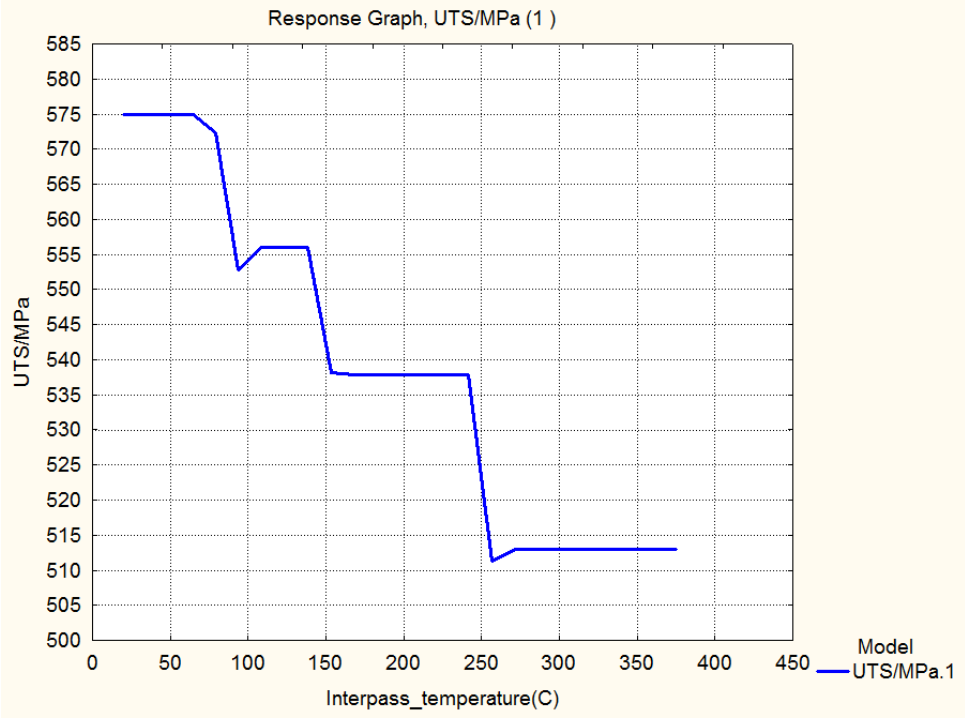


Fig. p Response Graph of Ultimate Tensile Strength MPa and Interpass temperature (C)

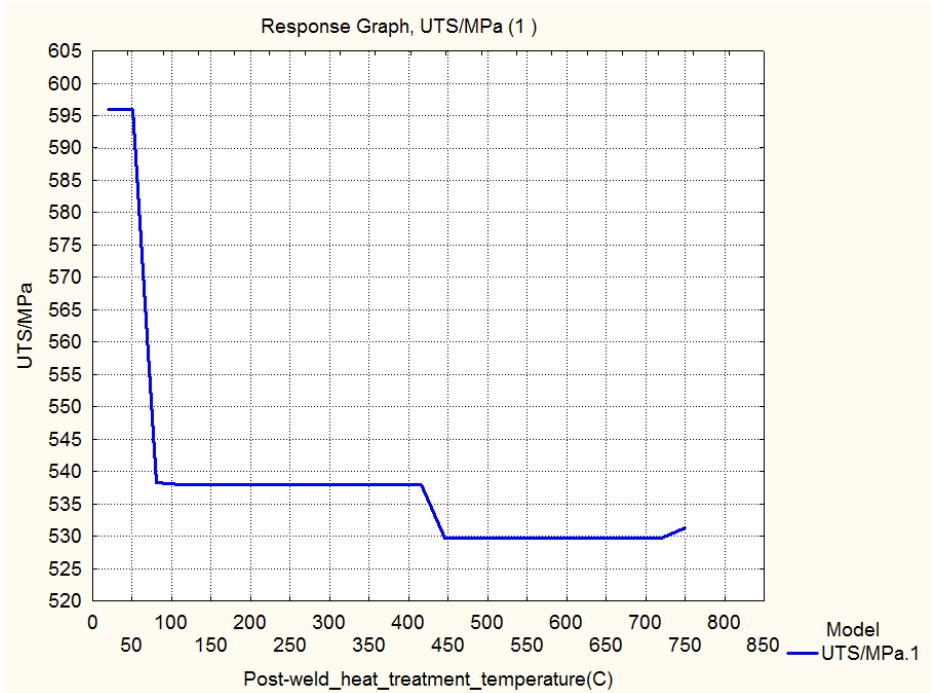


Fig. q Response Graph of Ultimate Tensile Strength MPa and Post-weld heat treatment temperature (C)

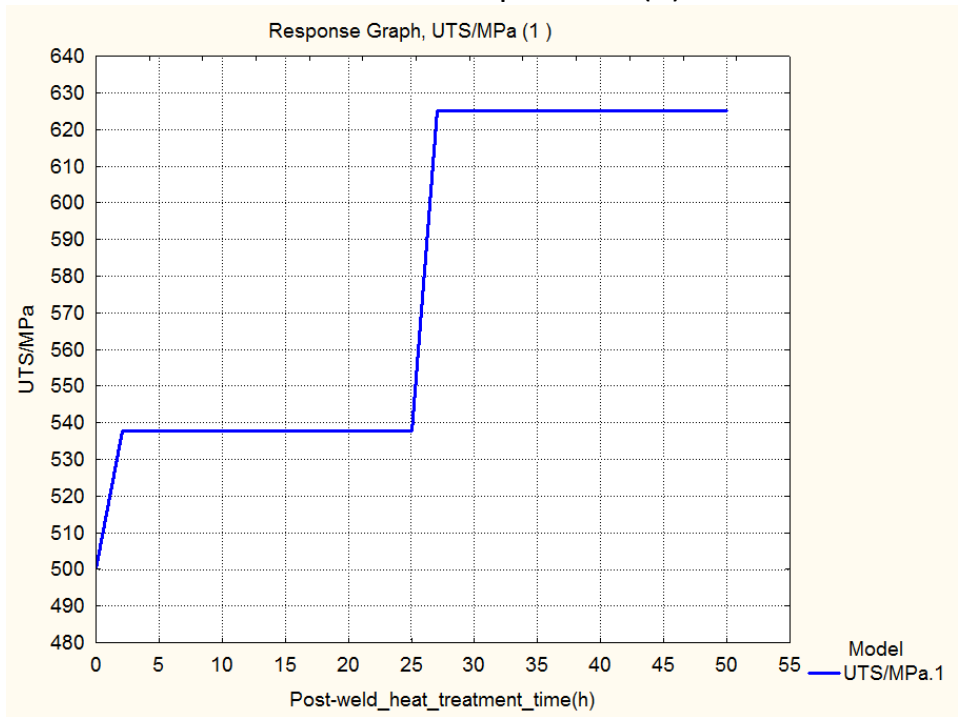


Fig. r Response Graph of Ultimate Tensile Strength MPa and Post-weld heat treatment time(h)

Figure 4.5 (a to r) Response graphs of Input variables Ultimate Tensile Strength of Ferritic Steel Welds

The influence of each of the variables on the ultimate tensile strength of welding alloys, which is discussed here. The carbon increases the ultimate tensile strength up to 635 MPa near to 0.13%, and the minimum at 530 MPa at 0.02%. Overall %C increases between 0.02% to 0.22%, give a general increase in the ultimate tensile strength. Some points are observed to decrease maximum up to 27 MPa at 0.08%C and 25 MPa at 0.198%C. In the case of silicon between 0.1% to 0.8%, there is an increase of the 505 MPa to 580 MPa in the ultimate tensile strength and then constant to 570 MPa between 0.9% to 1.3% Si with drop in 10MPa at 0.82% Si. At 1.35%, the ultimate tensile strength is maximum 625 MPa. The trend of manganese shows the increase in the Mn% from 0.2% to 2.08%, the value of the ultimate tensile strength is also increased from 478 MPa to 648 MPa. After 2.08% Mn, there is reduced to 592 MPa at 2.4% Mn. The sulphur shows the first decrease in the ultimate tensile strength from 548 MPa to 523 MPa. At 0.08%, it is increased from 523 MPa to 625MPa. The Phosphorus gives the increase in the ultimate tensile strength from 536 MPa to 625 MPa. The nickel has the maximum ultimate tensile strength of 680 MPa at 5.8% and minimum 538 MPa at 1.3%. In the figure, it shows at 2.5% the ultimate tensile strength value drops from 622 MPa to 605 MPa. More than 5.8 % Ni gives a further drop in ultimate tensile strength 625 MPa. The Chromium has a maximum ultimate tensile strength of 809 MPa between 3% to 5.5%. More than 5.5% Cr reduces the ultimate tensile strength to 623 MPa. Increase in the ultimate tensile strength from 538 MPa to 809 MPa only by the gradual addition of chromium up to 4%. Molybdenum increases the ultimate tensile strength from 547 MPa to 880 MPa at 1.68%. At 1.68% Mo gives a maximum ultimate tensile strength 880 MPa. More than 1.68% Mo decreases ultimate tensile strength from 880 MPa to 625 MPa. Vanadium increases the ultimate tensile strength from a minimum 532 MPa to a maximum 626 MPa at 0.17%. At 0.17% V, ultimate tensile strength is constant to 626 MPa. Copper increases the ultimate tensile strength from 538 MPa to 638 MPa at 1.45%. Between 0.48% to 0.74% Cu, the ultimate tensile strength decreases to 535 MPa. Cu gives maximum tensile strength of 638 MPa when it is in range, from 1.45% to 2.0%. Oxygen lowers the ultimate tensile strength of 570 MPa to 500 MPa when it is in the range of 820 ppm to 1020 ppm Oxygen content. Higher than 1020ppm Oxygen, there is an increase in the ultimate tensile strength from 500 MPa to 625 MPa. Titanium gives a minimum ultimate tensile strength of 539 MPa to maximum 625 MPa. At 775 ppm ultimate tensile strength is the highest. In between some range of Titanium from 40 ppm to 675 ppm, up and down in range of 5 MPa to 20MPa in the ultimate tensile strength. Boron shows

maximum ultimate tensile strength of 587 MPa at 58 ppm. More than 58 ppm, there is an up and down in ultimate tensile strength between the difference of 50MPa to 20 MPa. Niobium has a trend of increase in ultimate tensile strength from 542 MPa to 708 MPa with an increase from 180 to 1400 ppm.

Heat Input has stated that the maximum ultimate tensile strength of 625 MPa at 5.5 kJ mm⁻¹. Between 0.5 kJ mm⁻¹ to 5.5 kJ mm⁻¹ reduces from 540 MPa to 500 MPa. When the Interpass temperature is less than 70 C, the ultimate tensile strength is 575 MPa. More than 70 C, a decrease in ultimate tensile strength is observed to 513 MPa with increase in Interpass temperature up to 270 C. Post weld heat treatment temperature increases from 50 C to 750 C, shows ultimate tensile strength decrease from 596 MPa to 530 MPa. Post weld heat treatment time has a trend of increase in ultimate tensile strength from 500 to 539 MPa between 2 to 25 hours. More than 25 hours, it increases maximum ultimate tensile strength to 625 MPa.

The relationship between the input variables and the ultimate tensile strength is a nonlinear as seen above in response graphs (Figure 4.5 (a to r)).

The GRNN model has good accuracy in prediction of ultimate tensile strength of ferritic steel welds on unseen data which is excellent for the design of welds.(Table.4.5) The predicted yield strength for the unseen data of three weld alloys are compared with measured values of yield strength shows the prediction capacity of the GRNN model. This GRNN model can be used for practical applications, research and development of ferritic steel alloys.

4.2.3 3D Contour plots of the Ultimate Tensile Strength GRNN model

The effect in combination of any two input variables (Independent variables) from Carbon, Silicon, Manganese, Sulphur, Phosphorus, Nickel, Chromium, Molybdenum, Vanadium, Copper, Oxygen, Titanium, Boron, Niobium, Heat_input, Interpass_temperature, Post- weld heat treatment temperature and Post-weld heat treatment time on the Ultimate Tensile Strength of Ferritic Steel Welds are given in form of 3D contour plots. (Figure.4.6.1 to 4.6.19)

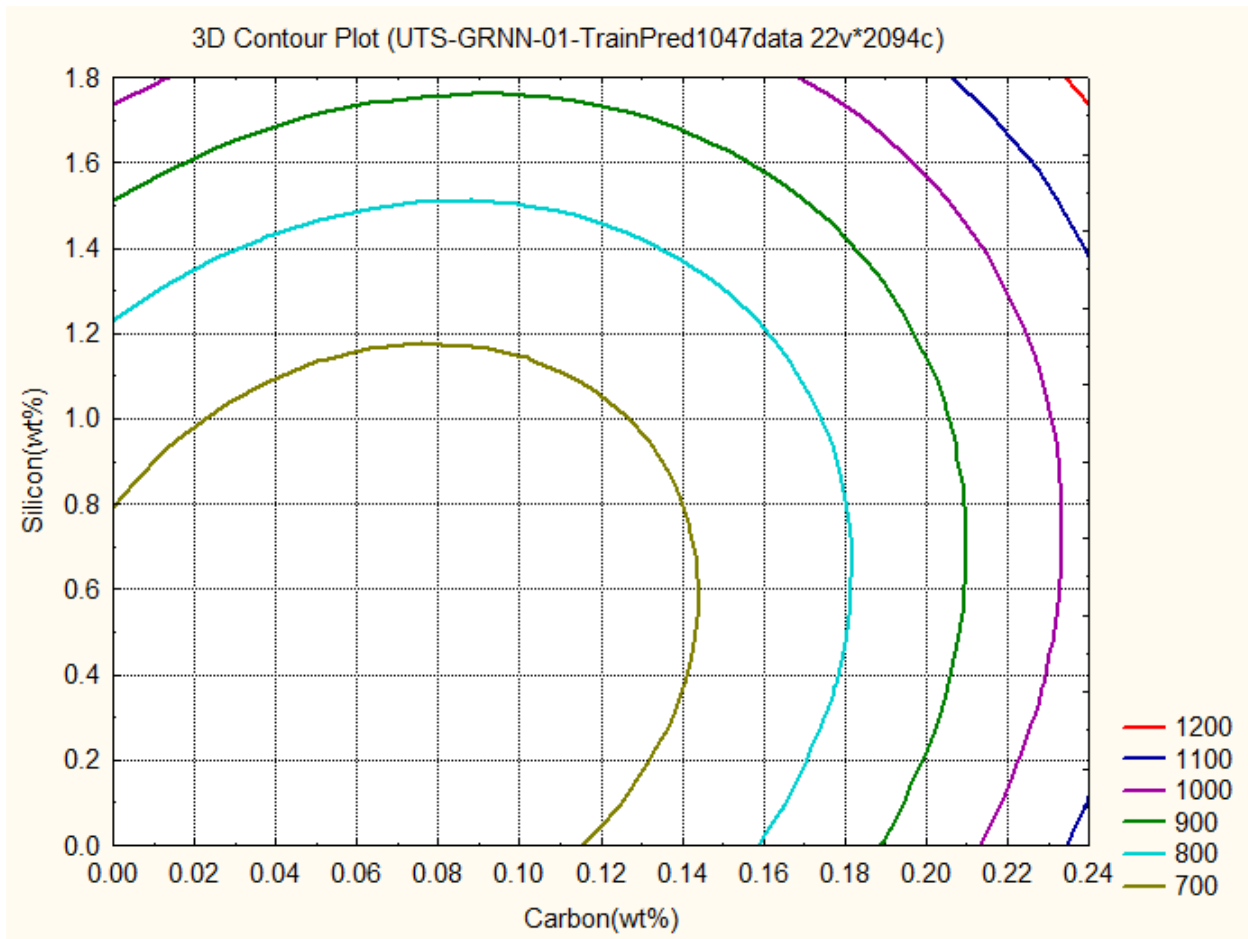


Figure.4.6.1 Predicted variations in Ultimate Tensile Strength (MPa) as a function of the Carbon and Silicon concentrations

3D contour Plot gives the relations between the **two input variables** and **one output variable**. **Figure.4.6.1** shows the relations between Carbon, Silicon and Ultimate Tensile Strength by **GRNN**. The graph gives the information about how these two, Carbon and Silicon control the Ultimate Tensile Strength from **700MPa to 1200 MPa**.

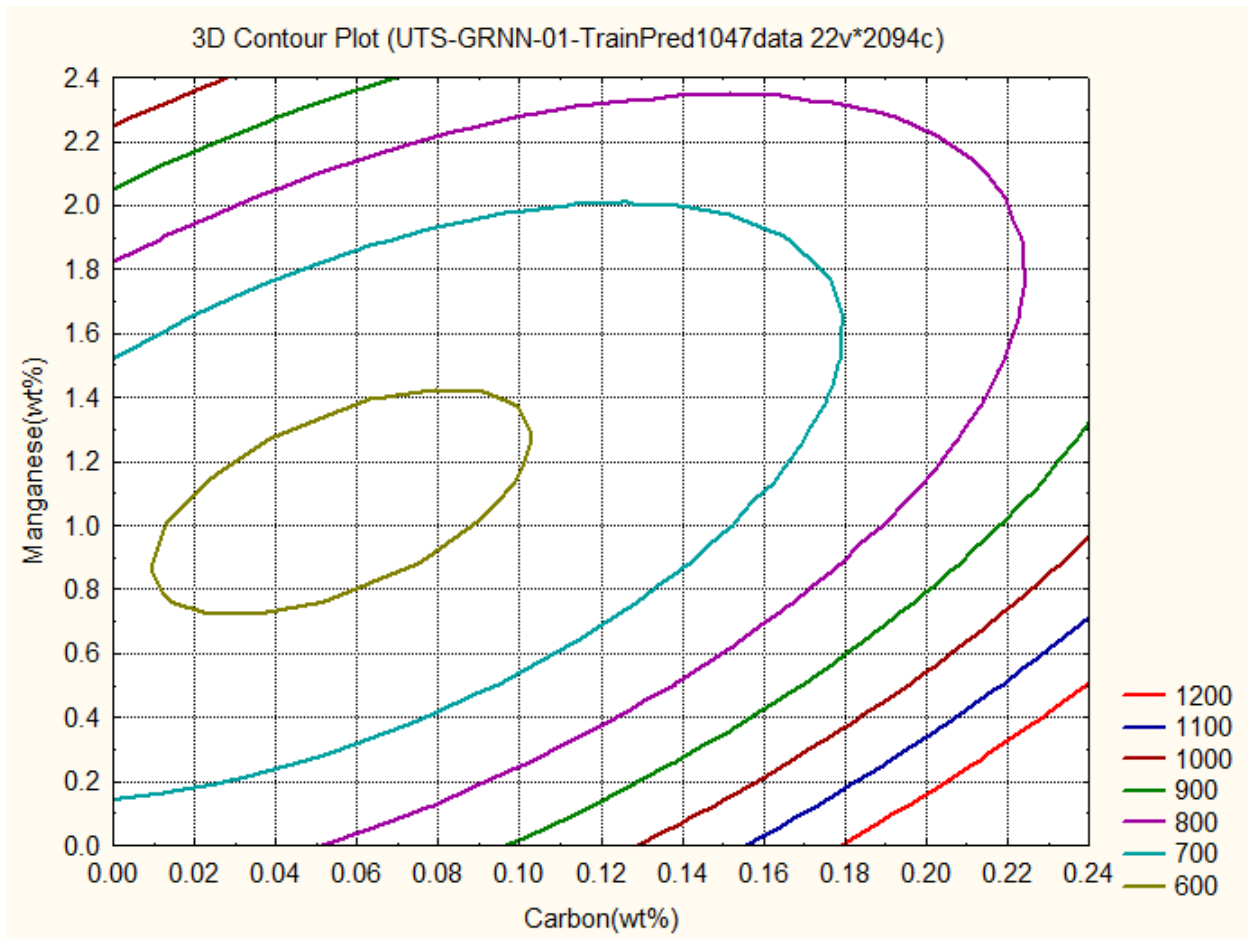


Figure.4.6.2 Predicted variations in Ultimate Tensile Strength (MPa) as a function of the Carbon and Manganese concentrations

3D contour Plot gives the relations between the **two input variables** and **one output variable**. **Figure.4.6.2** shows the relations between Carbon, **Manganese** and Ultimate Tensile Strength by **GRNN**. The graph gives the information about how these two, Carbon and **Manganese** control the Ultimate Tensile Strength from 600MPa to 1200 MPa.

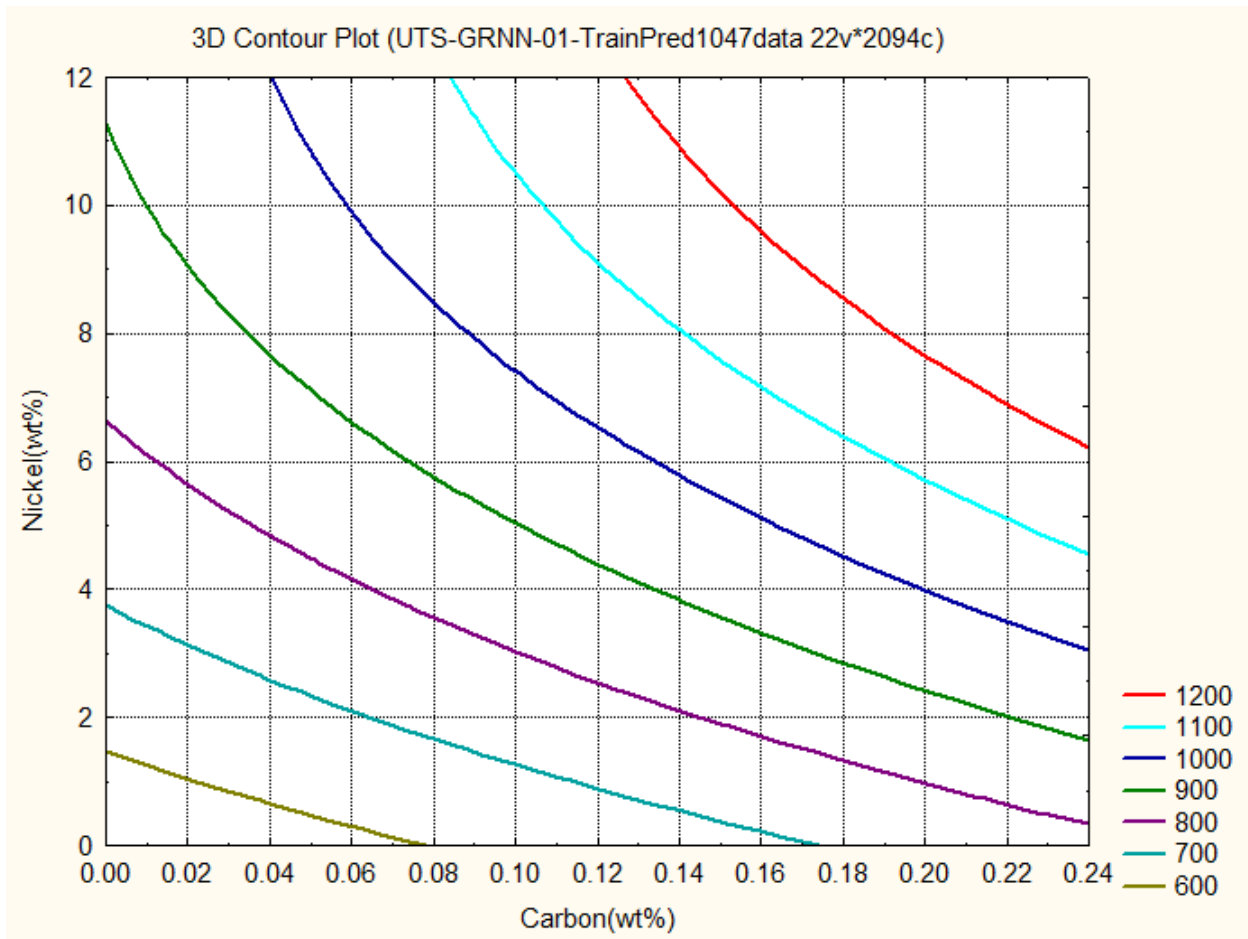


Figure.4.6.3 Predicted variations in Ultimate Tensile Strength (MPa) as a function of the Carbon and Nickel concentrations

3D contour Plot gives the relations between the **two input variables** and **one output variable**. **Figure.4.6.3** shows the relations between Carbon, Nickel and Ultimate Tensile Strength by **GRNN**. The graph gives the information about how these two, Carbon and Nickel control the Ultimate Tensile Strength from 600MPa to 1200 MPa.

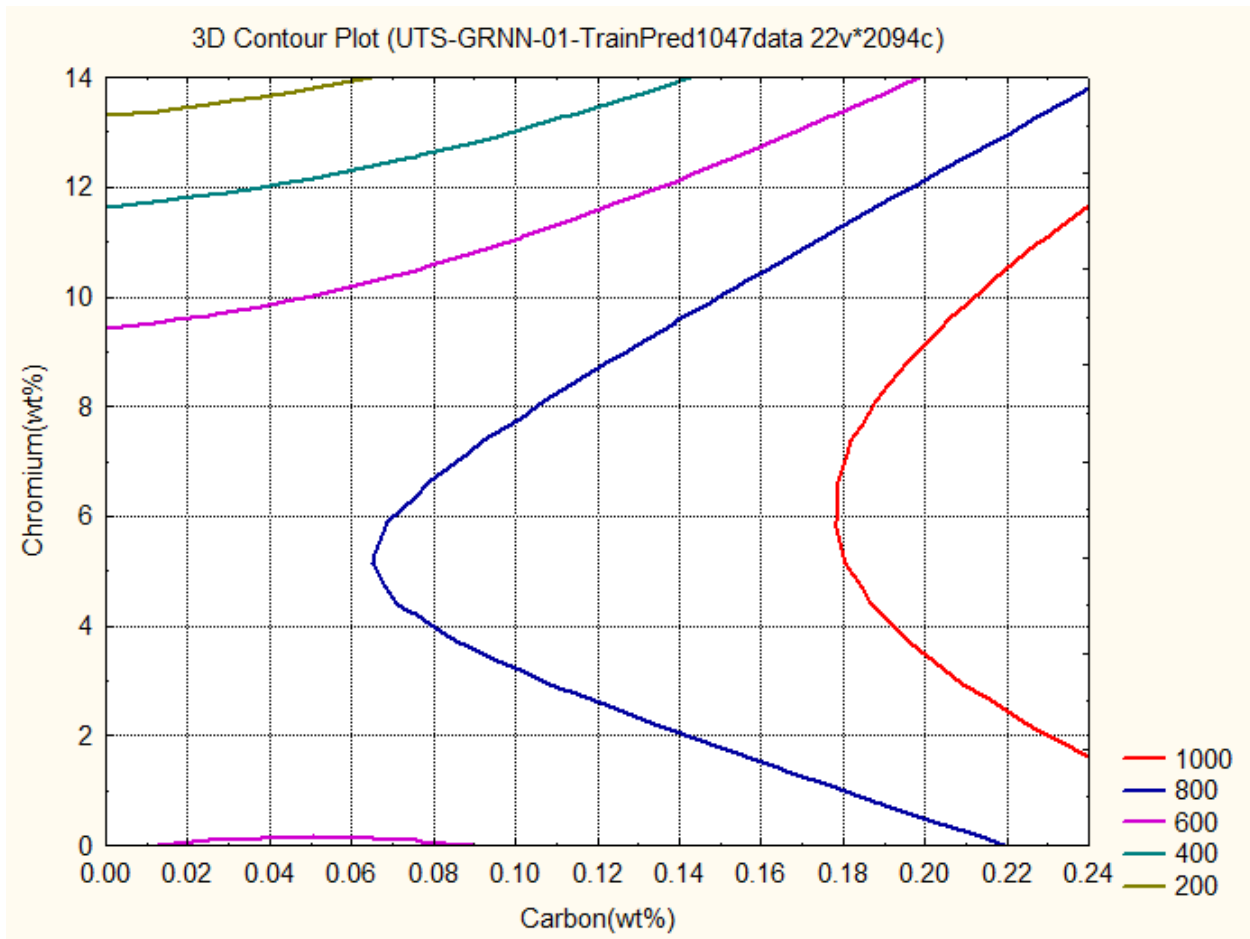


Figure.4.6.4 Predicted variations in Ultimate Tensile Strength (MPa) as a function of the Carbon and Chromium concentrations

3D contour Plot gives the relations between the **two input variables** and **one output variable**. **Figure.4.6.4** shows the relations between Carbon, Chromium and Ultimate Tensile Strength by **GRNN**. The graph gives the information about how these two, Carbon and Chromium control the Ultimate Tensile Strength from **200MPa to 1000MPa**.

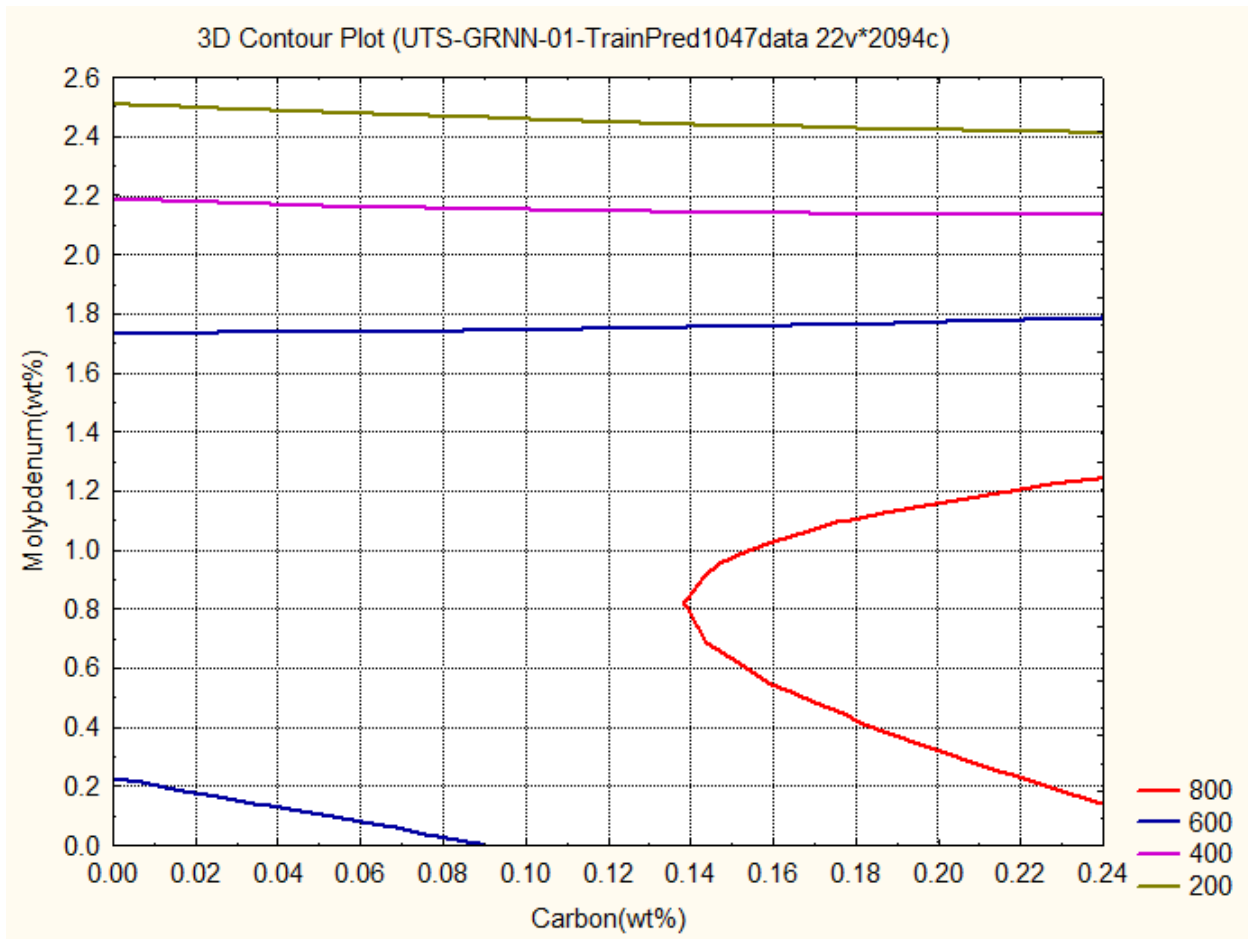


Figure.4.6.5 Predicted variations in Ultimate Tensile Strength (MPa) as a function of the Carbon and Molybdenum concentrations

3D contour Plot gives the relations between the **two input variables** and **one output variable**. **Figure.4.6.5** shows the relations between Carbon, Molybdenum and Ultimate Tensile Strength by **GRNN**. The graph gives the information about how these two, Carbon and Molybdenum control the Ultimate Tensile Strength from 200MPa to 800MPa.

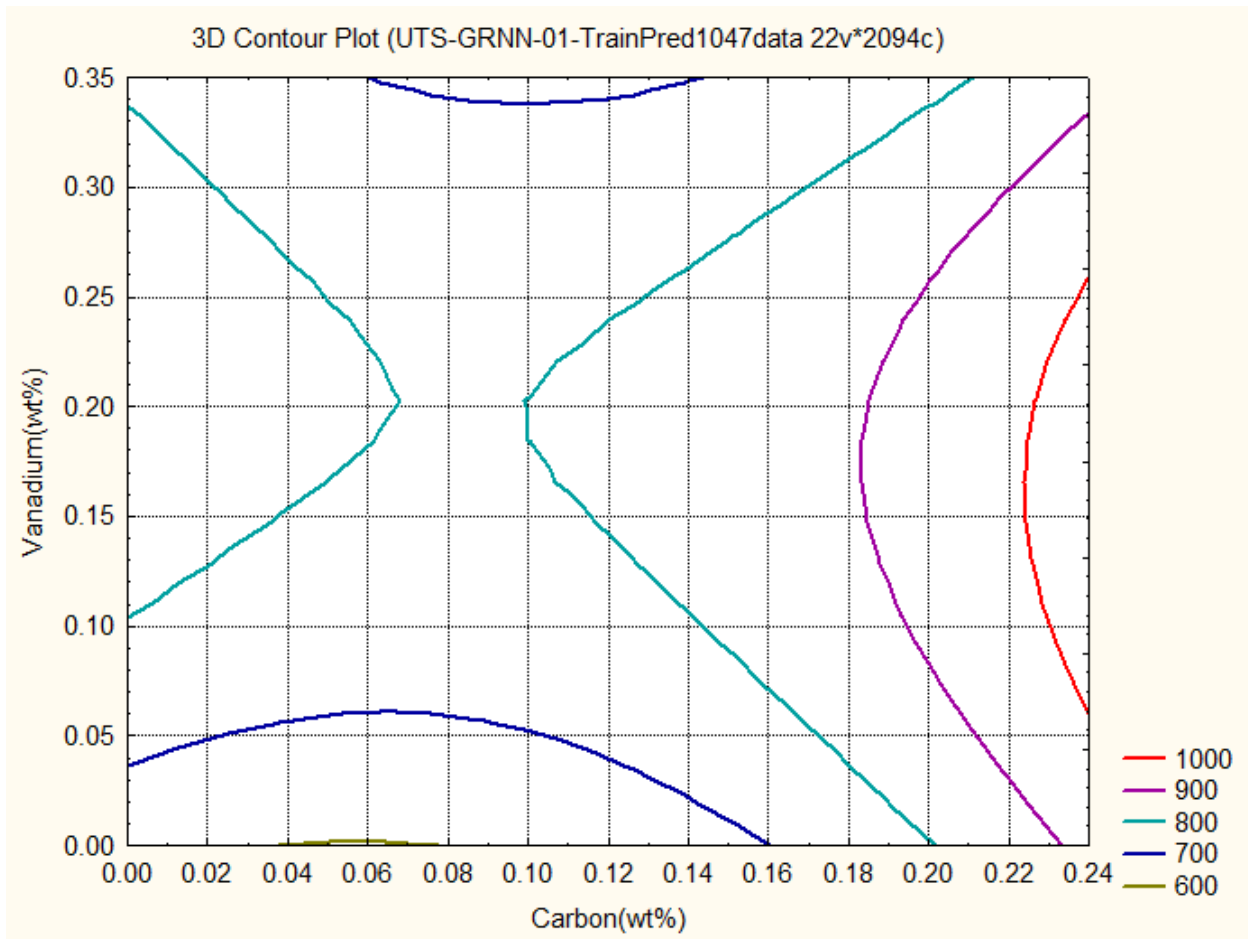


Figure.4.6.6 Predicted variations in Ultimate Tensile Strength (MPa) as a function of the Carbon and Vanadium concentrations

3D contour Plot gives the relations between the **two input variables** and **one output variable**. **Figure.4.6.6** shows the relations between Carbon, Vanadium and Ultimate Tensile Strength by **GRNN**. The graph gives the information about how these two, Carbon and Vanadium control the Ultimate Tensile Strength from 600MPa to 1000MPa.

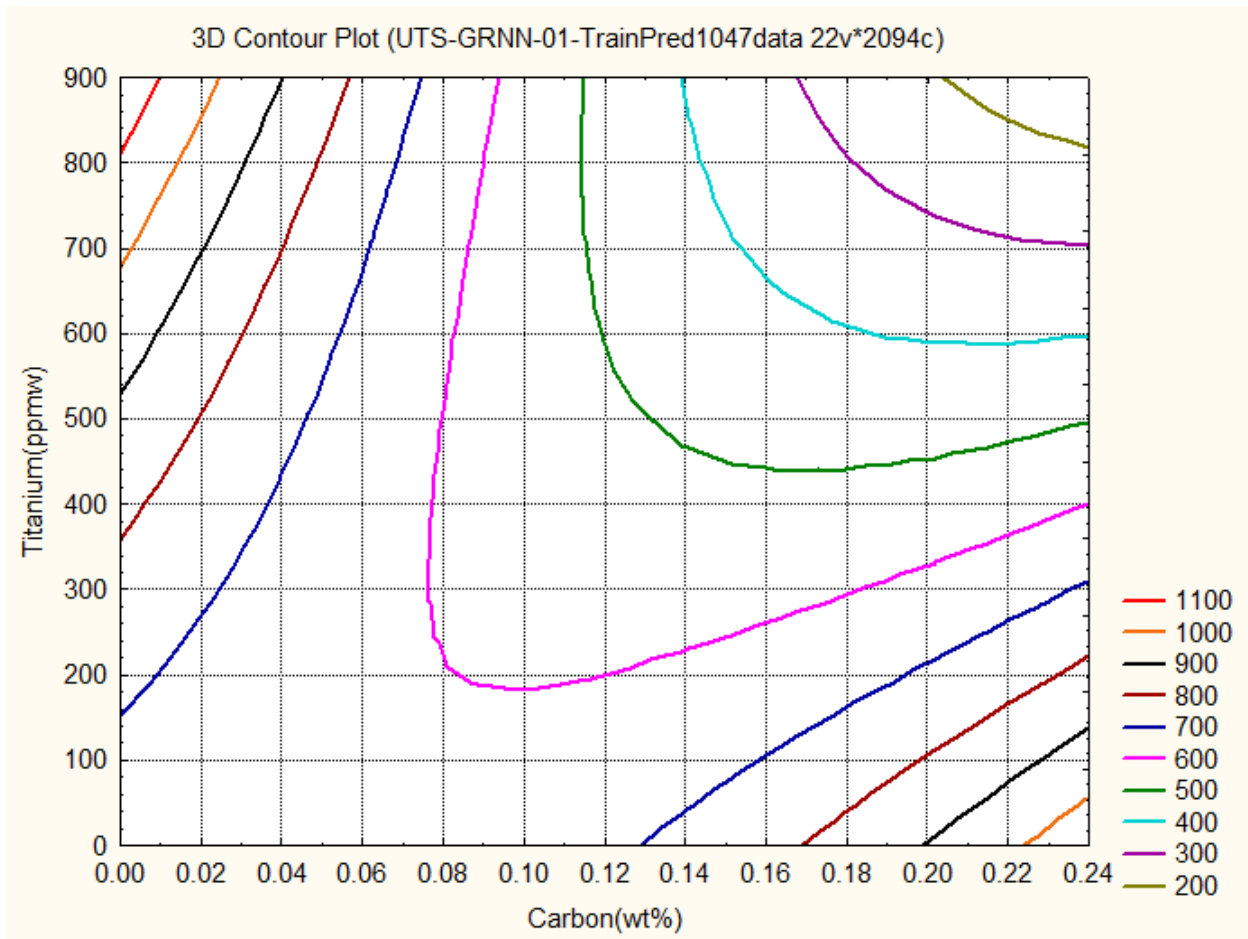


Figure.4.6.7 Predicted variations in Ultimate Tensile Strength (MPa) as a function of the Carbon and Titanium concentrations

3D contour Plot gives the relations between the **two input variables** and **one output variable**. **Figure.4.6.7** shows the relations between Carbon, Titanium and Ultimate Tensile Strength by **GRNN**. The graph gives the information about how these two, Carbon and Titanium control the Ultimate Tensile Strength from 200MPa to 1100MPa.

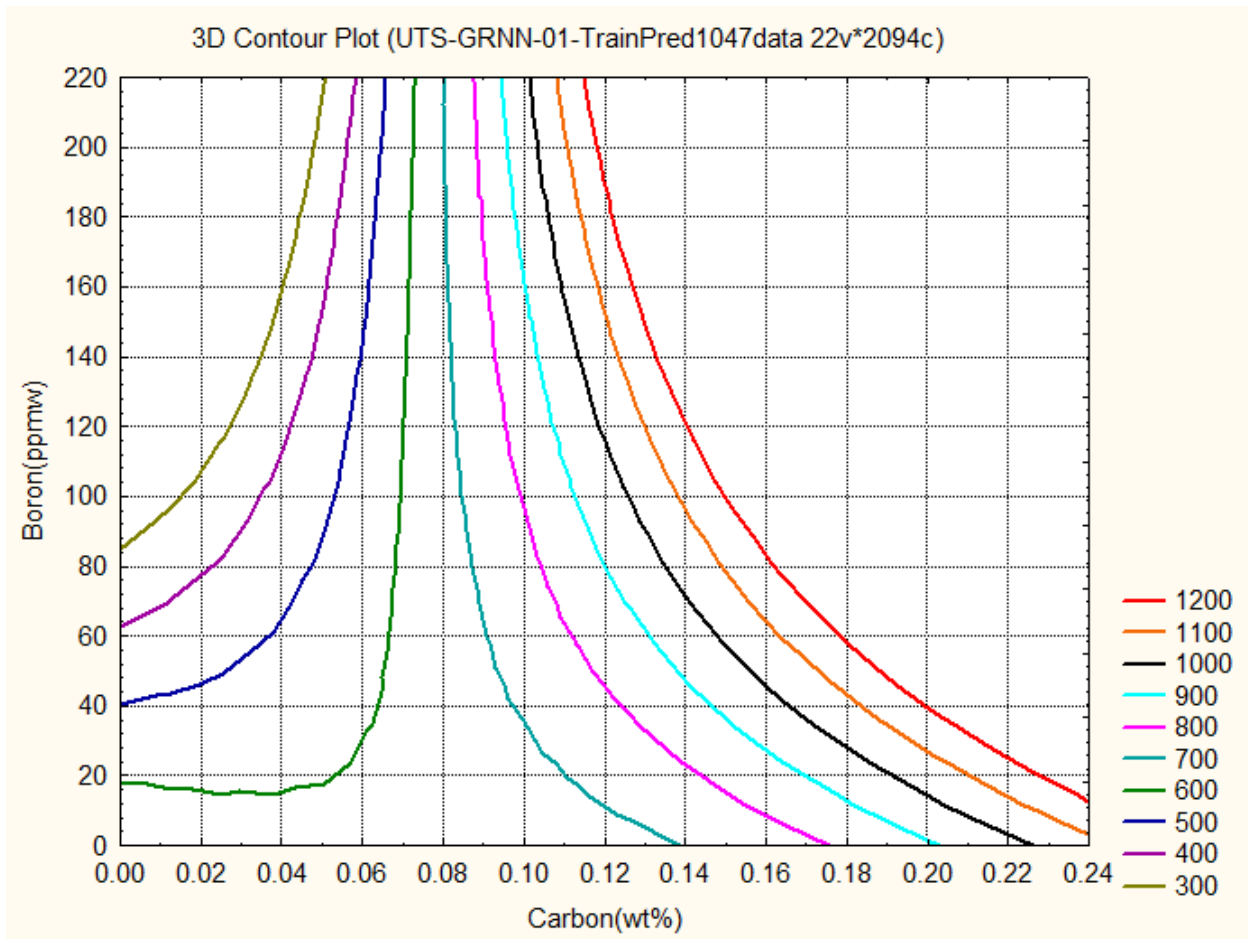


Figure.4.6.8 Predicted variations in Ultimate Tensile Strength (MPa) as a function of the Carbon and Boron concentrations

3D contour Plot gives the relations between the **two input variables** and **one output variable**. **Figure.4.6.8** shows the relations between Carbon, Boron and Ultimate Tensile Strength by **GRNN**. The graph gives the information about how these two, Carbon and Boron control the Ultimate Tensile Strength from 300MPa to 1200MPa.

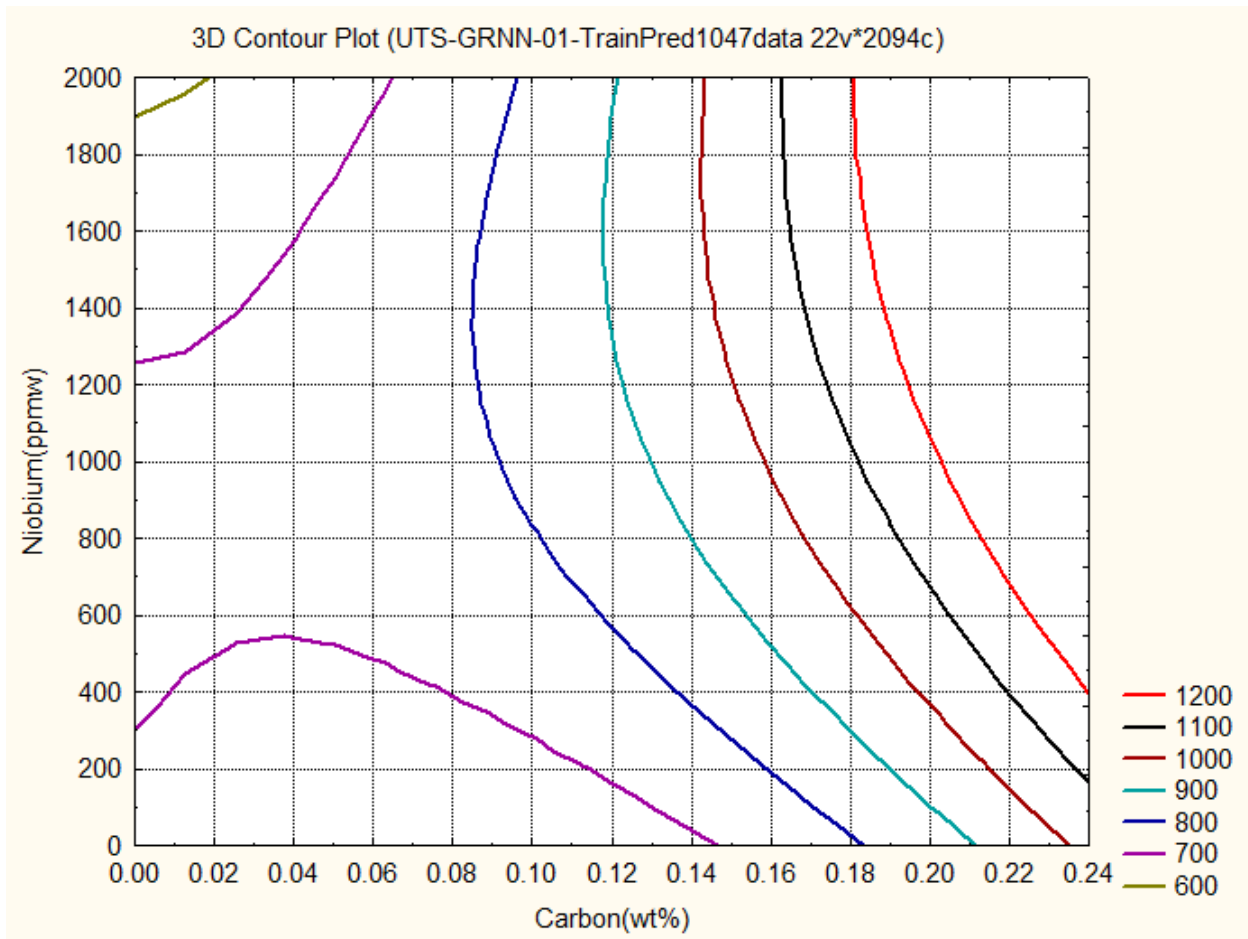


Figure.4.6.9 Predicted variations in Ultimate Tensile Strength (MPa) as a function of the Carbon and Niobium concentrations

3D contour Plot gives the relations between the **two input variables** and **one output variable**. **Figure.4.6.9** shows the relations between Carbon Niobium and Ultimate Tensile Strength by **GRNN**. The graph gives the information about how these two, Carbon and Niobium control the Ultimate Tensile Strength from 600MPa to 1200MPa.

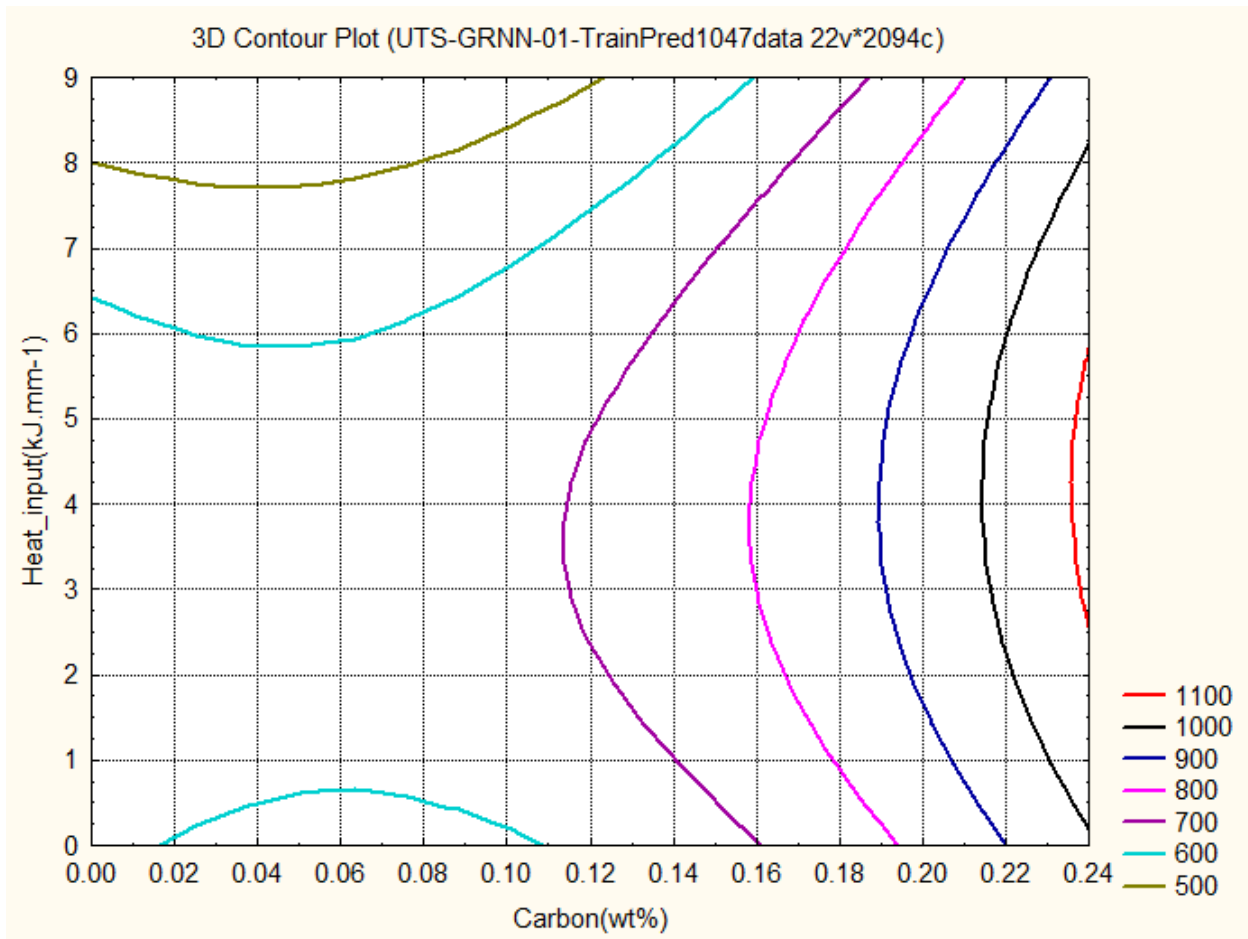


Figure.4.6.10 Predicted variations in Ultimate Tensile Strength (MPa) as a function of the Carbon concentration and Heat input

3D contour Plot gives the relations between the **two input variables** and **one output variable**. **Figure.4.6.10** shows the relations between Carbon Heat input and Ultimate Tensile Strength by **GRNN**. The graph gives the information about how these two, Carbon and Heat input control the Ultimate Tensile Strength from 500MPa to 1100MPa.

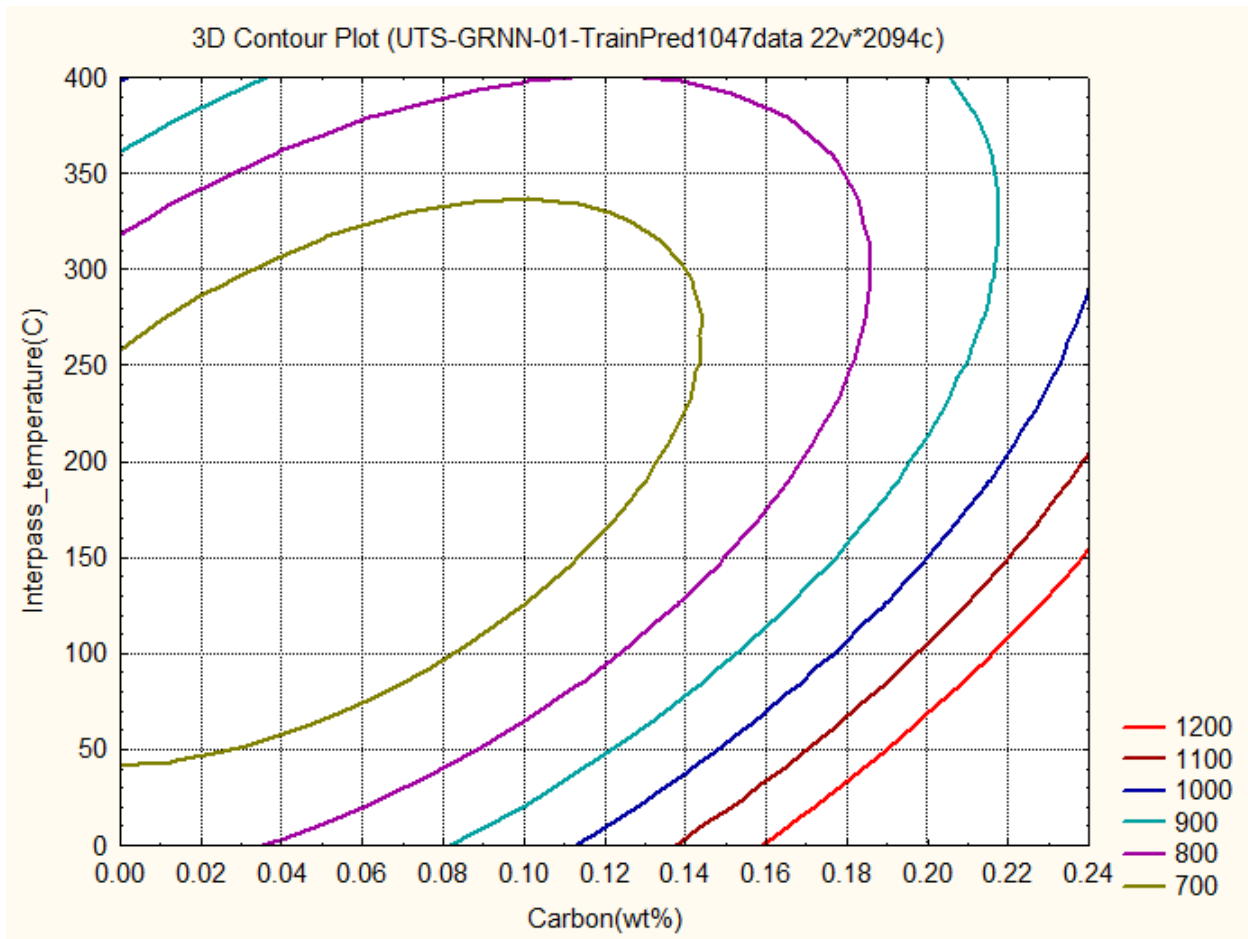


Figure.4.6.11 Predicted variations in Ultimate Tensile Strength (MPa) as a function of the Carbon concentration and Interpass temperature

3D contour Plot gives the relations between the **two input variables** and **one output variable**. **Figure.4.6.11** shows the relations between Carbon, Interpass temperature and Ultimate Tensile Strength by **GRNN**. The graph gives the information about how these two, Carbon and Interpass temperature control the Ultimate Tensile Strength from 700MPa to 1200MPa.

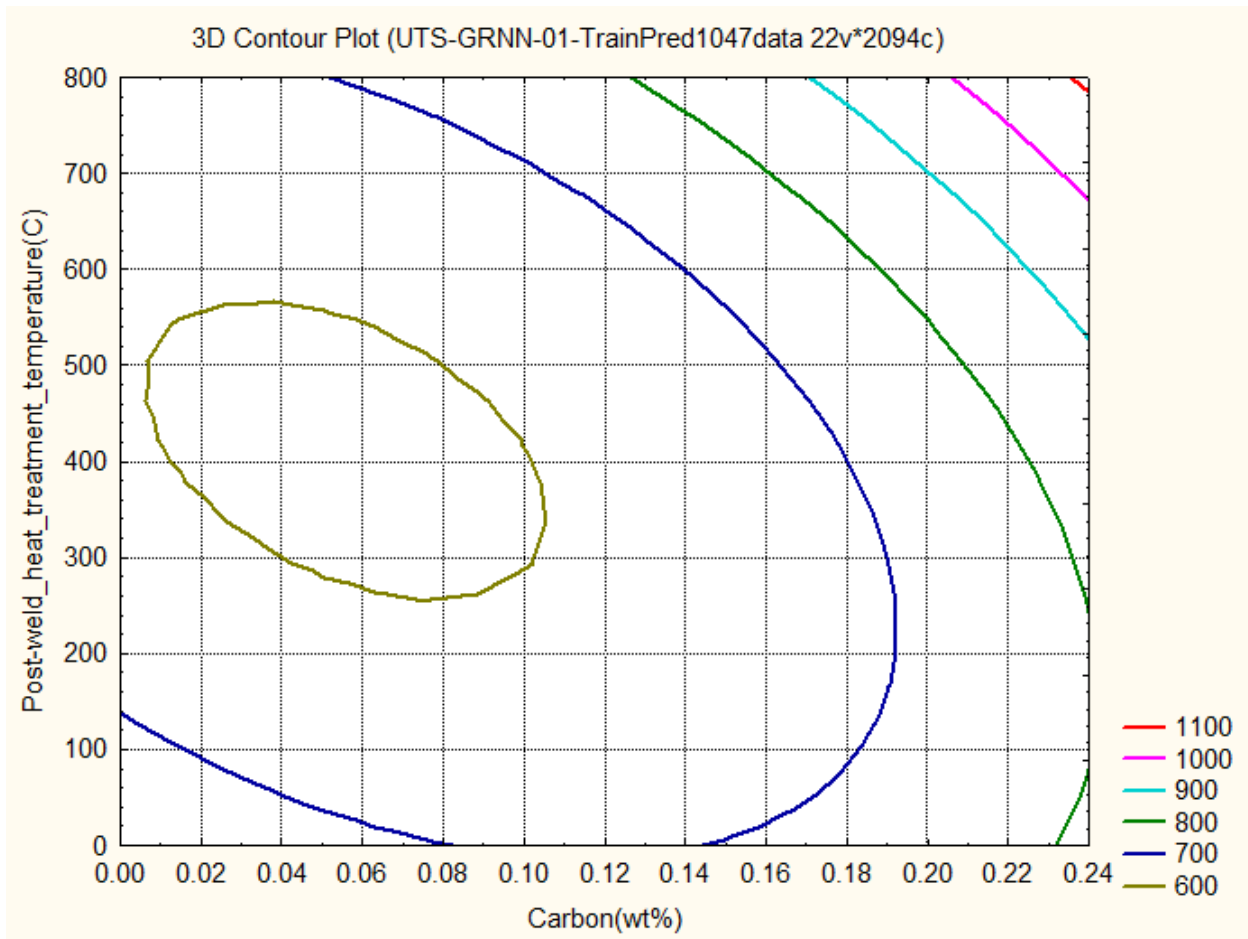


Figure.4.6.12 Predicted variations in Ultimate Tensile Strength (MPa) as a function of the Carbon concentration and Post-weld heat treatment temperature

3D contour Plot gives the relations between the **two input variables** and **one output variable**. **Figure.4.6.12** shows the relations between Carbon, Post-weld heat treatment temperature and Ultimate Tensile Strength by **GRNN**. The graph gives the information about how these two, Carbon and Post-weld heat treatment temperature control the Ultimate Tensile Strength from 600MPa to 1100MPa.

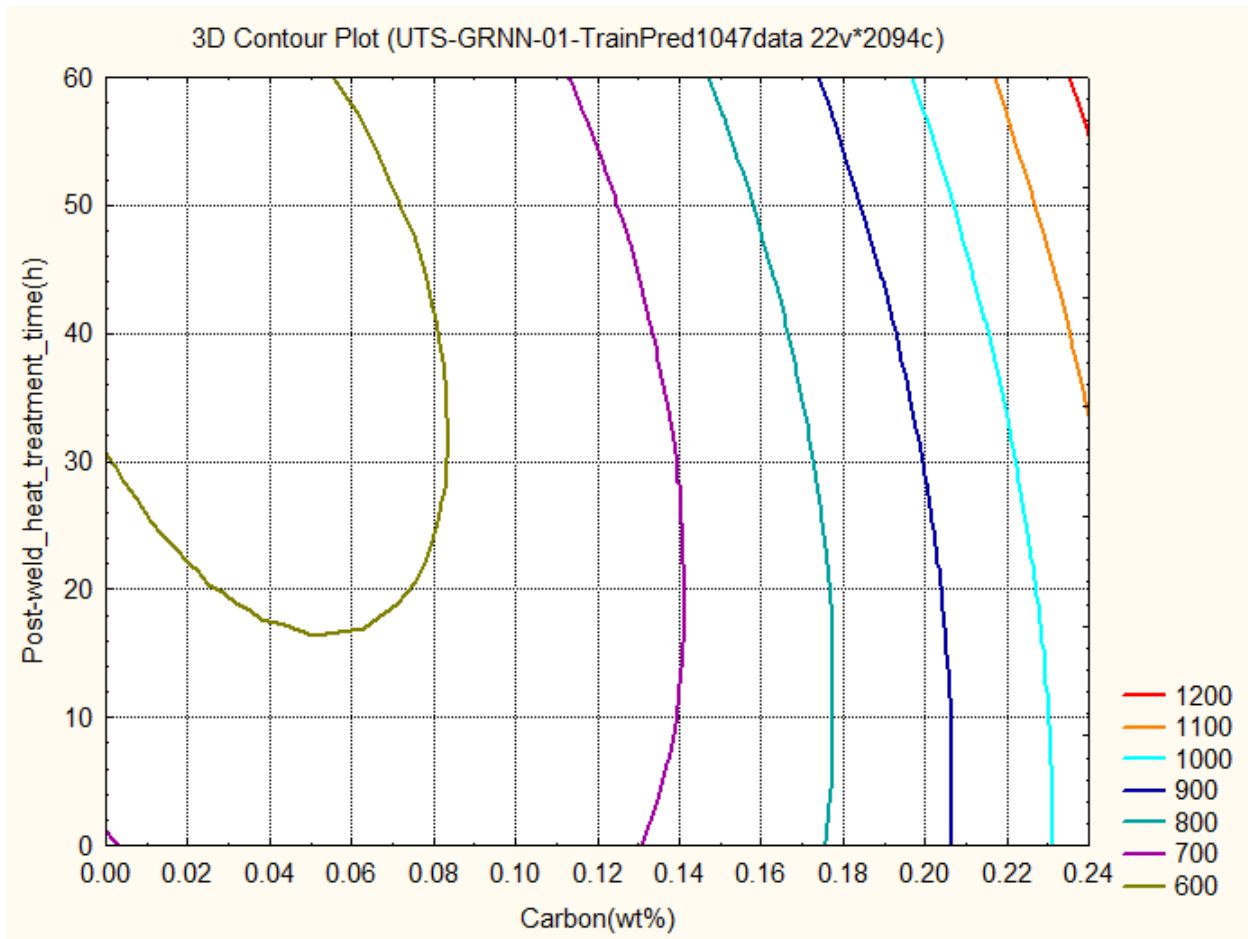


Figure.4.6.13 Predicted variations in Ultimate Tensile Strength (MPa) as a function of the Carbon concentration and Post-weld heat treatment time

3D contour Plot gives the relations between the **two input variables** and **one output variable**. **Figure.4.6.13** shows the relations between Carbon, Post-weld heat treatment time and Ultimate Tensile Strength by **GRNN**. The graph gives the information about how these two, Carbon and Post-weld heat treatment time control the Ultimate Tensile Strength from 600MPa to 1200MPa.

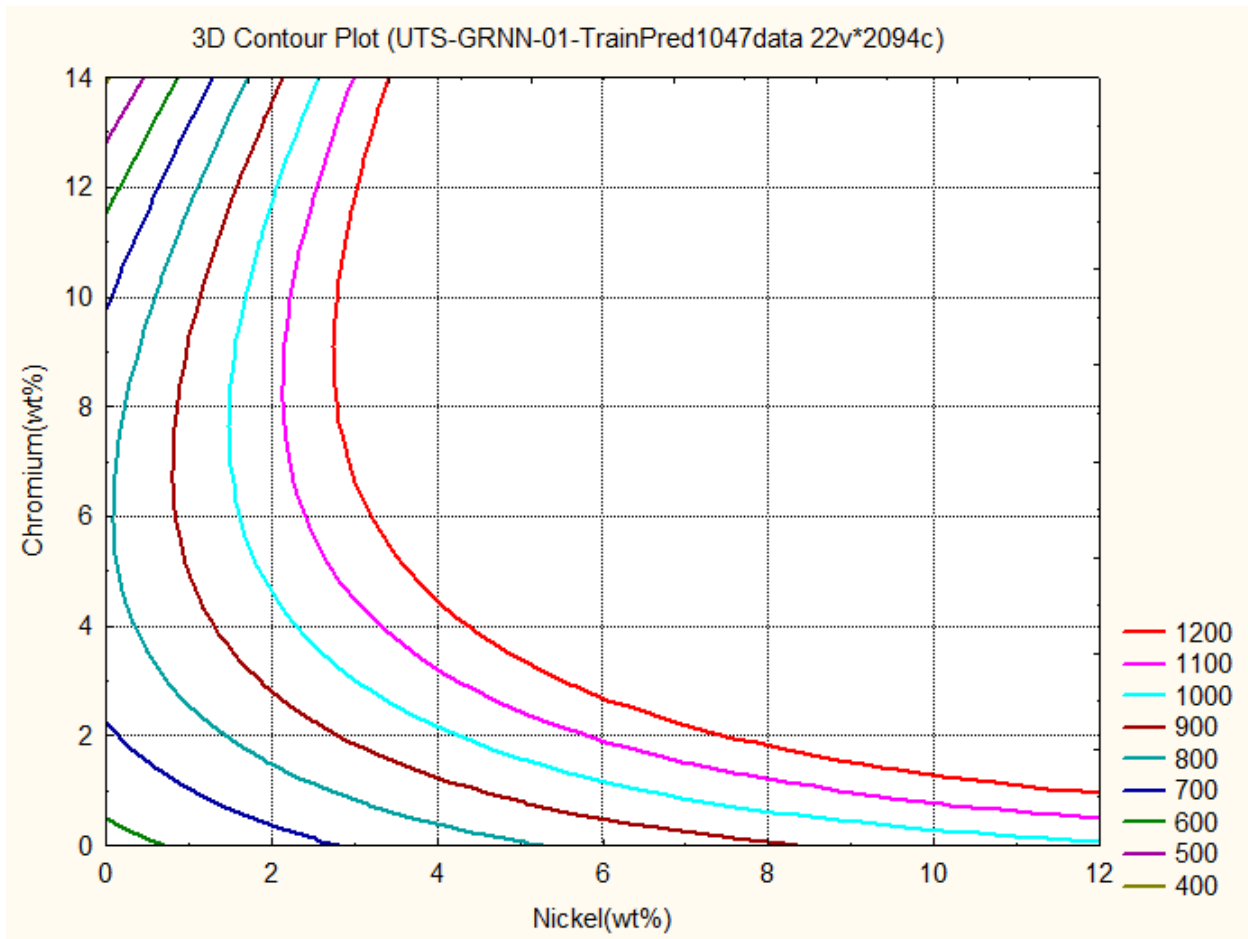


Figure.4.6.14 Predicted variations in Ultimate Tensile Strength (MPa) as a function of the Nickel and Chromium concentrations

3D contour Plot gives the relations between the **two input variables** and **one output variable**. **Figure.4.6.14** shows the relations between Nickel, Chromium and Ultimate Tensile Strength by **GRNN**. The graph gives the information about how these two, Nickel and Chromium control the Ultimate Tensile Strength from **400MPa to 1200MPa**

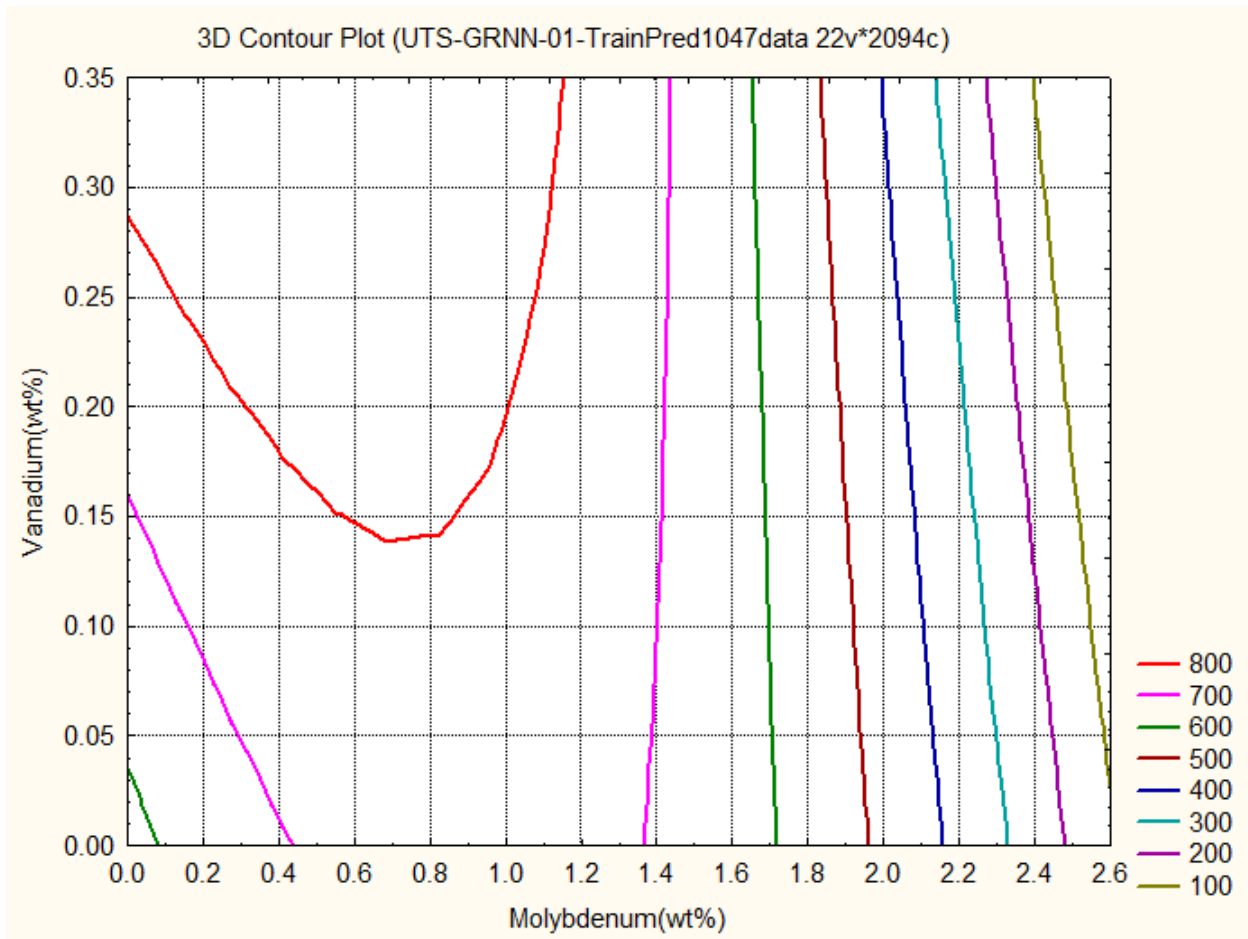


Figure.4.6.15 Predicted variations in Ultimate Tensile Strength (MPa) as a function of the Molybdenum and Vanadium concentrations

3D contour Plot gives the relations between the **two input variables** and **one output variable**. **Figure.4.6.15** shows the relations between Molybdenum, Vanadium and Ultimate Tensile Strength by **GRNN**. The graph gives the information about how these two, Molybdenum and Vanadium control the Ultimate Tensile Strength from 100MPa to **800MPa**

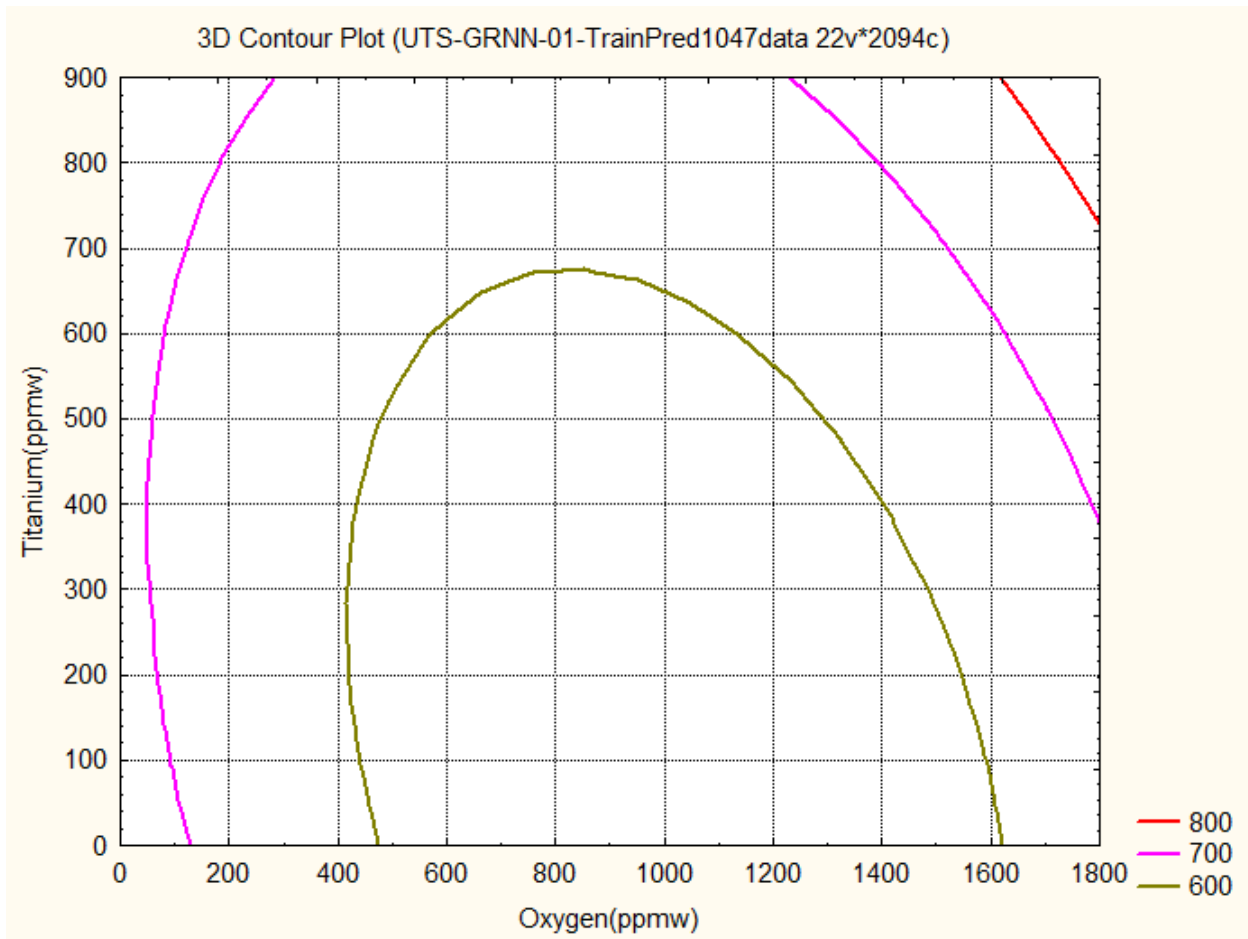


Figure.4.6.16 Predicted variations in Ultimate Tensile Strength (MPa) as a function of the Oxygen and Titanium concentrations

3D contour Plot gives the relations between the **two input variables** and **one output variable**. **Figure.4.6.16** shows the relations between Oxygen, Titanium and Ultimate Tensile Strength by **GRNN**. The graph gives the information about how these two, Oxygen and Titanium control the Ultimate Tensile Strength from 600MPa to 800MPa.

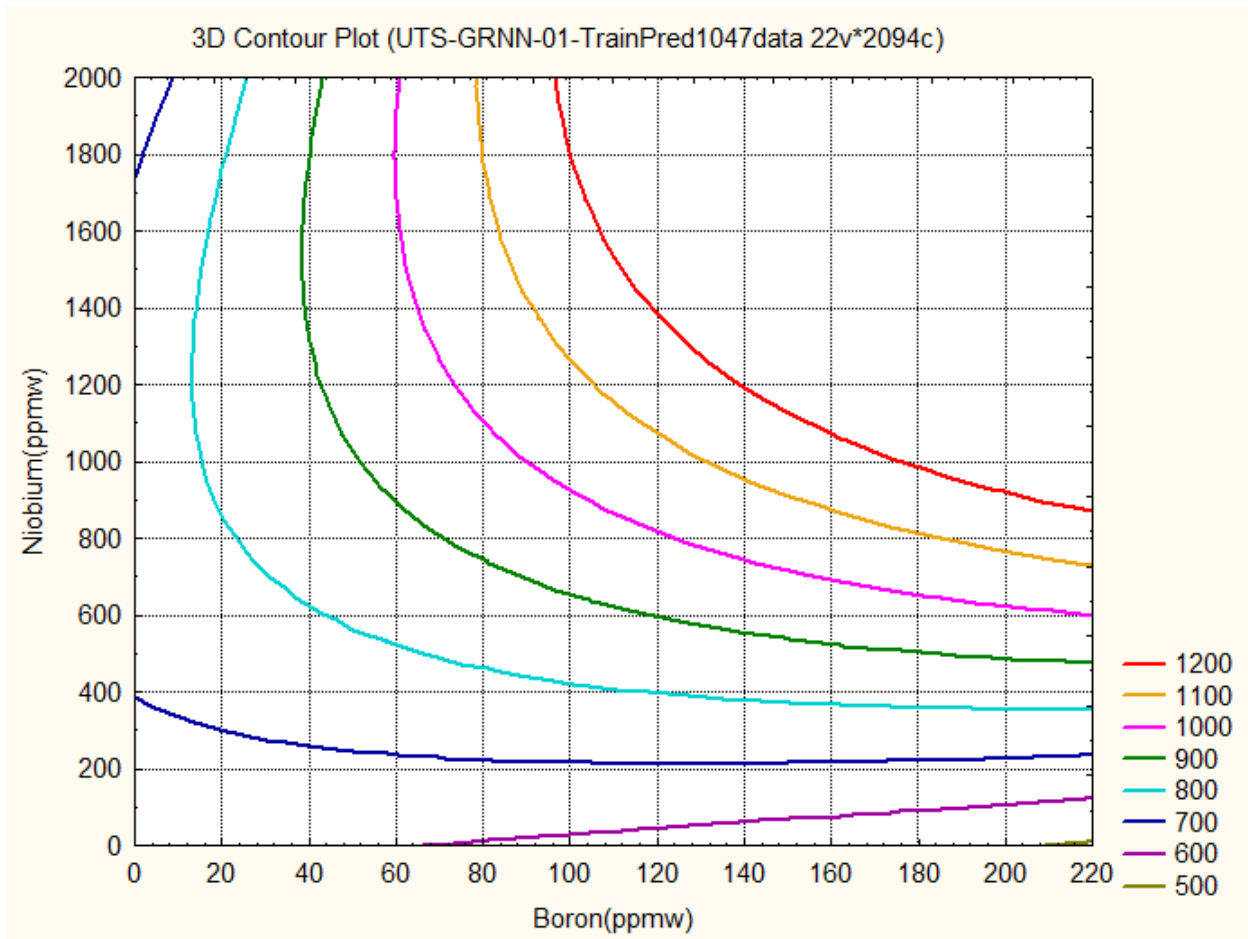


Figure.4.6.17 Predicted variations in Ultimate Tensile Strength (MPa) as a function of the Boron and Niobium concentrations

3D contour Plot gives the relations between the **two input variables** and **one output variable**. **Figure.4.6.17** shows the relations between Boron, Niobium and Ultimate Tensile Strength by **GRNN**. The graph gives the information about how these two, Boron and Niobium control the Ultimate Tensile Strength from 500MPa to 1200MPa.

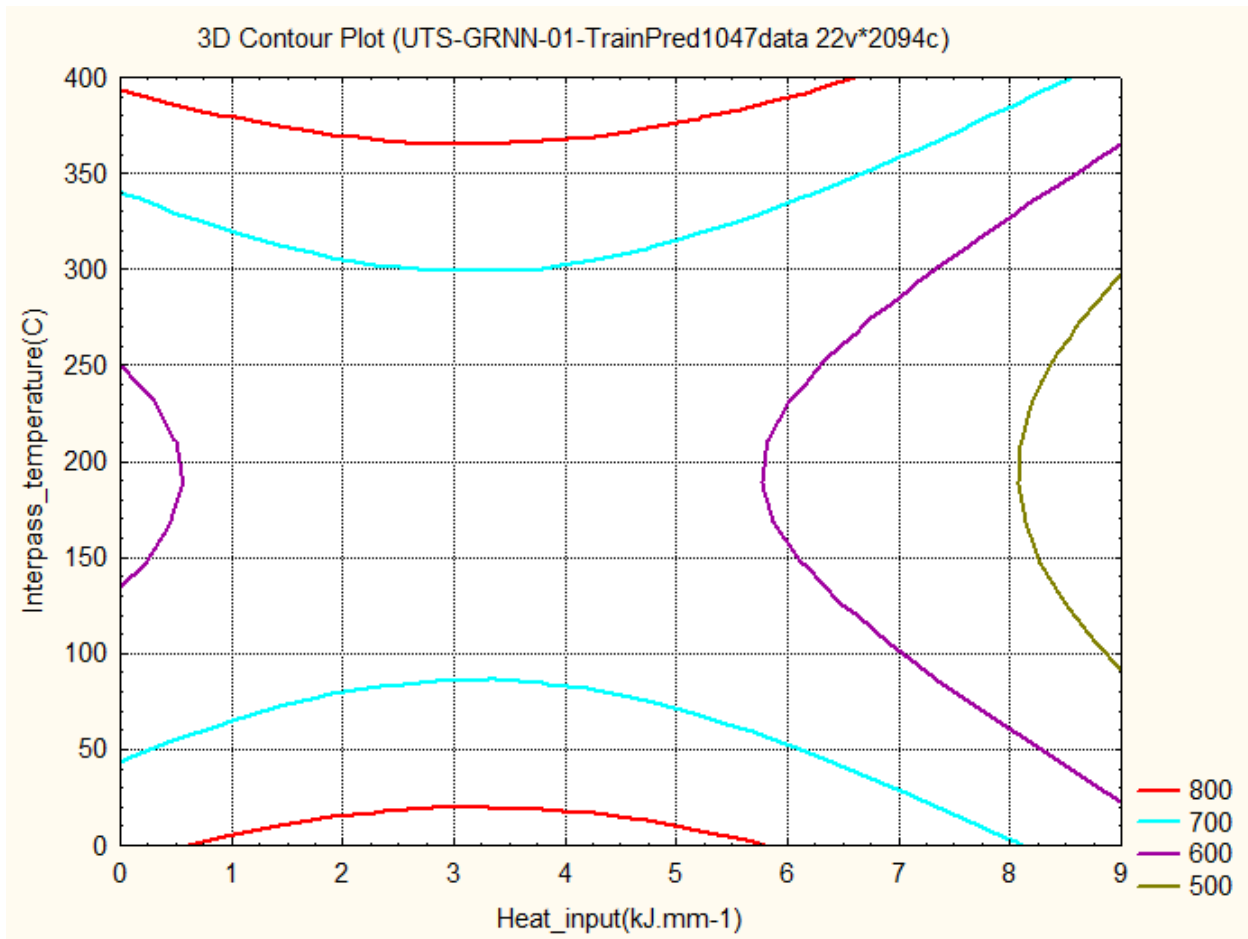


Figure.4.6.18 Predicted variations in Ultimate Tensile Strength (MPa) as a function of the Heat input and Interpass temperature

3D contour Plot gives the relations between the **two input variables** and **one output variable**. **Figure.4.6.18** shows the relations between the Heat input, Interpass temperature and Ultimate Tensile Strength by **GRNN**. The graph gives the information about how these two, the Heat input and Interpass temperature control the Ultimate Tensile Strength from **500MPa to 800MPa**.

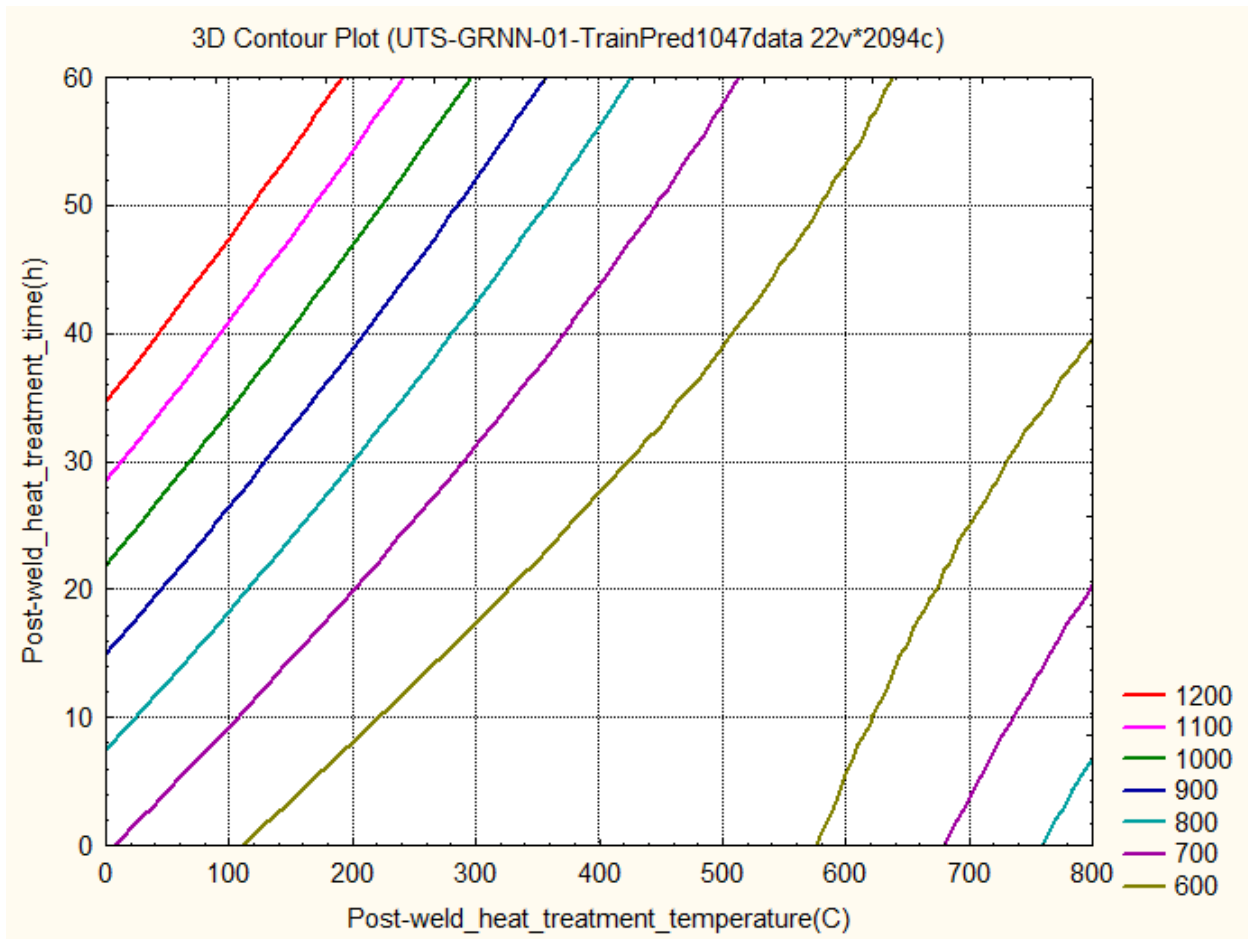


Figure.4.6.19 Predicted variations in Ultimate Tensile Strength (MPa) as a function of the Post-weld heat treatment temperature and Post-weld heat treatment time

3D contour Plot gives the relations between the **two input variables** and **one output variable**. **Figure.4.6.19** shows the relations between the Post-weld heat treatment temperature, Post-weld heat treatment time and Ultimate Tensile Strength by **GRNN**. The graph gives the information about how these two, the Post-weld heat treatment temperature and Post-weld heat treatment time control the Ultimate Tensile Strength from 600MPa to 1200MPa.

Figure 4.6.1. UTS (z) - Si (y) - C (x) 3D plot.

Figure 4. 6.1. shows the increase in the Ultimate Tensile Strength from 700 MPa to 1200 MPa with increase in the concentration of both Carbon and Silicon. The increase in the Ultimate Tensile Strength is also achieved by keeping Carbon constant and Silicon concentration varies and vice versa. The contour of Ultimate Tensile Strength 700 MPa has a wt% Carbon in range from 0.116% to 0.144% and wt% Silicon in the range from 0.8% to 1.18%. The trends of the both independent variables are not simple, but more flexible for designing the Ultimate Tensile Strength in wide range as shown in the plot from less than 700 MPa to 1200 MPa.

Figure 4.6.2. UTS (z) - Mn (y) - C (x) 3D plot.

Figure 4. 6.2. shows the contour of Ultimate Tensile Strength 600 MPa with the Carbon in the range from 0.01% to 0.104% and the Manganese in the range from 0.72% to 1.44%. The increase in the Ultimate Tensile Strength is achieved outside the 600 MPa contour by keeping Manganese constant and Carbon concentration varies and vice versa. The concentration of %C and %Mn give the Ultimate Tensile Strength in wide range from less than 600MPa to 1200 MPa. The trends of both the independent variables are less complex and flexible for designing the Ultimate Tensile Strength.

Figure 4. 6.3. UTS (z) - Ni (y) - C (x) 3D plot.

Figure 4. 6.3. shows the increase in the Ultimate Tensile Strength from 600 MPa to 1200 MPa with an increase in the concentrations of both Carbon and Nickel. The increase in the Ultimate Tensile Strength is also achieved by keeping Carbon constant and Nickel concentration varies and vice versa. The higher value of Ultimate Tensile Strength 1200 MPa is obtained with %wt C in the range from 0.128% to 0.24% and %wt Ni in the range from 6.4% to 12%. The trends of both the independent variables are less complex and flexible for designing the Ultimate Tensile Strength.

Figure 4. 6.4. UTS (z) - Cr (y) - C (x) 3D plot.

Figure 4. 6.4. shows the increase in the Ultimate Tensile Strength from 800 MPa to more than 1000 MPa with the increase and decrease in the concentrations Chromium from 0% to 13.8% and the increase in concentrations of Carbon from 0.065% to 0.24%. The Chromium in the

range from 9.4% to 14% and Carbon in the range from 0% to 0.198% decrease the Ultimate Tensile Strength from 600MPa to less than 200 MPa. The Ultimate Tensile Strength

800MPa is obtained with %wt C in the range from 0.066% to 0.24% and %wt Cr in the range from 0% to 14%. The Ultimate Tensile Strength 1000 MPa and higher are obtained with %wt C in the range from 0.179% to 0.24% and %wt Cr in the range from 1.70% to 11.6%. The independent variables Carbon and Chromium both have a wide range for designing the Ultimate Tensile Strength between 600 MPa to 800 MPa. The trends of both the independent variables are complex for designing the Ultimate Tensile Strength 1000 MPa and higher.

Figure 4. 6.5. UTS (z) - Mo (y) - C (x) 3D plot

Figure 4. 6.5. shows the Ultimate Tensile Strength 600 MPa and higher are obtained with %wt C in the range from 0% to 0.24% and %wt Mo in the range from 0% to 1.8%. The Ultimate Tensile Strength 800 MPa and higher are obtained with %wt C in the range from 0.14% to 0.24% and %wt Mo in the range from 0.16% to 1.25%. The content of %wt Mo more than 1.8% and %wt C in the range from 0% to 0.24% decrease the Ultimate Tensile Strength from 600 MPa to less than 200 MPa. The trends of both the independent variables are complex for designing the Ultimate Tensile Strength with a wide range of combinations available.

Figure 4.6.6 UTS (z) - V (y) - C (x) 3D plot

Figure 4.6.6. shows the Ultimate Tensile Strength values 800 MPa and more than 800MPa are observed in the left side and right side of the graph. Right side of the graph has almost full range of the Vanadium from 0% to 0.35% and the Carbon from 0.1% to 0.24%. Left side of the graph has the range of Vanadium from 0.101% to 0.335% and the Carbon from 0% to 0.066%. The Ultimate Tensile Strength 900MPa and higher are obtained with the range of %wt V from 0% to 0.35% and by maintaining the Carbon, in the range from 0.184% to 0.24%. The Ultimate Tensile Strength 1000MPa and higher are obtained with the range of %wt V from 0.065% to 0.26% and the %wt C in the range from 0.224% to 0.24%. The Upper side and bottom side of the plot show the contours of the decrease in the Ultimate Tensile Strength from 700MPa and less than 700MPa. Both the independent variables have a complex relationship with the Ultimate Tensile Strength. The trends of the independent variables is significant for designing the Ultimate Tensile Strength.

Figure 4. 6.7. UTS (z) - Ti (y) - C (x) 3D plot

Figure 4. 6.7 shows the decrease in the Ultimate Tensile Strength from 600 MPa to 200 MPa with an increase in the concentration of both Carbon and Titanium. The Ultimate Tensile Strength 700 MPa and more than 1100 MPa are obtained with %wt C in the range from 0% to 0.074% and Titanium ppm in the range from 160 ppm to 900 ppm. The Ultimate Tensile Strength 700 MPa and more than 1000 MPa are also achieved with %wt C in the range from 0.129% to 0.24% and Titanium ppm in the range from 0 ppm to 310 ppm. Selection of these two independent variables is very important for the design of the Ultimate Tensile Strength. Because both the independent variables have a nonlinear complex relationship with the Ultimate Tensile Strength.

Figure 4. 6.8. UTS (z) - B (y) - C (x) 3D plot

Figure 4. 6.8 shows the contours of the Ultimate Tensile Strength increase from 300 MPa to 1200 MPa with an increase in wt% C in the range from 0% to 0.24% and Boron ppm in the range from 0 ppm to 220 ppm. The increase in the Ultimate Tensile Strength is achieved by keeping Boron ppm constant and Carbon concentration varies in the range from 0% to 0.24%. The increase Ultimate Tensile Strength is obtained by maintaining the increase wt% C and the constant Boron ppm and vice versa. The trends of both the independent variables are not complex for designing the Ultimate Tensile Strength.

Figure 4. 6.9 UTS (z) - Nb (y) - C (x) 3D plot

Figure 4. 6.9 shows the increase in the Ultimate Tensile Strength from 800 MPa to 1200 MPa with an increase in the concentration of both Carbon and Niobium. The Ultimate Tensile Strength 800 MPa and more than 1200 MPa are obtained with %wt C in the range from 0.086% to 0.24%C and Niobium ppm in the range from 0 ppm to 2000 ppm. In this range 800 MPa to 1200 MPa is obtained by keeping the Nb ppm constant and varying the wt% of Carbon. The decrease in the Ultimate Tensile Strength from less than 700 MPa to less than 700 MPa are obtained with %wt C less than 0.146% and Niobium ppm in the range from 0 ppm to 560 ppm at bottom contour of 700 MPa. The decrease in the Ultimate Tensile Strength from less than 700 MPa to 600 MPa are obtained with %wt C less than 0.064% and Niobium ppm in the range from 1260 ppm to 2000 ppm at upper left corner of the graph. Both the independent variables have a

complex relationship with the Ultimate Tensile Strength. The trends of the independent variables are significant for designing the Ultimate Tensile Strength.

Figure 4. 6.10 UTS (z) - HI (y) - C (x) 3D plot

Figure 4. 6.10 shows the increase in the Ultimate Tensile Strength from 700 MPa to 1100 MPa with an increase in the concentration of both Carbon and Heat input. The Ultimate Tensile Strength 700 MPa and more than 1100 MPa are obtained with %wt C in the range from 0.114% to 0.24%C and Heat input kJmm⁻¹ in the range from 0 kJmm⁻¹ to 9 kJmm⁻¹. In this range 700 MPa to 1000 MPa is obtained by keeping the Heat input constant and varying the wt% of Carbon. But for the Ultimate Tensile Strength 1100 MPa and higher is obtained with the Heat input in the range from 2.6 kJmm⁻¹ to 5.7 kJmm⁻¹ and the wt% C in the range from 0.236% to 0.24%. The decrease in the Ultimate Tensile Strength from less than 700 MPa to less than 500 MPa are obtained with %wt C less than 0.114% and the Heat input in the range from 0 kJmm⁻¹ to 9 kJmm⁻¹. Both the independent variables have a complex relationship with the Ultimate Tensile Strength. The trends of the independent variables are significant for designing the Ultimate Tensile Strength.

Figure 4. 6.11 UTS (z) - IPT (y) - C (x) 3D plot

Figure 4. 6.11 shows the contour of Ultimate Tensile Strength 700 MPa with the Carbon in the range from 0% to 0.146% and the Interpass temperature in the range from 45 C to 330 C. The increase in the Ultimate Tensile Strength is achieved outside the 700 MPa contour by keeping Interpass temperature constant and increasing Carbon concentration. The decrease in the Ultimate Tensile Strength is achieved outside the 700 MPa contour by keeping Carbon concentration constant and increasing the Interpass temperature. The concentration of the Carbon and the Interpass temperature combinations give the Ultimate Tensile Strength in wide range from less than 700MPa to 1200 MPa. The trends of both the independent variables are a complex and flexible for designing the Ultimate Tensile Strength. The trends of the independent variables are significant for designing the Ultimate Tensile Strength.

Figure 4. 6.12 UTS (z) - PWHTT(y) - C (x) 3D plot

Figure 4, 6,12 shows the contour of Ultimate Tensile Strength 600 MPa with the Carbon in the range from 0.006% to 0.106% and the Post Weld Heat Treatment Temperature in the range from

250 C to 560 C. The increase in the Ultimate Tensile Strength from 700 MPa to 1100 MPa are achieved outside the 600 MPa contour by an increasing both the %Carbon in the range from 0.106% to 0.24% and the Post Weld Heat Treatment Temperature in the range from 300 C to 800 C. The Ultimate Tensile Strength less than 600 MPa is obtained inside the contour of 600 MPa. Below the Post Weld Heat Treatment Temperature 300 C, the Ultimate Tensile Strength values are obtained in the range more than 600 MPa to 800 MPa with a full range of wt% C from 0% to 0.24%. Both independent variables show complexity in their trends. The independent variables are significant for designing the Ultimate Tensile Strength.

Figure 4. 6.13 UTS (z) – PWHTtime (y) - C (x) 3D plot

Figure 4. 6.13 shows the contour of Ultimate Tensile Strength 600 MPa with the Carbon in the range from 0% to 0.084% and the Post Weld Heat Treatment Time in the range from 16 h to 60 h. The increase in the Ultimate Tensile Strength from 700 MPa to 1000 MPa are achieved outside the 600 MPa contour by an increasing both the %Carbon in the range from 0.084% to 0.232% and the Post Weld Heat Treatment Time in the range from 0 h to 60 h. The Ultimate Tensile Strength 1100 MPa and higher are achieved with wt% C in the range from 0.218% to 0.24% and Post Weld Heat Treatment Time in the range from 35 h to 60 h. The Ultimate Tensile Strength less than 600 MPa is obtained inside the contour of 600 MPa. The increase in the Ultimate Tensile Strength is achieved more than 600 MPa to 1000 MPa by keeping Post Weld Heat Treatment Time constant and increasing Carbon concentration. The trends of both the independent variables are less complex and flexible for designing the Ultimate Tensile Strength.

Figure 4. 6.14 UTS (z) - Cr (y) - Ni (x) 3D plot

Figure 4. 6.14 shows the increase in the Ultimate Tensile Strength from 600 MPa to 1200 MPa with equally increase in wt% Chromium from 0% to 4.4% and wt% Nickel from 0% to 4.4%. The increase in the Ultimate Tensile Strength is also achieved by keeping Chromium constant and Nickel concentration varies and vice versa. Both independent variables show complexity and uniqueness in their trends. The independent variables are significant for designing the Ultimate Tensile Strength.

Figure 4. 6.15 UTS (z) - V (y) - Mo (x) 3D plot

Figure 4. 6.15 shows the contour of Ultimate Tensile Strength 800 MPa with the Molybdenum in the range from 0% to 1.14% and the Vanadium in the range from 0.135% to 0.35%. More than 800 MPa Ultimate Tensile Strength is obtained inside the contour of 800MPa. The decrease in the Ultimate Tensile Strength from 700 MPa to 100 MPa are obtained by keeping Vanadium concentration constant and increasing Molybdenum concentration. The Molybdenum less than 0.44% and more than 1.38% decreases the Ultimate Tensile Strength. Both independent variables show complexity in their trends. The independent variables are significant for designing the Ultimate Tensile Strength.

Figure 4. 6.16 UTS (z) - Ti (y) - O (x) 3D plot

Figure 4. 6.16 shows the contour of Ultimate Tensile Strength 600 MPa with the Oxygen in the range from 410 ppm to 1620 ppm and the Titanium in the range from 0 ppm to 670 ppm. Inside the 600 MPa contour the Values of the Ultimate Tensile Strength are less than 600 MPa for the combinations of the Oxygen ppm and the Titanium ppm. The increase in the Ultimate Tensile Strength is achieved outside the 600 MPa contour by keeping Oxygen in the range between 0 ppm to 410 ppm and Titanium in the range between 0 ppm to 900 ppm concentration. The increase in the Ultimate Tensile Strength 700 MPa, 800 MPa and higher are achieved with increase in the Oxygen in the range from 1240 ppm to 1800 ppm and in the Titanium in the range from 370 ppm to 900 ppm. Tensile Strength. Both independent variables show complexity in their trends. The independent variables are significant for designing the Ultimate Tensile Strength.

Figure 4. 6.17 UTS (z) - Nb (y) - B (x) 3D plot

Figure 4. 6.17 shows the increase in the Ultimate Tensile Strength from 700 MPa to 1200 MPa with an increase in the Niobium from 200 ppm to 1200 ppm and the Boron from 40 ppm to 140 ppm. The increase in the Ultimate Tensile Strength is also achieved by keeping Niobium constant and Boron concentration varies and vice versa. These trends are observed for higher values of both the Niobium in range, from 800 ppm to 2000 ppm and the Boron in the range from 80 ppm to 220 ppm. The Ultimate Tensile Strength 600 MPa and less is obtained with the Niobium in the range from 0 ppm to 120 ppm and the Boron in the range from 65 ppm to 220

ppm. Both independent variables show complexity and uniqueness in their trends. The independent variables are significant for designing the Ultimate Tensile Strength.

Figure 4.6.18 UTS (z) - ITP (y) - HI (x) 3D plot

Figure 4.6.18 shows the Ultimate Tensile Strength values 700 MPa and more than 700MPa are observed in the upper side and bottom side of the graph. Right side of the graph has the range of the Interpass Temperature from 25 C to 365 C and the Heat Input from 5.7 kJmm⁻¹ to 9 kJmm⁻¹. Left side of the graph has the range of the Interpass Temperature from 140 C to 250 C and the Heat Input from 0 kJmm⁻¹ to 0.6 kJmm⁻¹. The Ultimate Tensile Strength 800MPa and higher are obtained with the range of the Interpass Temperature from 320 C to 400 C and by maintaining the Heat Input, in the range from 0 kJmm⁻¹ to 6.5 kJmm⁻¹ at the upper side of the plot. The Ultimate Tensile Strength 800MPa and higher are obtained with the range of the Interpass Temperature from 0 C to 20 C and by maintaining the Heat Input, in the range from 0.7 kJmm⁻¹ to 5.7 kJmm⁻¹ at the bottom side of the plot. The Upper side and bottom side of the plot show the contours of the increase in the Ultimate Tensile Strength from 700MPa and more than 700MPa. Both the independent variables have a complex relationship with the Ultimate Tensile Strength. The trends of the independent variables are significant for designing the Ultimate Tensile Strength.

Figure 4.7.19 UTS (z) - PWHTt (y) - PWHTT (x) 3D plot

Figure 4.7.19 shows the increase in the Ultimate Tensile Strength from 600 MPa to 1200 MPa with the increase in the Post Weld Heat Treatment Time in the range from 0 h to 60 h and the decrease in the Post Weld Heat Treatment Temperature in the range from 630 C to 0 C. The increase in the Ultimate Tensile Strength from 600 MPa to 800 MPa with the decrease in the Post Weld Heat Treatment Time in the range from 39 h to 0 h and the increase in the Post Weld Heat Treatment Temperature in the range from 575 C to 800 C at the bottom right corner of the graph. Both the independent variables have a complex relationship with the Ultimate Tensile Strength. The trends of the independent variables are significant for designing the Ultimate Tensile Strength.

4.2.4. Application of Trained Best Models

4.2.4.1 Prediction of The Ultimate Tensile Strength on unseen data by BNN Model

The BNN model has good accuracy in prediction of ultimate tensile strength of ferritic steel welds on unseen data which is excellent for the design of welds. (Table.4.4) The predicted ultimate tensile strength of the unseen data of three weld alloys are compared with measured values of ultimate tensile strength shows the prediction capacity of the BNN model. This BNN model can be used for practical applications, research and development of ferritic steel alloys.

Table 4.4 Predicted Ultimate Tensile strength by BNN model for unseen data of three ferritic weld deposits

Variable	Weld alloy 1	Weld alloy 2	Weld alloy 3
Carbon(wt%)	0.041	0.088	0.11
Silicon(wt%)	0.3	0.35	0.28
Manganese(wt%)	0.62	0.54	0.6
Sulphur(wt%)	0.007	0.007	0.007
Phosphorus(wt%)	0.010	0.009	0.016
Nickel(wt%)	2.38	7.0	10.62
Chromium(wt%)	0.03	0.15	1.13
Molybdenum(wt%)	0.005	0.4	0.3
Vanadium(wt%)	0.012	0.016	0.006
Copper(wt%)	0.03	0.01	0.3
Oxygen(ppm)	440	290	290
Titanium(ppm)	55	0.0	0.0
Boron(ppm)	2.0	1.0	1.0
Niobium(ppm)	20	10	10
Heat_input(kJ.mm-1)	1.0	1.4	1.4
Interpass_temperature(C)	200	150	200
Postweld_heat_treatment_temperature(C)	250	250	250
Post-weld_heat_treatment_time(h)	14	16	16
Measured UTS/MPa	538	972	1194
Predicted UTS/MPa	523.44	978.12	1176.12

4.2.4.2 Prediction of The Ultimate Tensile Strength on unseen data by GRNN Model

The GRNN model has good accuracy in prediction of ultimate tensile strength of ferritic steel welds on unseen data which is excellent for the design of welds. (Table.4.5) The predicted ultimate tensile strength of the unseen data of three weld alloys are compared with measured values of ultimate tensile strength shows the prediction capacity of the GRNN model. This GRNN model can be used for practical applications, research and development of ferritic steel alloys.

Table 4.5 Predicted Ultimate Tensile strength by GRNN model for unseen data of three ferritic weld deposits

Variable	Weld alloy 1	Weld alloy 2	Weld alloy 3
Carbon(wt%)	0.041	0.088	0.11
Silicon(wt%)	0.3	0.35	0.28
Manganese(wt%)	0.62	0.54	0.6
Sulphur(wt%)	0.007	0.007	0.007
Phosphorus(wt%)	0.010	0.009	0.016
Nickel(wt%)	2.38	7.0	10.62
Chromium(wt%)	0.03	0.15	1.13
Molybdenum(wt%)	0.005	0.4	0.3
Vanadium(wt%)	0.012	0.016	0.006
Copper(wt%)	0.03	0.01	0.3
Oxygen(ppm)	440	290	290
Titanium(ppm)	55	0.0	0.0
Boron(ppm)	2.0	1.0	1.0
Niobium(ppm)	20	10	10
Heat_input(kJ.mm-1)	1.0	1.4	1.4
Interpass_temperature(C)	200	150	200
Postweld_heat_treatment_temperature(C)	250	250	250
Post-weld_heat_treatment_time(h)	14	16	16
Measured UTS/MPa	538	972	1194
Predicted UTS/MPa	538	978	1183

Prediction of The Ultimate Tensile Strength for new data of input variables can be achieved accurately with best trained models by BNN and GRNN as given in above Table 4.4. and Table 4.5. These Models have capacity for changing any individual input variable, any combination of more than one input variables or all input variables to predict the The Ultimate Tensile Strength of Ferritic Steel Welds. These are only possible with the BNN and GRNN Models which are impossible practically. By simply running these Models the various design of the Ferritic Steel Welds are possible which save money, time and labour during Research and Development of the Ferritic Steel Welds.

4.2.5 Genetic Algorithms and applications to the Ultimate Tensile Strength of Ferritic Steel Welds

4.2.5.1 Target Ultimate tensile strength of 538 MPa and High value of Ultimate tensile strength 1300 MPa

The first simulation is made to check the behaviour of the genetic algorithm. The target value of ultimate tensile strength is set to -0.7. which correspond to an unnormalised value of 538 MPa. The dataset provides such values of yield strength and the aim of this simulation is to check the results of the genetic algorithm.. The 18 parameters(input variables) are allowed to vary, in between -1 and + 1 during the genetic algorithm process. After 3000 generations, the best results obtained is shown Table 4.6.

The second simulation is made to check the genetic algorithm for high value of the Ultimate tensile strength.. The target value of ultimate tensile strength is set to 0.13 which correspond to an unnormalised value of 1300 MPa. The dataset does not provide such value of ultimate tensile strength and the aim of this simulation is to check the results of the genetic algorithm.. The 18 parameters (input variables) are allowed to vary, in between -1 and + 1 during the genetic algorithm process. After 3000 generations, the best results obtained are shown Table 4.6.

According to Table 4.6, the genetic algorithm has managed to reach the target after 3000 generations.

Moreover, the associated error obtained is very reasonable.

To check if the given input variables correspond to Ferritic Steel Weld, compare with the actual data of Ultimate tensile strength.

Table 4.6 Predicted Input variables by NN-GA model for two targeted Ultimate Tensile Strength of ferritic weld deposits

Variable	Weld 1	Weld 1	Weld 2
	Result GA	Data	Result GA
Carbon(wt%)	0.04	0.041	0.098
Silicon(wt%)	0.28	0.3	0.35
Manganese(wt%)	0.59	0.62	0.74
Sulphur(wt%)	0.007	0.007	0.007
Phosphorus(wt%)	0.010	0.010	0.009
Nickel(wt%)	2.24	2.38	8.0
Chromium(wt%)	0.03	0.03	0.25
Molybdenum(wt%)	0.006	0.005	0.4
Vanadium(wt%)	0.014	0.012	0.02
Copper(wt%)	0.03	0.03	0.01
Oxygen(ppm)	436	440	290
Titanium(ppm)	52	55	55
Boron(ppm)	2.0	2.0	1.0
Niobium(ppm)	20	20	20
Heat_input(kJ.mm-1)	1.1	1.0	1.4
Interpass_temperature(C)	210	200	150
Postweld_heat_treatment_temperature(C)	240	250	250
Post-weld_heat_treatment_time(h)	13	14	16
GA calculated UTS/MPa	534	---	1281
Target Value UTS/MPa	538	---	1300
Error UTS/MPa	28	---	45
Measured UTS/MPa	---	538	---

The NNGA models have good accuracy in predicting 18 input variables of the Ultimate Tensile Strength of ferritic steel welds, which is excellent for weld design.(Table.4.6) The predicted results of the targeted values of the two weld deposits are very close. The results of Genetic Algorithms are match with trends of measured data and fundamental of metallurgy. The output results show the predictive capacity of the NNGA model.

This NNGA model can be used in practical applications, research and development of ferritic steel alloys. [Appendix-B]

4.2.6 Summary

The Neural Network and Genetic algorithms Methods have been used for efficient design of the Ultimate Tensile strength of Ferritic Steel Welds. From the Modelling works and Results and Discussion of this Chapter some useful conclusions can be drawn:

The distribution of the Data of the Ultimate Tensile Strength of Ferritic Steel Welds is uniform for some Input variables and non-uniform for some Input variables. The distribution is clearly observed in Scatter plots.

In this case, of Bayesian Neural Network method, all the response graphs show error bars when the concentration of Nickel and Chromium is respectively below 8 and 6 wt%, the prediction can be reliable but above those limits (8 wt% for Ni and 6 wt% for Cr), the model can no more be trusted and this is inferred by the large error bars. Similarly it is applicable to other graphs where larger error bars are present. More experiments with concentrations in this range of values need to be carried out to improve the model. Uncertainty because of a lack of data is one of the limitations of a neural network. The error bars and output variable (Ultimate Tensile Strength) sometimes showing unphysical (negative) values, this is because of the empirical equation in Neural Network modelling. This error bars feature of Bayesian Neural Network is excellent guideline for research and Development.

In the case of General Regression Neural Network method, there is no problems of noisy data. It can handle noises in the Inputs. The Response graphs of the GRNN show more define about the non linearity or complexity between the Input variables and the Ultimate Tensile Strength of Ferritic Steel Welds.

The Response Graphs show about the individual relationship between the input variables and Output variable (Ultimate Tensile Strength). The 3D contour plots show the relationship between the two Input variables with Output variable (Ultimate Tensile Strength).

These trends are confirmed in the present analysis as illustrated in both the types of the Graphs Figure 4.4 (a to r) and Figure 4.5 (a to r). They are impossible to reproduce in practice. They give a clear understanding of the relationship between the Input variables and the Ultimate Tensile Strength of Ferritic Steel Welds. These pieces of information are very valuable for design, as well as understanding the existing theory and also guiding about new research and new finding for the Ferritic steel Welds.

The 3D contour plots show the relationship between the two Input variables with Ultimate Tensile Strength. There is a total combination of 153 3D contour plots formed by 18 Input variables with the Ultimate Tensile Strength. In the present work, 19 3D contour plots are selected with their important relationship with the Ultimate Tensile Strength. These 3D contour plots show some hidden complex behaviour of the input variables with the Ultimate Tensile Strength which is not available and not well understood . Some innovative theoretical relations

can be established by the proper interpretation of these 3D contour plots which become the new knowledge base for the future work on Ferritic Steel Welds. The Input variables show complex trends because during welding, there are formation of various types of the microstructures in Ferritic Steel Welds, qualitatively and quantitatively.

The trained BNN and GRNN models give the accurate predictions of unseen data which is useful in designing the Ferritic Steel Welds for the welding electrodes industries. With simply change the quantity of Input variables in model and run it, the predicted Ultimate Tensile Stength is obtained in the seconds.

The Genetic Algorithms method gives the prediction of the Input Variables for the Targeted Ultimate Tensile Strength value. It also predicted Input variables for the Targeted Ultimate Tensile Strength value which is beyond the range of data. The results are excellent.

4.3 Elongation Models

4.3.1 Response graphs of Input variables and Elongation of Ferritic Steel Welds using committee model of Bayesian Neural Network

The Trends of the Input Variables (Independent Variables) and Elongation of Ferritic Steel Welds are given below in the form of the graphs.

Trends of Elongation Model

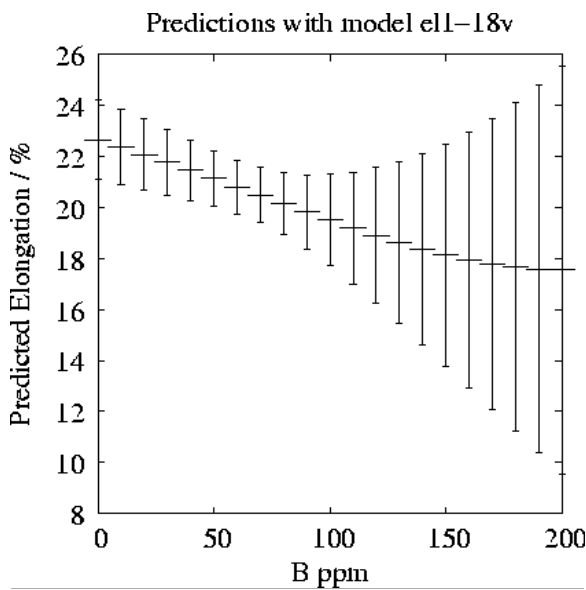


Fig a. Predicted variations in Elongation with Boron variation.

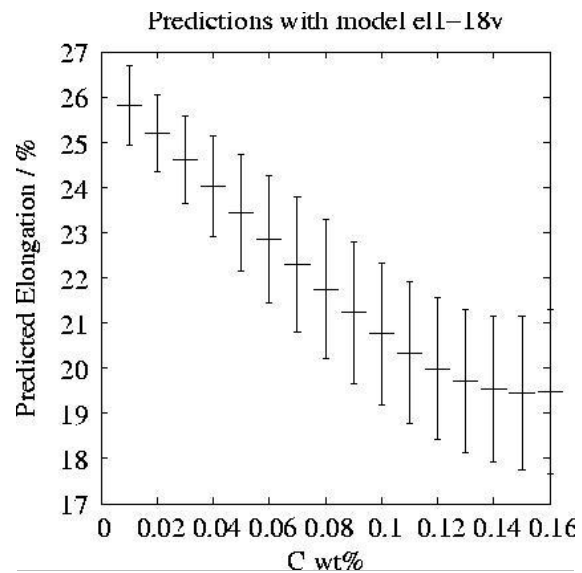


Fig b. Predicted variations in Elongation with Carbon variation.

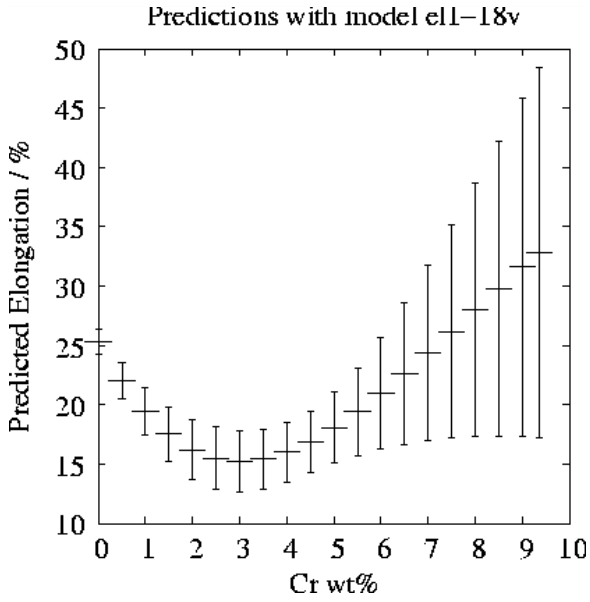


Fig c. Predicted variations in in Elongation with Chromium variation.

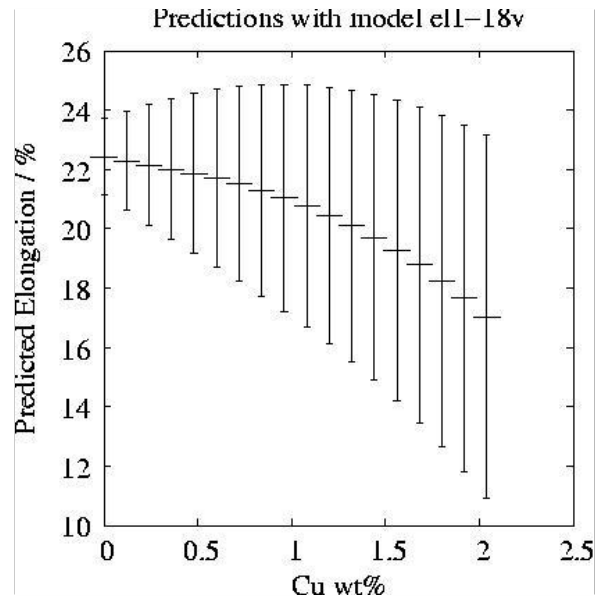


Fig d. Predicted variations in in Elongation with Copper variation.

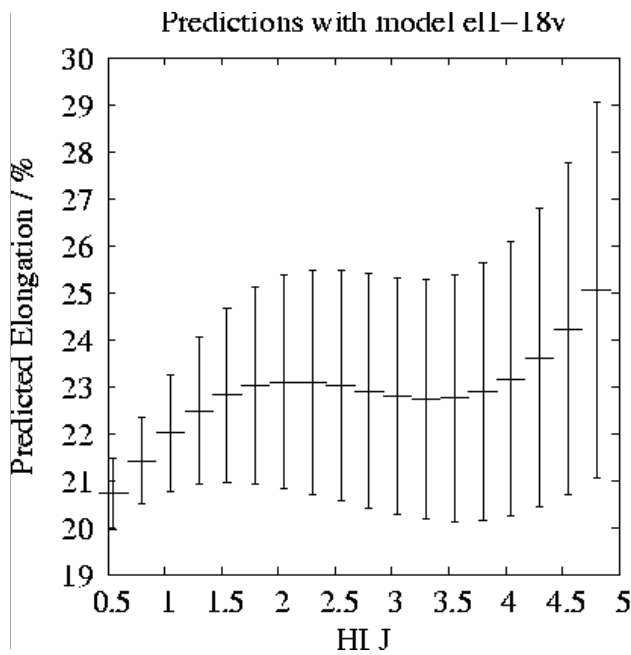


Fig e. Predicted variations in in Elongation with Heat input variation.

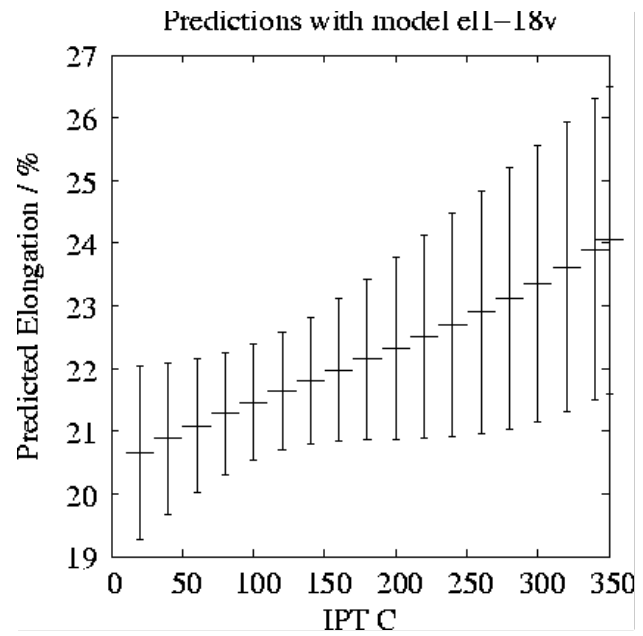


Fig f. Predicted variations in in Elongation with Interpass Temperature variation.

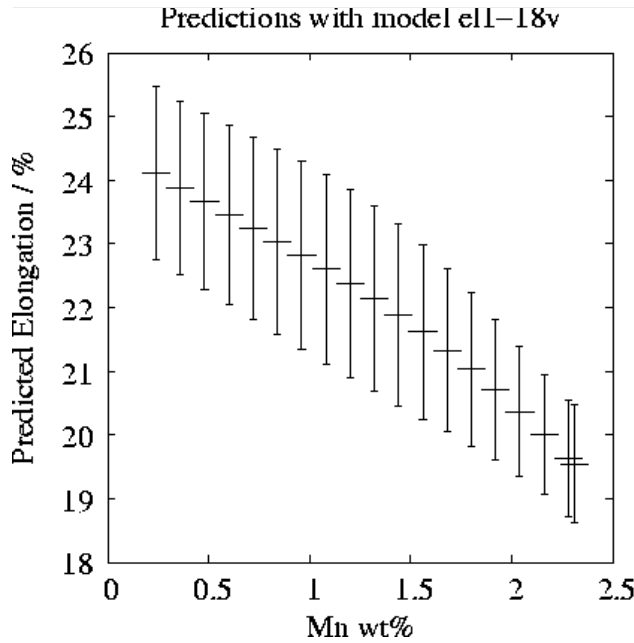


Fig g. Predicted variations in in Elongation with Manganese variation.

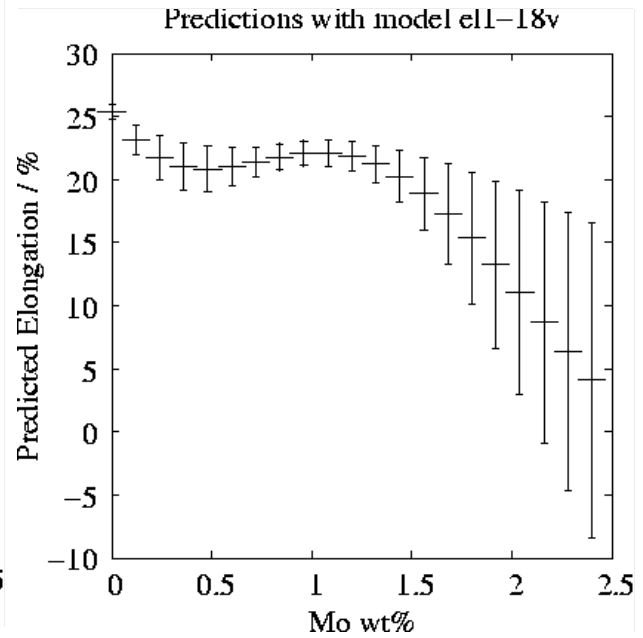


Fig h. Predicted variations in in Elongation with Molybdenum variation.

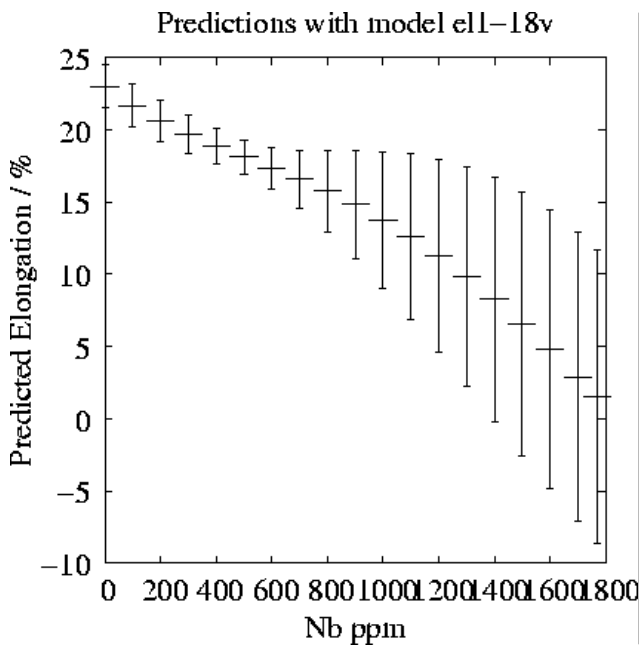


Fig i. Predicted variations in in Elongation with Niobium variation.

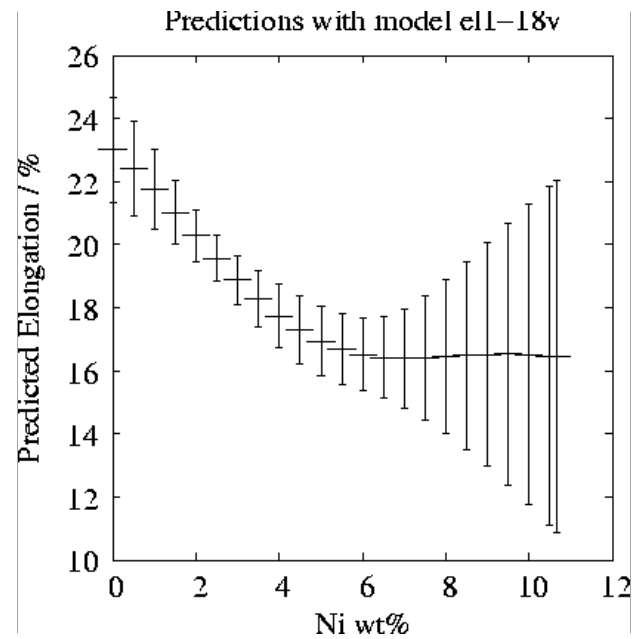


Fig j. Predicted variations in in Elongation with Nickel variation.

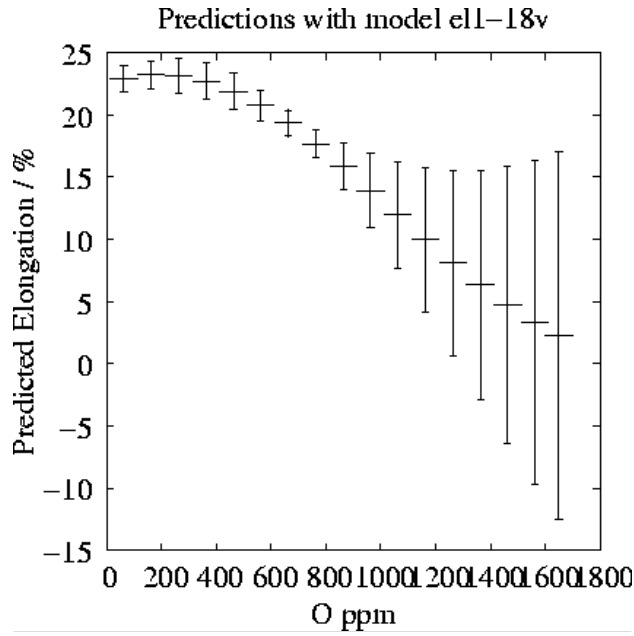


Fig k. Predicted variations in in Elongation with Oxygen variation.

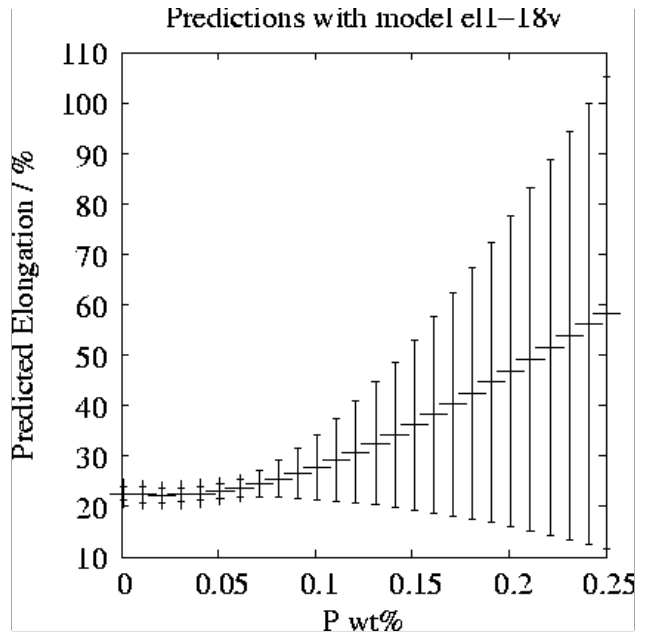


Fig l. Predicted variations in in Elongation with Phosphorus variation.

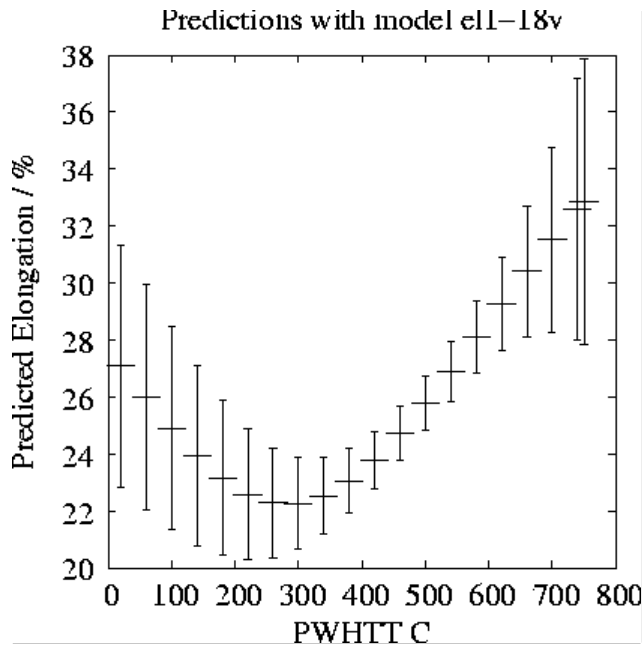


Fig m. Predicted variations in in Elongation with Post Weld Heat Treatment Temperature variation.

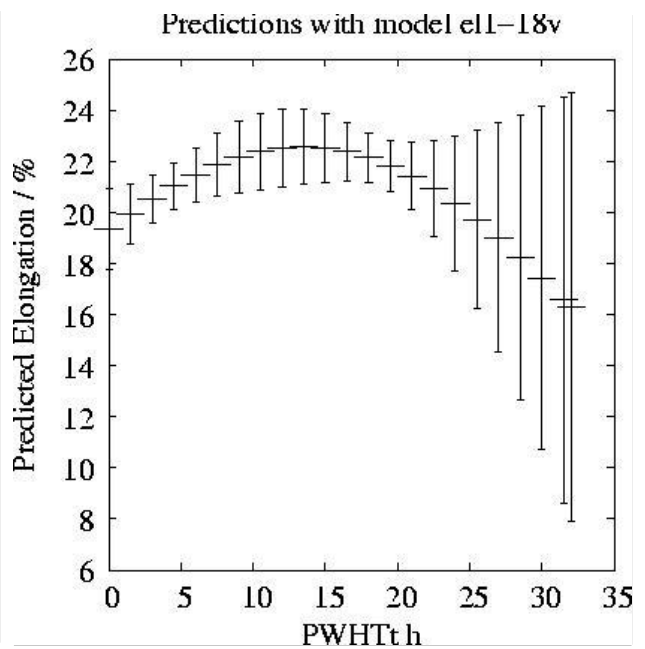


Fig n. Predicted variations in in Elongation with Post Weld Heat Treatment Time variation.

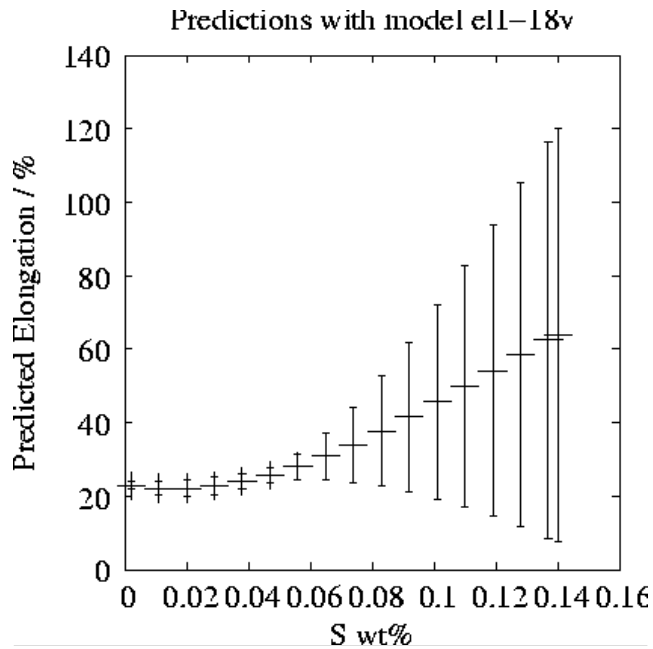


Fig o. Predicted variations in in Elongation with Sulphur variation.

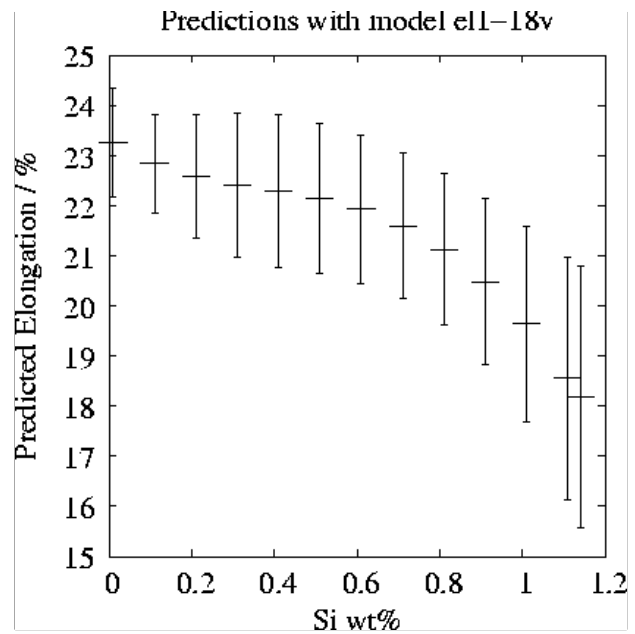


Fig p. Predicted variations in in Elongation with Silicon variation.

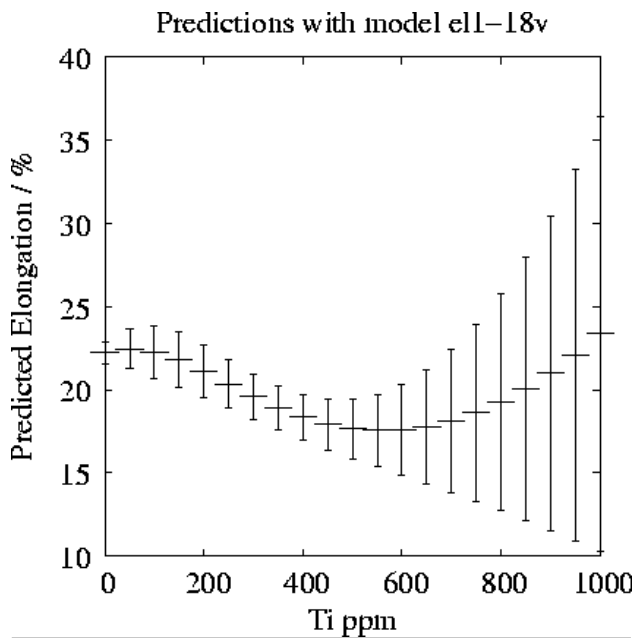


Fig q. Predicted variations in in Elongation with Titanium variation.

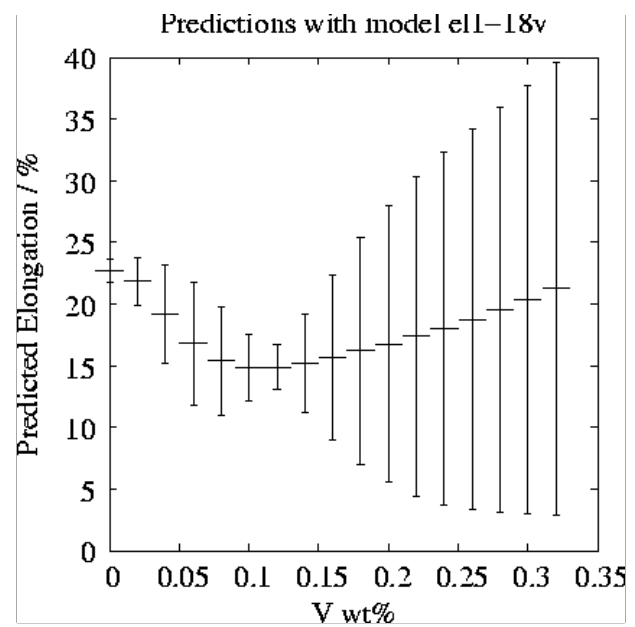


Fig r. Predicted variations in in Elongation with Vanadium variation.

Figure 4.7 (a to r) Response graphs of Input variables and Elongation of Ferritic Steel Welds using committee model of Bayesian Neural Network

These trends are confirmed in the present analysis as illustrated in Figure 4.7 (a to r). It is emphasised that these calculations are done without permitting any of the other variables to change. They are impossible to reproduce in practice.

All the graphs show the error bars. The error bars are uniform in size indicate that the uniformity of data, like the graph the prediction of the Elongation, as a function of Manganese. The error bars are large in size indicate non-uniformity of data, like the graph the prediction of the Elongation as a function of Chromium.

In this case, when the concentration of Nickel and Chromium is respectively below 8 and 6 wt%, the prediction can be reliable. But above those limits (7 wt% for Ni and 6 wt% for Cr), the model can no more be trusted and this is inferred by the large error bars. Similarly it is applicable to other graphs where larger error bars are present. More experiments with concentrations in this range of values need to be carried out to improve the model. Uncertainty because of a lack of data is one of the limitations of a neural network. The error bars and output variable (Elongation) sometimes showing unphysical (negative) values, this is because of the empirical equation in Neural Network modelling.

The input variables like Interpass Temperature, and Sulphur are increasing in concentration or in amount, increase the Elongation of ferritic Steel welds. The Sulphur has shown an increase on the Elongation too high 62% which is not reliable.

The input variables like Boron, Carbon, Copper, Manganese, Niobium, Oxygen, and Silicon increase in content or in amount quantitatively, decrease the Elongation of ferritic Steel welds. The Phosphorus has shown an increase on the Elongation too high 58% which is not reliable.

The input variable like Chromium, Heat Input, Molybdenum, Nickel, Post Weld Heat Treatment Temperature, Post Weld Heat Treatment Time, Titanium and Vanadium indicate their non linear behaviour with the Elongation.

The trends of the graphs of Bayesian Neural network model are useful to design the Elongation of Ferritic Steel welds efficiently.

In summary, a reasonable committee model has been obtained for Yield Strength. It appears that these input variables are affected on the Elongation of Ferritic Steel Welds, as could be expected from a metallurgical point of view.

4.3.2 Response Graphs of the Elongation GRNN model

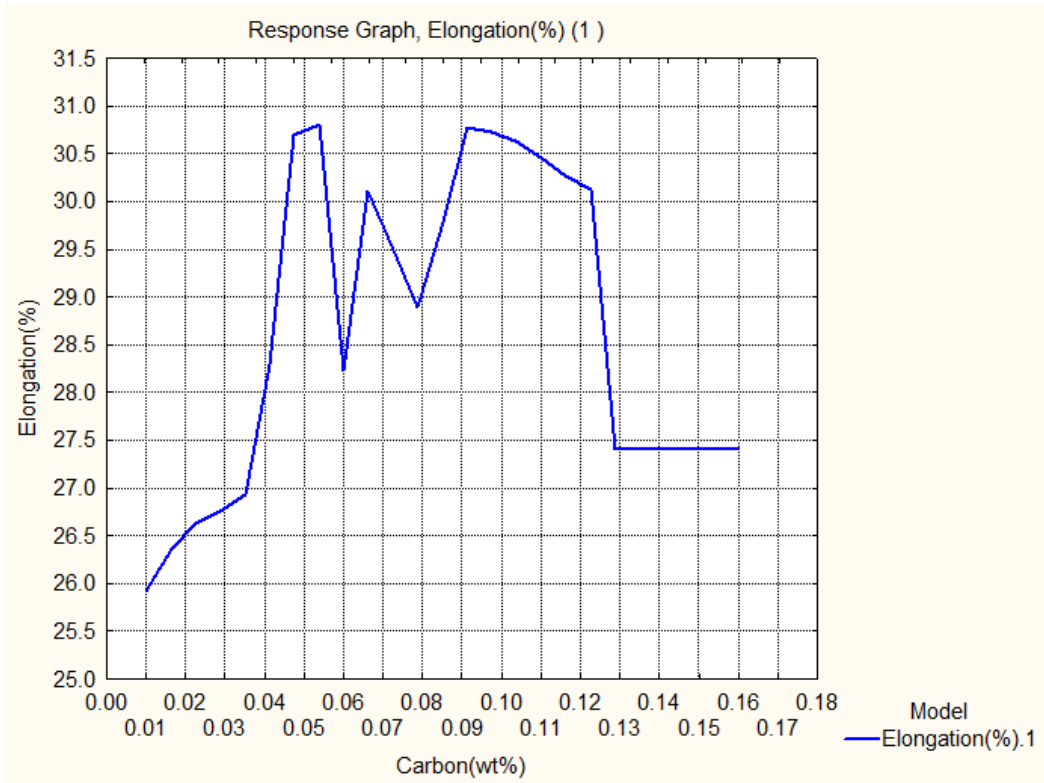


Fig. a Response Graph of Elongation % and Carbon(wt%)

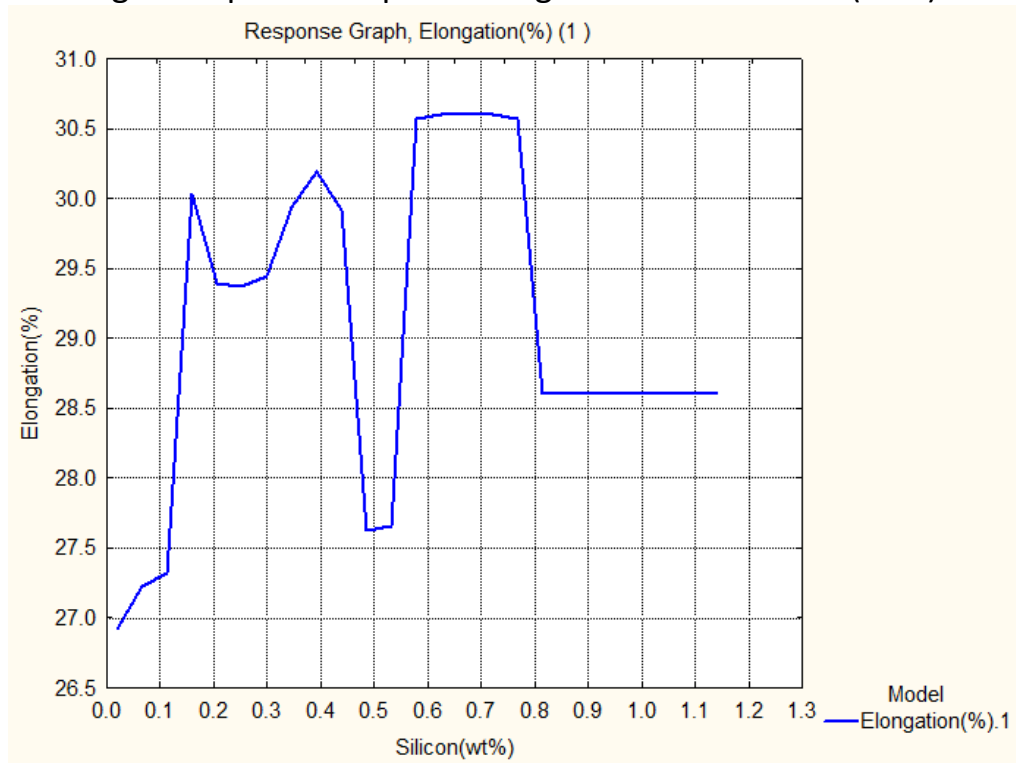


Fig. b Response Graph of Elongation % and Silicon(wt%)

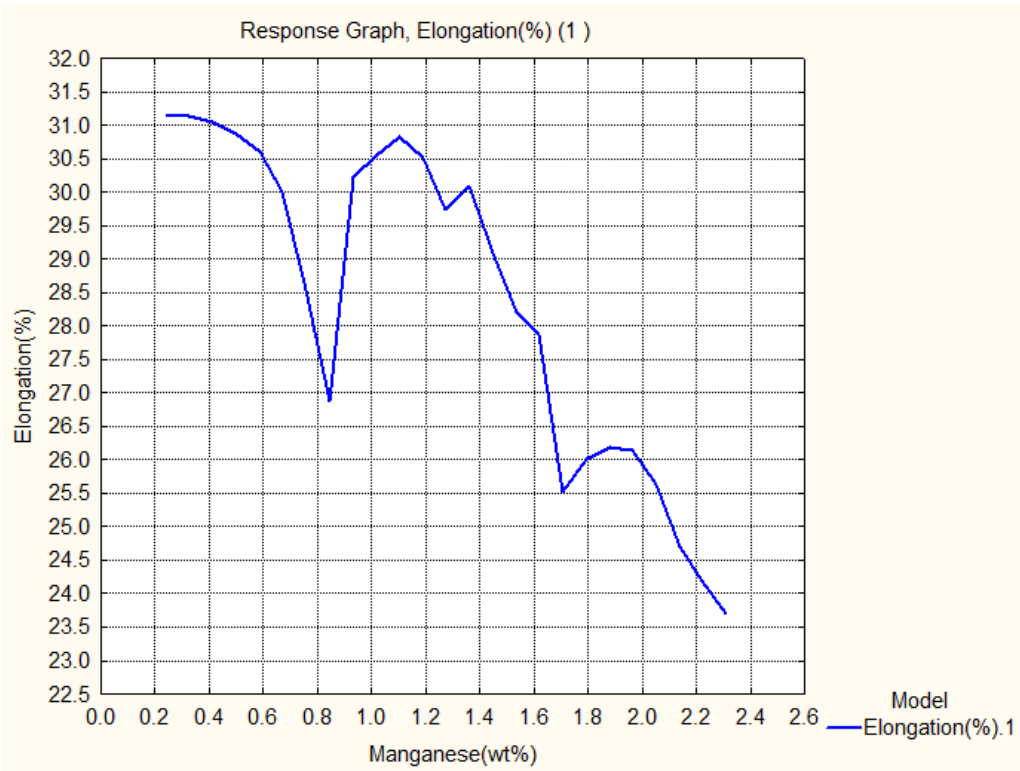


Fig. c Response Graph of Elongation % and Manganese(wt%)

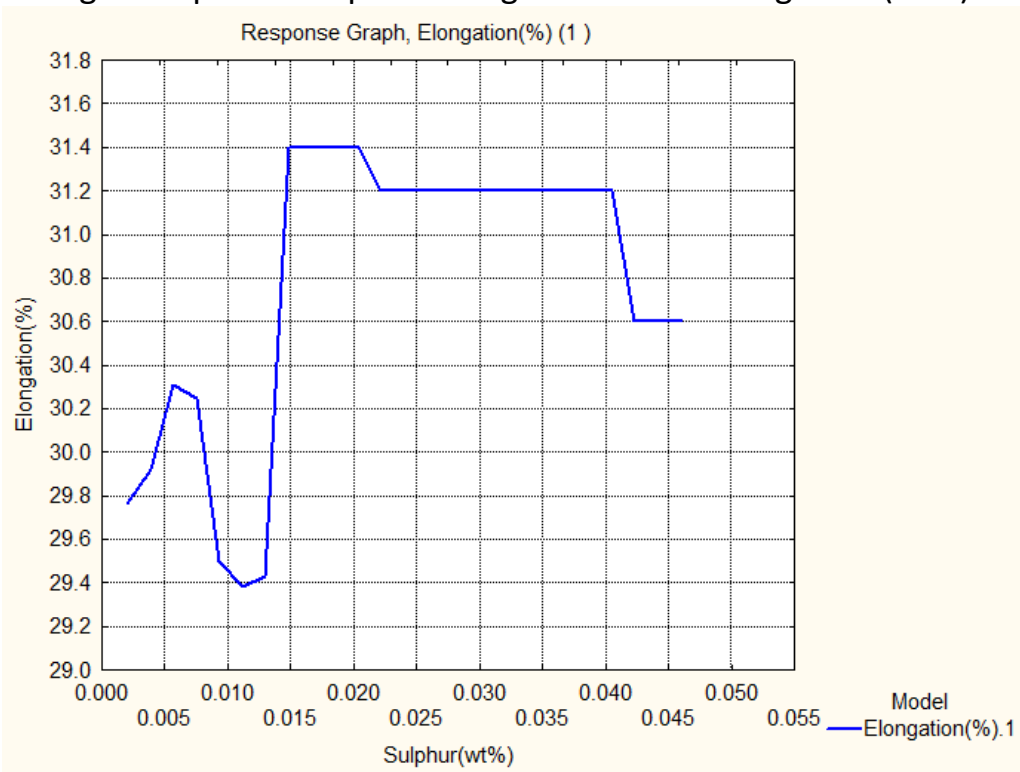


Fig. d Response Graph of Elongation % and Sulphur(wt%)

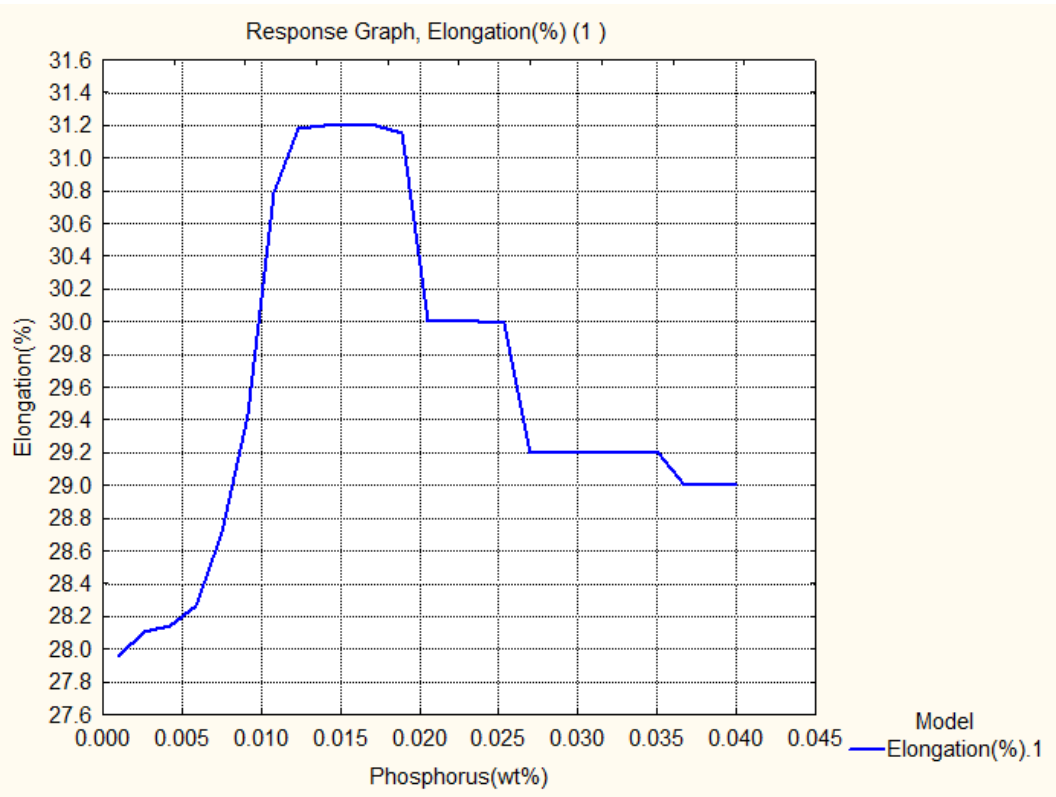


Fig. e Response Graph of Elongation % and Phosphorus(wt%)

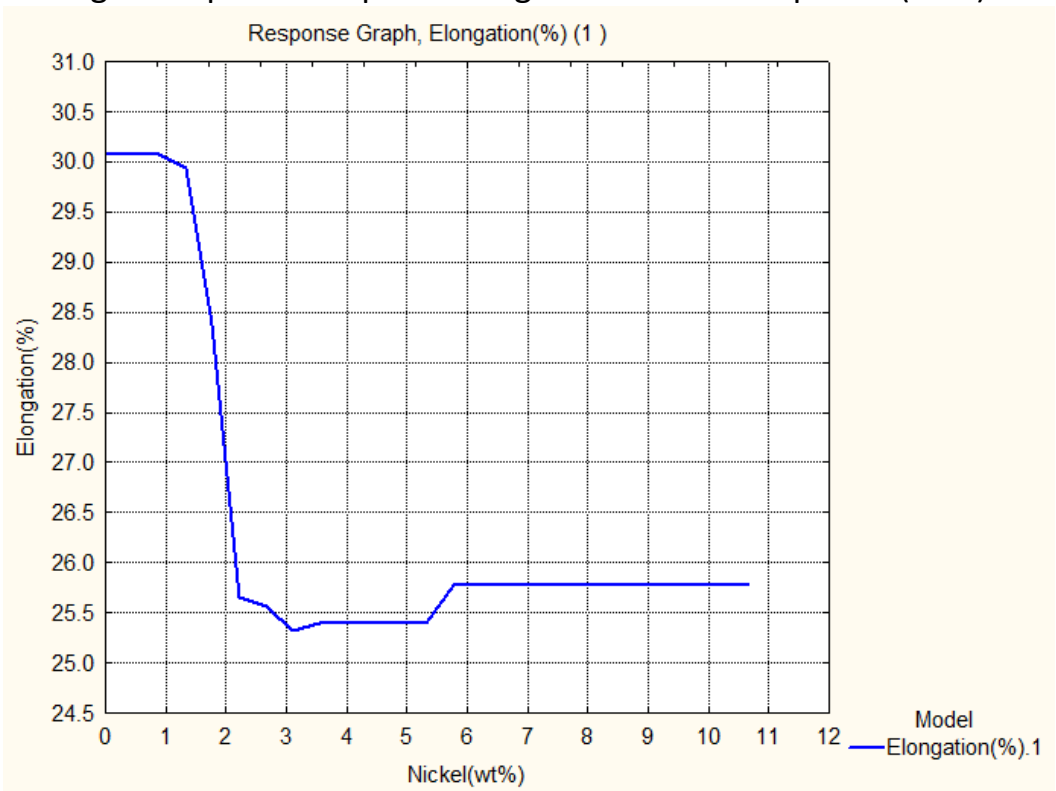


Fig. f Response Graph of Elongation % and Nickel(wt%)

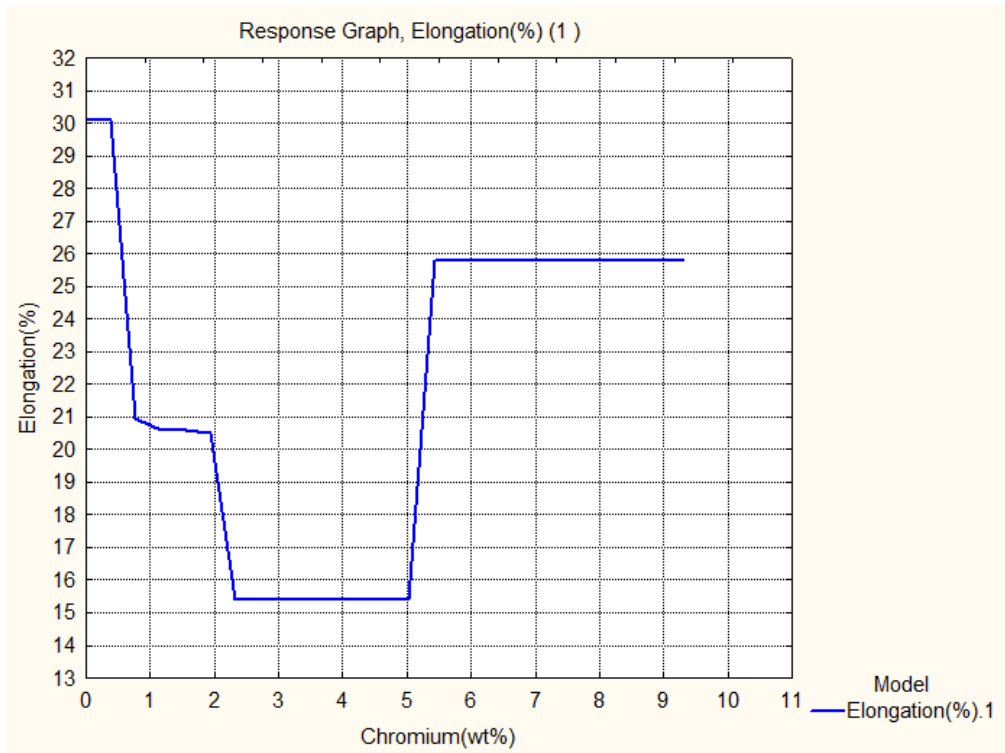


Fig. g Response Graph of Elongation % and Chromium(wt%)

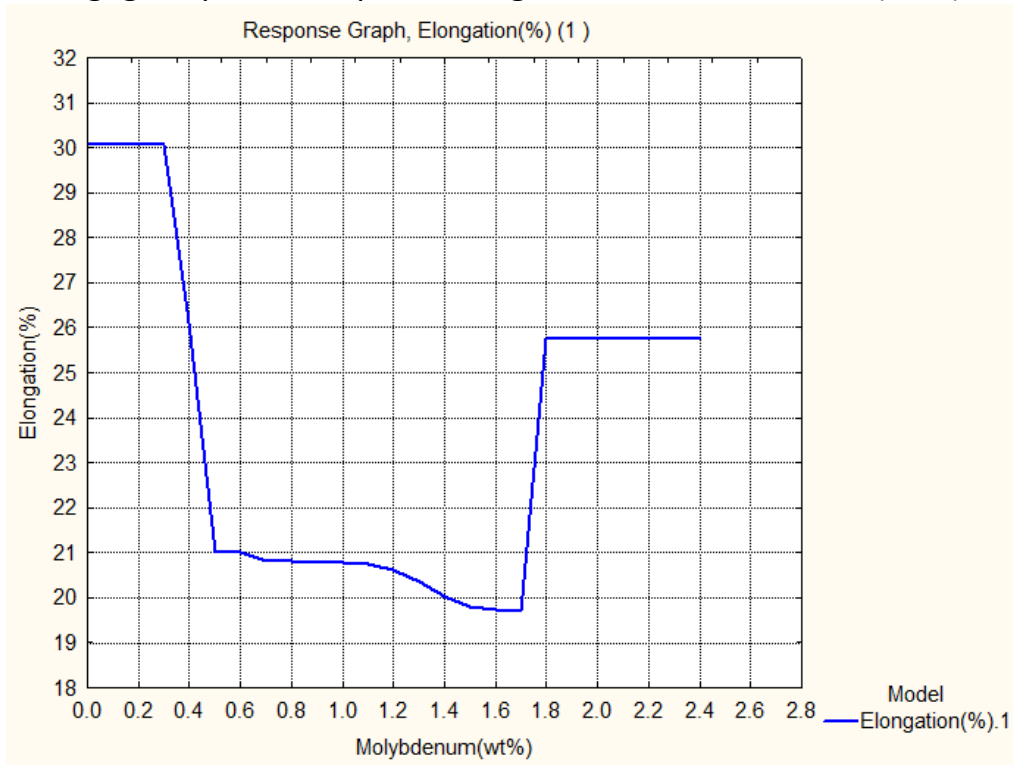


Fig. h Response Graph of Elongation % and Molybdenum(wt%)

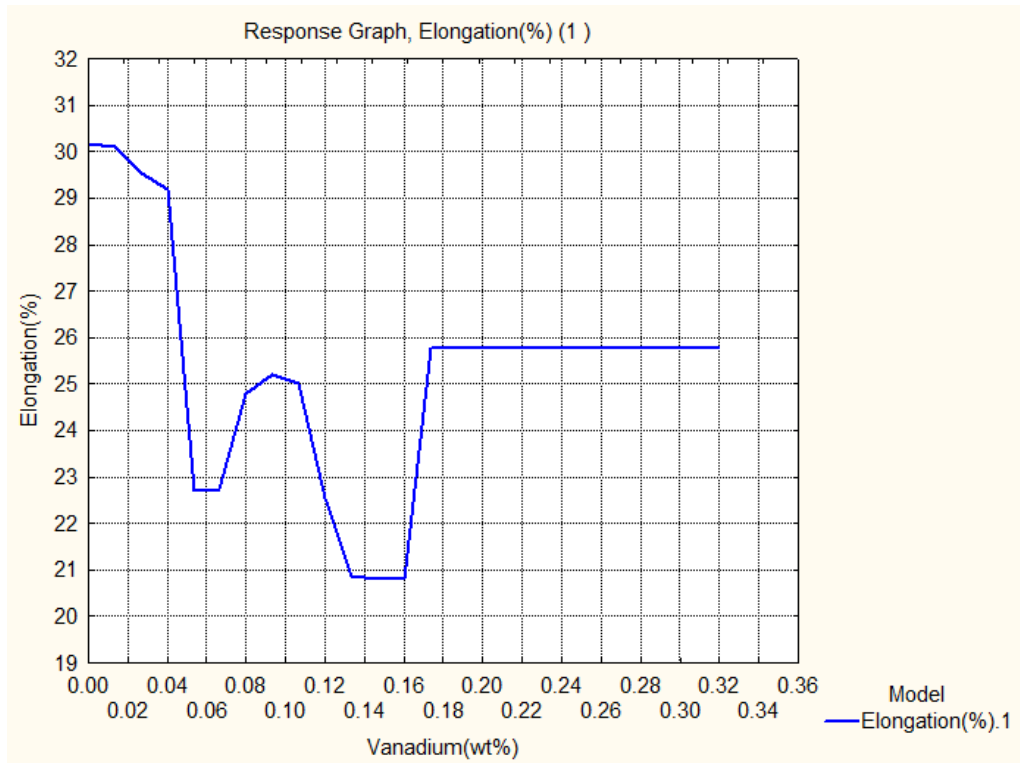


Fig. i Response Graph of Elongation % and Vanadium(wt%)

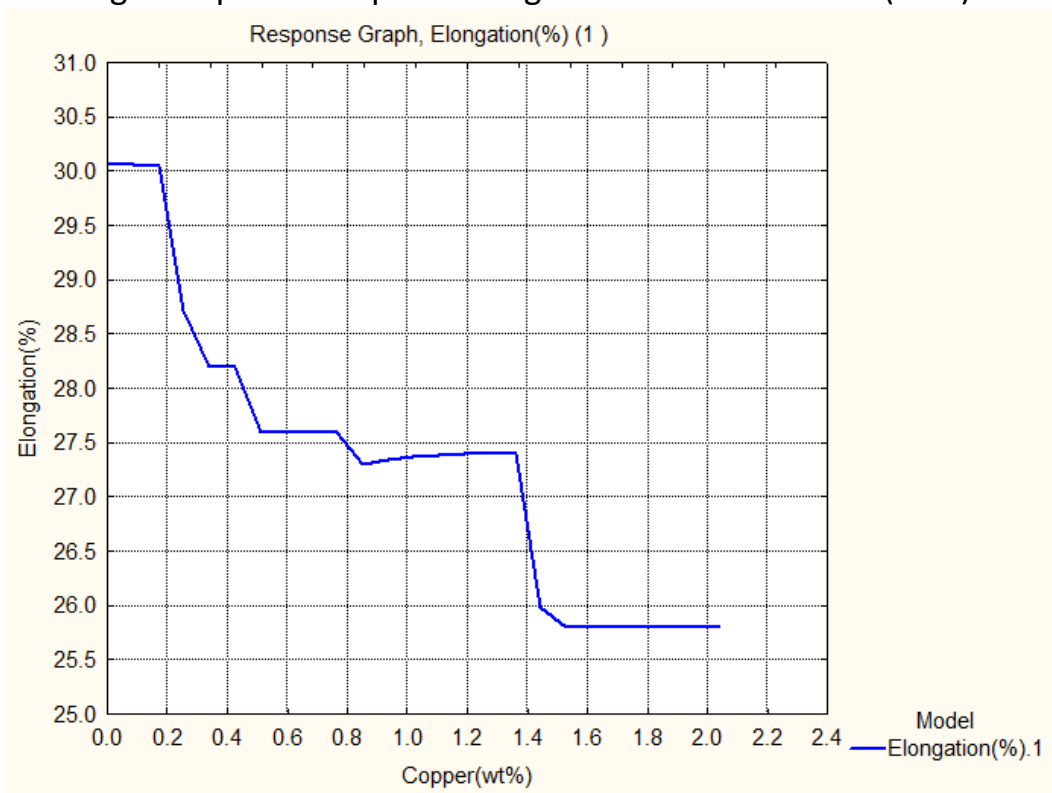


Fig. j Response Graph of Elongation % and Copper(wt%)

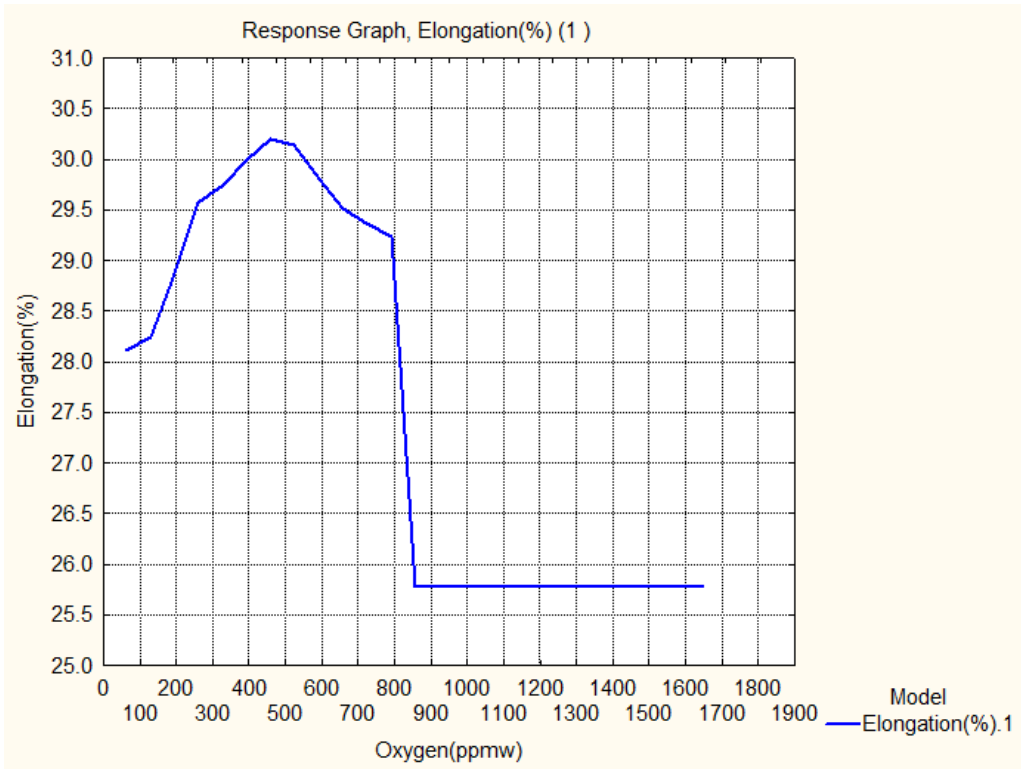


Fig. k Response Graph of Elongation % and Oxygen(ppmw)

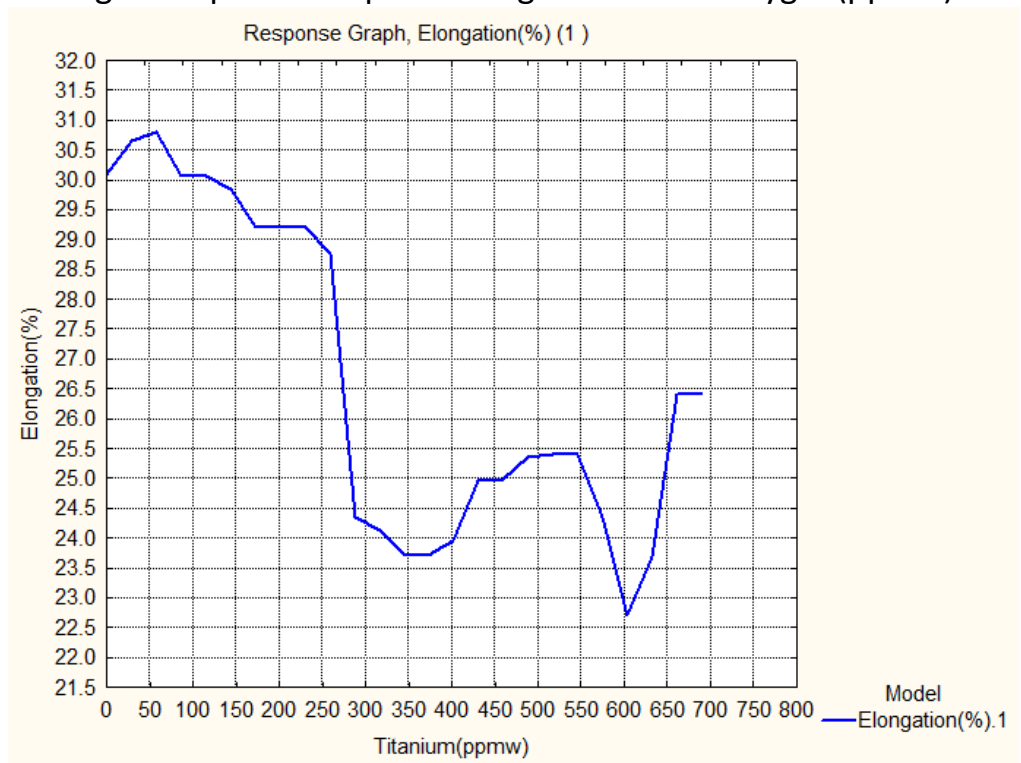


Fig. l Response Graph of Elongation % and Titanium(ppm)

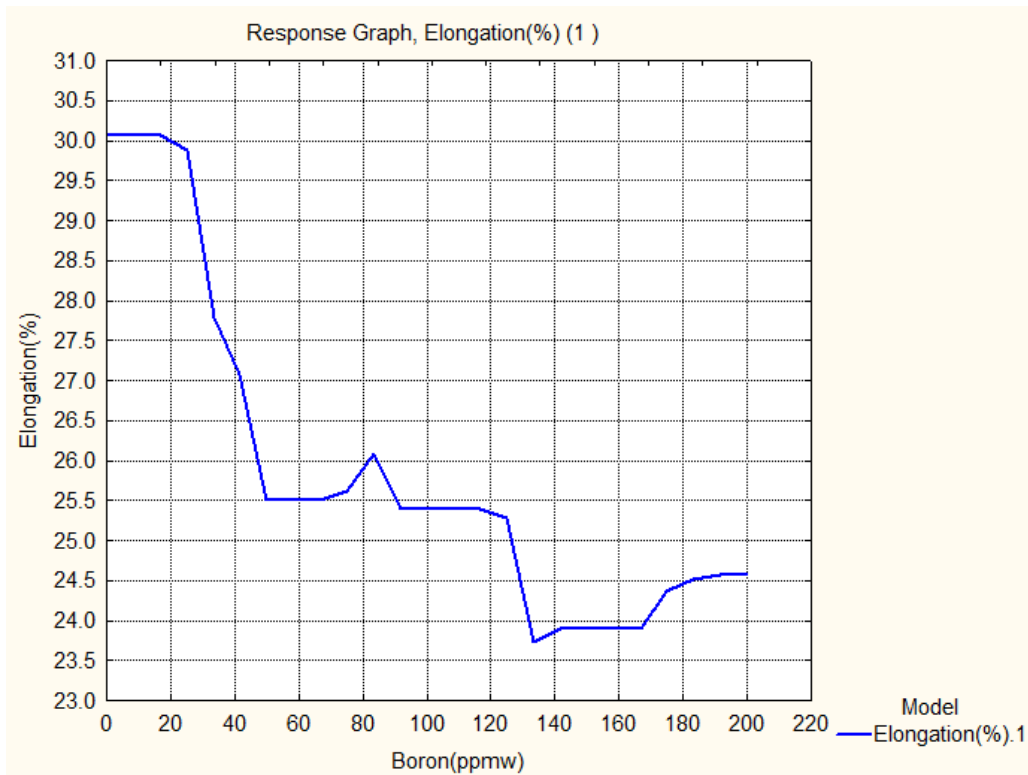


Fig. m Response Graph of Elongation % and Boron(ppm)

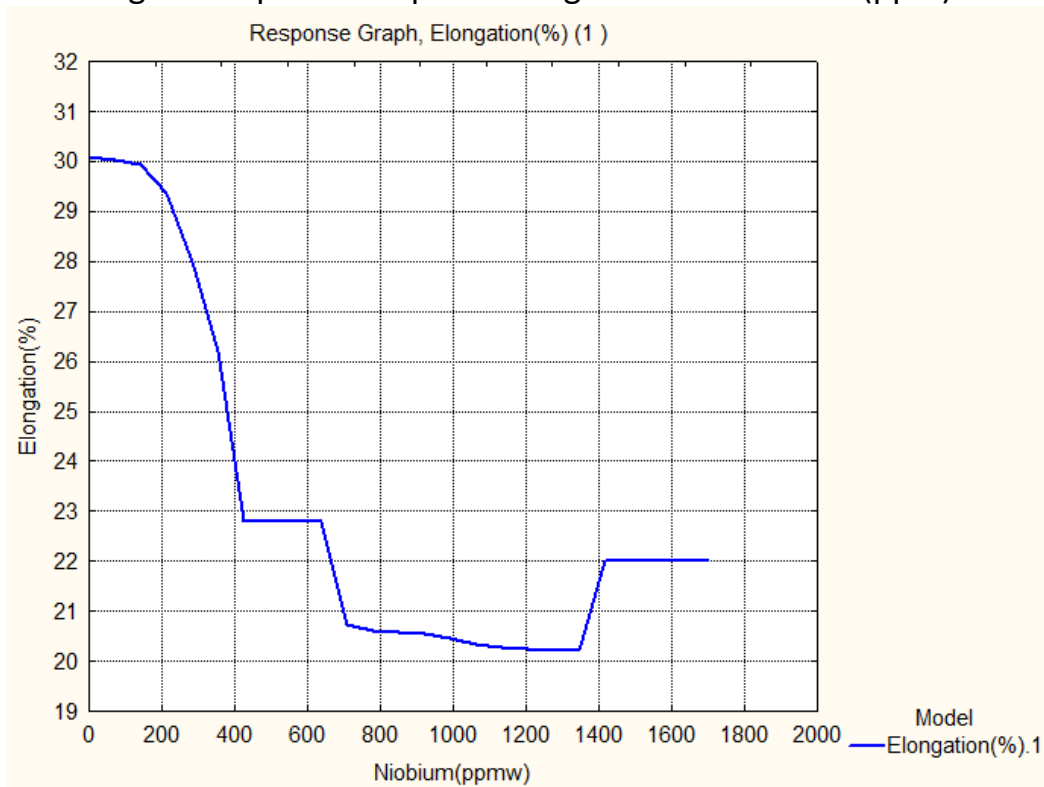


Fig. n Response Graph of Elongation % and Niobium(ppmw)

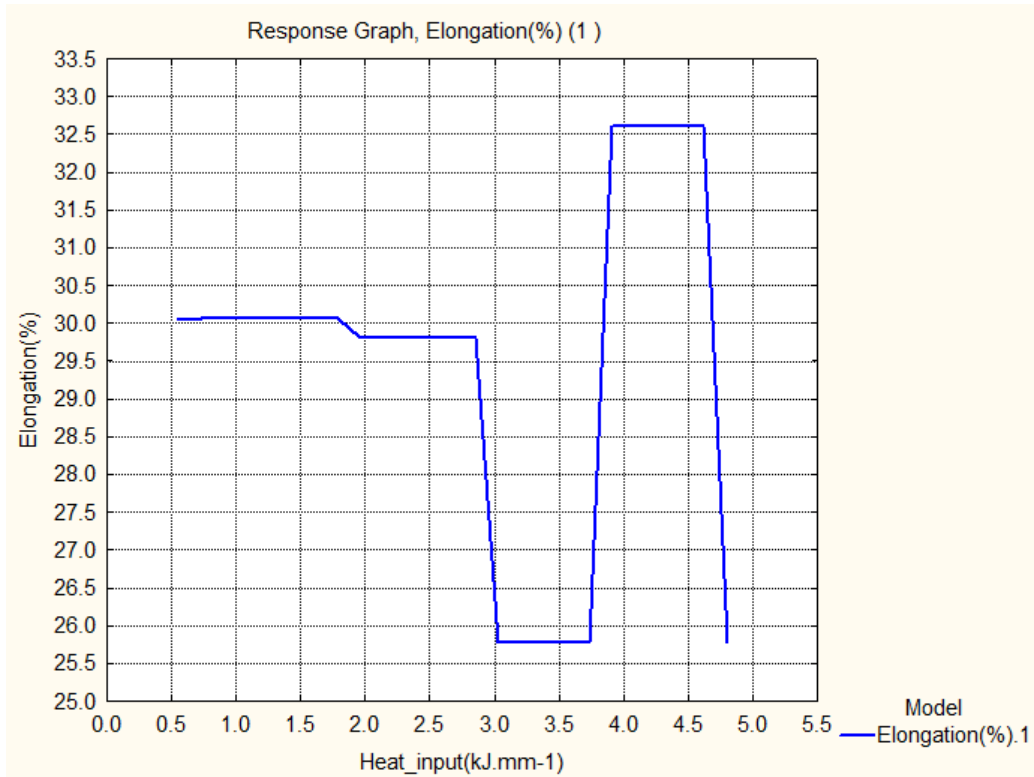


Fig. o Response Graph of Elongation % and Heat input(kj mm-1)

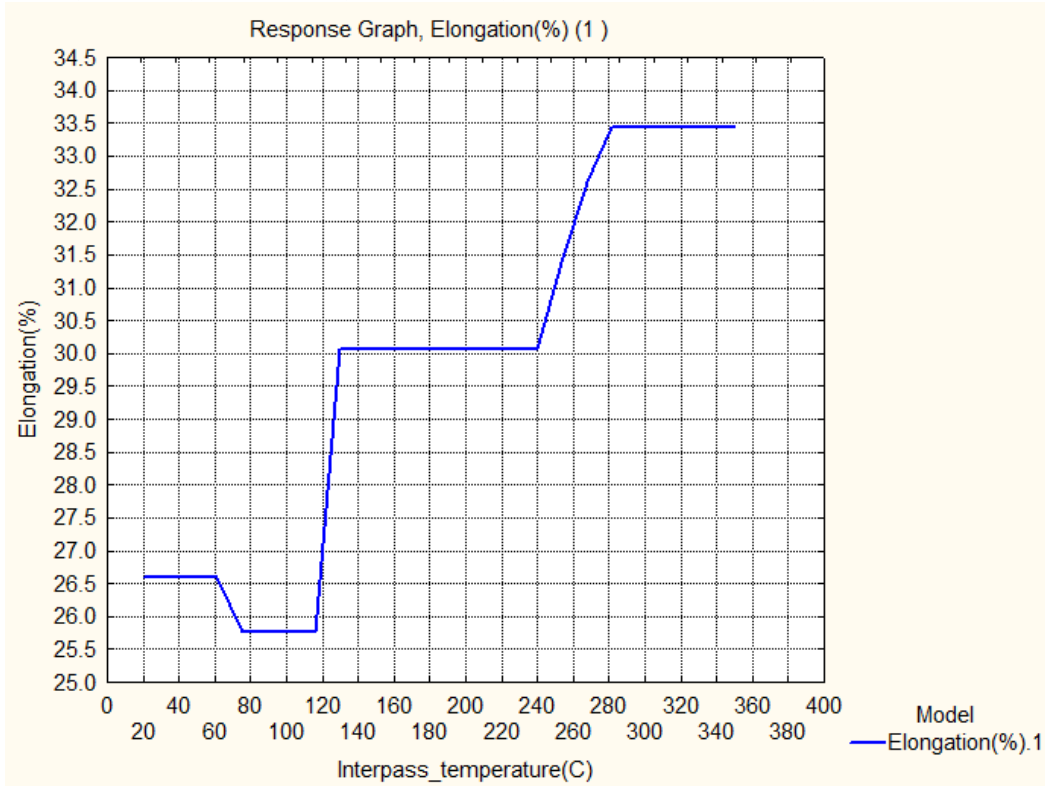


Fig. p Response Graph of Elongation % and Interpass temperature(C)

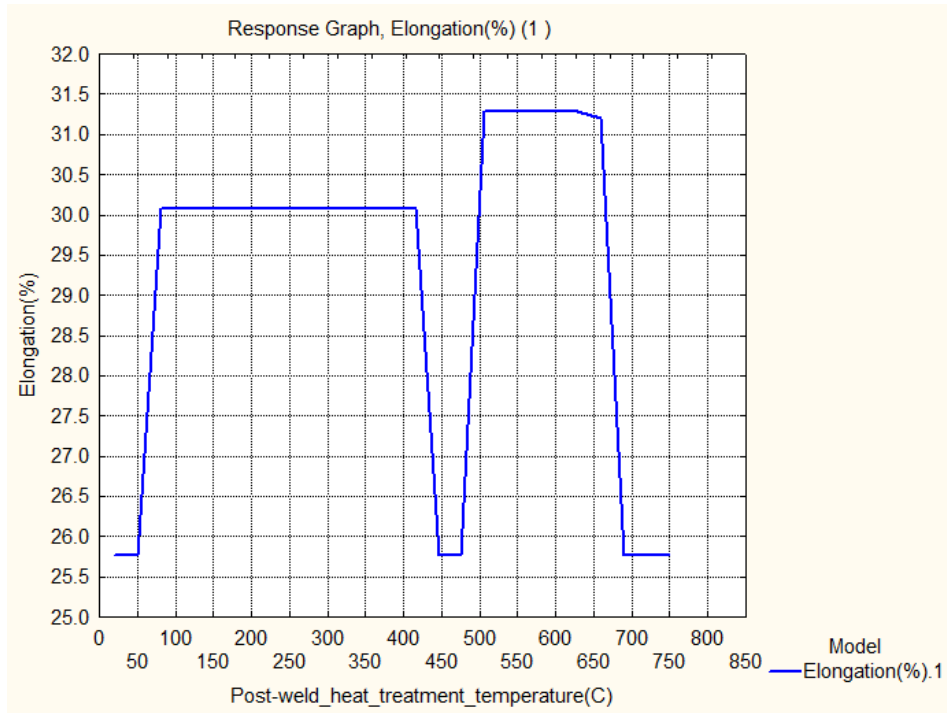


Fig. q Response Graph of Elongation % and Post-weld heat treatment temperature(°C)

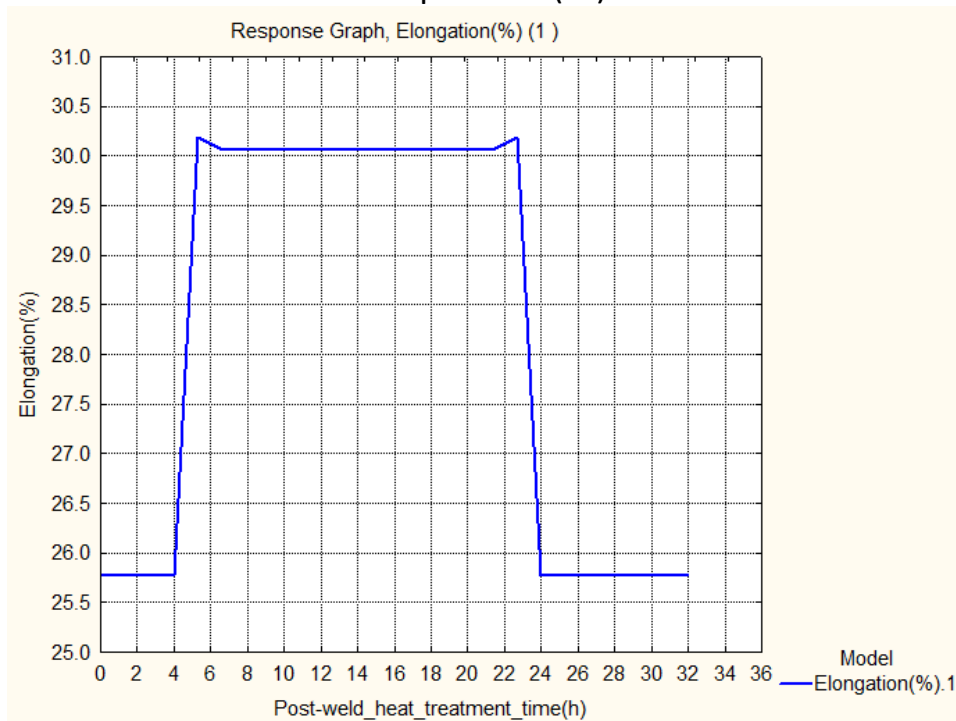


Fig. r Response Graph of Elongation % and Post-weld heat treatment time(h)

Figure 4.8 (a to r) Response graphs(a to r) of Input variables Elongation of Ferritic Steel Welds

The influence of each of the variables on the elongation of welding alloys, which is discussed here. The % elongation starts increasing from 26% at 0.01% C up to 30.7 % near to 0.055% C. Up and down of % elongation is maximum 2.5%, between the 0.055%C to 0.09%C. There is a decrease in %elongation after 0.09% C and it goes to 27.4 % at 0.0129% C. . In the case of silicon between 0.01% to 1.14%, there is an increase from the 26.9% to 30% (at 0.16%Si) in the elongation and then further decrease to 29.4% Elongation in the range of 0.2% to 0.3% Si. At near to 0.4% Si, Elongation is 30.2%. Reduction of the Elongation of 27.7% is observed near to 0.5% Si in the graph. Highest value of 30.7% Elongation is observed between the 0.58% Si to 0.78% Si. The drop in Elongation to 28.7% at 0.8% Si and then, it remains constant. The trend of manganese shows the increase in the Mn% from 0.24% to 2.3%, the value of the elongation also decreases from 31.2% to 23.7%. Between 0.24% Mn to 0.84% Mn, there is decrease in % elongation to 26.8% and further increases to 30.8% at 1.1% Mn. Over 1.1% Mn, there is generally decreased in %Elongation with increase in %Mn, with little fluctuation of 0.6% Elongation at 1.9% Mn. The sulphur shows the first increase in the Elongation from 29.79% to 30.3%, between 0.002%S to 0.006%S. Between 0.006%S to 0.012%S, Elongation is decreased from 30.0% to 29.4%. After 0.012%S, it starts increasing to a maximum 31.4%, at 0.015%S. The only reduction in 0.8% Elongation is observed between 0.02 %S to 0.045%S. The Phosphorus gives the increase in the Elongation from 27.95% to 31.2% in the range of 0.001%P to 0.0175%P. Reduction in the Elongation from 31.2% to 29.2% is observed with increase in amount of Phosphorus up to 0.04%. The nickel has the maximum Elongation of 30% at 0.85% and decrease with increase in %Ni more than 0.85%. In the figure, it shows at 0.85% the Elongation value drops from 30% to 25.3%. More than 5.8 % Ni gives a constant value of the Elongation 25.8%. The Chromium has a maximum Elongation of 30.1% at less than and equal to 0.4% Cr. More than 0.4% Cr reduces the Elongation to 21%. Further increase in %Cr between 0.7% to 5%, the Elongation drop from 21% to 15.4%. More than 5% Cr the Elongation increases of 25.8% and constant up to a maximum 9.3% Cr. Molybdenum has a maximum Elongation 30.1% at less than and equal to 0.3% concentration. More than 0.3% Mo decreases the Elongation from 30.1% to 21% at 0.5% Mo. At 1.7% Mo, the value of Elongation is a minimum to 20.7%. More than 1.7% Mo increases Elongation up to 25.7% and then it is constant till 2.4% Mo. Vanadium decreases the Elongation from a maximum 30.2% to a minimum 22.7% between 0.01% to 0.068%. At 0.092% V, the Elongation is 25.2%, then decrease to 20.8%

between 0.131% V to 0.16% V. More than 0.16% V increases the Elongation from 20.8% to 25.8% and 25.8% is constant up to a concentration of 0.32% V. Copper decreases the Elongation from 30.2% to 25.8% between more than 0% Cu to 2.05% Cu. Oxygen increases the Elongation of 28.15% to 30.2% when it is in the range of 50 ppm to 450 ppm. Higher than 450ppm Oxygen, there is a decrease in the Elongation from 30.2% to 25.75%. At 850 ppm Oxygen, the Elongation is 25.75% and remains constant up to maximum 1650 ppm Oxygen. Titanium gives a minimum the Elongation of 22.7% to maximum 30.8%. At 60 ppm the Elongation is the highest. In between the range of Titanium from 60 ppm to 340 ppm, the Elongation reduces from 30.8% to 23.7%. In the Elongation approximately 3.7% variation is observed between 350 ppm and 685 ppm Titanium. Boron shows the maximum Elongation of 30.1% in between 0 ppm to 18 ppm. More than 18 ppm to , there is a reduction in the Elongation from 30.1% to 23.75% (at 134 ppm Boron) and the increase in 0.5% is observed at 84 ppm Boron and 200 ppm Boron. Niobium has a trend of decrease in the Elongation from 30.1% to 20.3% with an increase from 0 to 1350 ppm. More than 1420 ppm to 1700ppm, the Elongation is a constant value of 22%

Heat Input has stated that the maximum Elongation of 32.65% between 3.8 kJ mm⁻¹ to 4.65 kJ mm⁻¹. Heat Input between 2.7 kJ mm⁻¹ to 3.8 kJ mm⁻¹ reduces the Elongation from 29.7% to 25.75%. Heat Input starts from 0.5 kJ mm⁻¹ with 30.1% an Elongation. The Elongation has a little change of 0.3% between 0.5 kJ mm⁻¹ to 2.7kJ mm⁻¹. When the Interpass temperature is 20⁰C, the Elongation is 26.6%. More than 60⁰C, a decrease in the Elongation is observed to 25.8%. To increase in Interpass temperature more than 119⁰C, there is an increase in the Elongation from 25.8% at 72⁰C to 33.45% at 350⁰C. Post weld heat treatment temperature increases from 50⁰ C to 750⁰ C, shows the Elongation have higher values, 30.1% and 31.3%. Reduction in the Elongation, 28.5% is observed between 4200C to 470⁰C and more than 660⁰C. Post weld heat treatment time has a trend of increase in the Elongation from 25.75% to 30.1% between 2 to 22.8 hours. More than 22.8 hours PWHTt, it decreases to minimum Elongation of 25.75%.

The relationship between the input variables and the elongation is a nonlinear as seen above in response graphs (Figure 4.8).

4.3.3 3D Contour plots of the Elongation GRNN model

The effect in combination of any two input variables (Independent variables) from Carbon, Silicon, Manganese, Sulphur, Phosphorus, Nickel, Chromium, Molybdenum, Vanadium, Copper, Oxygen, Titanium, Boron, Niobium, Heat_input, Interpass_temperature, Post-weld heat treatment temperature and Post-weld heat treatment time on the Elongation of Ferritic Steel Welds are given in form of 3D contour plots. (Figure. 4.9.1 to 4.9.13)

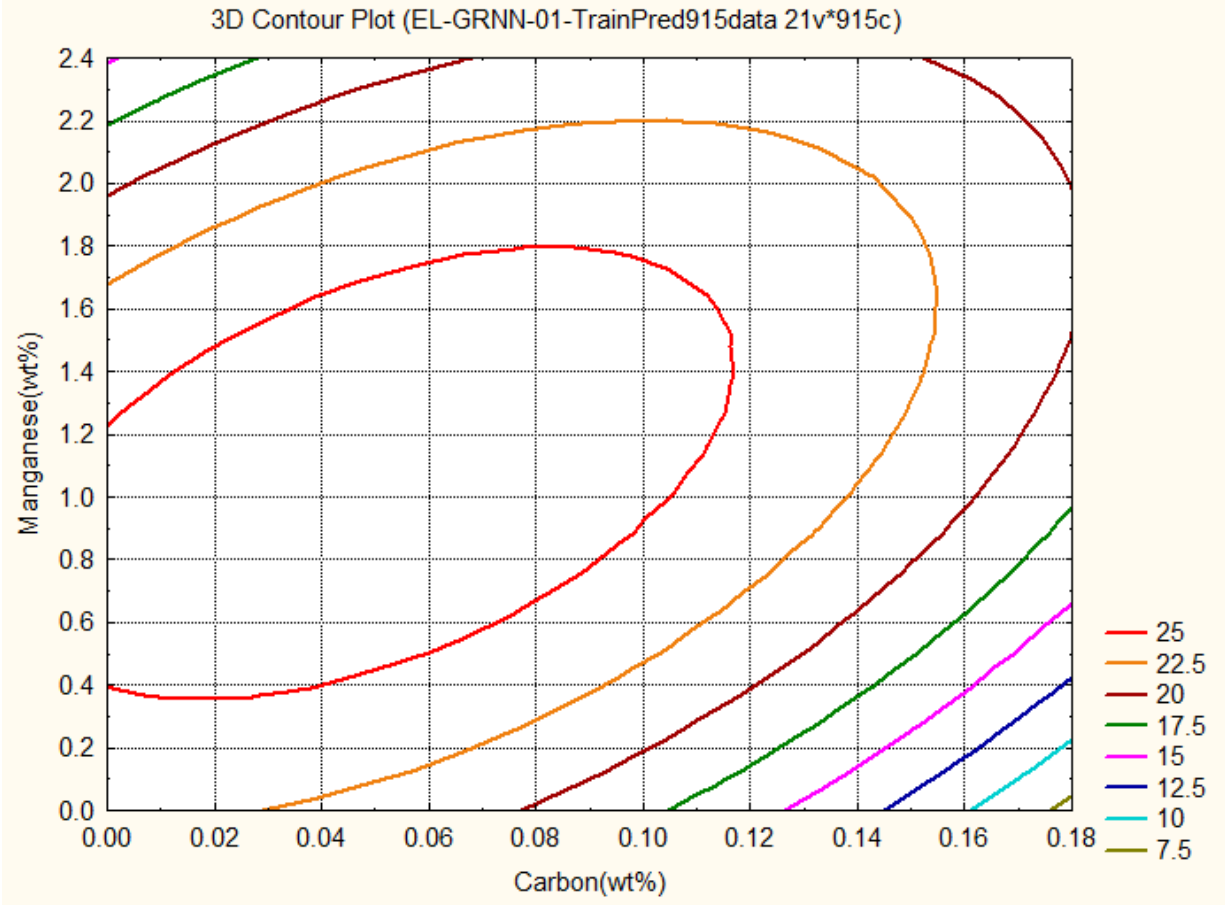


Figure.4.9.1 Predicted variations in Elongation (%) as a function of the Carbon and Manganese concentrations

3D contour Plot gives the relations between the **two input variables** and **one output variable**. **Figure. 4.9.1** shows the relations between Carbon, **Manganese** and Elongation by **GRNN**. The graph gives the information about how these two, Carbon and **Manganese** control the Elongation from 7.5% to **25%**.

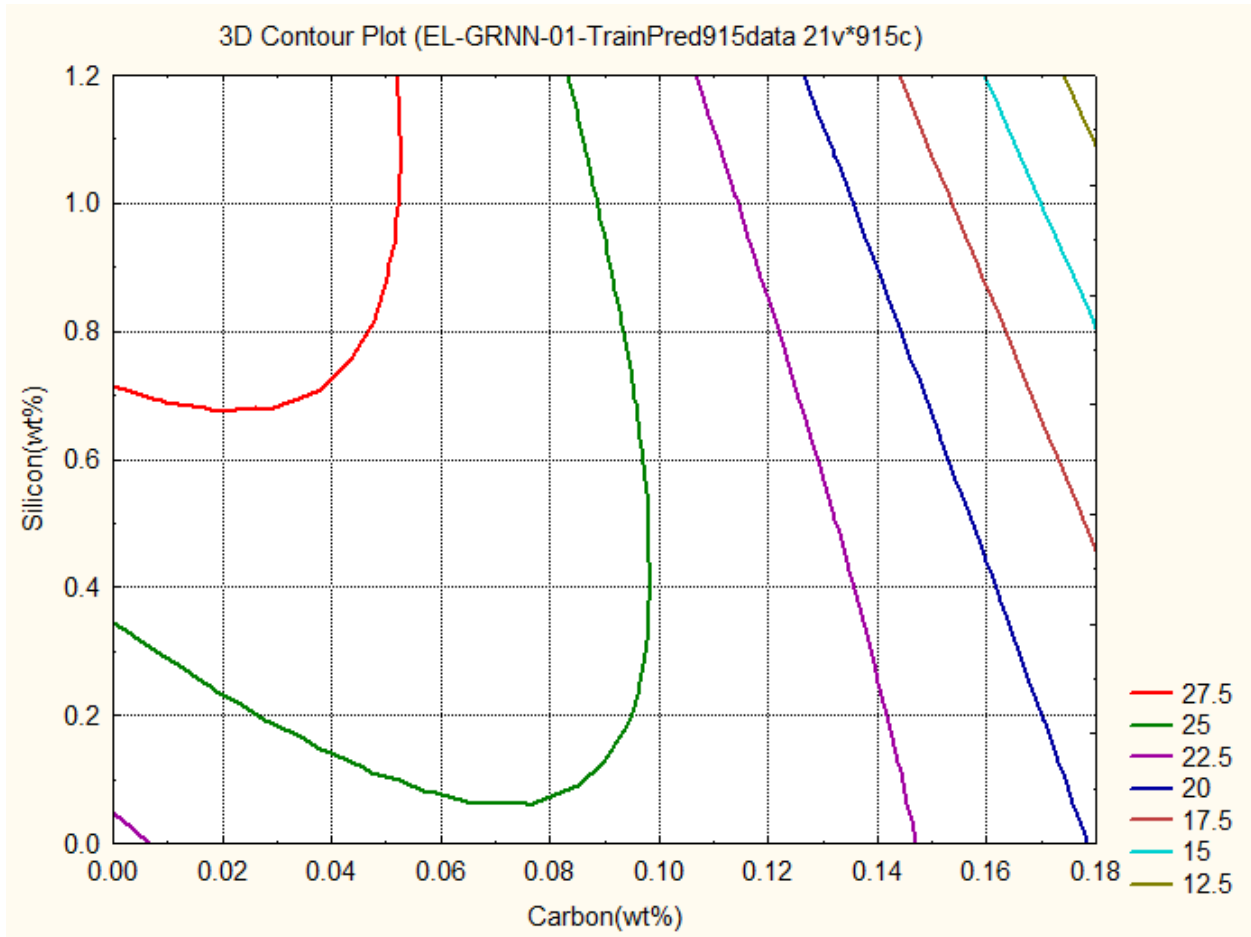


Figure. 4.9.2 Predicted variations in Elongation (%) as a function of the Carbon and Silicon concentrations

3D contour Plot gives the relations between the **two input variables** and **one output variable**. **Figure. 4.9.2** shows the relations between Carbon, Silicon and Elongation by **GRNN**. The graph gives the information about how these two, Carbon and Silicon control the Elongation from 12.5 % to 27.5 %.

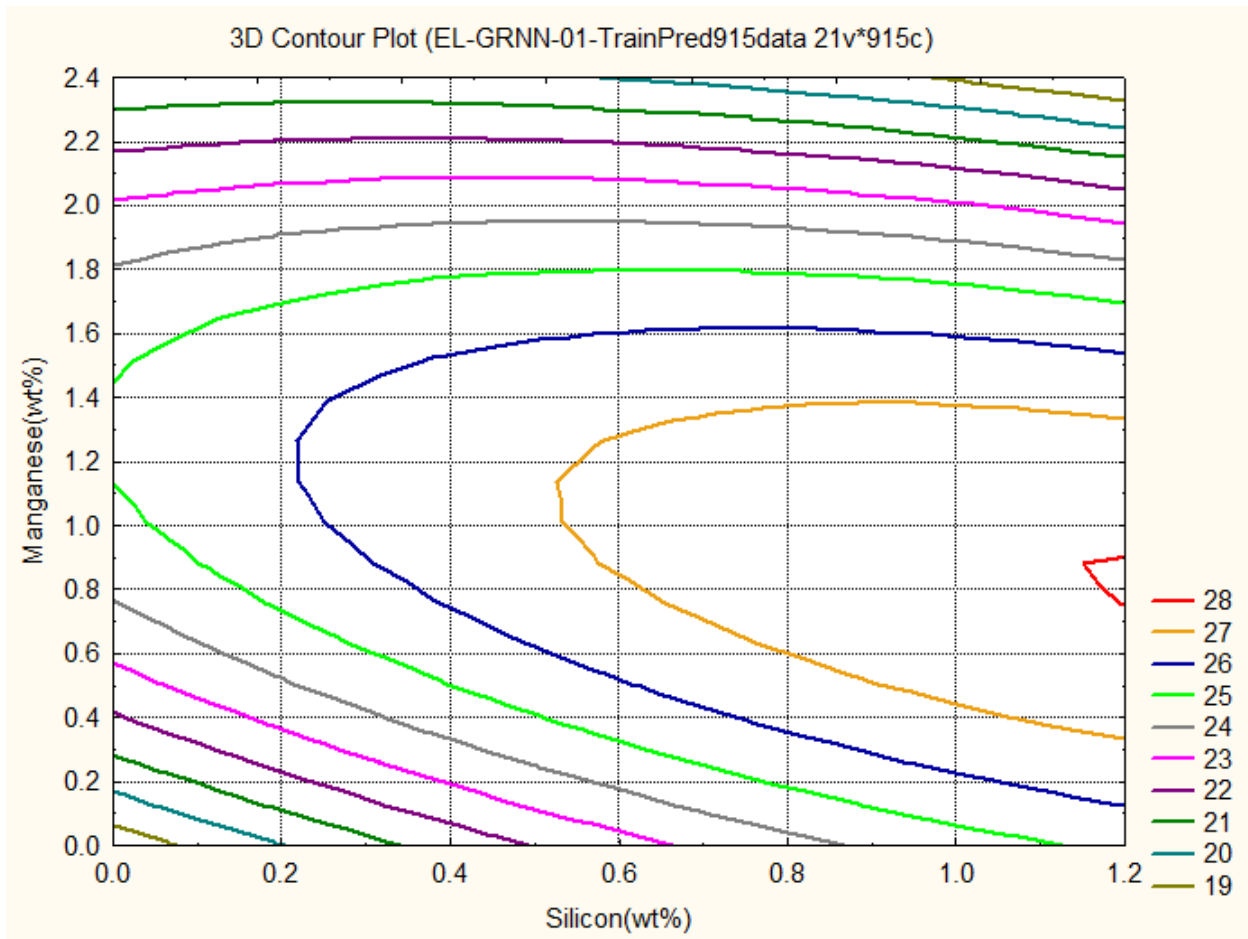


Figure. 4.9.3 Predicted variations in Elongation (%) as a function of the Silicon and Manganese concentrations

3D contour Plot gives the relations between the **two input variables** and **one output variable**. **Figure. 4.9.3** shows the relations between Silicon, Manganese and Elongation by **GRNN**. The graph gives the information about how these two, Silicon and Manganese control the Elongation from 19 % to 28 %.

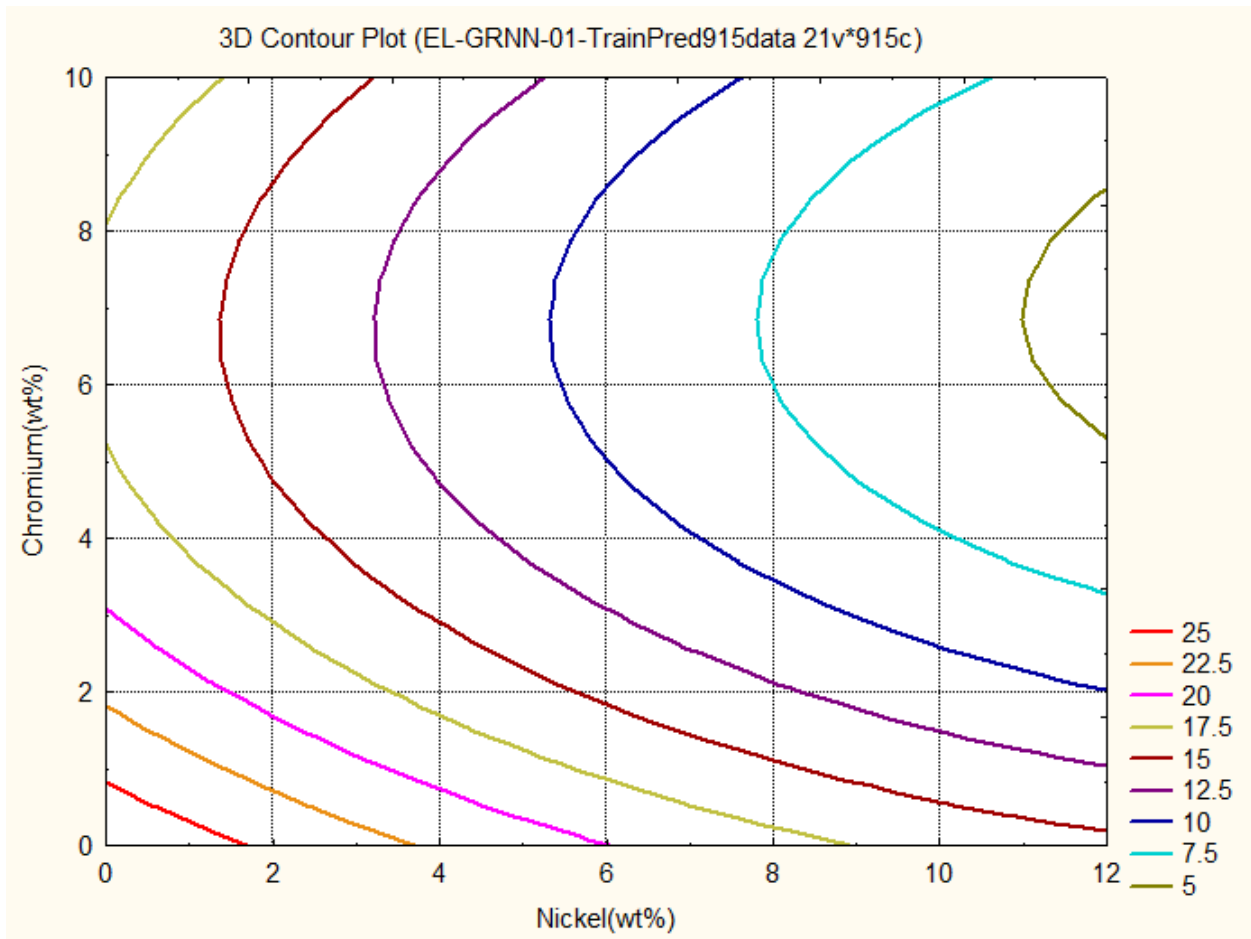


Figure. 4.9.4 Predicted variations in Elongation (%) as a function of the Nickel and Chromium concentrations

3D contour Plot gives the relations between the **two input variables** and **one output variable**. **Figure. 4.9.4** shows the relations between Nickel, Chromium and Elongation by **GRNN**. The graph gives the information about how these two, Nickel and Chromium control the Elongation from 5 % to 25 %.

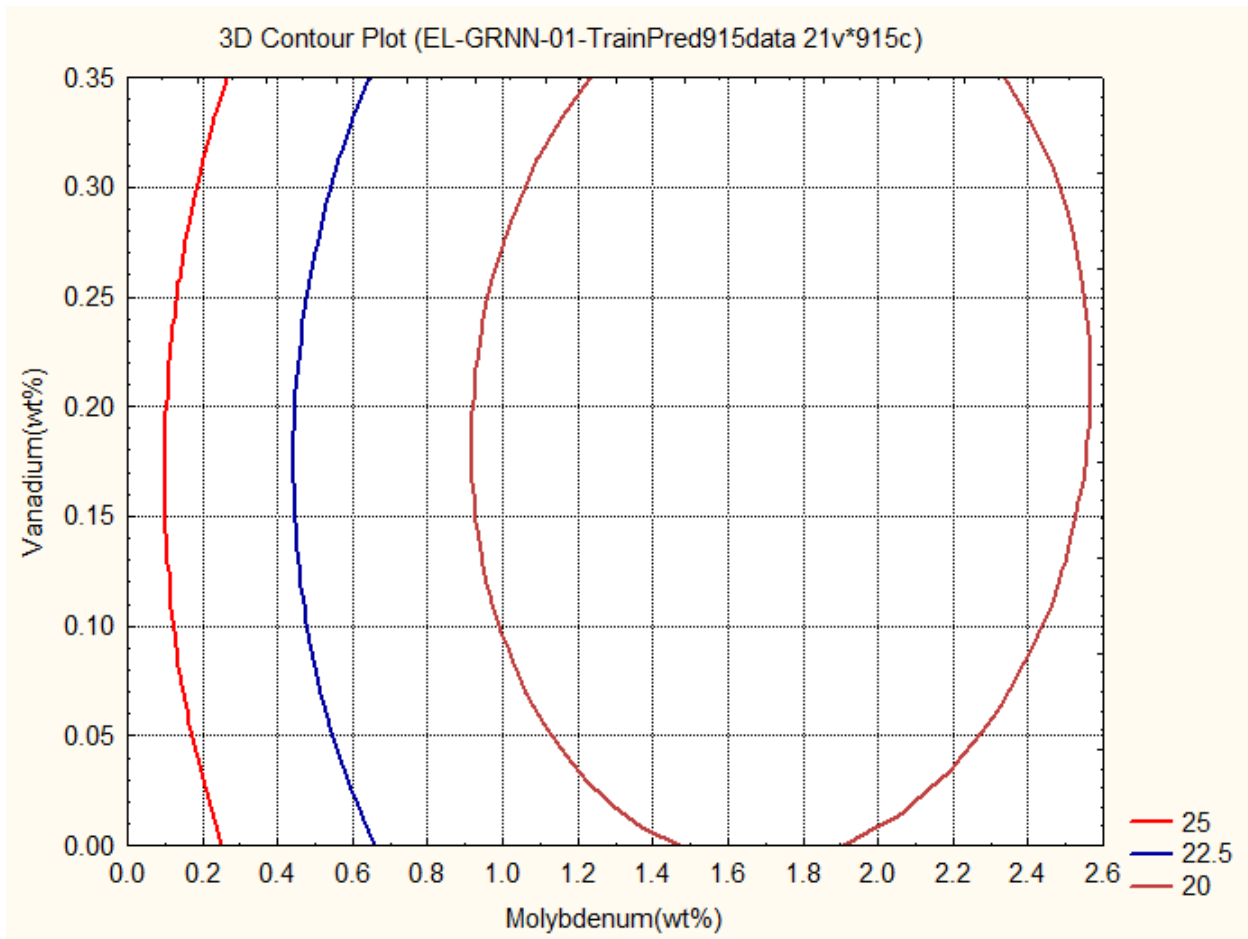


Figure. 4.9.5 Predicted variations in Elongation (%) as a function of the Molybdenum and Vanadium concentrations

3D contour Plot gives the relations between the **two input variables** and **one output variable**. **Figure. 4.9.5** shows the relations between Molybdenum, Vanadium and Elongation by **GRNN**. The graph gives the information about how these two, Molybdenum and Vanadium control the Elongation from 20 % to 25 %.

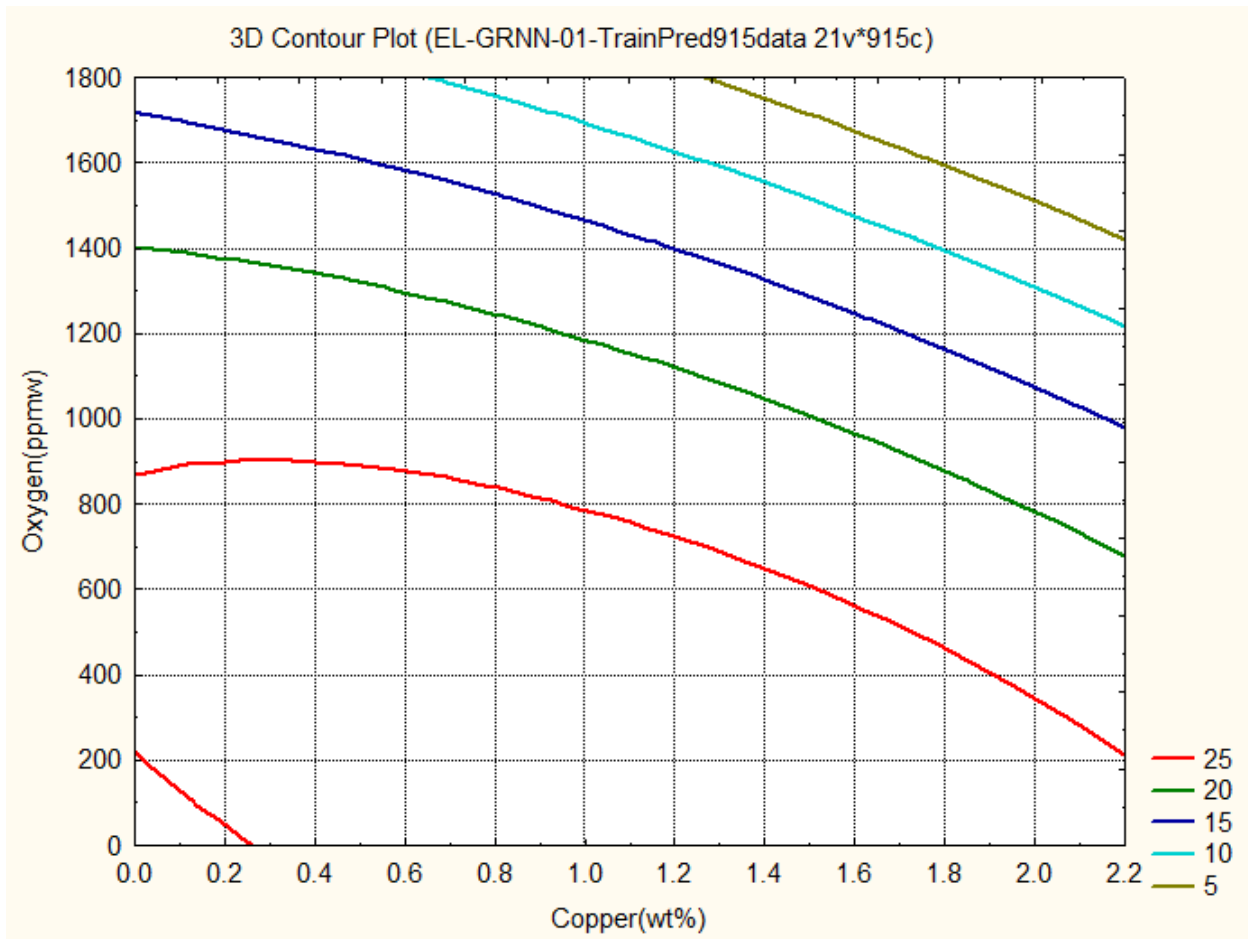


Figure. 4.9.6 Predicted variations in Elongation (%) as a function of the Copper and Oxygen concentrations

3D contour Plot gives the relations between the **two input variables** and **one output variable**. **Figure. 4.9.6** shows the relations between Copper, Oxygen and Elongation by **GRNN**. The graph gives the information about how these two, Copper and Oxygen control the Elongation from 5% to 25 %.

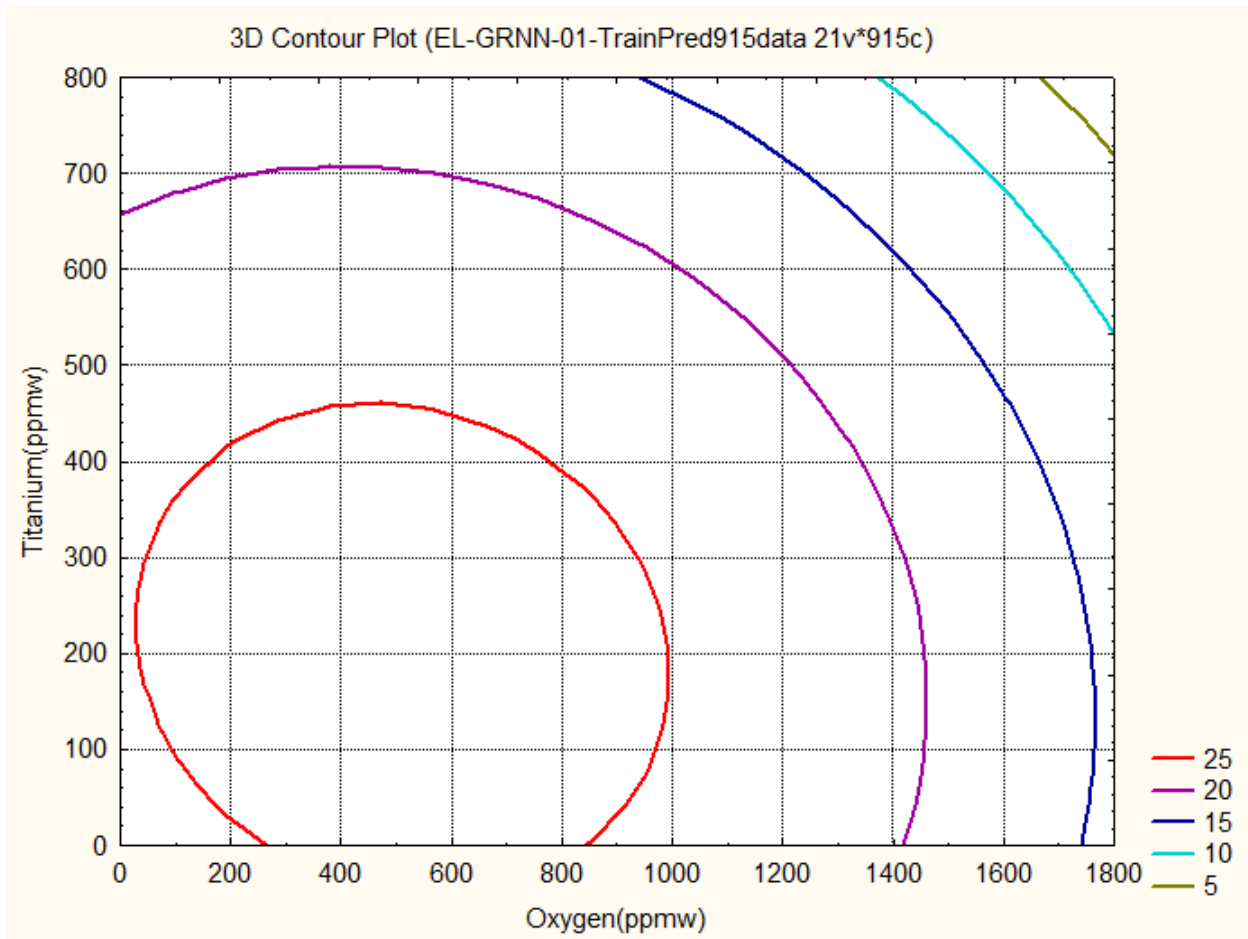


Figure. 4.9.7 Predicted variations in Elongation (%) as a function of the Oxygen and Titanium concentrations

3D contour Plot gives the relations between the **two input variables** and **one output variable**. **Figure. 4.9.7** shows the relations between Copper, Oxygen and Elongation by **GRNN**. The graph gives the information about how these two, Copper and Oxygen control the Elongation from 5% to 25 %.

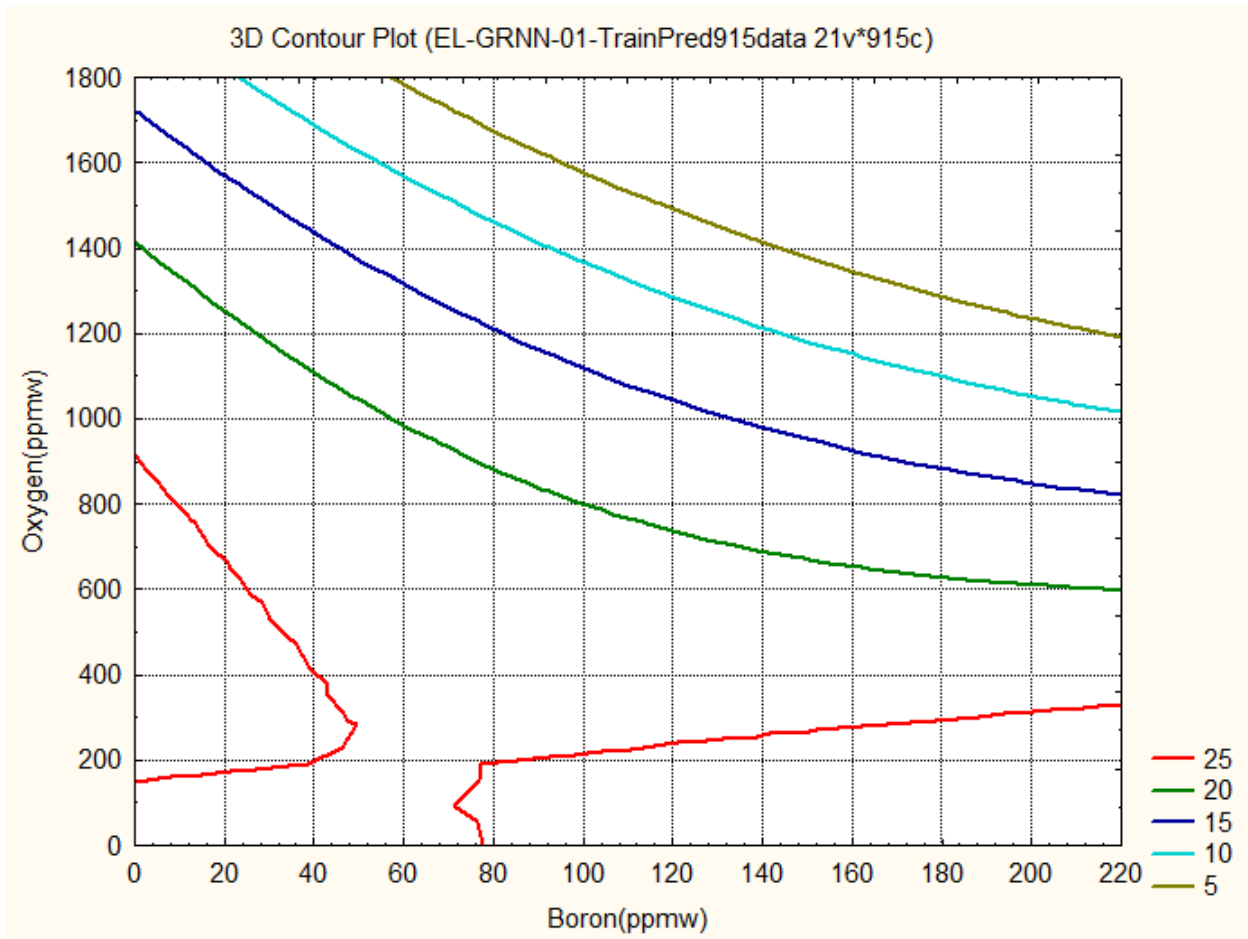


Figure. 4.9.8 Predicted variations in Elongation (%) as a function of the Boron and Oxygen concentrations

3D contour Plot gives the relations between the **two input variables** and **one output variable**. **Figure. 4.9.8** shows the relations between Boron, Oxygen and Elongation by **GRNN**. The graph gives the information about how these two, Boron and Oxygen control the Elongation from 5% to 25 %.

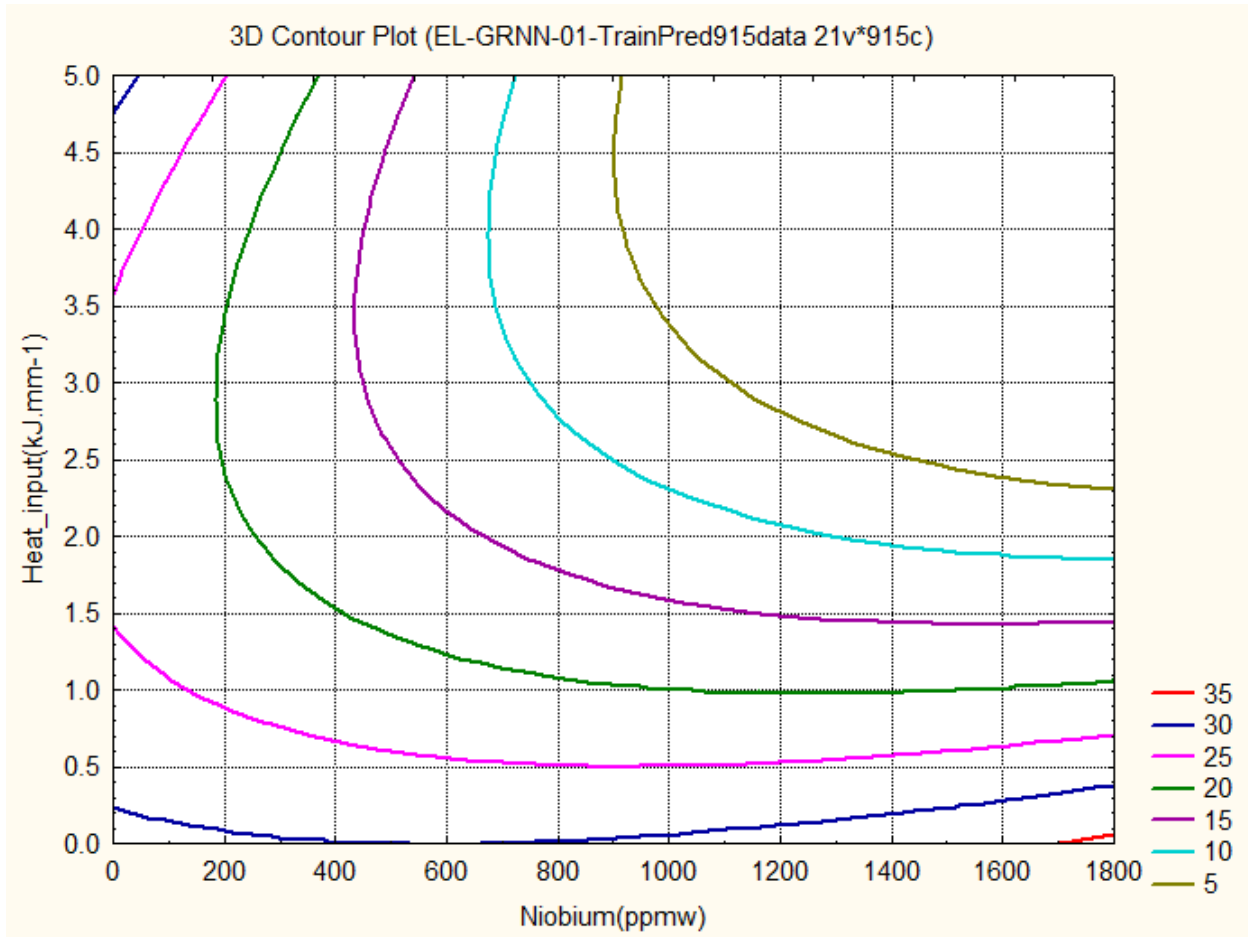


Figure. 4.9.9 Predicted variations in Elongation (%) as a function of the Niobium concentration and Heat input

3D contour Plot gives the relations between the **two input variables** and **one output variable**. **Figure. 4.9.9** shows the relations between Niobium, Heat input and Elongation by **GRNN**. The graph gives the information about how these two, Niobium and Heat input control the Elongation from **5% to 35 %**.

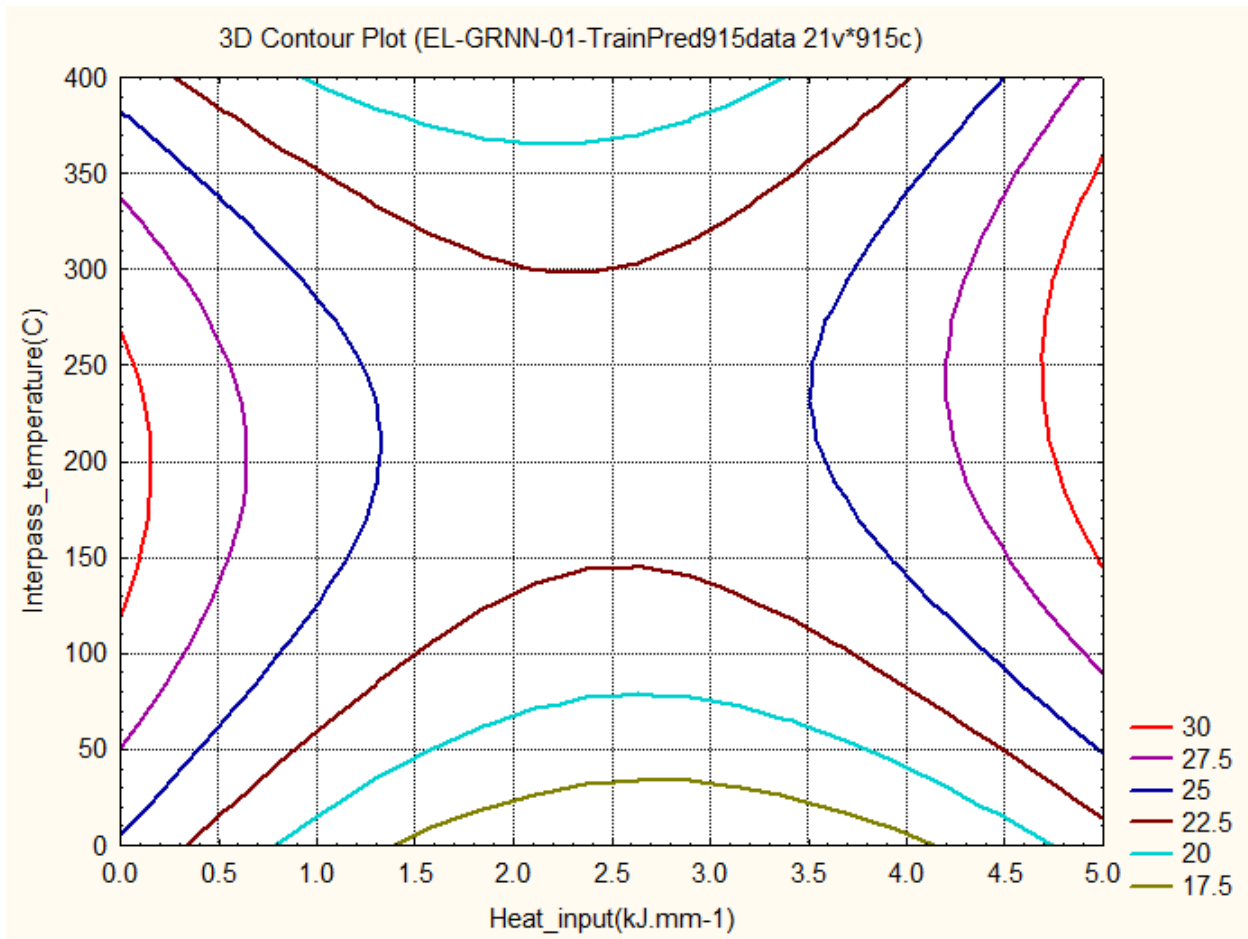


Figure. 4.9.10 Predicted variations in Elongation (%) as a function of the Heat input and Interpass temperature

3D contour Plot gives the relations between the **two input variables** and **one output variable**. **Figure. 4.9.10** shows the relations between Heat input, Interpass temperature and Elongation by **GRNN**. The graph gives the information about how these two, Heat input and Interpass temperature control the Elongation from 17.5% to 30 %.

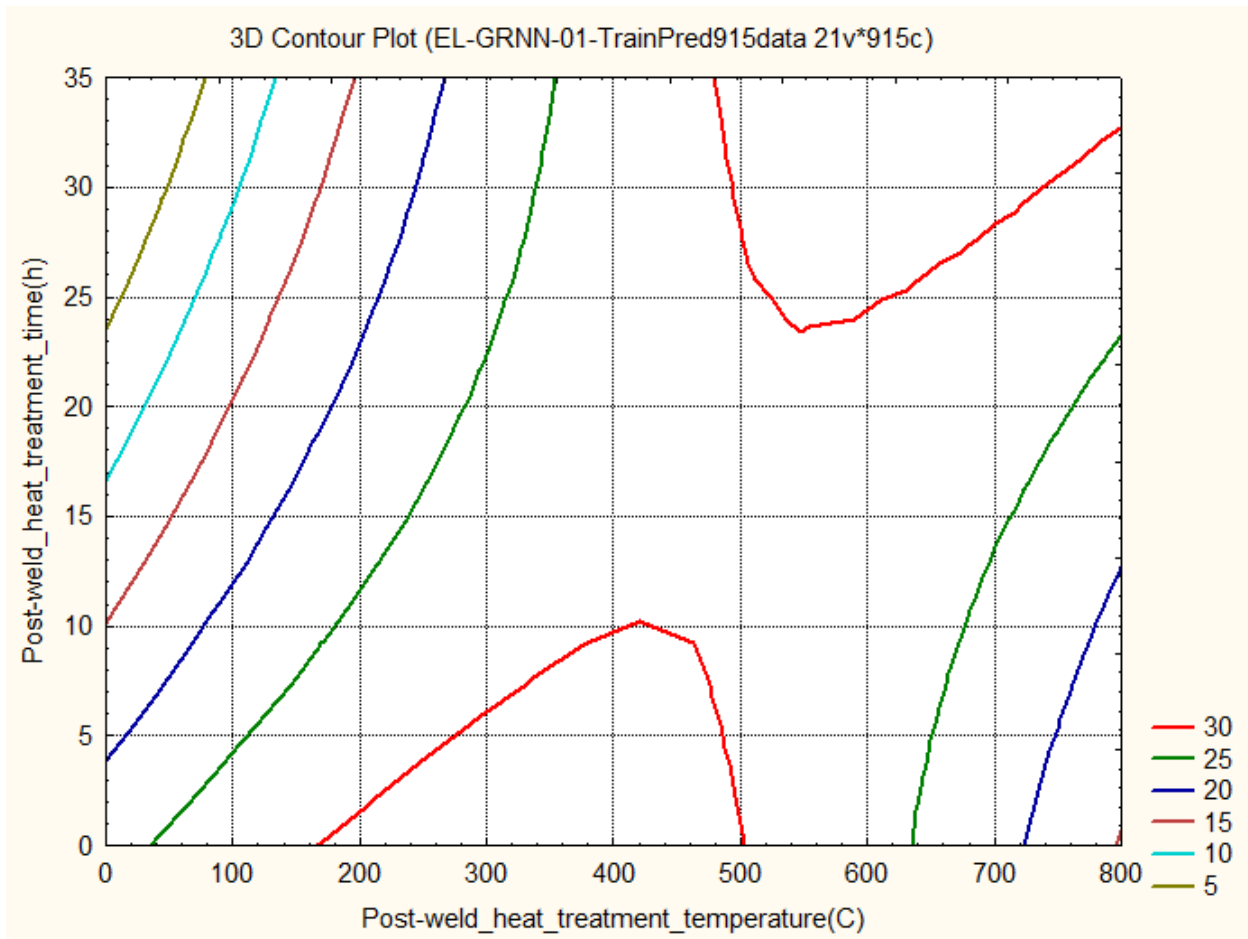


Figure. 4.9.11 Predicted variations in Elongation (%) as a function of the Post-weld Heat treatment temperature and Post-weld Heat treatment time

3D contour Plot gives the relations between the **two input variables** and **one output variable**. **Figure. 4.9.11** shows the relations between Post-weld Heat treatment temperature, Post-weld Heat treatment time and Elongation by **GRNN**. The graph gives the information about how these two, Post-weld Heat treatment temperature and Post-weld Heat treatment time control the Elongation from 5% **to 30 %**.

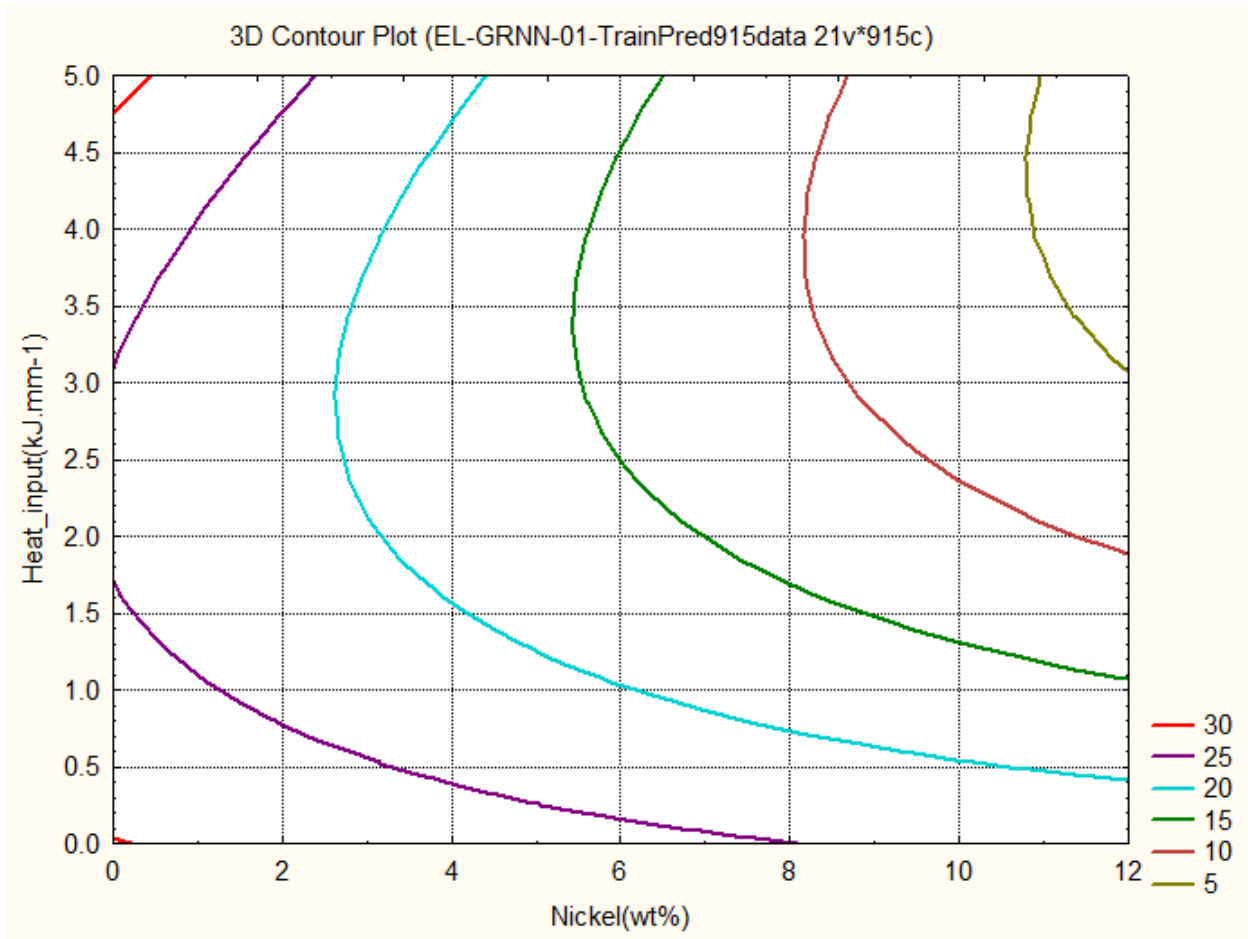


Figure. 4.9.12 Predicted variations in Elongation (%) as a function of the Nickel concentration and Heat input

3D contour Plot gives the relations between the **two input variables** and **one output variable**. **Figure. 4.9.12** shows the relations between Nickel, Heat input and Elongation by **GRNN**. The graph gives the information about how these two, Nickel and Heat input control the Elongation from 5% to 30 %.

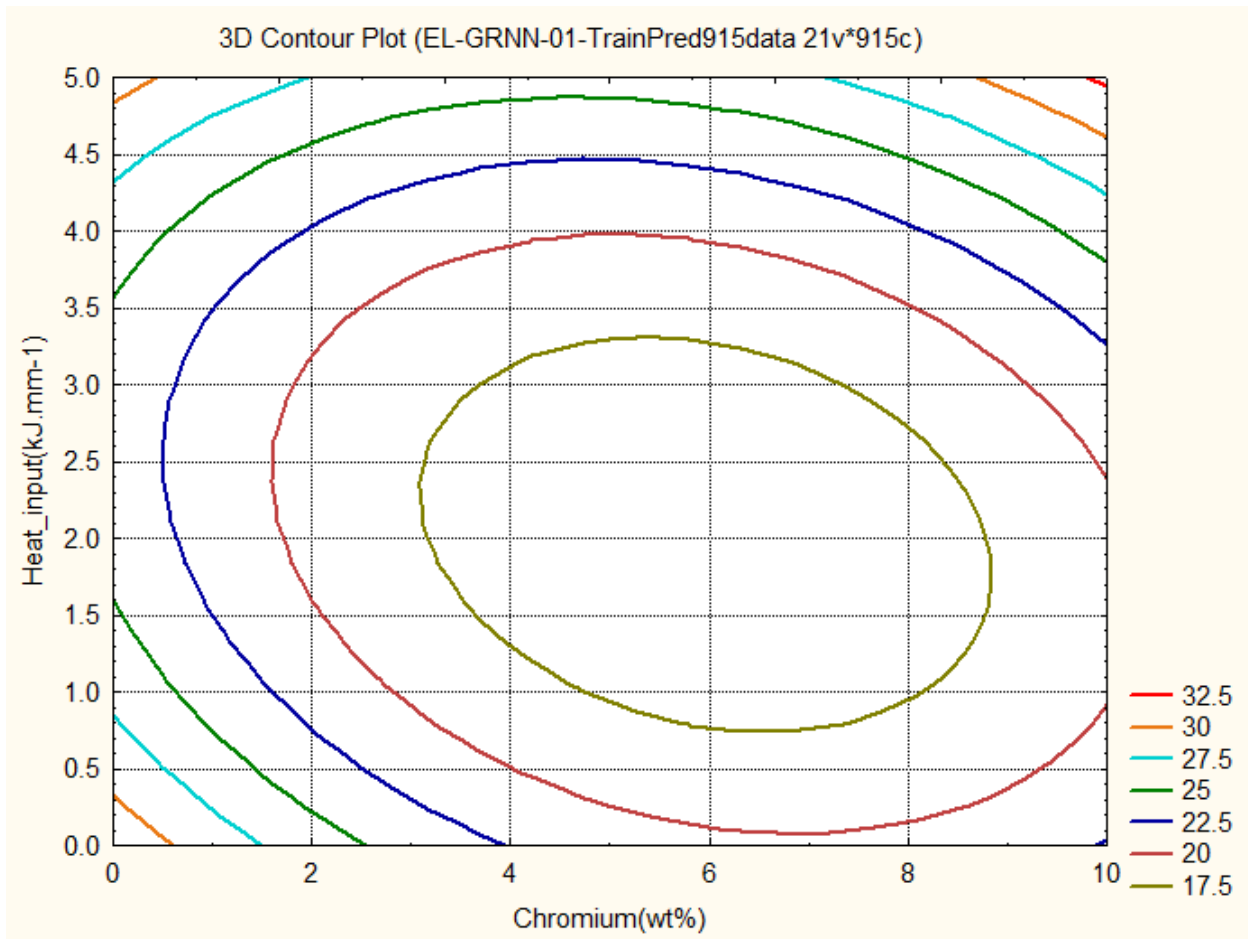


Figure. 4.9.13 Predicted variations in Elongation (%) as a function of the Chromium concentration and Heat input

3D contour Plot gives the relations between the **two input variables** and **one output variable**. **Figure. 4.9.13** shows the relations between Chromium, Heat input and Elongation by **GRNN**. The graph gives the information about how these two, Chromium and Heat input control the Elongation from 17.5% to **32.5 %**.

Figure 4.9.1. EL (z) - Mn (y) - C (x) 3D plot.5

Figure 4.9.1. shows the increase in the Elongation 25% and more than 25% inside the area covered by the contour of 25% Elongation. The contour of 25% Elongation has the range of %wt Carbon from 0% to 0.116% and %wt Manganese from 0.36% to 1.6%. Any other combination of concentration of wt% C and wt% Mn gives the reduction in the % Elongation which is clearly observed by the contours of lower % Elongation from 22.5% to less than 7.5%. For design of higher % Elongation, both the variables wt% C and wt% Mn must be controlled in specific range as mentioned above for Ferritic Steel Welds.

Figure 4.9.2. EL (z) - Si (y) - C (x) 3D plot.

Figure 4.9.2. The Elongation contours 27.5%, and more than 27.5% are observed in the range of wt% C from 0% to 0.052% and the range of wt% Silicon from 0.68% to 1.2%. The Elongation 25% and more than 25% can be achieved in the range of wt% C from 0% to 0.1% and in the range of Si from 0.06% to 1.2%. Higher amount of the both wt% C and wt% Si decreases the Elongation from less than 25% to 12.5%. The trends of the both the independent variables are less complex for the Elongation of Ferritic Steel Welds.

Figure 4.9.3. EL (z) - Mn (y) - Si (x) 3D plot.

Figure 4.9.3. shows an increase in the Elongation from 25% to more than 28% with the wt% Si in the range from 0% to 1.2% and the wt% Mn in the range from 0% to 1.8%. The Elongation 28% and more than 28% are obtained with the wt% Si in the range from 1.15% to 1.2% and the wt% Mn in the range from 0.78% to 0.9%. These are the very small range of the both independent variables for higher values of the Elongation of Ferritic Steel Welds. Any other combination of Si and Mn gradually decreases the Elongation from less than 25% to 19%. The selection of the Mn concentration is more critical compared to the concentration of Si for the design of Ferritic Steel welds.

Figure 4.9.4. EL (z) - Cr (y) - Ni (x) 3D plot.

Figure 4.9.4. shows the decreasing trends in the Elongation from more than 25% to less than 5% with the increase in the %wt Ni and the %wt Cr. The higher values of Elongation 25% more

than 25% are observed with the Ni in the range from 0% to 1.6% and the Cr in the range from 0% to 0.7% Cr. The bottom left of the plot indicates that for higher Elongation from more than 25% to 20 % in Ferritic Steel Welds require more 5 %Ni and less %Cr. The relationship of the both the independent variables %Ni and %Cr is less complex with Elongation.

Figure 4.9.5. EL (z) - V (y) - Mo (x) 3D plot.

Figure 4.9.5. shows the decreasing trends in the Elongation from more than 25% to less than 20% with the increase in the %wt Mo in the range from 0% to less than 2.5% and the %wt V in the range from 0% to 0.35%. Less than 0.68% Mo gives the % Elongation in higher side, more than 22.5% with a full %wt range of the Vanadium. More than 0.94% Mo reduces the Elongation which is less than 20%. The molybdenum is more effective variable compared to the Vanadium. The behaviour between the Molybdenum and the Vanadium is not much complex.

Figure 4.9.6. EL (z) - O (y) - Cu (x) 3D plot.

Figure 4.9. 6. shows the decreasing trends in the Elongation with an increase in the %wt Cu and Oxygen ppm from 25% to less than 5%. The high value of the Elongation 25% is observed with %wt Cu in the range, from 0.024% to 2.2% and Oxygen ppm in range from 200 ppm to 880 ppm. The Oxygen is more effective variable compare to copper for controlling the Elongation in specific range as indicated by the different Elongation contours.

Figure 4.9.7. EL (z) – Ti (y) - O (x) 3D plot.

Figure 4.9.7. shows the decreasing trends in the Elongation with an increase in the Oxygen ppm and Titanium ppm, from 25% to less than 5%. Higher values of Elongation of 25% and more than 25% are observed with Oxygen ppm in range, from 20 ppm to 1000 ppm and Titanium ppm in the range from 0 ppm to 460 ppm. The behaviour of both variables is very critical for achieving higher Elongation.

Figure 4.9.8. EL (z) – O (y) - B (x) 3D plot.

Figure 4.9.8. shows the decreasing trends in the Elongation with an increase in the Boron ppm and Oxygen ppm, from 25% to less than 5%. Higher values of Elongation of 25% and more than 25% are observed with Oxygen ppm in range, from 170 ppm to 910 ppm and Boron ppm in the range from 0 ppm to 48 ppm. Other contour of higher values of Elongation of 25% and more

than 25% is also observed with Oxygen ppm in range, from 0 ppm to 320 ppm and Boron ppm in the range from 72 ppm to 220 ppm. The Elongation between 20% and 25%, are observed with Oxygen ppm below the range from 600 ppm to 1000 ppm and the Boron ppm in range from 0 ppm to 220 ppm. For higher Elongation the Oxygen is a very important independent variable compare to Boron.

Figure 4.9.9. EL (z) – HI (y) - Nb (x) 3D plot.

Figure 4.9.9. shows the decreasing trends in the Elongation with an increase in the Niobium ppm and Heat Input kJmm-1, from 25% to less than 5%. For higher values of the Elongation 20% and more than 20%, are observed with the Niobium ppm in range, from 0 ppm to 1800 ppm and Heat Input kJmm-1 in the range from 0 kJmm-1 to 5.0 kJmm-1. Both the independent variables have a significant role in designing the Elongation of the Ferritic Steel Welds. The values of the Heat Input which is below 0.5 kJmm-1 indicate that means these are the properties of welding electrodes not welds.

Figure 4.9.10. EL (z) – IPT (y) - HI (x) 3D plot.

Figure 4.9.10. shows the maximum Elongation values 25% and more than 25% are observed in the left side and right side of the graph. Left side of graph has almost full range of the Interpass temperature from 10 C to 380 C and the Heat Input less than 1.15 kJmm-1. Right side of graph has the range of Interpass temperature from 50 C to 400 C and the Heat Input more than 3.5 kJmm-1. The Elongation are obtained between the range from 22.5% to 25% by maintaining the Heat Input, in the range from 1.15 kJmm-1 to 3.5 kJmm-1 and the Interpass temperature in the range from 145 C to 300 C. Both the independent variables have complex relationship with the Elongation.

Figure 4.9.11. EL (z) – PWHTt (y) - PWHTT (x) 3D plot.

Figure 4.9.11. shows a decrease in the Elongation values from 25% to 5%, are observed in the left side and right side of the graph. Left side of graph has almost full range of the Post Weld Heat Treatment Time h from 0 h to 35 h and the Post Weld Heat Treatment Temperature from 0 C to 350 C. Right side of graph has the range of the Post Weld Heat Treatment Time h from 0 h to 23 h and the Post Weld Heat Treatment Temperature from 630 C to 800 C. The Elongation are obtained between the range from 25% to 30% and more by maintaining the Post Weld Heat

Treatment Time, in the range from 0 h to 35 h and Post Weld Heat Treatment Temperature in the range from 40 C to 800 C. Both the independent variables have complex relationship with the Elongation.

Figure 4.9.12. EL (z) – HI (y) - Ni (x) 3D plot.

Figure 4.9.12. shows increase in the Elongation more than 20%, with lower than 2.6% Ni and any value of Heat Inputs from 0 to 5 kJmm⁻¹. Heat Input in range from 2.5 kJmm⁻¹ to 5 kJmm⁻¹, the Elongation decreases with an increase in %Ni. Heat Input from 2.5 kJmm⁻¹ to less than 2.5 kJmm⁻¹, the Elongation increases with an increase in %Ni.

Figure 4.9.13. EL (z) – HI (y) - Cr (x) 3D plot.

Figure 4.9.13. shows the Elongation 17.5% and less than 17.5%, are observed with the Chromium in the range from 3.2% to 8.8% and Heat Input in the range from 0.75 kJmm⁻¹ to 3.3 kJmm⁻¹. Outside of the Elongation contour 17.5%, the %Elongation values are increased for all combinations of Heat Input and Chromium. The nature of both independent variables is observed complex and significant for designing the %Elongation of Ferritic Steel Welds.

4.3.4 Application of Trained Best Models

4.3.4.1 Prediction of the Elongation on unseen data by BNN Model

The BNN model has good accuracy in prediction of elongation of ferritic steel welds on unseen data which is excellent for the design of welds. (Table. 4.7) The predicted elongation of the unseen data of three weld alloys are compared with measured values of elongation shows the prediction capacity of the BNN model. This BNN model can be used for practical applications, research and development of ferritic steel alloys.

Table 4.7 Predicted Elongation by BNN model for unseen data of three ferritic weld deposits

Variable	Weld alloy 1	Weld alloy 2	Weld alloy 3
Carbon(wt%)	0.041	0.088	0.11
Silicon(wt%)	0.300	0.35	0.28
Manganese(wt%)	0.62	0.54	0.6
Sulphur(wt%)	0.007	0.007	0.007
Phosphorus(wt%)	0.010	0.009	0.016
Nickel(wt%)	2.38	7.0	10.62
Chromium(wt%)	0.03	0.15	1.13
Molybdenum(wt%)	0.005	0.4	0.3
Vanadium(wt%)	0.012	0.016	0.006
Copper(wt%)	0.03	0.01	0.3
Oxygen(ppm)	440	290	290
Titanium(ppm)	55	0.0	0.0
Boron(ppm)	2.0	1.0	1.0
Niobium(ppm)	20	10	10
Heat_input(kj.mm-1)	1.0	1.4	1.4
Interpass_temperature(C)	200	150	200
Postweld_heat_treatment_temperature(C)	250	250	250
Post-weld_heat_treatment_time(h)	14	16	16
Measured Elongation %	31	13	11
Predicted Elongation %	30.03	17.02	13.62

4.3.4.2 Prediction of The Elongation on unseen data by GRNN Model

The GRNN model has good accuracy in prediction of elongation of ferritic steel welds on unseen data which is excellent for the design of welds. (Table.4.8) The predicted elongation of the unseen data of three weld alloys are compared with measured values of elongation shows the prediction capacity of the GRNN model. This GRNN model can be used for practical applications, research and development of ferritic steel alloys.

Table 4.8 Predicted Elongation by GRNN model for unseen data of three ferritic weld deposits

Variable	Weld alloy 1	Weld alloy 2	Weld alloy 3
Carbon(wt%)	0.041	0.088	0.11
Silicon(wt%)	0.300	0.35	0.28
Manganese(wt%)	0.62	0.54	0.6
Sulphur(wt%)	0.007	0.007	0.007
Phosphorus(wt%)	0.010	0.009	0.016
Nickel(wt%)	2.38	7.0	10.62
Chromium(wt%)	0.03	0.15	1.13
Molybdenum(wt%)	0.005	0.4	0.3
Vanadium(wt%)	0.012	0.016	0.006
Copper(wt%)	0.03	0.01	0.3
Oxygen(ppm)	440	290	290
Titanium(ppm)	55	0.0	0.0
Boron(ppm)	2.0	1.0	1.0
Niobium(ppm)	20	10	10
Heat_input(kJ.mm-1)	1.0	1.4	1.4
Interpass_temperature(C)	200	150	200
Postweld_heat_treatment_temperature(C)	250	250	250
Post-weld_heat_treatment_time(h)	14	16	16
Measured Elongation %	31	13	11
Predicted Elongation %	31	19	13

Prediction of The Elongation for new data of input variables can be achieved accurately with best trained models by BNN and GRNN as given in above Tables 4.7 and Table 4.8. These Models have capacity for changing any individual input variable, any combination of more than one input variables or all input variables to predict the The Elongation of Ferritic Steel Welds. These are only possible with the BNN and GRNN Models which are impossible practically. By simply running these Models the various design of the Ferritic Steel Welds are possible which save money, time and labour during Research and Development of the Ferritic Steel Welds.

4.3.5 Genetic Algorithms and applications to the Elongation of Ferritic Steel Welds

4.3.5.1 Target Elongation of 13% and High value of Elongation 45%

The first simulation is made to check the behaviour of the genetic algorithm. The target value of elongation is set to -0.8. Which correspond to an unnormalised value of 13%. The dataset provides such values of elongation and the aim of this simulation is to check the results of the genetic algorithm.. The 18 parameters (input variables) are allowed to vary, in between -1 and + 1 during the genetic algorithm process. After 3000 generations, the best results obtained are shown Table 4.9.

The second simulation is made to check the genetic algorithm for high value of the Elongation.The target value of Elongation is set to 0.12 which correspond to an unnormalised value of 45%. The dataset does not provide such value of Elongation and the aim of this simulation is to check the results of the genetic algorithm.. The 18 parameters(input variables) are allowed to vary, in between -1 and + 1 during the genetic algorithm process. After 3000 generations, the best results obtained are shown Table 5.6.

According to Table 4.9, the genetic algorithm has managed to reach the target after 3000 generations.

Moreover, the associated error obtained is very reasonable.

To check if the given input variables correspond to Ferritic Steel Weld, compare with the actual data of Elongation.

Table 4.9 Predicted Input variables by NN-GA model for two targeted Elongation of ferritic weld deposits

Variable	Weld 1 Result GA	Weld 1 Data	Weld 2 Result GA
Carbon(wt%)	0.078	0.088	0.036
Silicon(wt%)	0.34	0.35	0.290
Manganese(wt%)	0.47	0.54	0.670
Sulphur(wt%)	0.006	0.007	0.005
Phosphorus(wt%)	0.007	0.009	0.015
Nickel(wt%)	6.2	7.0	0.04
Chromium(wt%)	0.13	0.15	1.26
Molybdenum(wt%)	0.39	0.4	0.14
Vanadium(wt%)	0.014	0.016	0.25
Copper(wt%)	0.01	0.01	0.03
Oxygen(ppm)	280	290	540
Titanium(ppm)	0.0	0.0	90
Boron(ppm)	1.0	1.0	0
Niobium(ppm)	9	10	510
Heat_input(kJ.mm-1)	1.3	1.4	0.55
Interpass_temperature(C)	140	150	225
Postweld_heat_treatment_temperature(C)	280	250	690
Post-weld_heat_treatment_time(h)	17	16	2
GA calculated Elongation %	12	---	43
Targeted Elongation %	13	---	45
Error	21	---	39
Measured Elongation %	---	13	---

The NNGA models have good accuracy in predicting 18 input variables of the Elongation of ferritic steel welds, which is excellent for weld design. (Table.4.9) The predicted results of the targeted values of the two weld deposits are very close. The results of Genetic Algorithms are match with trends of measured data and fundamental of metallurgy. The output results show the predictive capacity of the NN-GA model.

This NNGA model can be used in practical applications, research and development of ferritic steel alloys. [Appendix-B]

4.3.6 Summary

The Neural Network and Genetic algorithms Methods have been used for efficient design of the Elongation of Ferritic Steel Welds. From the Modeling works and Results and Discussion of this Chapter some useful conclusions can be drawn:

The distribution of the Data of the Elongation of Ferritic Steel Welds is uniform for some Input variables and non-uniform for some Input variables. The distribution is clearly observed in Scatter plots.

In this case, of Bayesian Neural Network method, all the response graphs show error bars when the concentration of Nickel and Chromium is respectively below 8 and 6 wt%, the prediction can be reliable. But above those limits (7 wt% for Ni and 6 wt% for Cr), the model can no more be trusted and this is inferred by the large error bars. Similarly it is applicable to other graphs where larger error bars are present. More experiments with concentrations in this range of values need to be carried out to improve the model. Uncertainty because of a lack of data is one of the limitations of a neural network. The error bars and output variable (Elongation) sometimes showing unphysical (negative) values, this is because of the empirical equation in Neural Network modeling. This error bars feature of Bayesian Neural Network is excellent guideline for research and Development.

In the case of General Regression Neural Network method, there are no problems of noisy data. It can handle noises in the Inputs. The Response graphs of the GRNN show more define about the non linearity or complexity between the Input variables and the Elongation of Ferritic Steel Welds.

The Response Graphs show about the individual relationship between the input variables and Output variable (Elongation). The 3D contour plots show the relationship between the two Input variables with Output variable (Elongation).

These trends are confirmed in the present analysis as illustrated in both the types of the Graphs Figure 4.7 (a to r) and Figure 4.8 (a to r). They are impossible to reproduce in practice. They give a clear understanding of the relationship between the Input variables and the Elongation of Ferritic Steel Welds. These pieces of information are very valuable for design, as well

as understanding the existing theory and also guiding about new research and new finding for the Ferritic steel Welds.

The 3D contour plots show the relationship between the two Input variables with Elongation. There is a total combination of 153 3D contour plots formed by 18 Input variables with the Elongation. In the present work, 13 3D contour plots are given with their important relationship with the Elongation. These 3D contour plots show some hidden complex behavior of the input variables with the Elongation which is also not available and not well understood. Some innovative theoretical relations can be established by the proper interpretation of these 3D contour plots which become the new knowledge base for the future work on Ferritic Steel Welds. The Input variables show complex trends because during welding, there is formation of various types of the microstructures in Ferritic Steel Welds, qualitatively and quantitatively.

The trained BNN and GRNN models give the accurate predictions of unseen data which is useful in designing the Ferritic Steel Welds for the welding electrodes industries. With simply change the quantity of Input variables in model and run it, the predicted Elongation is obtained in the seconds.

The Genetic Algorithms method gives the prediction of the Input Variables for the Targeted Elongation value. It also predicted Input variables for the Targeted Elongation value which is beyond the range of data. The results are excellent.

4.4 Charpy Toughness Models

4.4.1 Response graphs of Input variables and Charpy Toughness of Ferritic Steel Welds using committee model of Bayesian Neural Network

The Trends of the Input Variables (Independent Variables) and Elongation of Ferritic Steel Welds are given below in the form of the graphs.

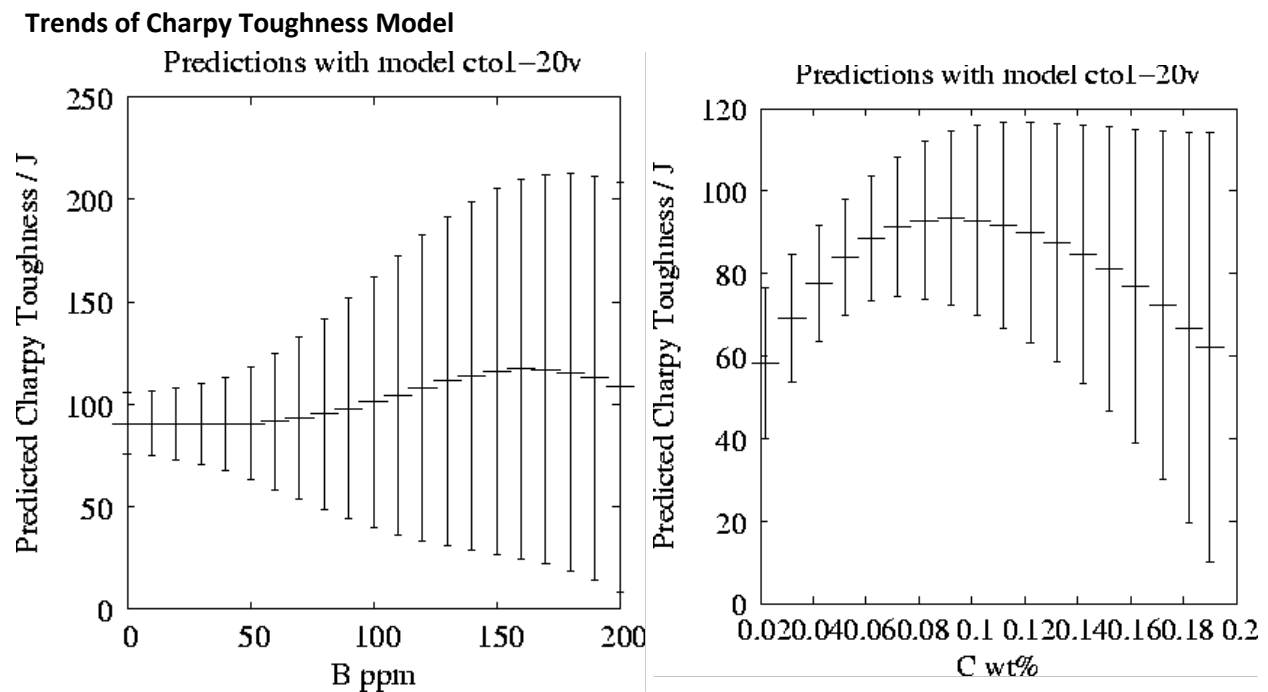


Fig a. Predicted variations in Charpy Toughness with Boron variation.

Fig b. Predicted variations in Charpy Toughness with Carbon variation.

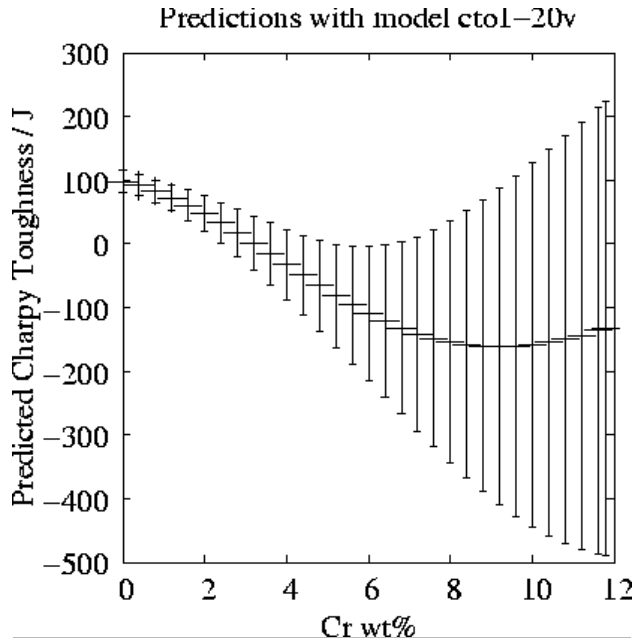


Fig c. Predicted variations in in Charpy Toughness with Chromium variation.

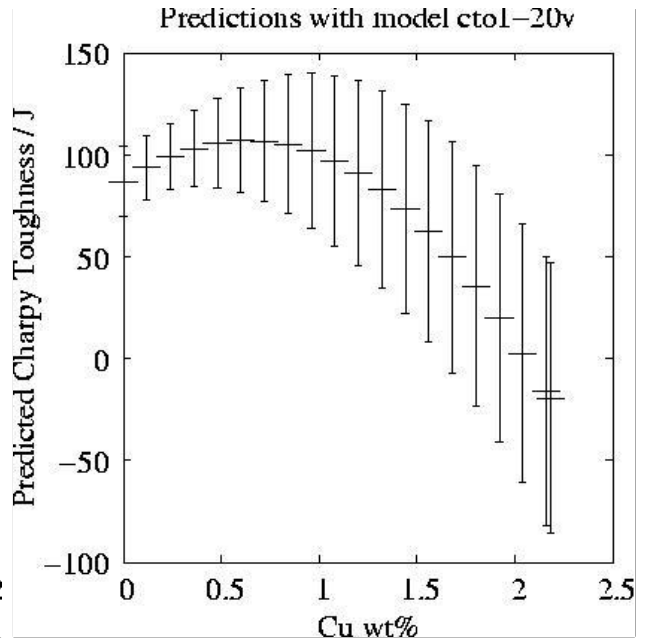


Fig d. Predicted variations in in Charpy Toughness with Copper variation.

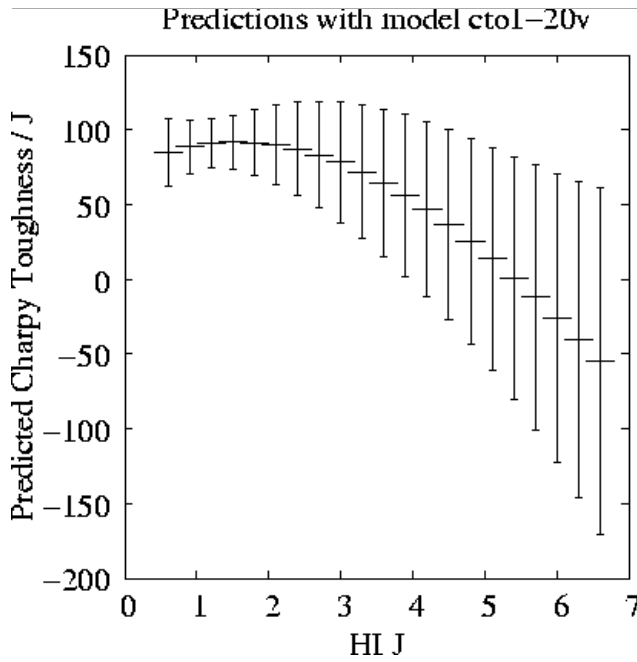


Fig e. Predicted variations in in Charpy Toughness with Heat input variation.

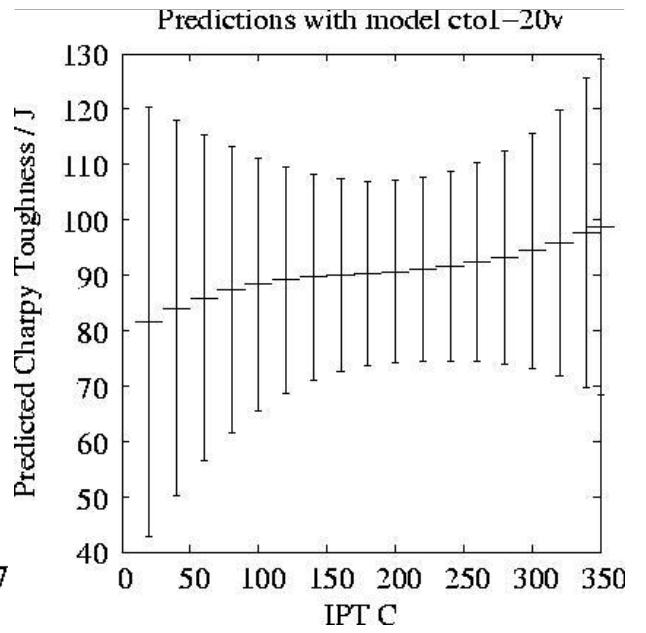


Fig f. Predicted variations in in Charpy Toughness with Interpass Temperature variation.

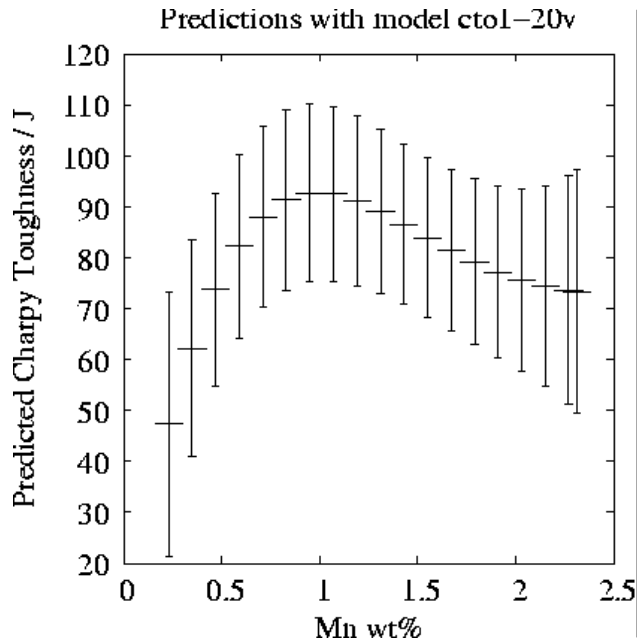


Fig g. Predicted variations in in Charpy Toughness with Manganese variation.

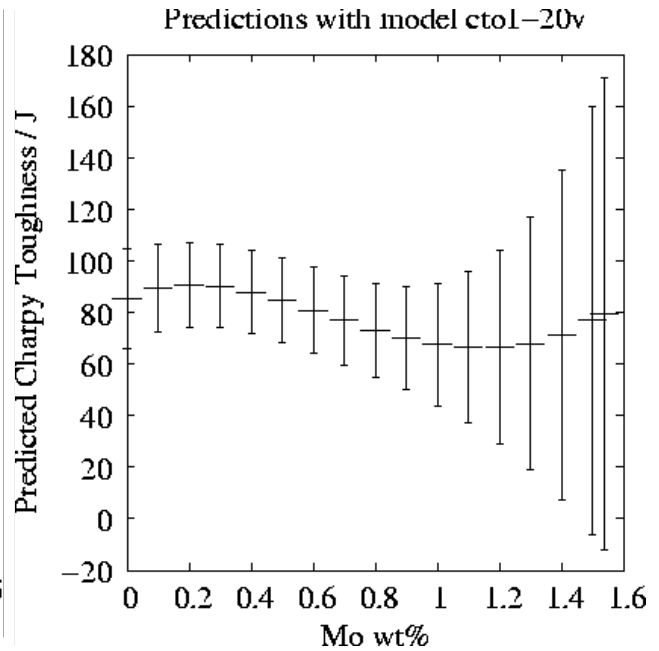


Fig h. Predicted variations in in Charpy Toughness with Molybdenum variation.

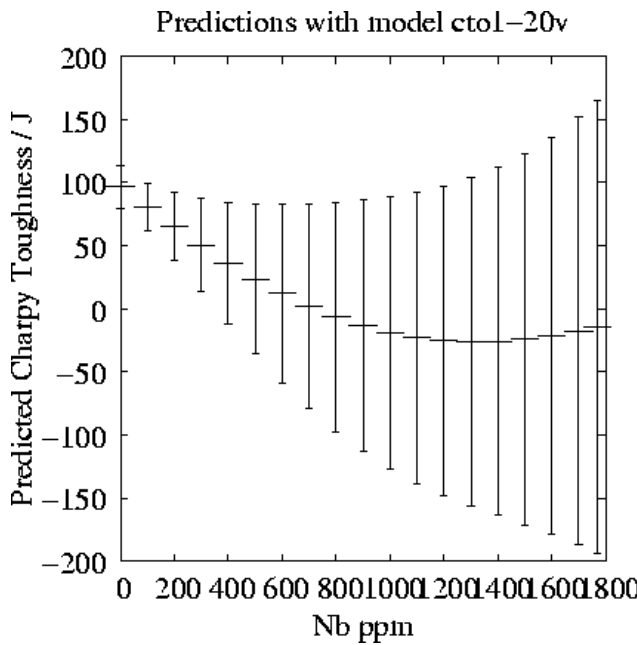


Fig i. Predicted variations in in Charpy Toughness with Niobium variation.

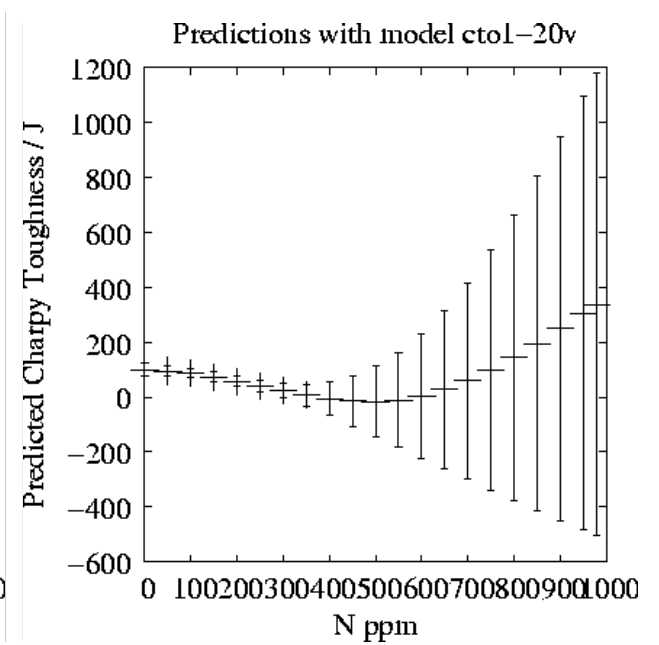


Fig j. Predicted variations in in Charpy Toughness with Nitrogen variation.

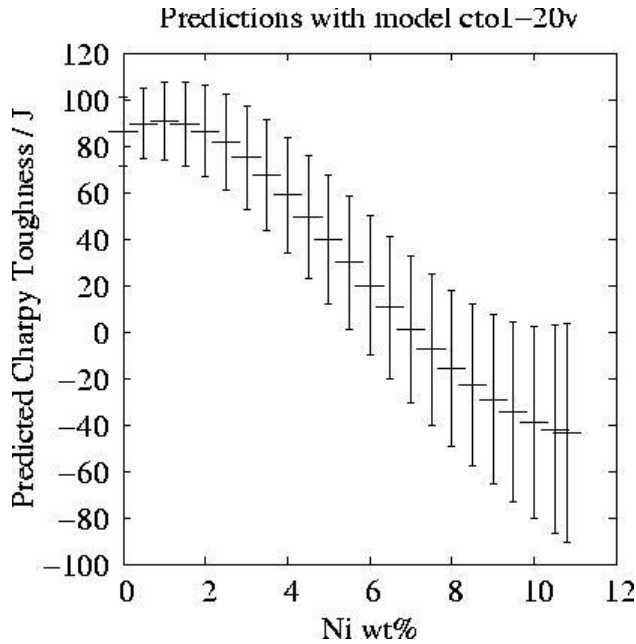


Fig k. Predicted variations in in Charpy Toughness with Nickel variation.

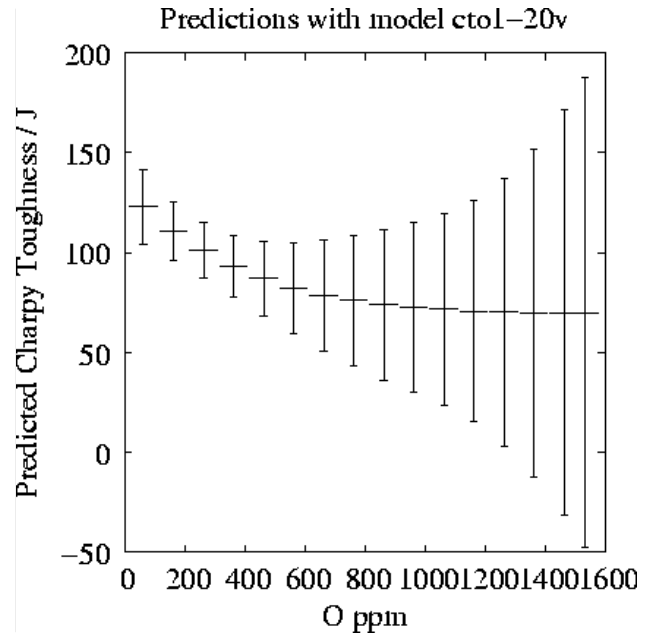


Fig l. Predicted variations in in Charpy Toughness with Oxygen variation.

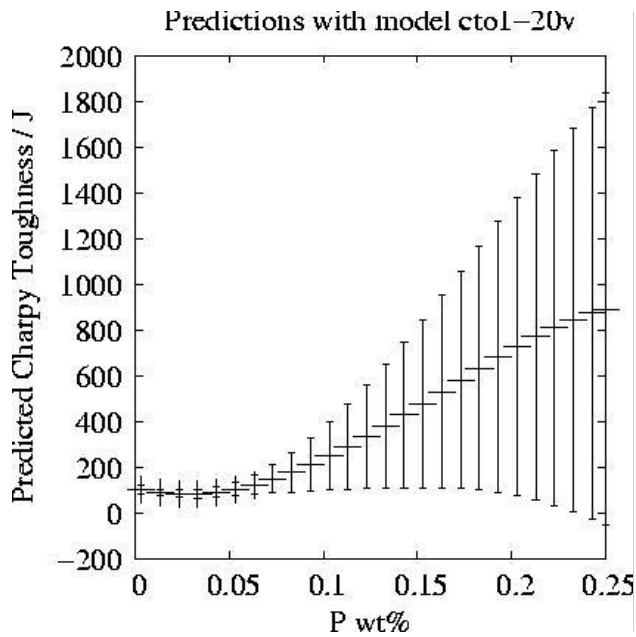


Fig m. Predicted variations in in Charpy Toughness with Phosphorus variation.

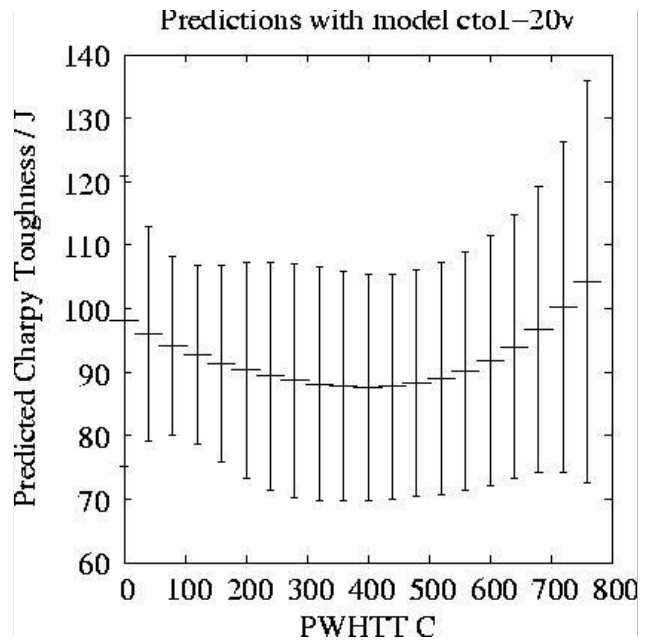


Fig n. Predicted variations in in Charpy Toughness with Post Weld Heat Treatment Temperature variation.

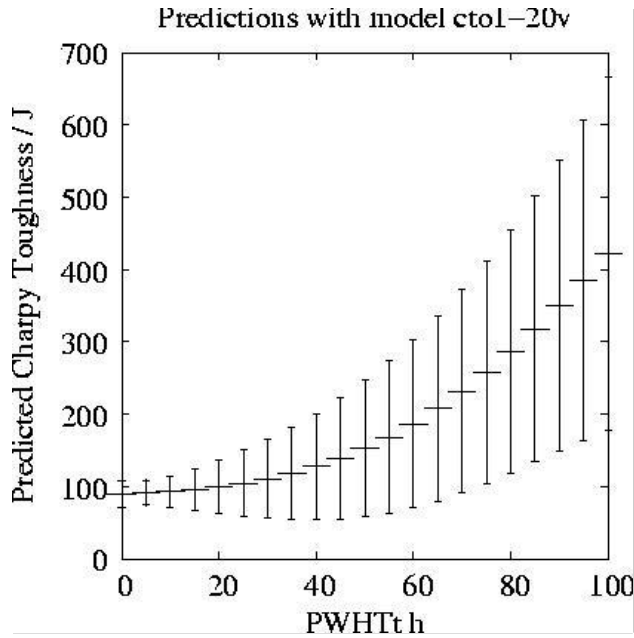


Fig o. Predicted variations in in Charpy Toughness with Post Weld Heat Treatment Time variation.

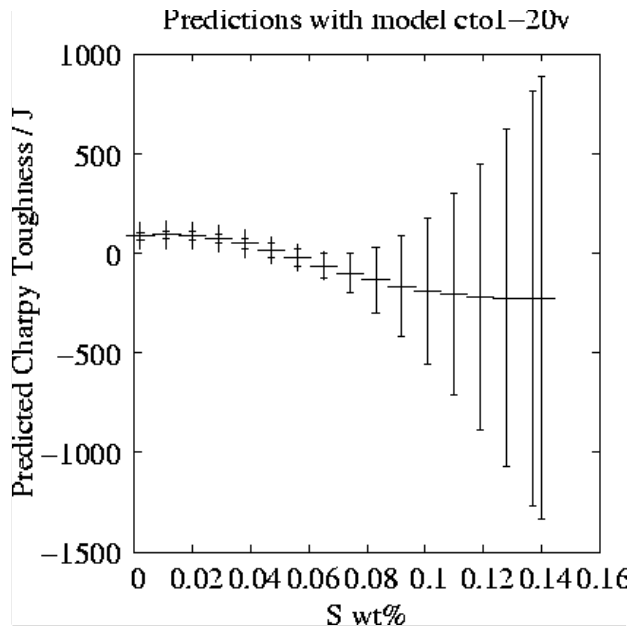


Fig p. Predicted variations in in Charpy Toughness with Sulphur variation.

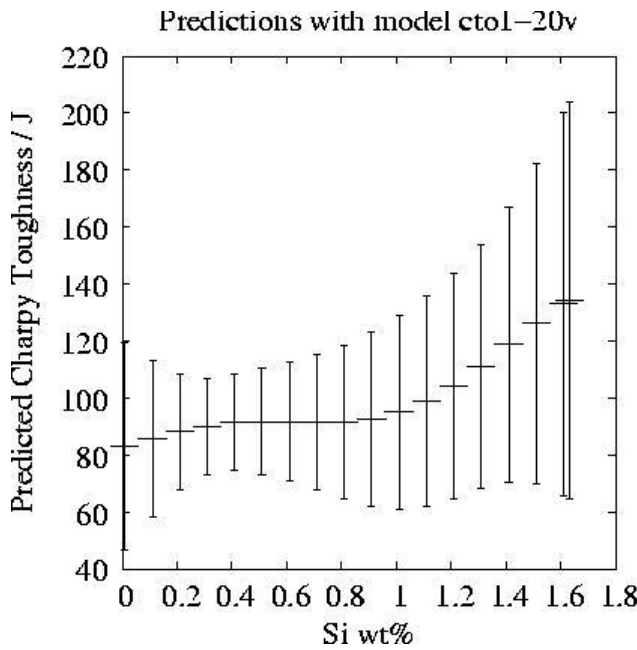


Fig q. Predicted variations in in Charpy Toughness with Silicon variation.

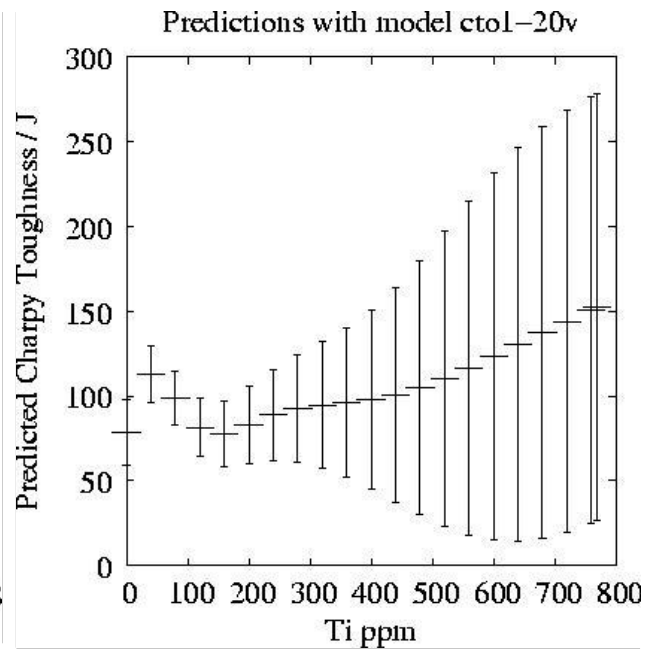


Fig r. Predicted variations in in Charpy Toughness with Titanium variation.

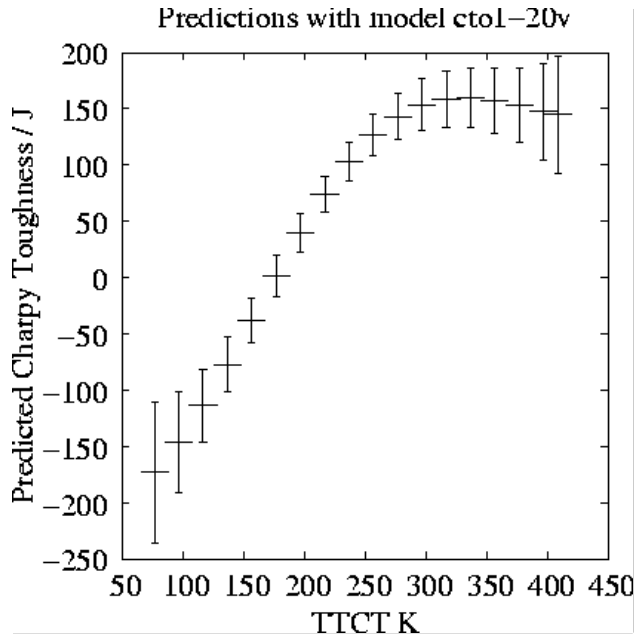


Fig s. Predicted variations in in Charpy Toughness with Testing Temperature Charpy Toughness variation.

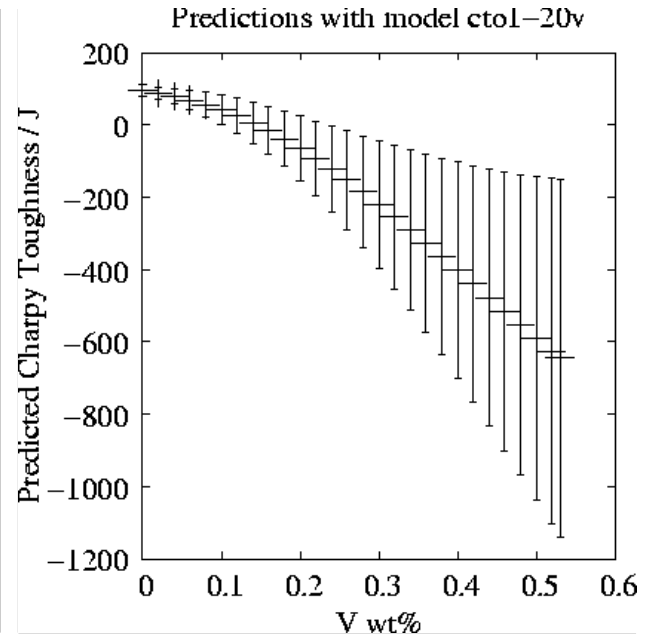


Fig t. Predicted variations in in Charpy Toughness with Vanadium variation.

Figure 4.10 (a to t) Response graphs (a to t) of Input variables and Charpy Toughness of Ferritic Steel Welds using committee model of Bayesian Neural Network

These trends are confirmed in the present analysis as illustrated in Figure 4.10 (a to t). It is emphasized that these calculations are done without permitting any of the other variables to change. They are impossible to reproduce in practice.

All the graphs show the error bars. The error bars are uniform in size indicate that the uniformity of data, like the graph the prediction of Charpy Toughness, as a function of Manganese. The error bars are large in size indicate non-uniformity of data, like the graph the prediction of the Charpy Toughness as a function of Chromium.

In this case, when the concentration of Nickel and Chromium is respectively below 6 and 2 wt%, the prediction can be reliable. But above those limits (6 wt% for Ni and 2 wt% for Cr), the model can no more be trusted and this is inferred by the large error bars. Similarly it is applicable to other graphs where larger error bars are present. More

experiments with concentrations in this range of values need to be carried out to improve the model. Uncertainty because of a lack of data is one of the limitations of a neural network. The error bars and output variable (Charpy Toughness) sometimes showing unphysical (negative) values, this is because of the empirical equation in Neural Network modelling.

The input variables like Interpass Temperature, Post Weld Heat Treatment Time, and Silicon are increasing in concentration or in amount, increase the Charpy Toughness of ferritic Steel welds. The Sulphur has shown an unphysical negative value of the Charpy Toughness which is not reliable. The Phosphorus has shown an increase on the Charpy Toughness too high 800 J which is not reliable.

The input variable like Boron, Carbon, Manganese, Molybdenum, Oxygen, Post Weld Heat Treatment Temperature, and Titanium indicate their non linear behavior with the Charpy Toughness.

The input variable like Boron, Chromium, Copper, Heat Input, Nitrogen, Niobium, Nickel, Vanadium and Testing Temperature Charpy Toughness show unphysical prediction of the Charpy Toughness.

The trends of the graphs of Bayesian Neural network model are useful to design the Charpy Toughness of Ferritic Steel welds efficiently.

In summary, a reasonable committee model has been obtained for Charpy Toughness. It appears that these input variables are affected on the Charpy Toughness of Ferritic Steel Welds, as could be expected from a metallurgical point of view.

4.4.2 Response Graphs of the Charpy Toughness GRNN model

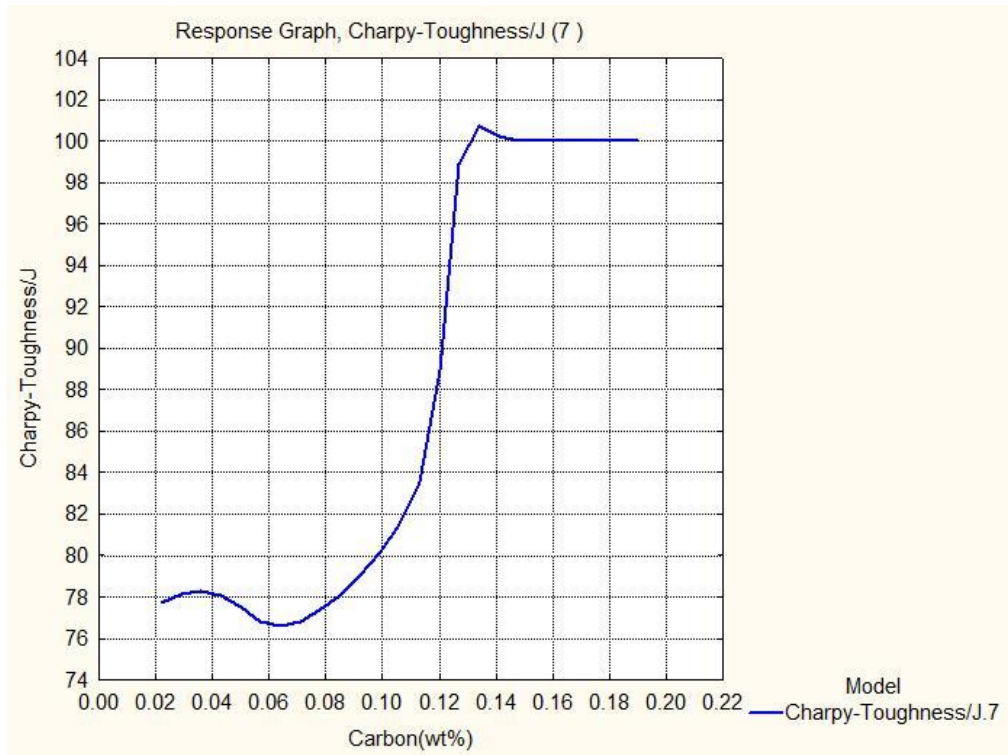


Fig. a Response Graph of Charpy Toughness J and Carbon (wt%)

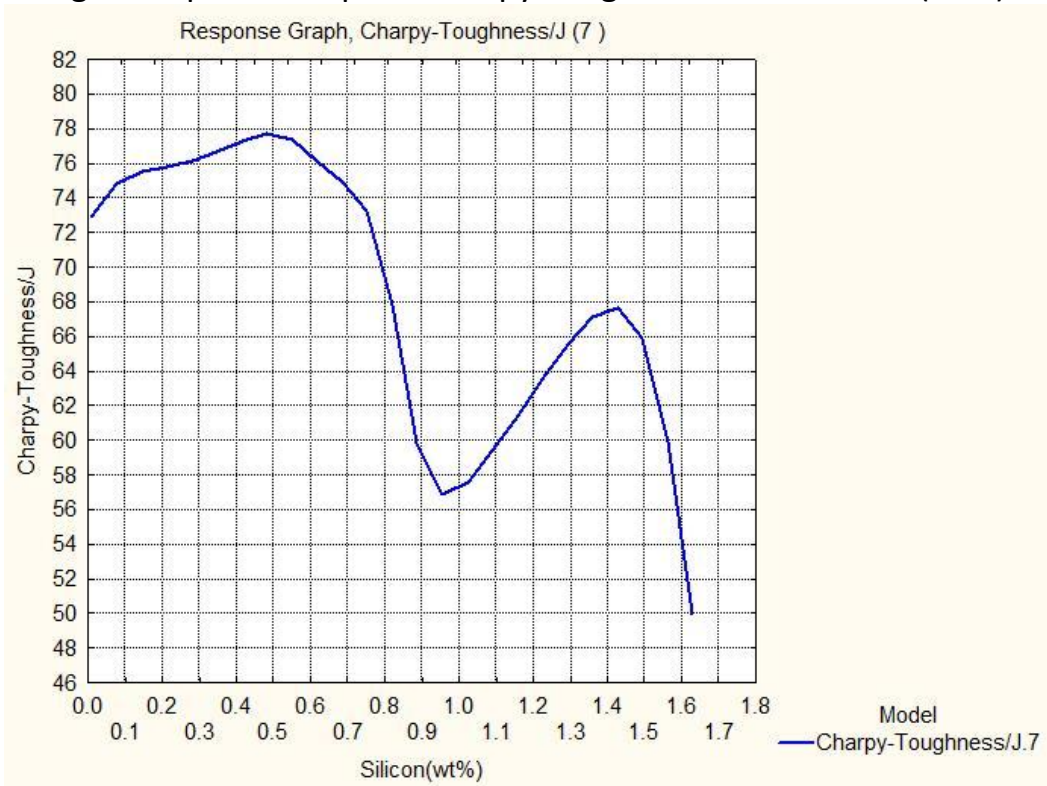


Fig. b Response Graph of Charpy Toughness J and Silicon (wt%)

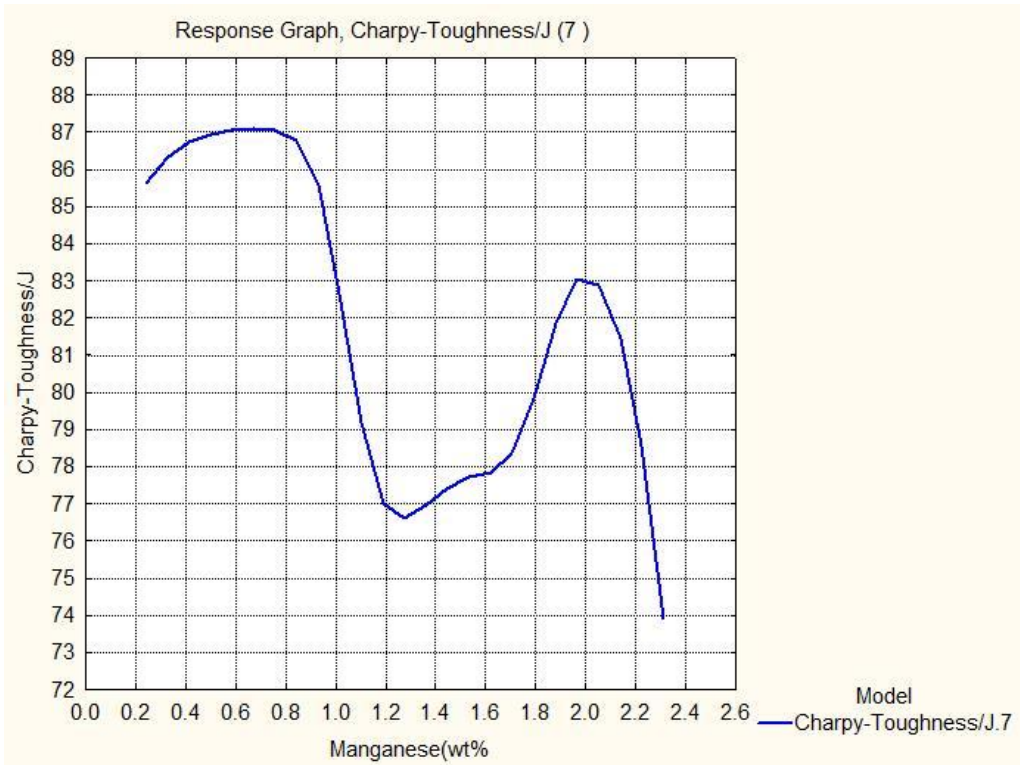


Fig. c Response Graph of Charpy Toughness J and Manganese(wt%)

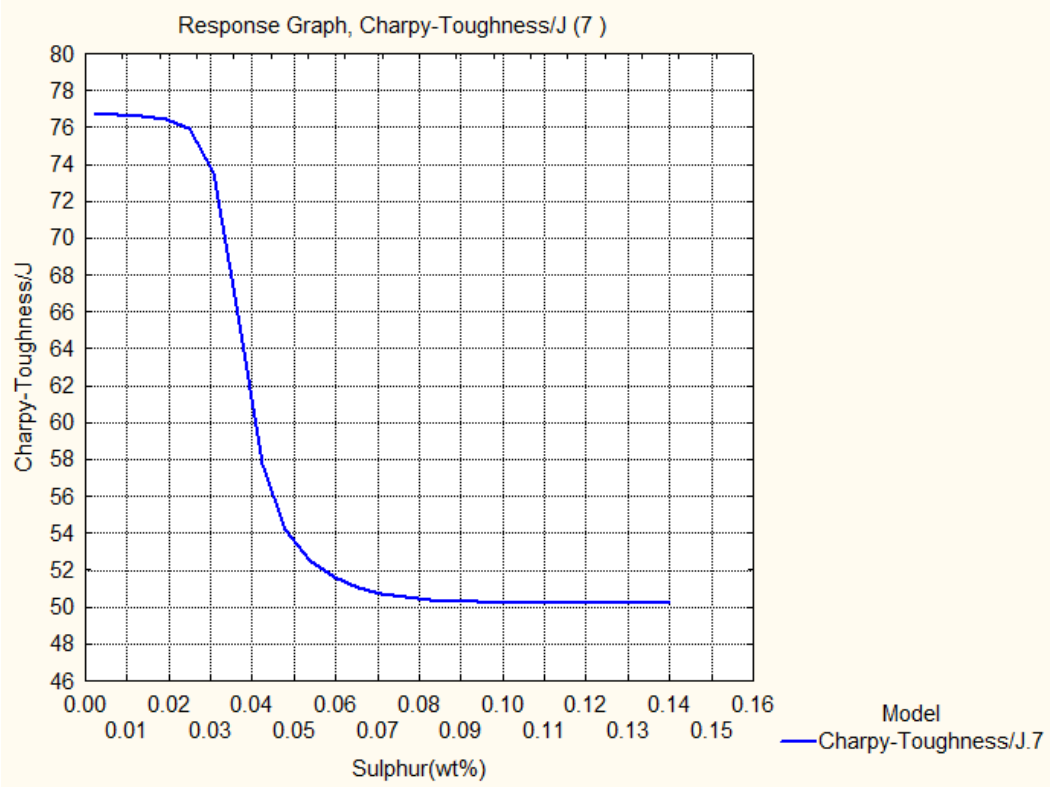


Fig.d Response Graph of Charpy Toughness J and Sulphur(wt%)

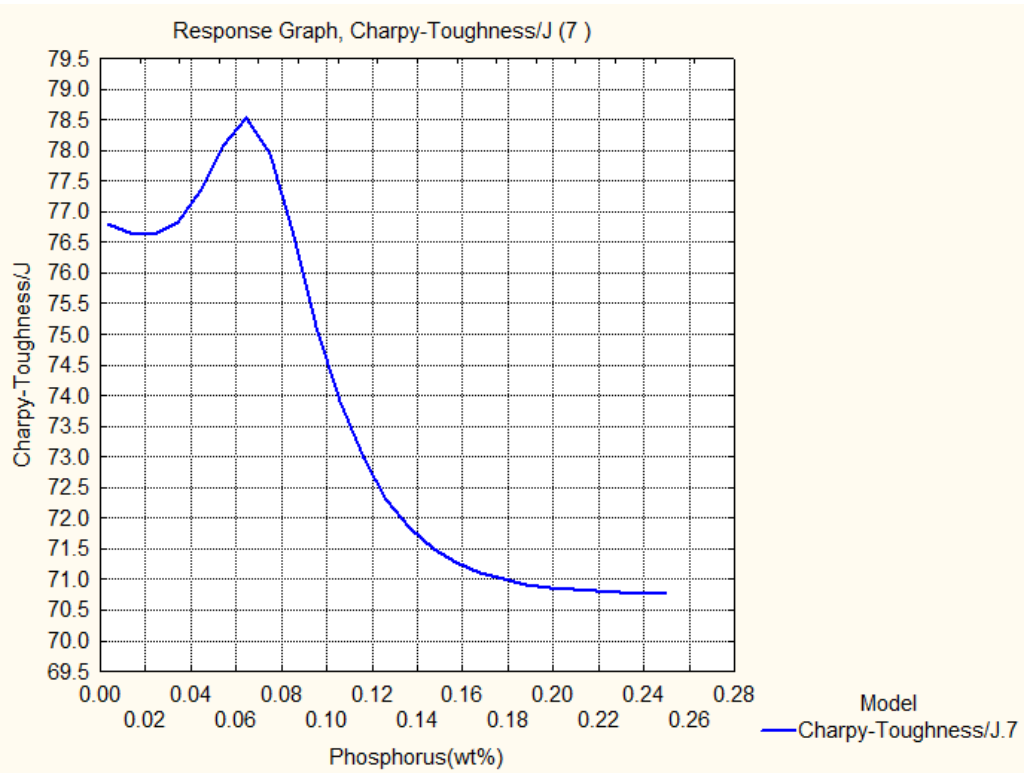


Fig.e Response Graph of Charpy Toughness J and Phosphorus(wt%)

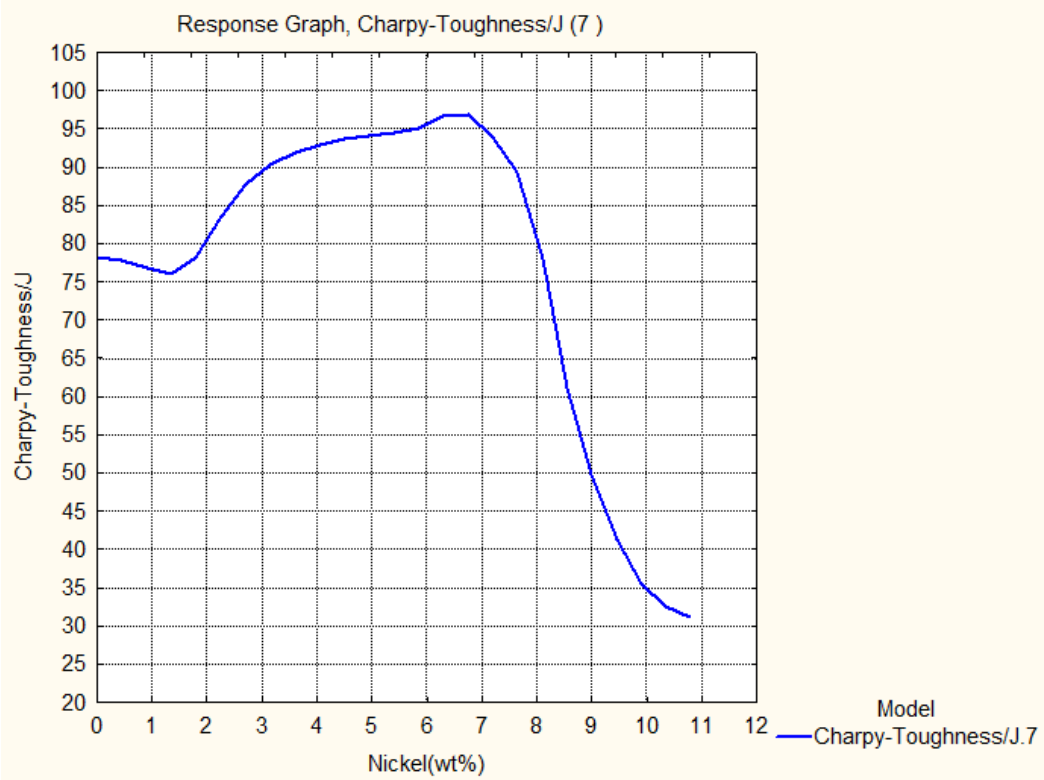


Fig.f Response Graph of Charpy Toughness J and Nickel(wt%)

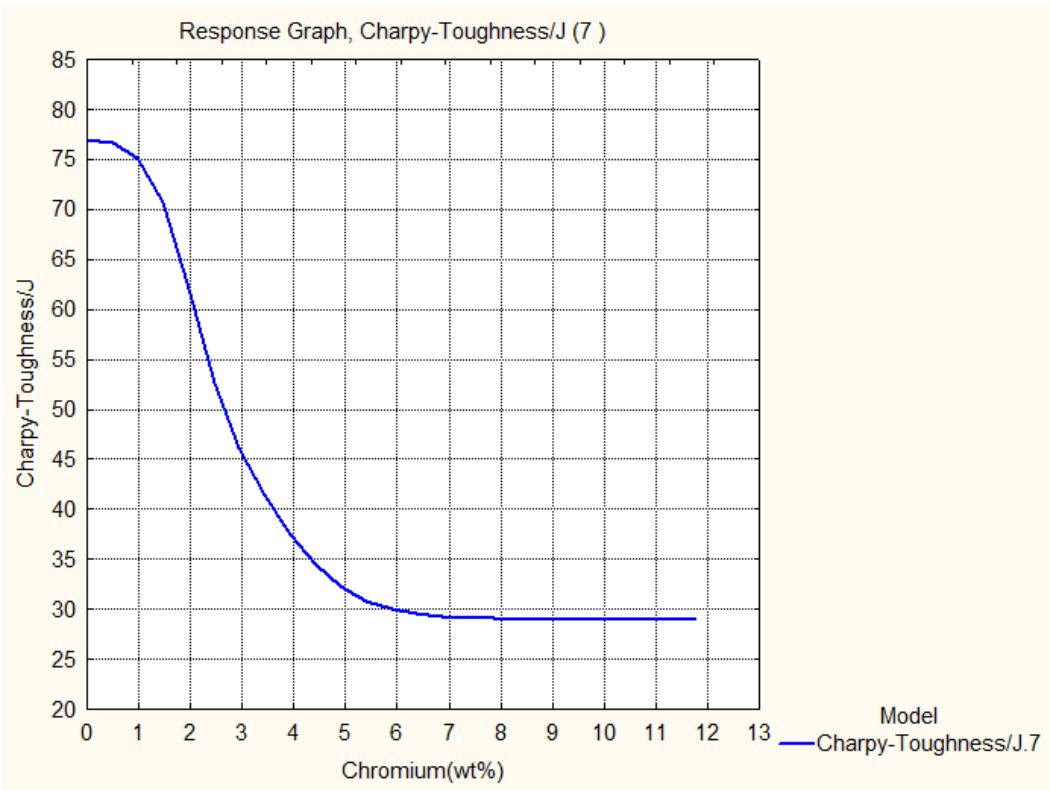


Fig.g Response Graph of Charpy Toughness J and Chromium(wt%)

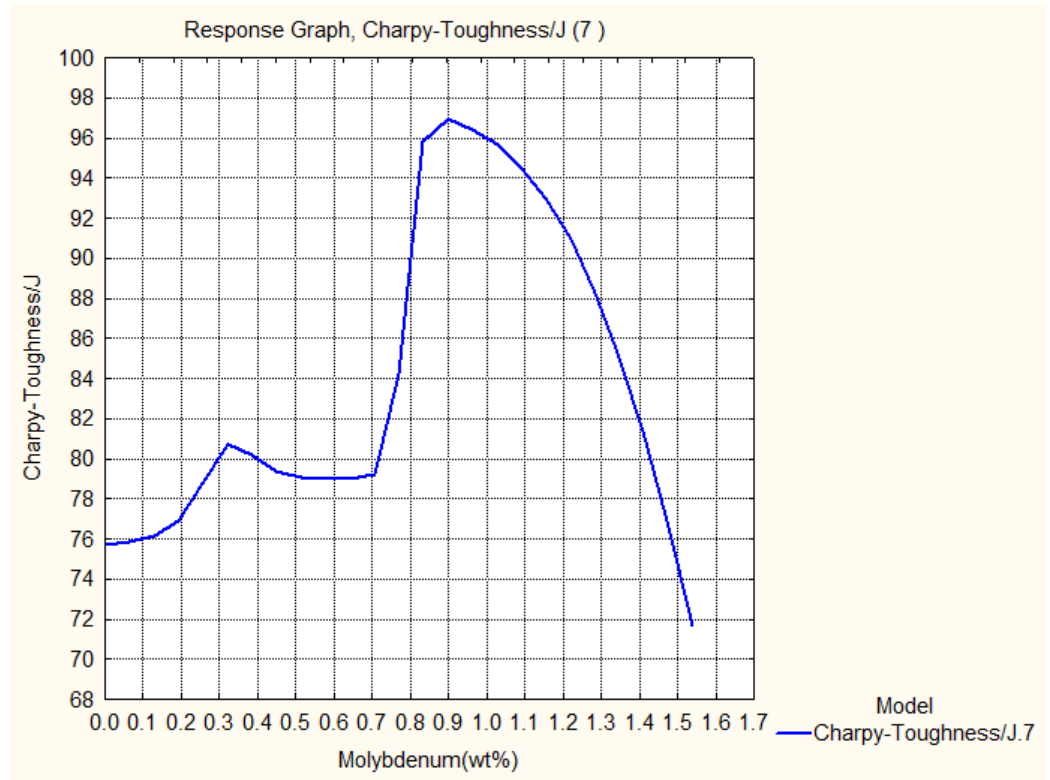


Fig.h Response Graph of Charpy Toughness J and Molybdenum(wt%)

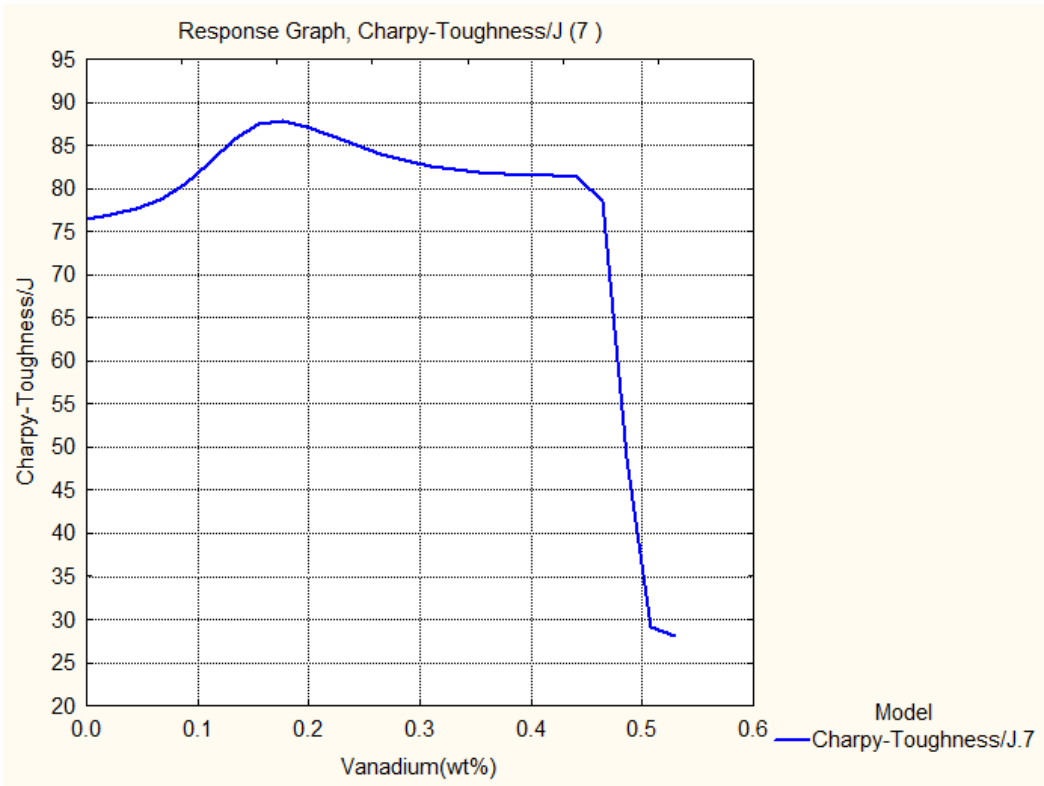


Fig.i Response Graph of Charpy Toughness J and Vanadium(wt%)

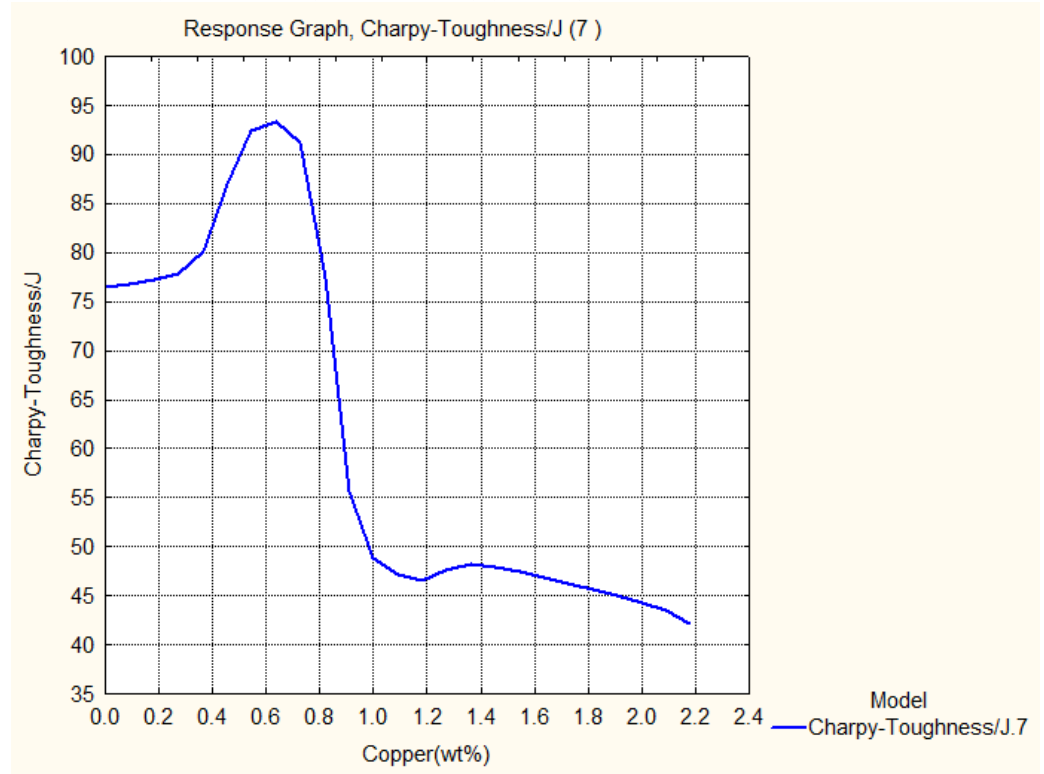


Fig.j Response Graph of Charpy Toughness J and Copper(wt%)

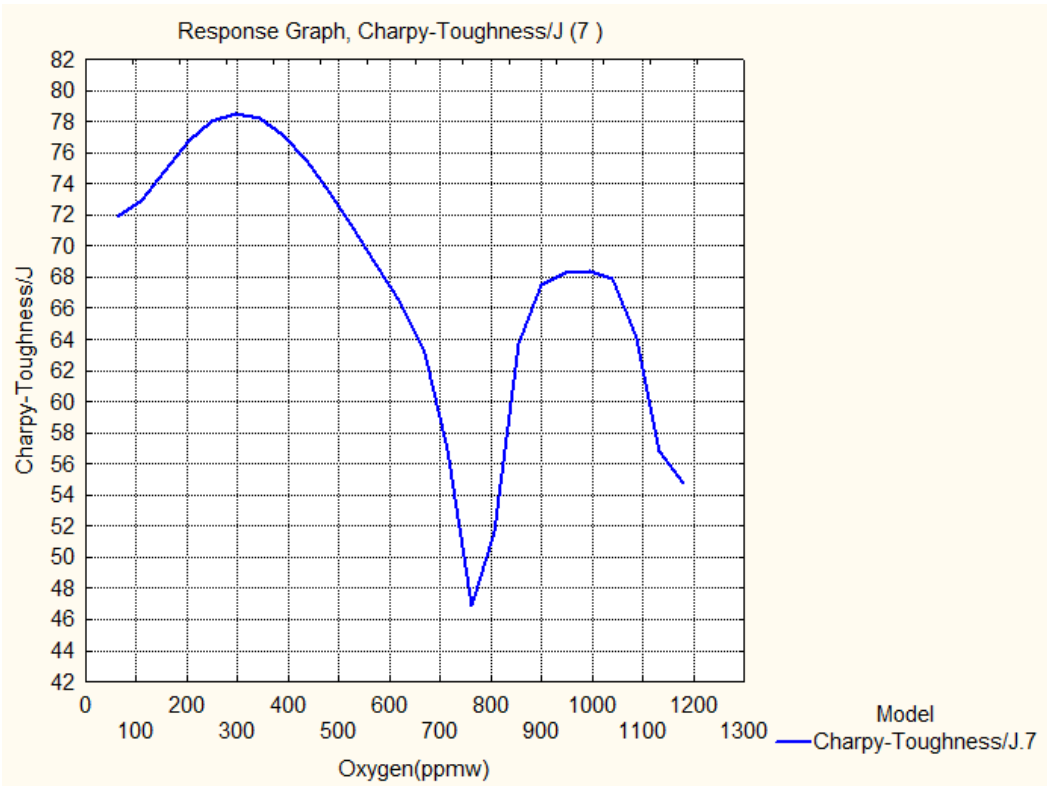


Fig.k Response Graph of Charpy Toughness J and Oxygen(wt%)

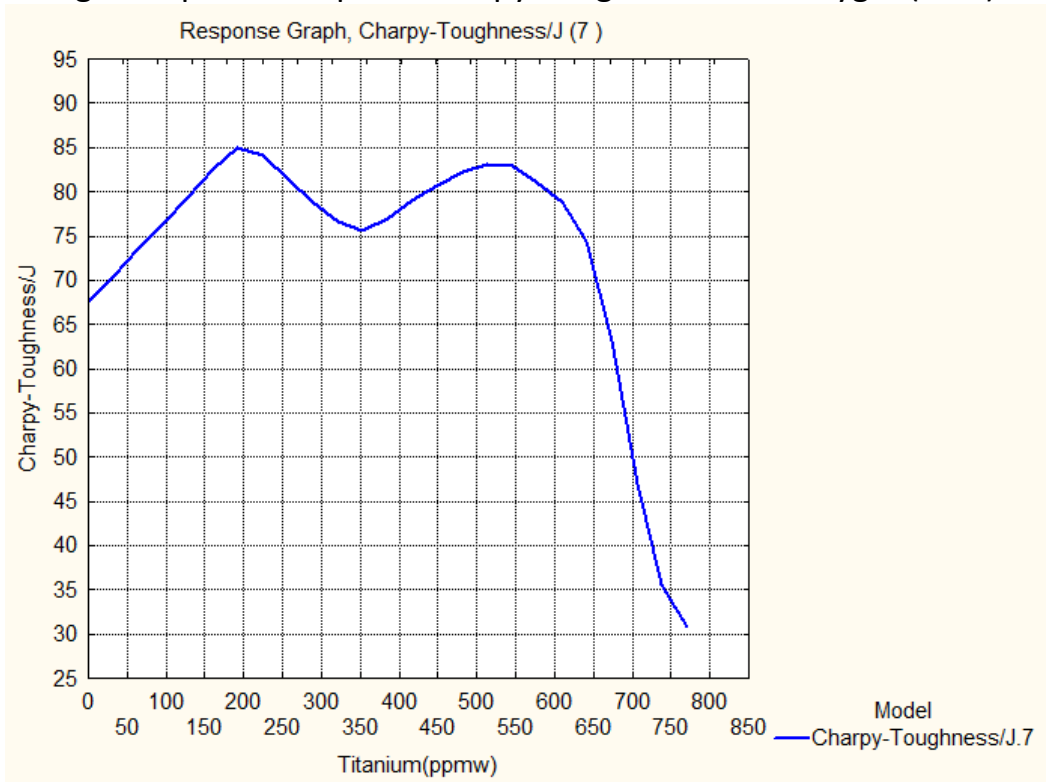


Fig.l Response Graph of Charpy Toughness J and Titanium(ppmw)

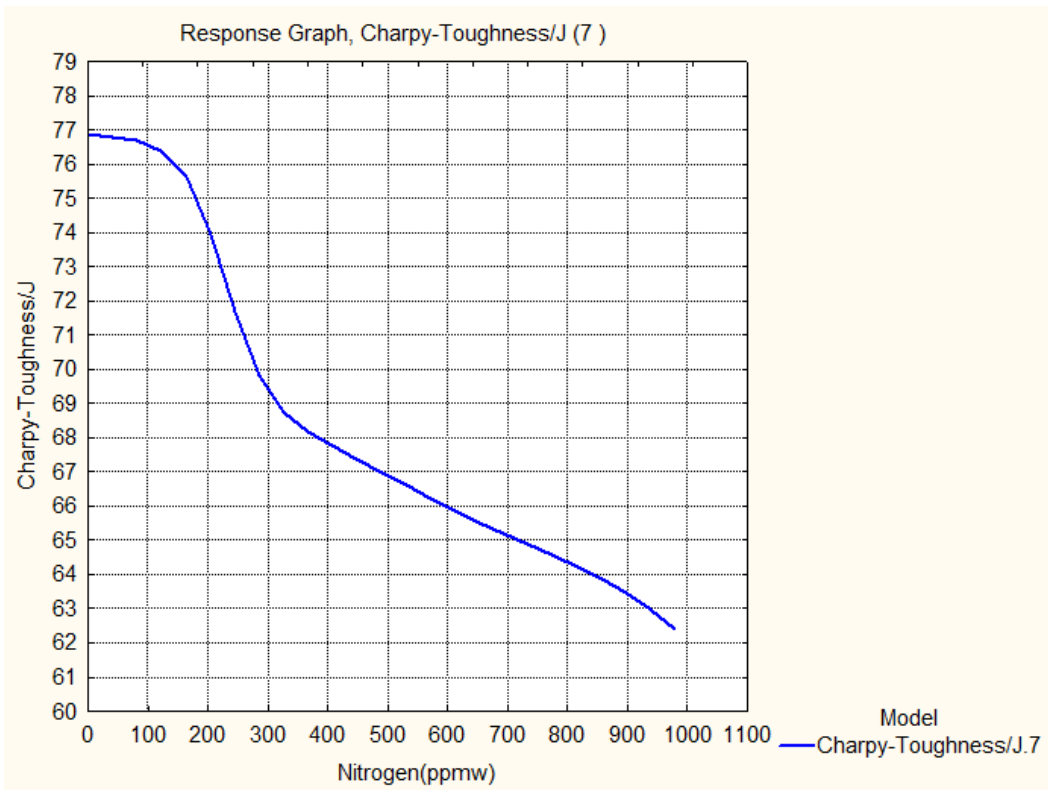


Fig.m Response Graph of Charpy Toughness J and Nitrogen(ppmw)

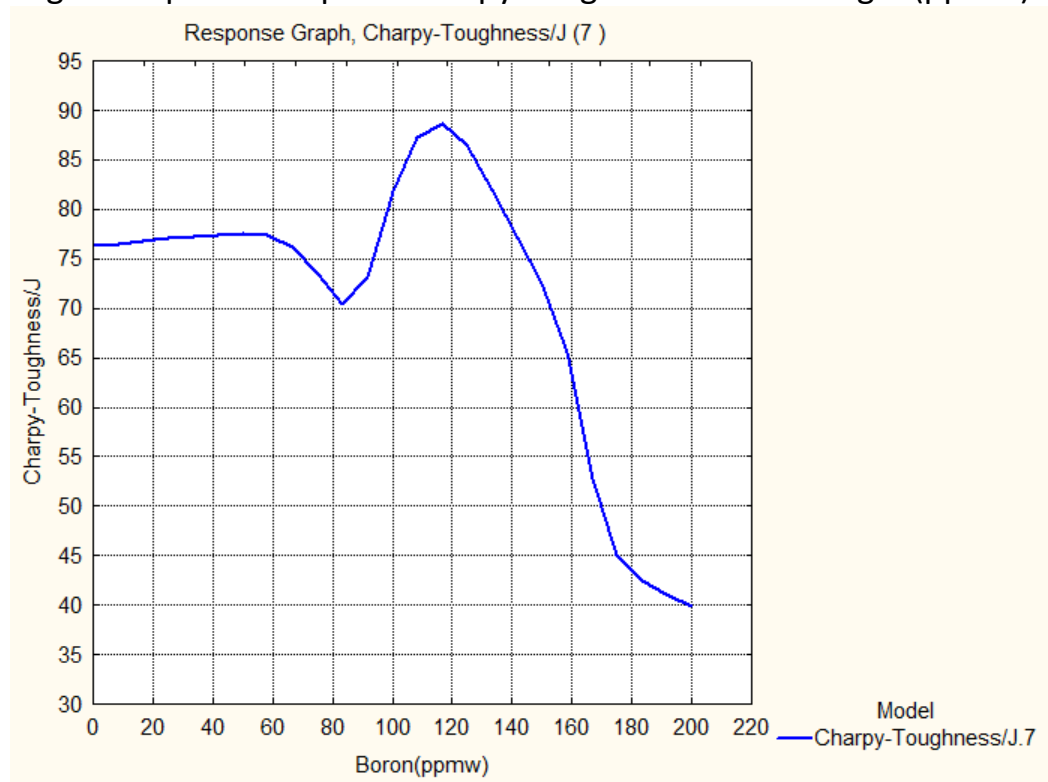


Fig.n Response Graph of Charpy Toughness J and Boron(ppmw)

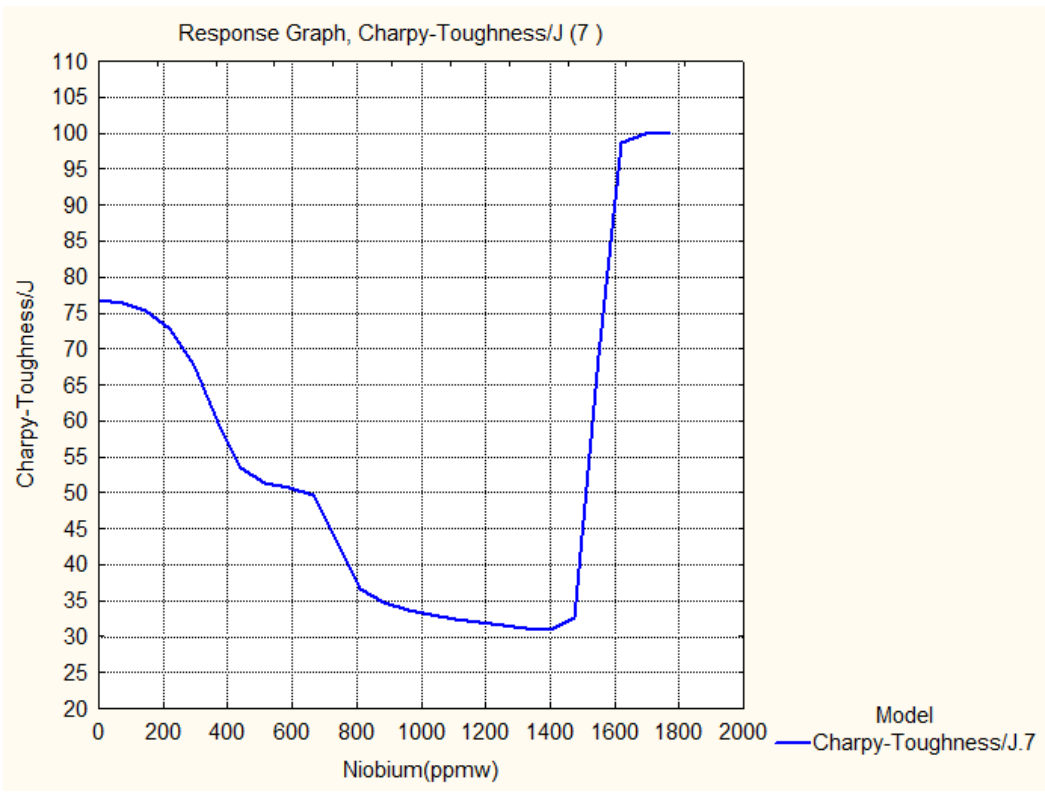


Fig.o Response Graph of Charpy Toughness J and Niobium(ppmw)

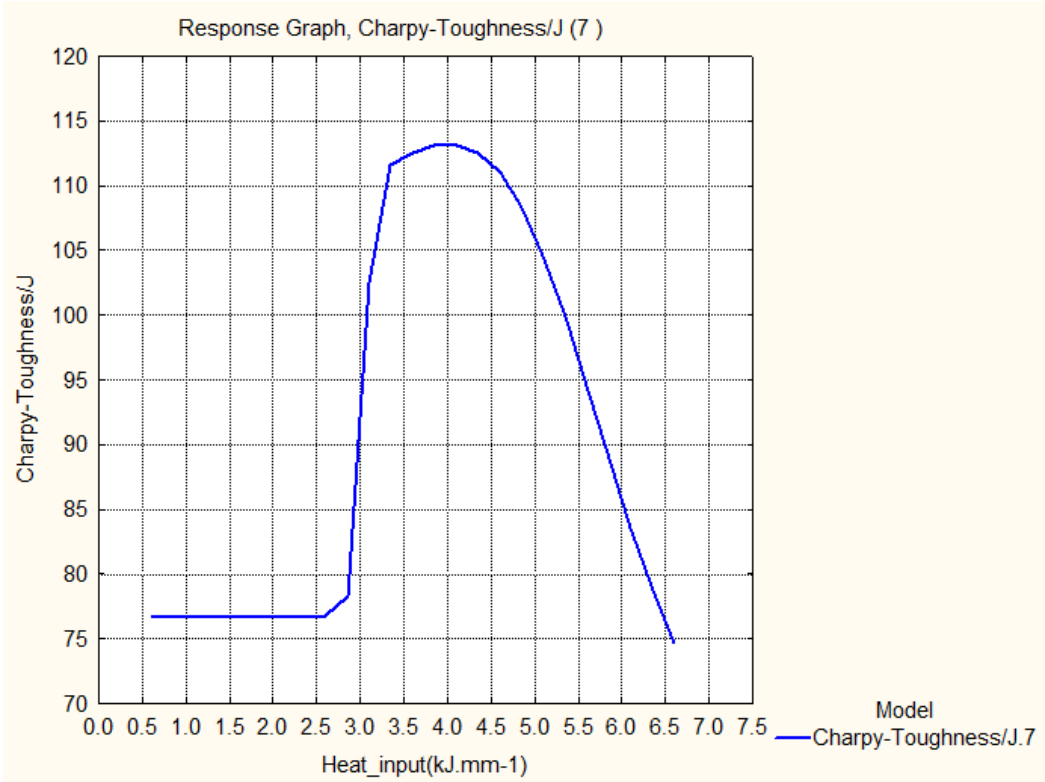


Fig.p Response Graph of Charpy Toughness J and Heat Input(kJ mm-1)

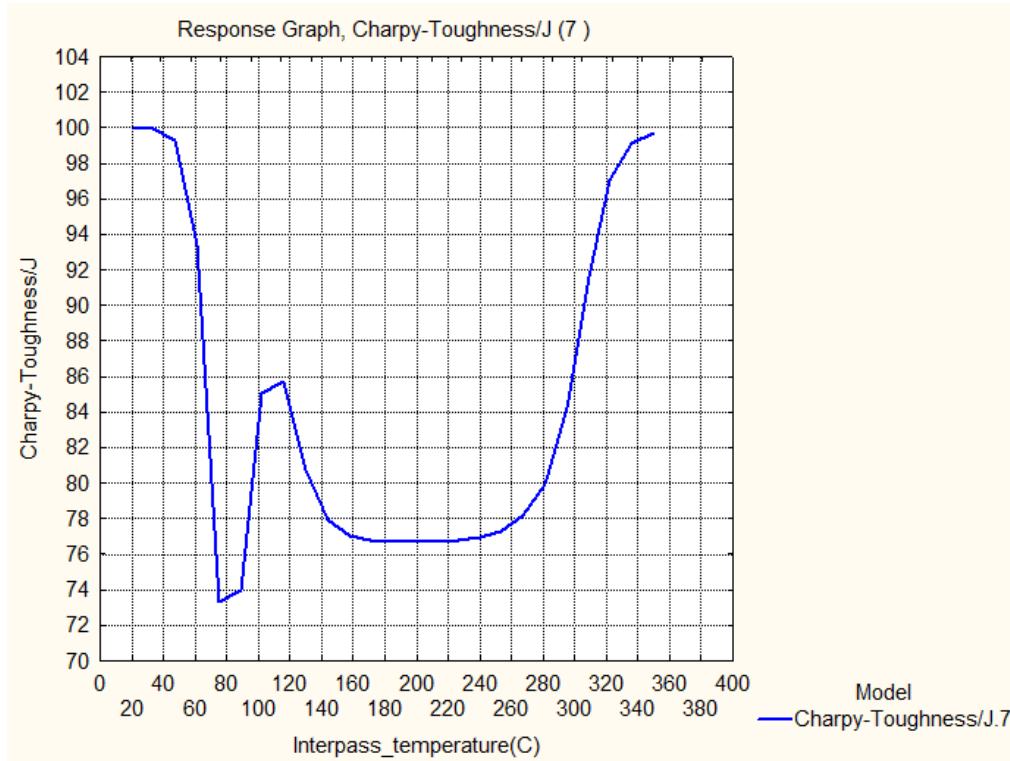


Fig.q Response Graph of Charpy Toughness J and Interpass temperature(C)

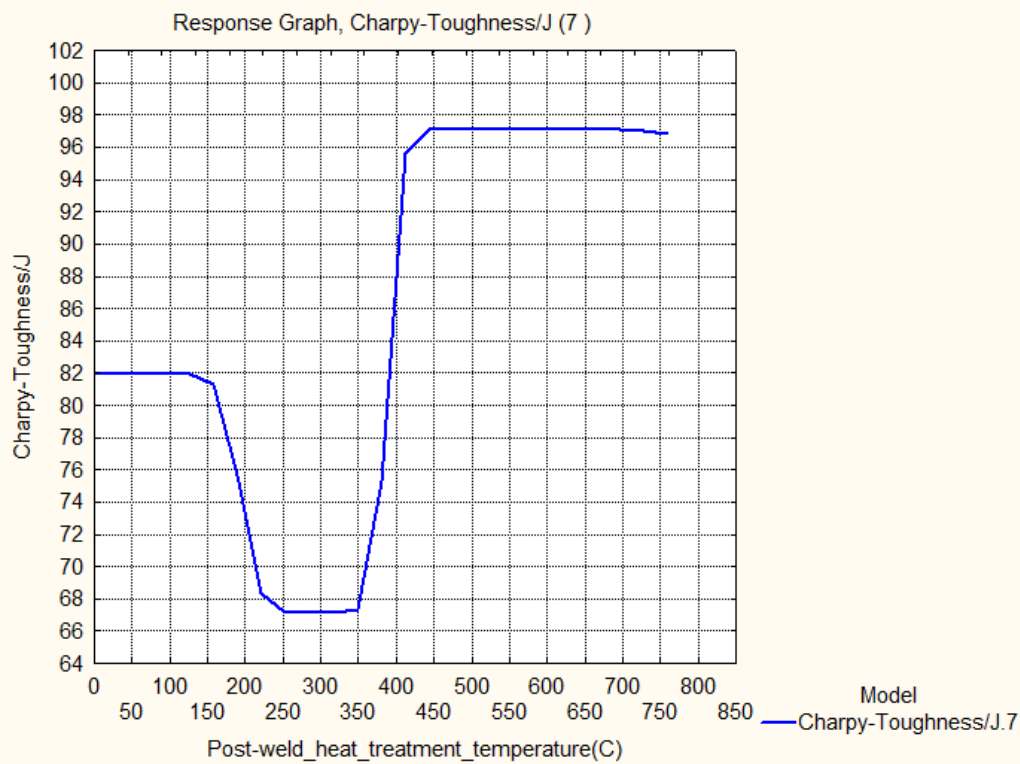


Fig.r Response Graph of Charpy Toughness J and Post-weld heat treatment(temperatureC)

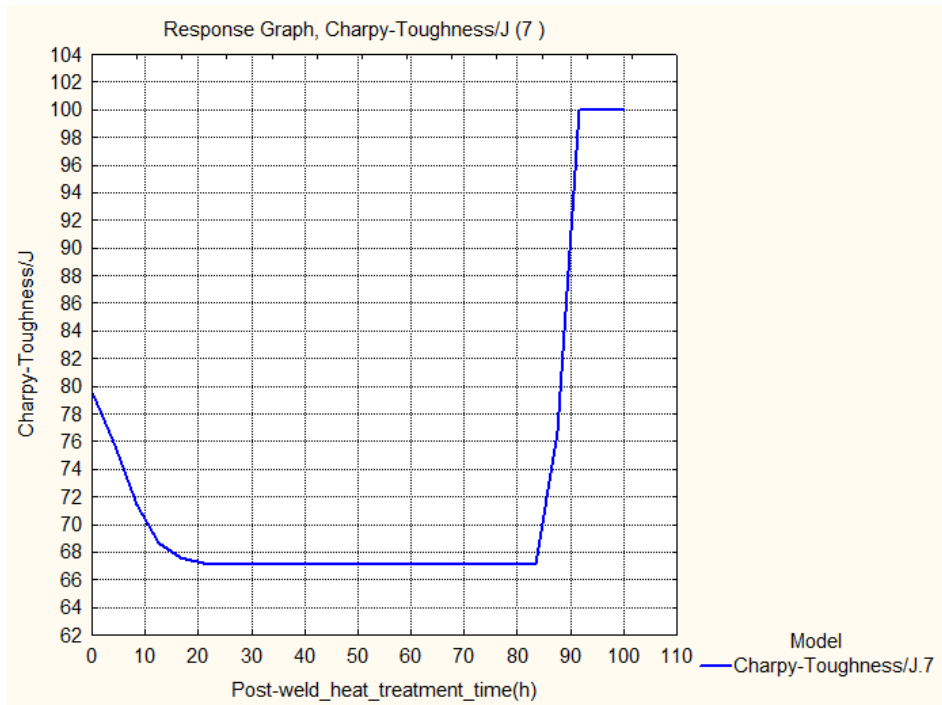


Fig.s Response Graph of Charpy Toughness J and Post-weld heat treatment time(h)

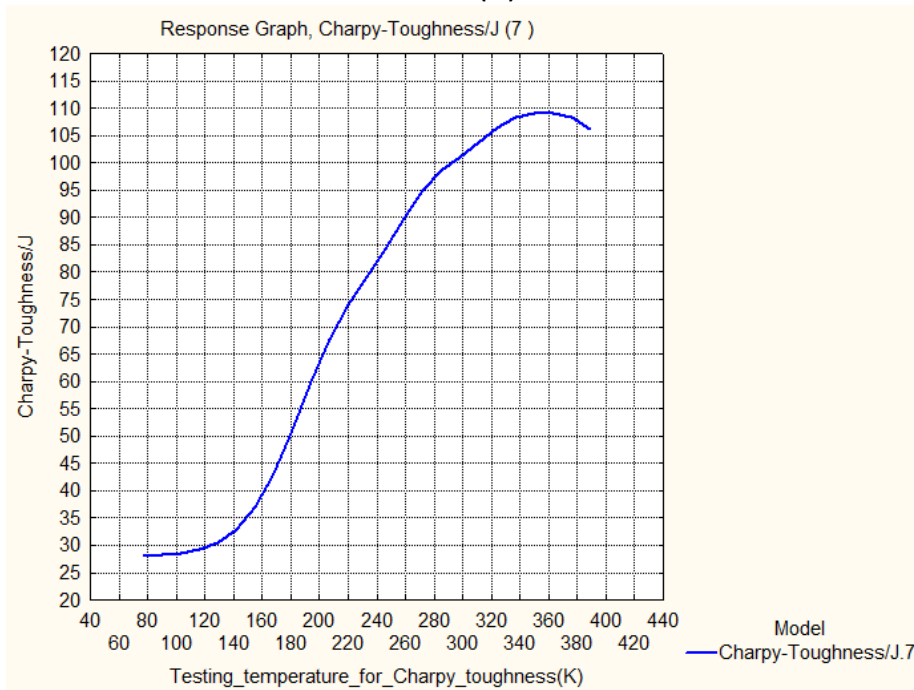


Fig.t Response Graph of Charpy Toughness J and Testing temperature for Charpy toughness(K)

Figure 4.11 (a to t) Response graphs of Input variables and Charpy Toughness of Ferritic Steel Welds (GRNN)

The influence of each of the variables on the Charpy toughness of welding alloys, which is discussed here. The Charpy toughness, initially decrease from 78.1 J to 76.8 J, between the 0.02% C to 0.065% C. The Carbon concentration of the welds in between 0.065% to 0.0134%, the Charpy toughness increases very high from 76.8 J to 100.9 J. Between 0.0134% C to 0.19% C, the Charpy Toughness is a constant value of 100 J after a slight increase of 0.9 J. In the case of silicon between more than 0.0% to 0.75%, there is an increase of the 73 J to 77.8 J in the Charpy toughness and then maximum 77.8 J at 0.48% Si. Between 0.75% to 0.95% Si, the Charpy toughness decreases from 73 J to 57 J. At 1.43%, the Charpy toughness increases to 67.8 J and then decreases to 50 J at 1.62% Si. The trend of manganese shows the increase in the Mn% from 0.22% to 0.9%, the value of the Charpy toughness is also increased from 85.6 J to 87.1 J. The Charpy toughness has a maximum value of 87.1 J between 0.58% Mn to 0.74% Mn. After 1.96% Mn, there is a reduction in the Charpy toughness from 83J to 74J at 2.3 Mn. The sulphur shows a maximum value of the Charpy toughness 76.6 J, upto 0.02%S. After 0.02% S, increase in sulphur decreases in the Charpy toughness from 76.6 J to 50.3 J at 0.09% S. More than 0.09% S gives constant Charpy toughness 50.3 J. The Phosphorus gives the maximum Charpy toughness 78.5 J at 0.064% P and increase in Phosphorus decreases the Charpy toughness to 70.7 J at 0.24% P. The nickel has the maximum 90 J to 97 J Charpy toughness between 6% Ni to 7% Ni. Between 2% Ni to 8% Ni, the charpy toughness is maintain minimum 80 J to maximum 97 J. More than 8% Ni reduces the Charpy toughness to 32 J at 10.8% Ni. The Chromium has a maximum Charpy toughness 77 J to 75 J up to 1% Cr. More than 1% Cr reduces the value of the Charpy toughness to 28 J at 8% Cr. The Charpy toughness is constant value of 28 J after 8% Cr. Molybdenum increases the Charpy toughness from 75.8 J to 80.8 J at 0.33%. At 0.9% Mo, the Charpy toughness is the highest 97 J. Increase more than 0.9% Mo the charpy toughness is reduced to 71.9 J at 1.53% Mo. Vanadium increases the Charpy toughness from a minimum 76.5 J to a maximum 87.5 J at 0.16V%. At 0.44% V, the Charpy toughness reduces and at 0.53% V, it is 27.5 J. Copper increases the Charpy toughness from 77 J to 93 J at 0.62%. Between 0.62% to 1.2% Cu, the Charpy toughness decreases from 93 J to 46.5 J. At 2.19% Cu, rhe Charpy toughness is the lowest 42.5 J. Oxygen increases the Charpy toughness from 72 J to 78.3 J at 300 ppm and it reduces to 47 J at 760 ppm. Further increases to 68.2 J at 940ppm Oxygen and then drops to 54.3 J at 1180ppm Oxygen. Titanium gives a minimum Charpy toughness of 67.5 J to maximum 85 J at 180ppm. At 350ppm Ti, the Charpy toughness has a value of 76 J. Between

500 ppm Ti to 550 ppm Ti, the Charpy toughness is 82.5 J. More than 550 ppm Ti, the Charpy toughness decreases from 82.5 J to 31.5 J at 770 ppm Ti. Nitrogen shows a decrease in the Charpy toughness from 76.9 J to 62.3 J with an increase in a Nitrogen ppm. Boron gives a little increase in the Charpy toughness from 76.5 J to 77.5 J between greater than 0 ppm to 58 ppm. Boron shows maximum Charpy toughness of 88 J at 118 ppm. More than 118 ppm Boron, there is a decrease in the Charpy toughness to 40 J at 200 ppm Boron. Niobium has a trend of a decrease in the Charpy toughness from 76.5 J to 31.5 J with an increase from a greater than 0 ppm Nb to 1400 ppm Nb. Between 1470 ppm Nb to 1780 ppm Nb, the Charpy toughness increases and attains the highest value of 100 J.

Heat Input has stated that the maximum Charpy toughness of 113 J at 4.0 kJ mm⁻¹. Between 0.5 kJ mm⁻¹ to 2.5 kJ mm⁻¹, the Charpy toughness is a constant 76.5 J. More than 2.8 kJ mm⁻¹ to 4.0 kJ mm⁻¹ Heat Input increases the Charpy toughness from 77.5 J to 113 J. Higher than 4.0 kJ mm⁻¹ Heat Input, the Charpy toughness reduces from 113 J to minimum 74.9 J at 6.5 kJ mm⁻¹. When the Interpass temperature is in range of 20 C to 75 C, the Charpy toughness decreases from 100 J to 73.5 J. Between 80 C to 118 C, the Charpy toughness increases from 74 J to 85.9 J and further it reduces to 76.8 J at 170 C and constant 76.8 J up to 220 C. More than 220 C Interpass temperature, the Charpy toughness value increases to 99.9 J at 350 C. Post weld heat treatment temperature increases from 50 C to 750 C, shows the Charpy toughness is 82 J up to 125 C then it decreases to 67.2 J between 250 C to 350 C. Between 350 C to 500 C, the Charpy toughness increases from 67.2 J to 97.2 J. More than 500 C Post weld heat treatment temperature, the Charpy toughness is almost constant 97.2 J upto 700 C. A little decrease, from 97.2 J to 96.8 J is observed between 700 C to 750 C Post weld heat treatment temperature. Post weld heat treatment time has a trend of a decrease in the Charpy toughness from 79.2 J to 67.2 J at 22 hours. Between 22 to 83 hours, post weld heat treatment time, the Charpy toughness is a constant 67.2 J. More than 83 hours, it increases a maximum Charpy toughness to 100 J at 91 hours, Post weld heat treatment time and a constant till 100 hours. Testing Temperature of Charpy toughness shows the trend towards of an increase in the Charpy toughness from 28 J to 109 J with an increase in Testing Temperature of Charpy toughness from 80 K to 360 K and then a little reduction from 109 J to 106 J between 360 K to 390 K.

The relationship between the input variables and the Charpy Toughness is a nonlinear as seen above in response graphs Figure 4.11 (a to t).

4.4.3 3D Contour plots of the Charpy Toughness GRNN model

The effect in combination of any two input variables (Independent variables) from Carbon, Silicon, Manganese, Sulphur, Phosphorus, Nickel, Chromium, Molybdenum, Vanadium, Copper, Oxygen, Titanium, Nitrogen, Boron, Niobium, Heat_input, Interpass_temperature, Post-weld heat treatment temperature, Post-weld heat treatment time and Testing Temperature Charpy Toughness on the Charpy Toughness of Ferritic Steel Welds are given in form of 3D contour plots. (Figure.4.12.1 to 4.12.18)

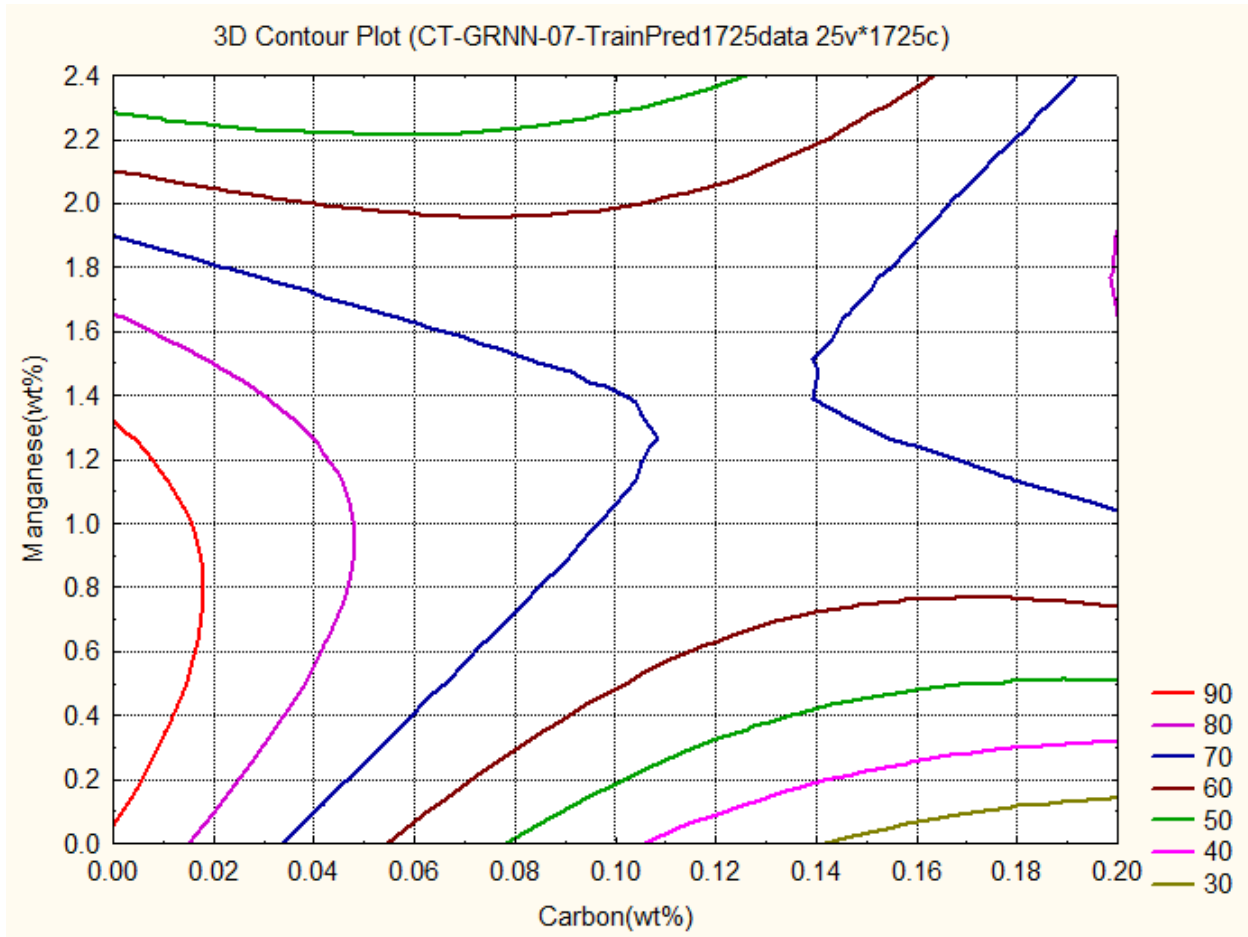


Figure. 4.12.1 Contour plot showing the variation in Predicted Charpy Toughness as a function of the Carbon and Manganese concentrations.

3D contour Plot gives the relations between the **two input variables** and **one output variable**. **Figure.4.12.1** shows the relations between Carbon, Manganese and Charpy Toughness by **GRNN**. The graph gives the information about how these two, Carbon and Manganese control the Charpy Toughness from 30J to 90J. Decrease in Charpy Toughness from 60J to 30J is achieved in the range of %C between 0.06 to 0.20 and %Mn in the range of 0.0 to 0.59. This same range of Charpy Toughness exists with %C in range of 0.0 to 0.162 and %Mn in the range of 1.9 to 2.4.

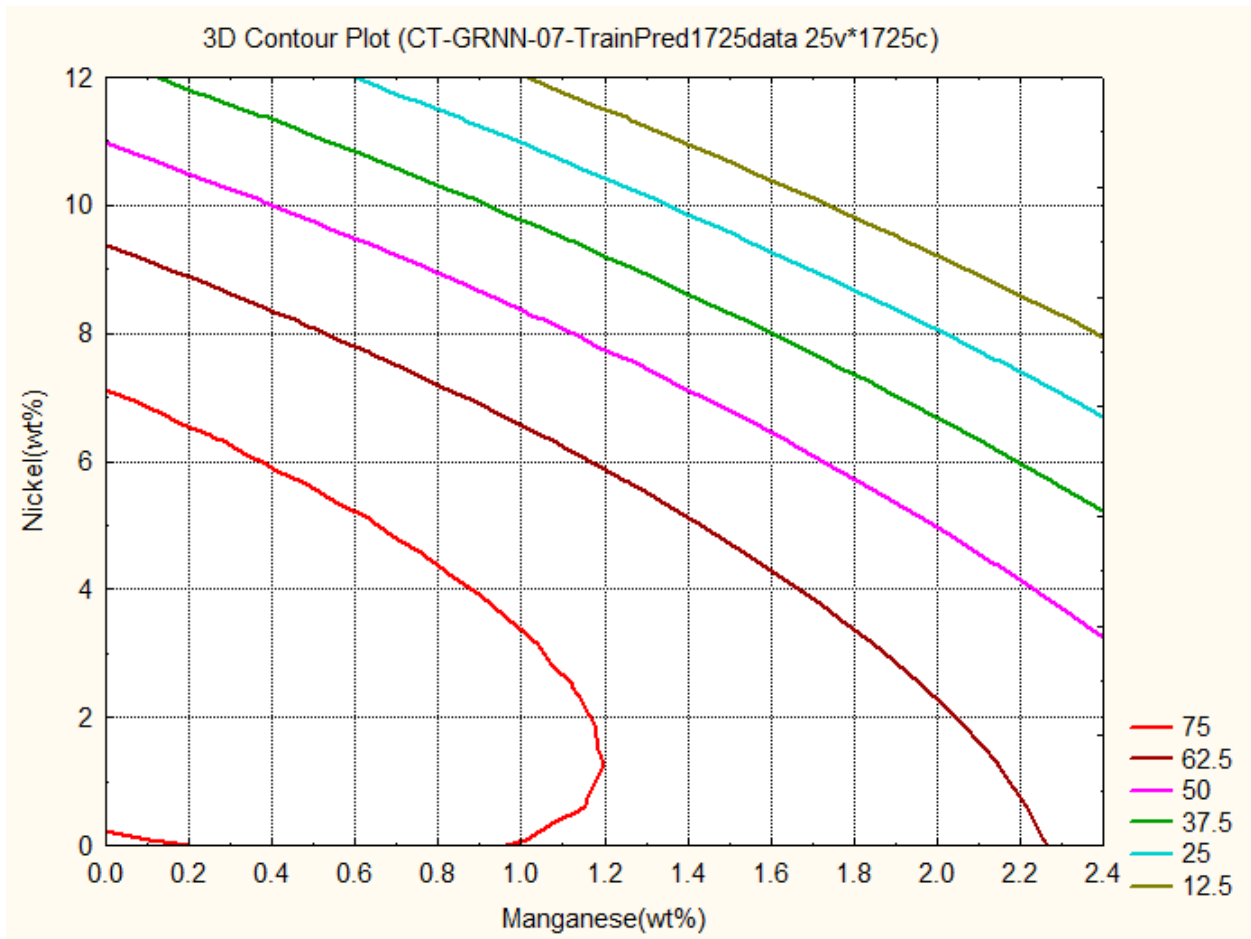


Figure. 4.12.2 Predicted variations in Charpy Toughness (J) as a function of the Manganese and Nickel concentrations

3D contour Plot gives the relations between the **two input variables** and **one output variable**. **Figure. 4.12.2** shows the relations between **Manganese**, Nickel and Charpy Toughness by **GRNN**. The graph gives the information about how these two, **Manganese** and Nickel control the Charpy Toughness from **12.5J to 75J**.

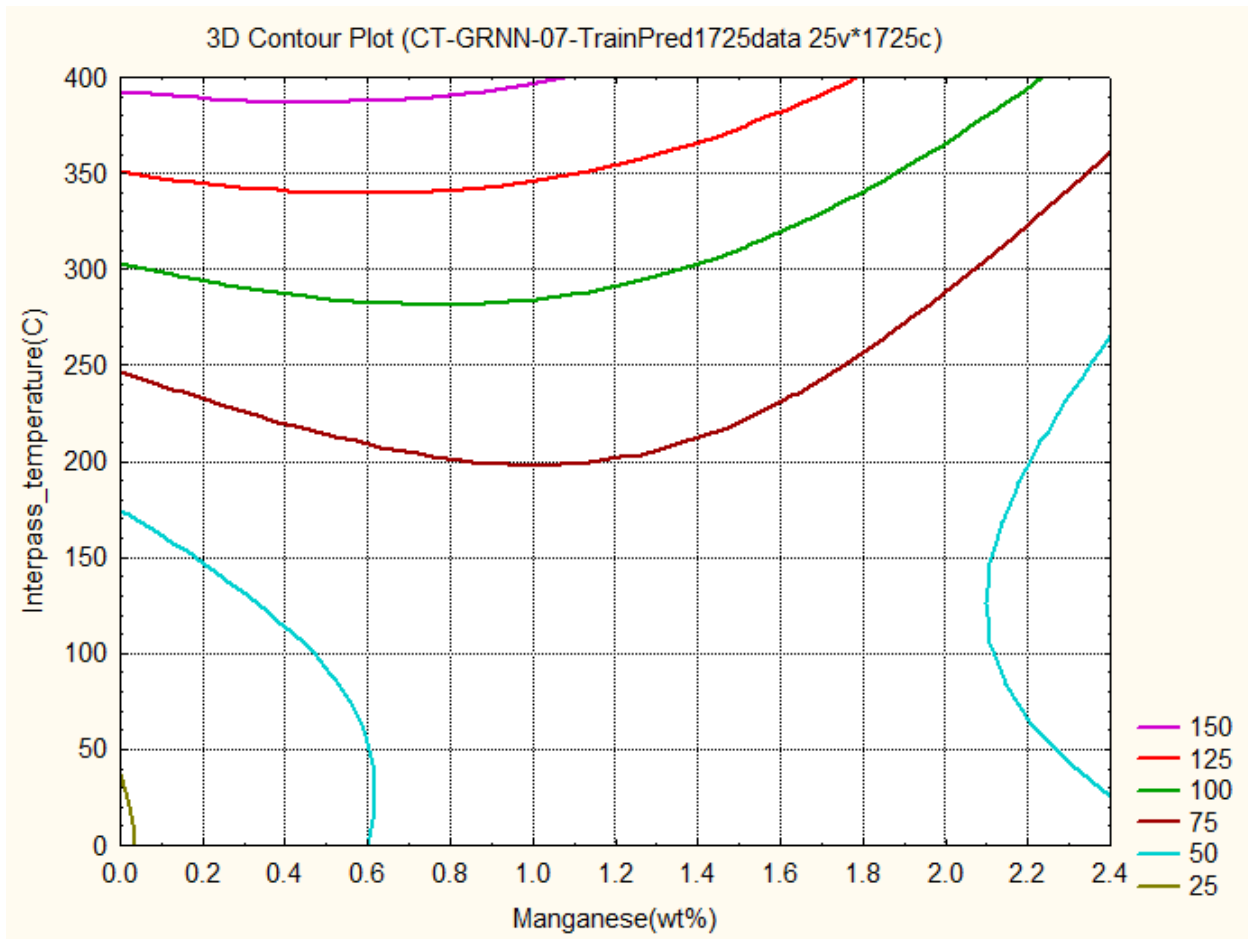


Figure. 4.12.3 Predicted variations in Charpy Toughness (J) as a function of the Manganese concentration and Interpass temperature

3D contour Plot gives the relations between the **two input variables** and **one output variable**. **Figure. 4.12.3** shows the relations between **Manganese**, Interpass temperature and Charpy Toughness by **GRNN**. The graph gives the information about how these two, **Manganese** and Interpass temperature control the Charpy Toughness from **25J to 150J**.

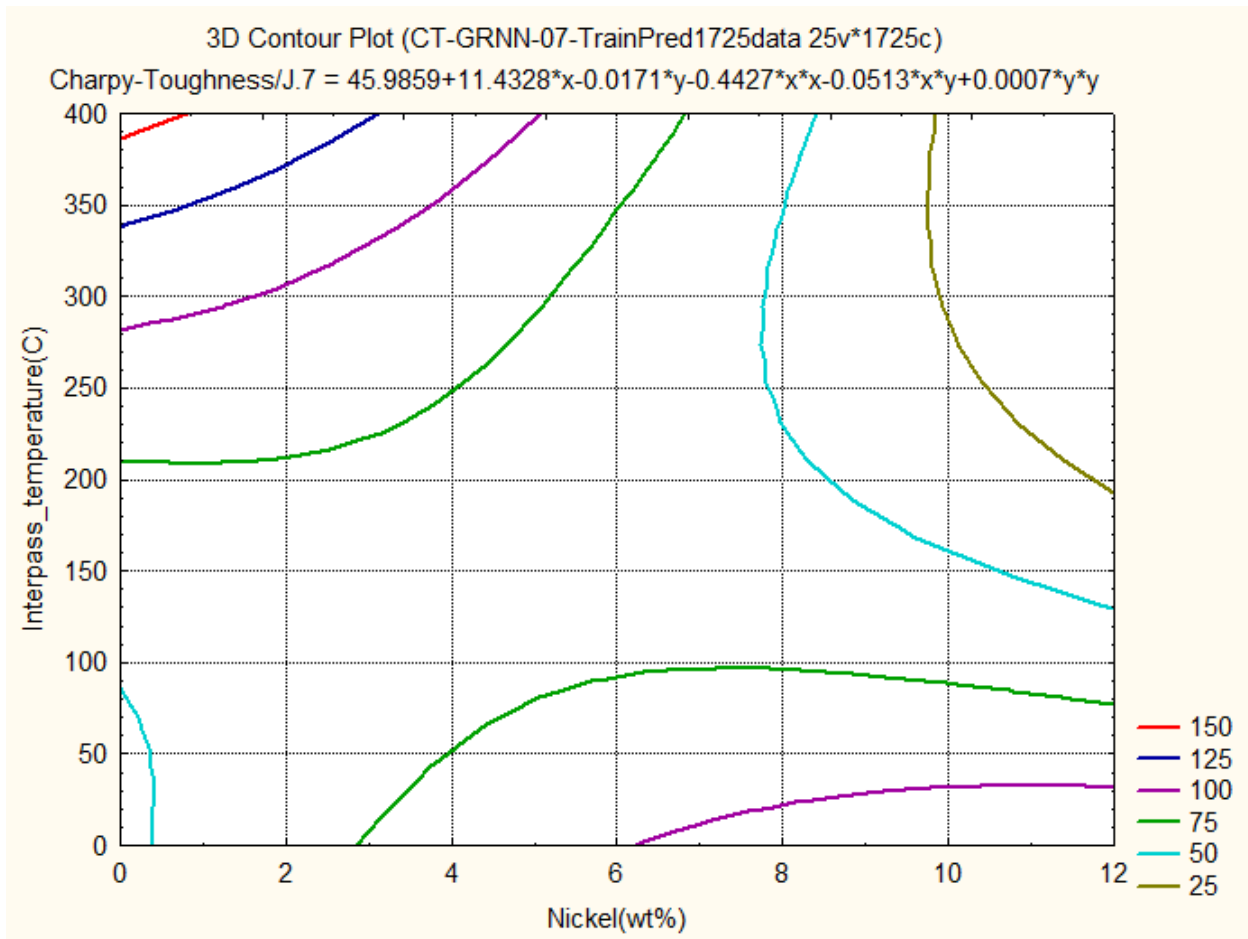


Figure. 4.12.4 Predicted variations in Charpy Toughness (J) as a function of the Nickel concentration and Interpass temperature

3D contour Plot gives the relations between the **two input variables** and **one output variable**. **Figure. 4.12.4** shows the relations between **Nickel**, Interpass temperature and Charpy Toughness by **GRNN**. The graph gives the information about how these two, **Nickel** and Interpass temperature control the Charpy Toughness from **25J to 150J**.

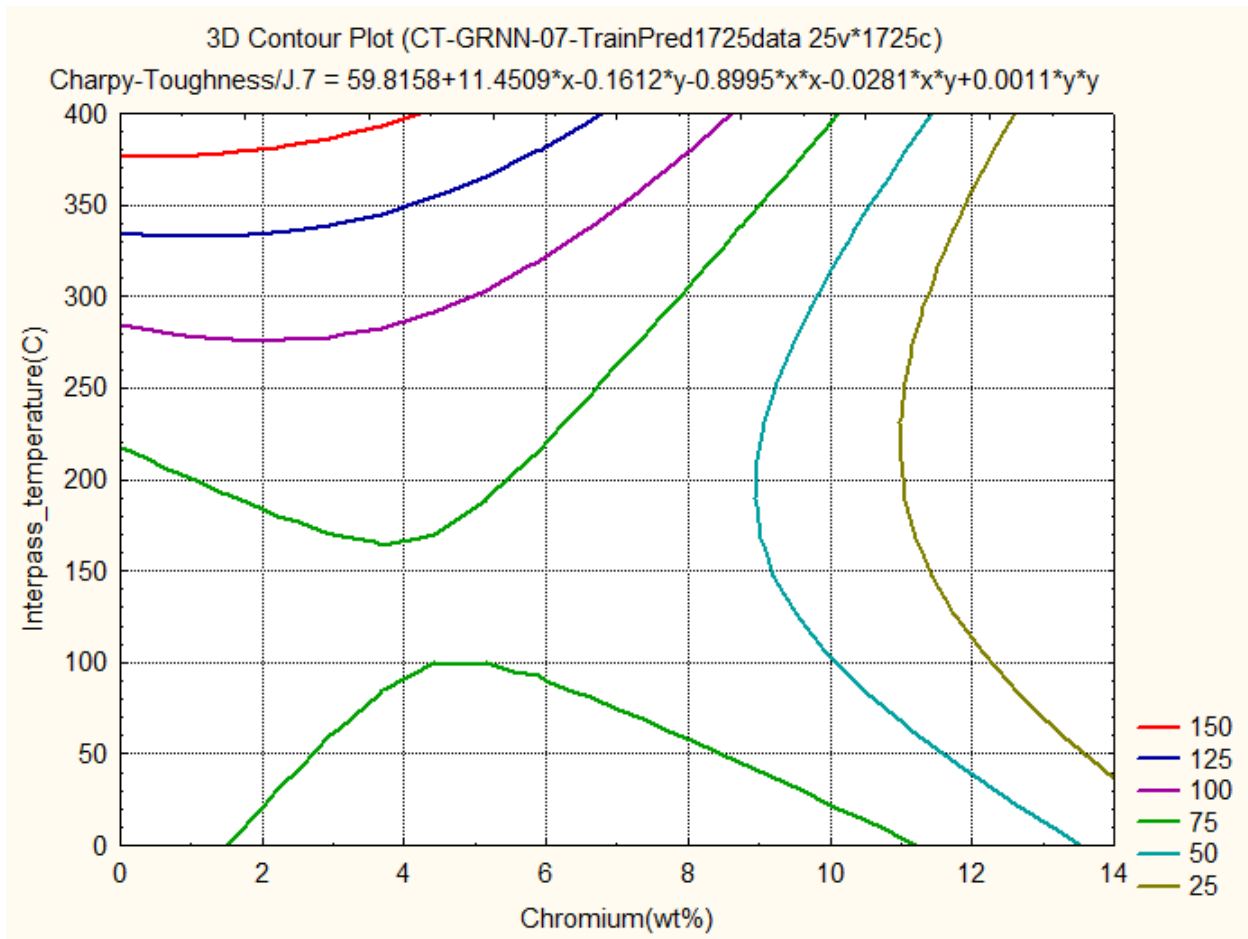


Figure. 4.12.5 Predicted variations in Charpy Toughness (J) as a function of the Chromium concentration and Interpass temperature

3D contour Plot gives the relations between the **two input variables** and **one output variable**. **Figure. 4.12.5** shows the relations between Chromium, Interpass temperature and Charpy Toughness by **GRNN**. The graph gives the information about how these two, Chromium and Interpass temperature control the Charpy Toughness from **25J to 150J**.

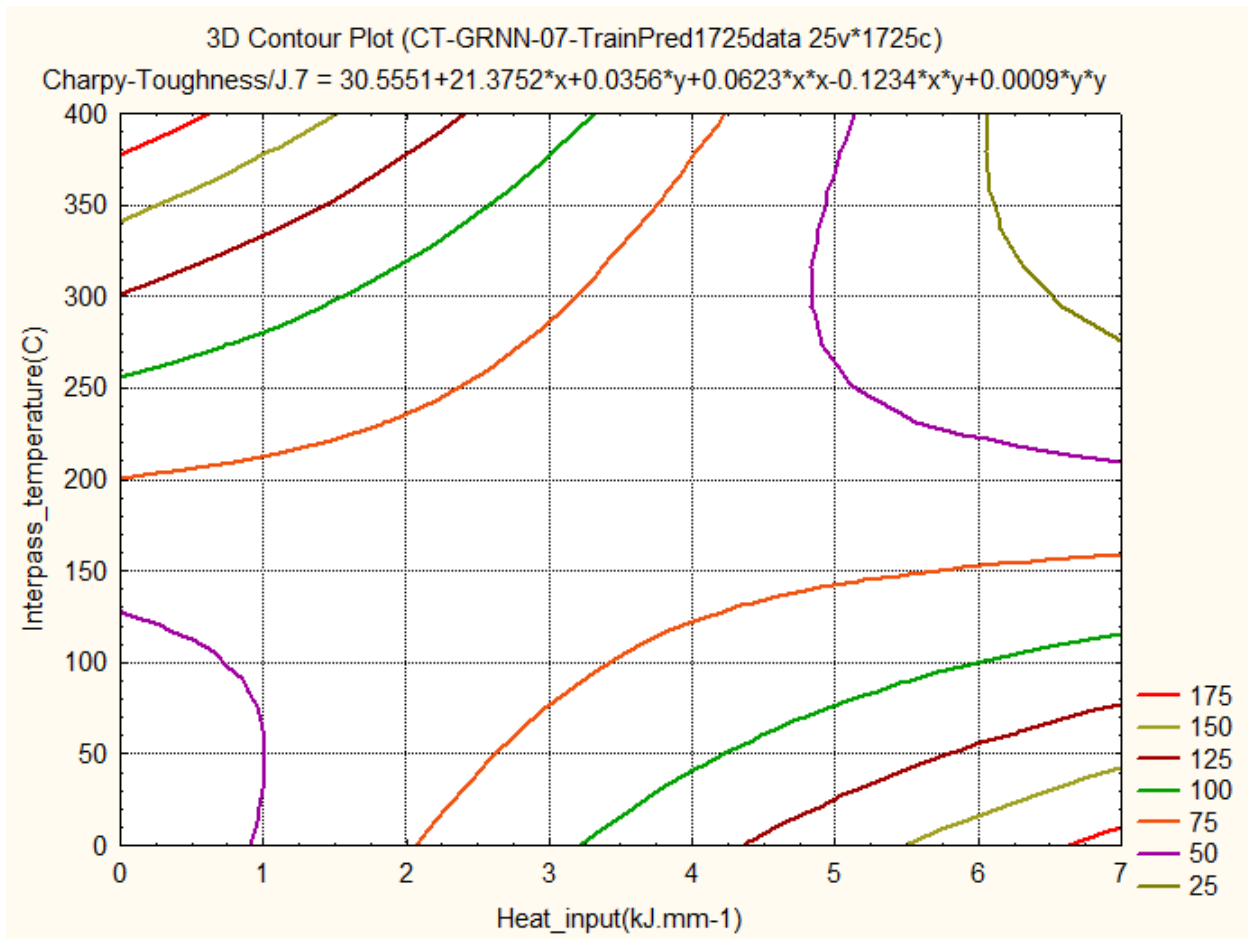


Figure. 4.12.6 Predicted variations in Charpy Toughness (J) as a function of the Heat Input(kJ mm-1) and Interpass temperature

3D contour Plot gives the relations between the **two input variables** and **one output variable**. **Figure. 4.12.6** shows the relations between Heat Input, Interpass temperature and Charpy Toughness by **GRNN**. The graph gives the information about how these two, Heat Input and Interpass temperature control the Charpy Toughness from **25J to 175J**.

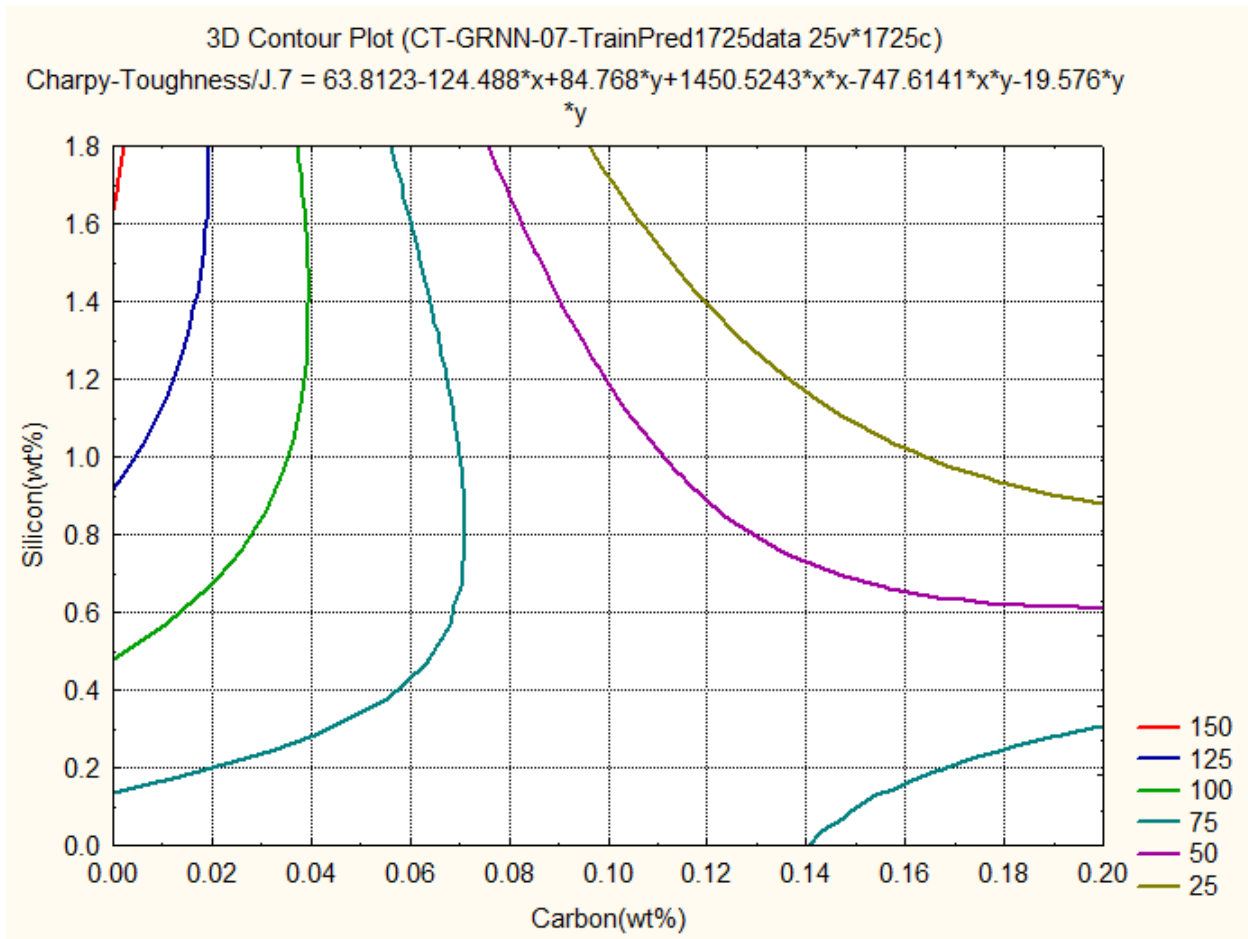


Figure. 4.12.7 Predicted variations in Charpy Toughness (J) as a function of the Carbon and Silicon concentrations

3D contour Plot gives the relations between the **two input variables** and **one output variable**. **Figure. 4.12.7** shows the relations between Carbon, Silicon and Charpy Toughness by **GRNN**. The graph gives the information about how these two, Carbon and Silicon control the Charpy Toughness from **25J to 150J**.

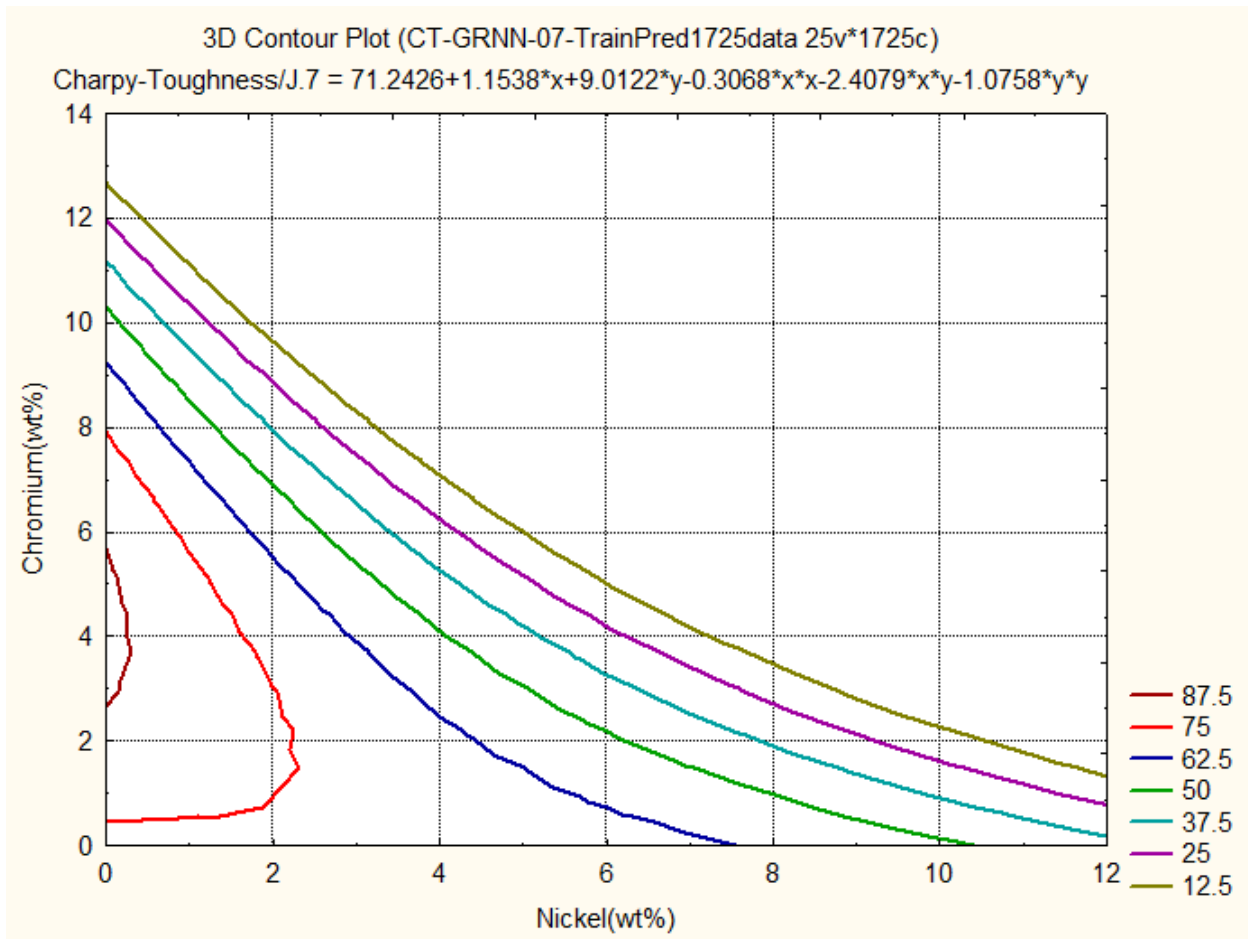


Figure. 4.12.8 Predicted variations in Charpy Toughness (J) as a function of the Nickel and Chromium concentrations

3D contour Plot gives the relations between the **two input variables** and **one output variable**. **Figure. 4.12.8** shows the relations between Nickel, Chromium and Charpy Toughness by **GRNN**. The graph gives the information about how these two, Nickel and Chromium control the Charpy Toughness from **12.5J to 87.5J**.

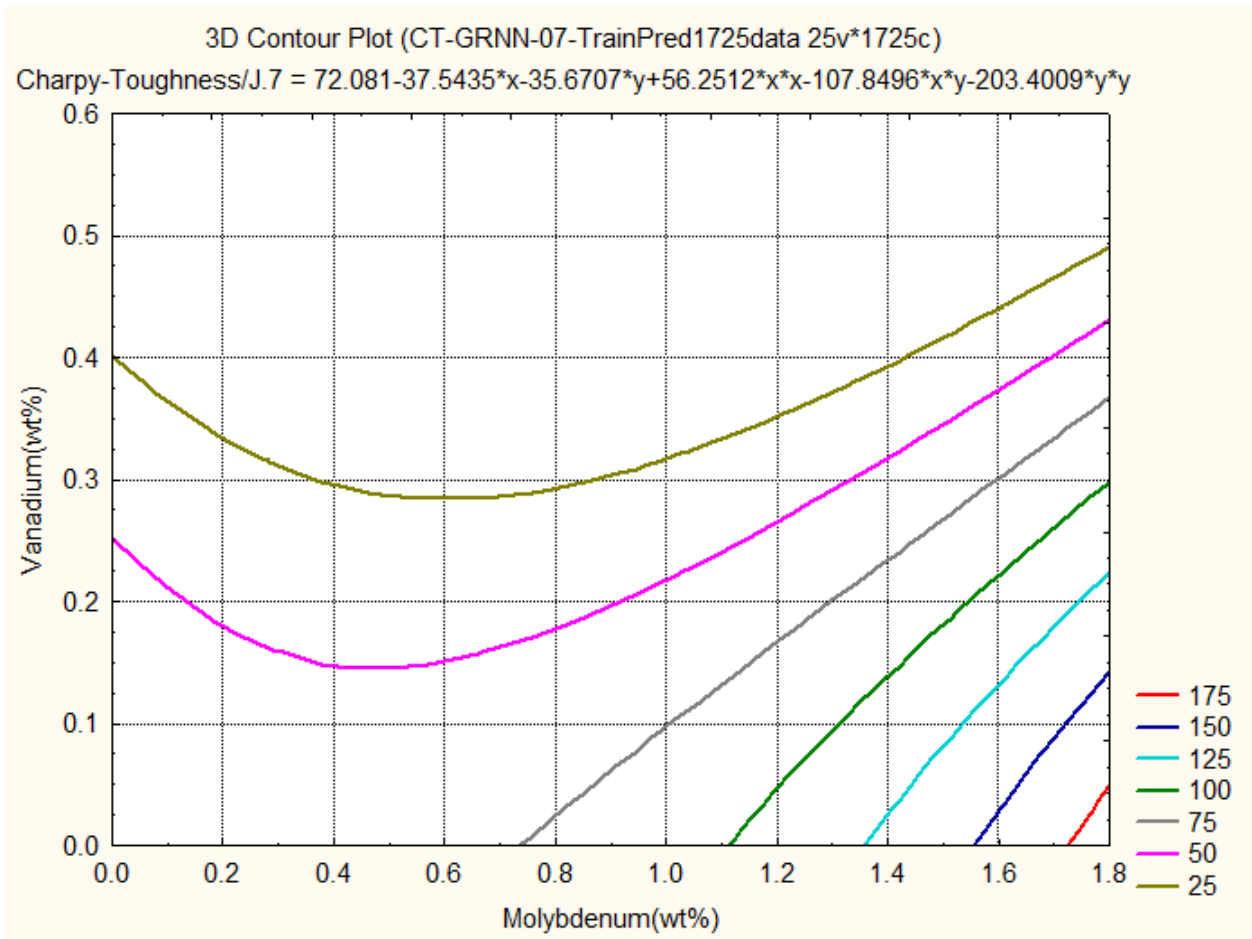


Figure. 4.12.9 Predicted variations in Charpy Toughness (J) as a function of the Molybdenum and Vanadium concentrations

3D contour Plot gives the relations between the **two input variables** and **one output variable**. **Figure. 4.12.9** shows the relations between Molybdenum, Vanadium and Charpy Toughness by **GRNN**. The graph gives the information about how these two, Molybdenum and Vanadium control the Charpy Toughness from **25J to 175J**.

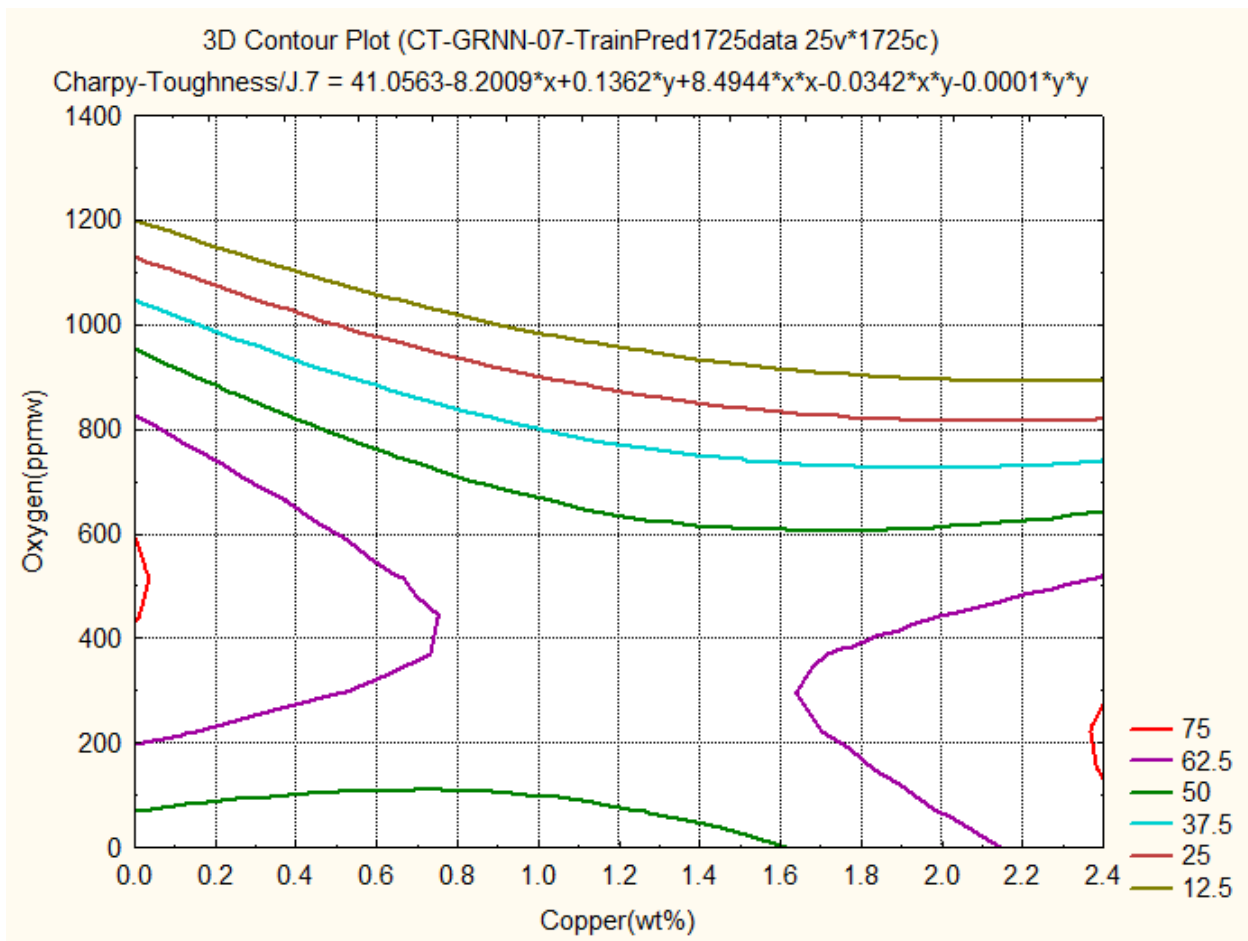


Figure. 4.12.10 Predicted variations in Charpy Toughness (J) as a function of the Copper and Oxygen concentrations

3D contour Plot gives the relations between the **two input variables** and **one output variable**. **Figure. 4.12.10** shows the relations between Copper, Oxygen and Charpy Toughness by **GRNN**. The graph gives the information about how these two, Copper and Oxygen control the Charpy Toughness from 12.5J to 75J.

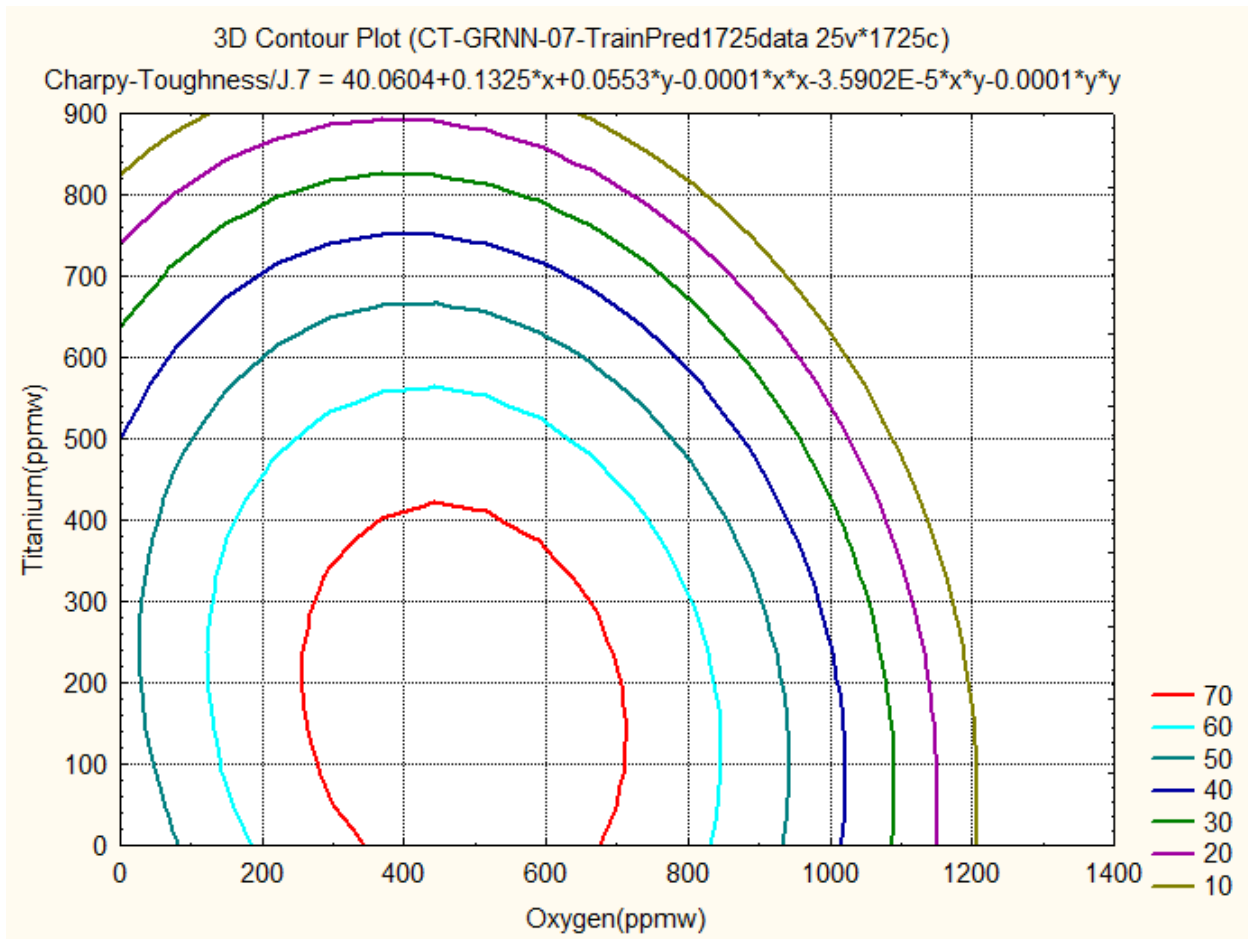


Figure. 4.12.11 Predicted variations in Charpy Toughness (J) as a function of the Qxygen and Titanium concentrations

3D contour Plot gives the relations between the **two input variables** and **one output variable**. **Figure. 4.12.11** shows the relations between Qxygen, Titanium and Charpy Toughness by **GRNN**. The graph gives the information about how these two, Qxygen and Titanium control the Charpy Toughness from **10J to 70J**.

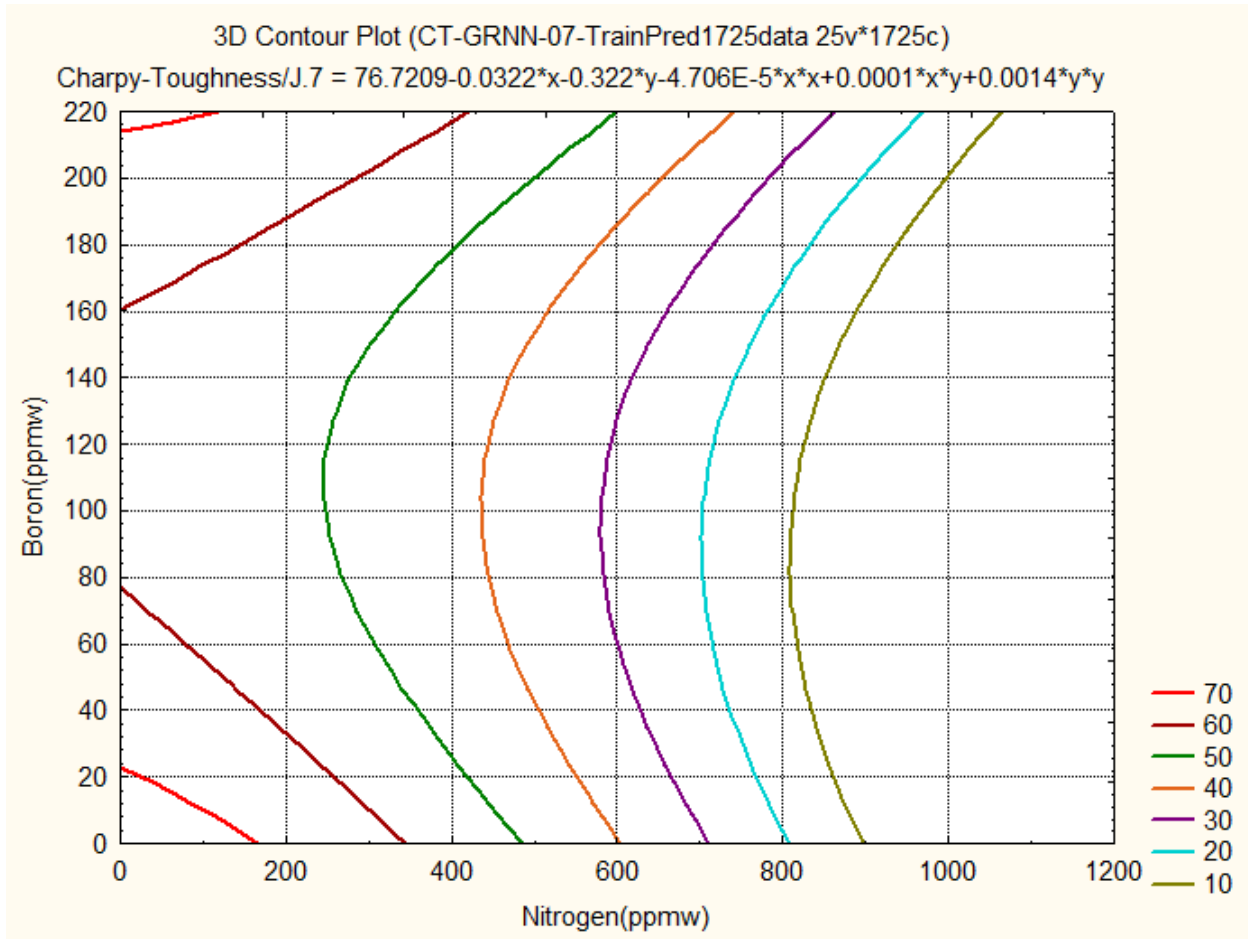


Figure. 4.12.12 Predicted variations in Charpy Toughness (J) as a function of the Nitrogen and Boron concentrations

3D contour Plot gives the relations between the **two input variables** and **one output variable**. **Figure. 4.12.12** shows the relations between Nitrogen, Boron and Charpy Toughness by **GRNN**. The graph gives the information about how these two, Nitrogen and Boron control the Charpy Toughness from **10J to 70J**.

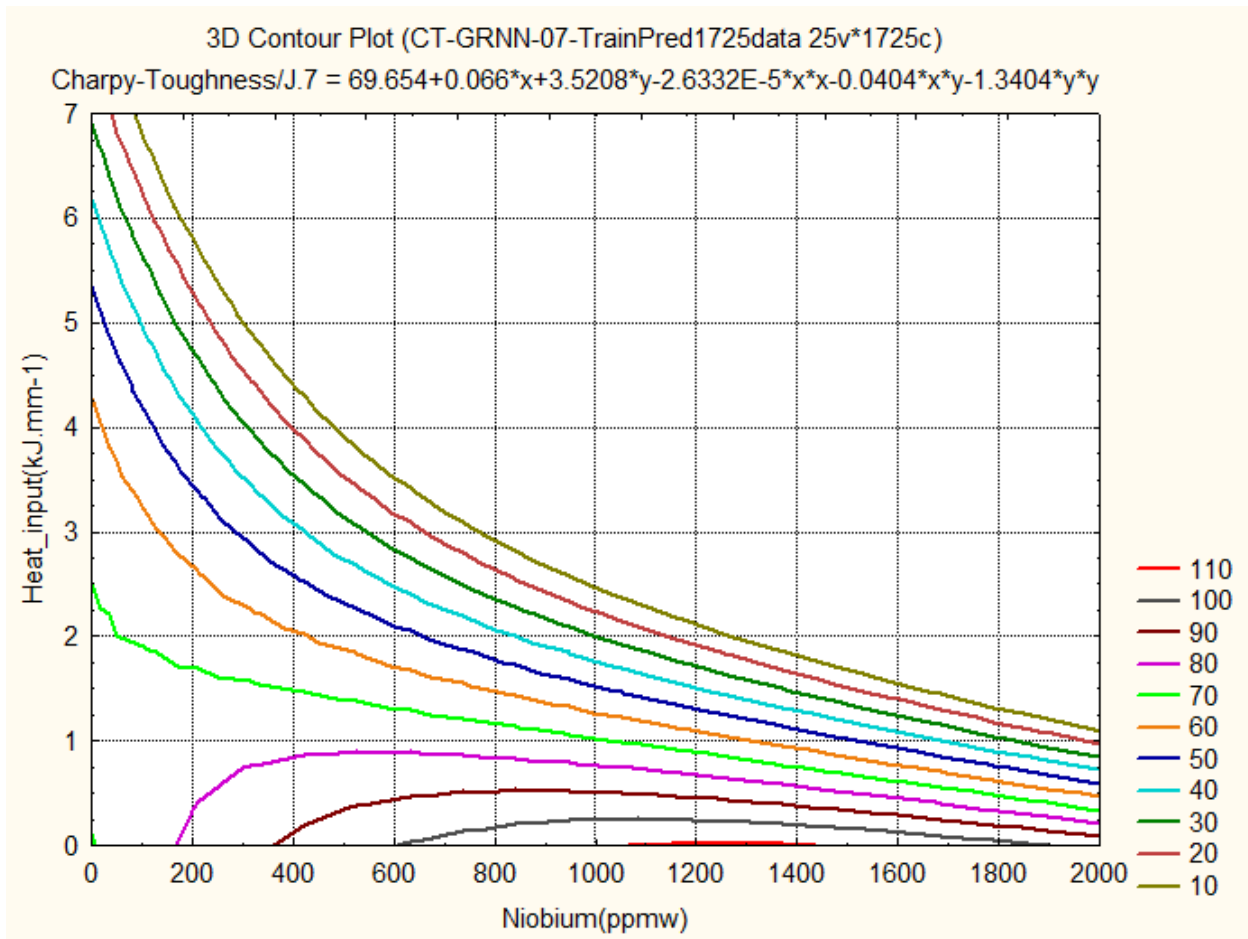


Figure. 4.12.13 Predicted variations in Charpy Toughness (J) as a function of the Niobium concentration and Heat input(kJ mm-1)

3D contour Plot gives the relations between the **two input variables** and **one output variable**. **Figure. 4.12.13** shows the relations between Niobium, Heat input and Charpy Toughness by **GRNN**. The graph gives the information about how these two, Niobium and Heat input control the Charpy Toughness from **10J to 110J**.

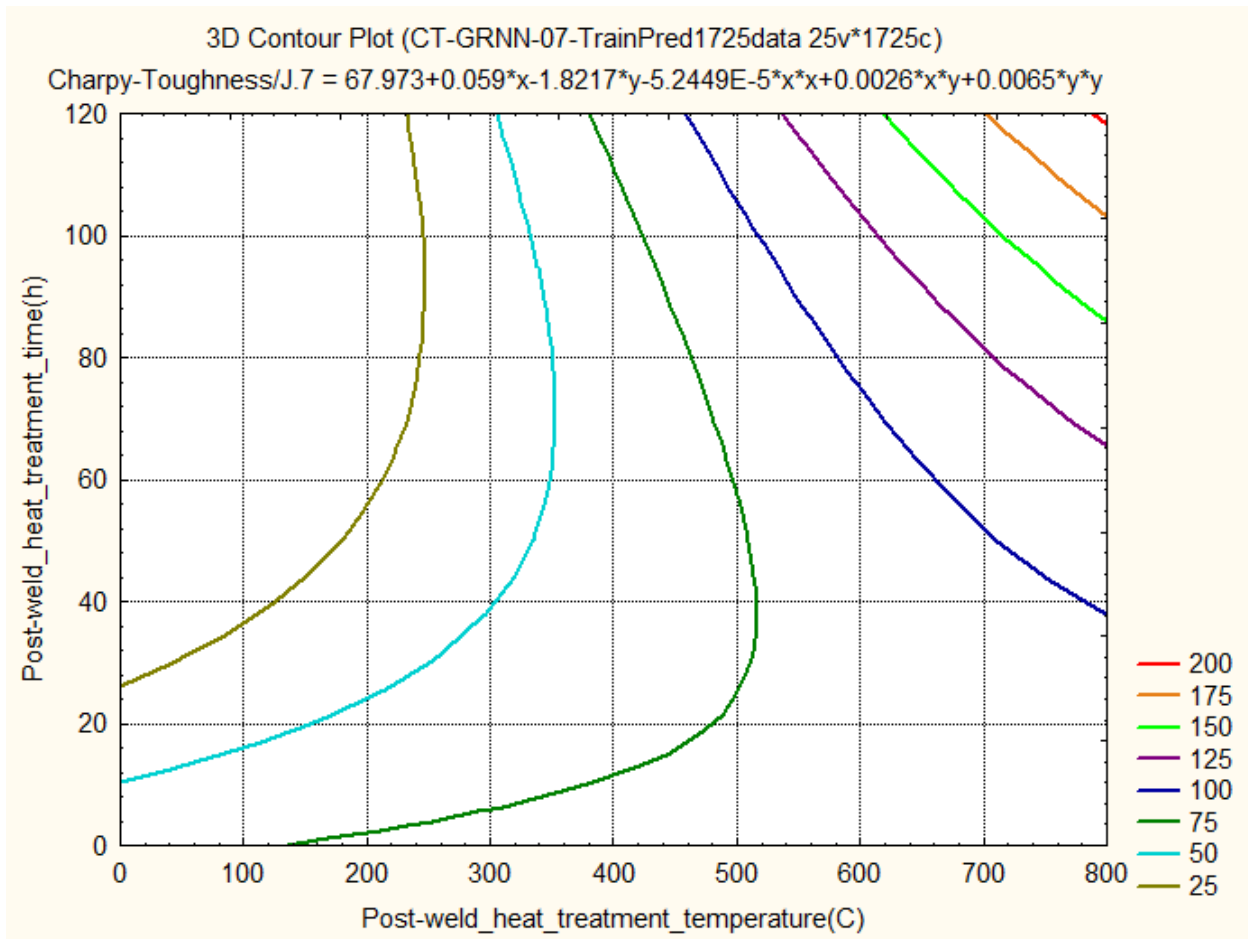


Figure. 4.12.14 Predicted variations in Charpy Toughness (J) as a function of the Post-weld Heat treatment temperature and Post-weld Heat treatment time

3D contour Plot gives the relations between the **two input variables** and **one output variable**. **Figure. 4.12.14** shows the relations between Post-weld Heat treatment temperature, Post-weld Heat treatment time and Charpy Toughness by **GRNN**. The graph gives the information about how these two, Post-weld Heat treatment temperature and Post-weld Heat treatment time control the Charpy Toughness from 25J to **200J**.

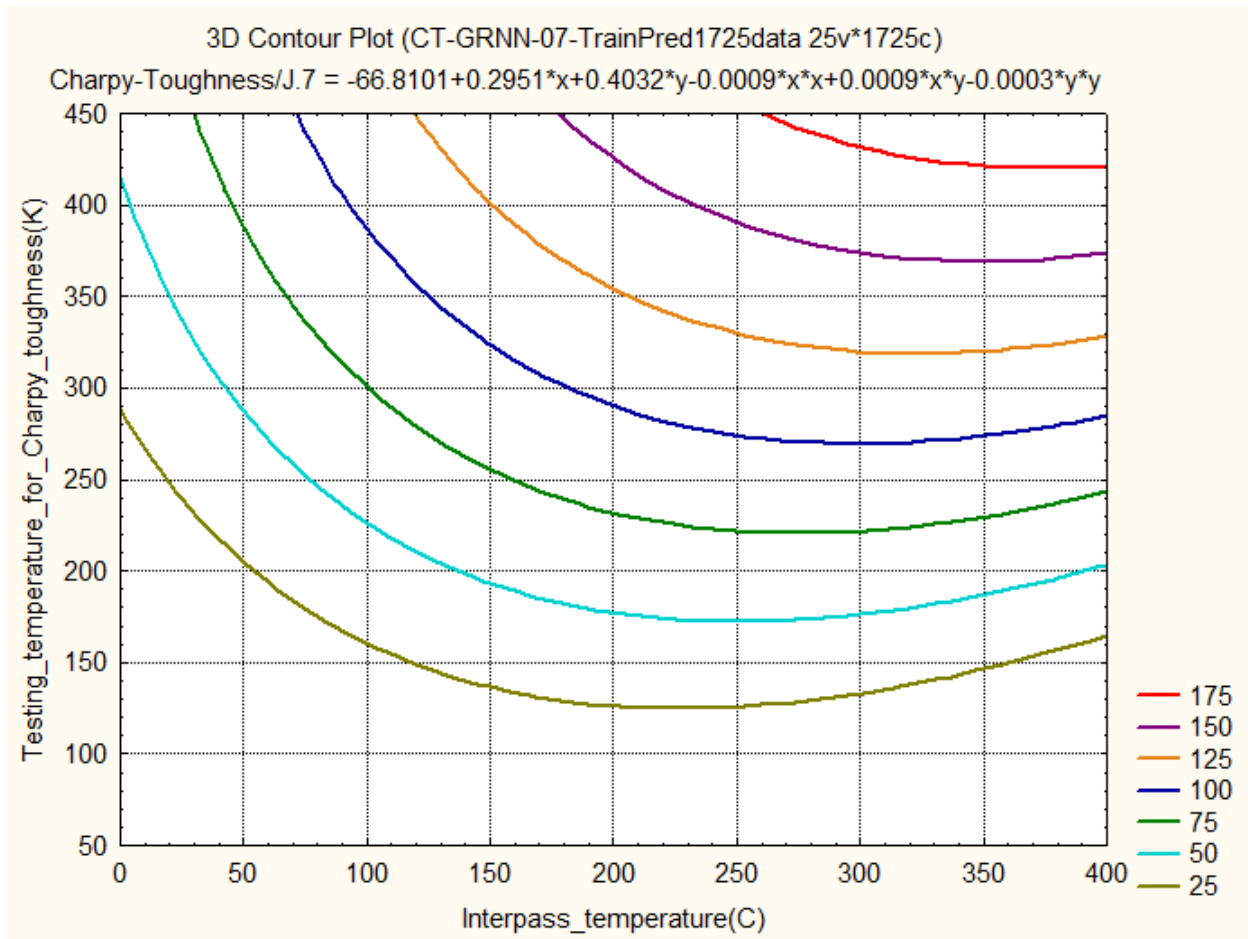


Figure. 4.12.15 Predicted variations in Charpy Toughness (J) as a function of the Interpass temperature and Testing temperature for Charpy Toughness

3D contour Plot gives the relations between the **two input variables** and **one output variable**. **Figure. 4.12.15** shows the relations between Interpass temperature, Testing temperature for Charpy Toughness and Charpy Toughness by **GRNN**. The graph gives the information about how these two, Interpass temperature and Testing temperature for Charpy Toughness control the Charpy Toughness from **25J to 175J**.

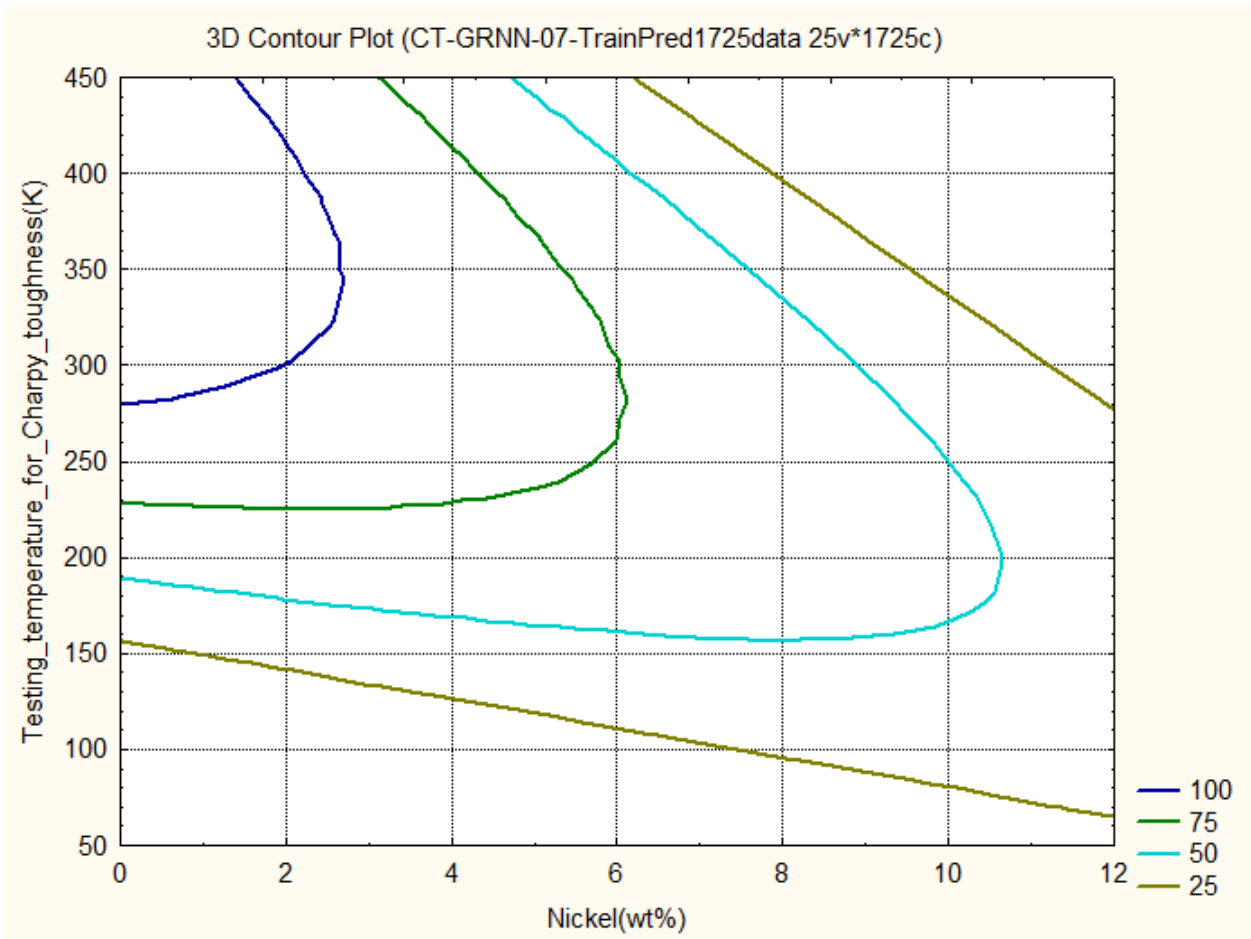


Figure. 4.12.16 Predicted variations in Charpy Toughness (J) as a function of the Nickel and Testing temperature for Charpy Toughness

3D contour Plot gives the relations between the **two input variables** and **one output variable**. **Figure. 4.12.16** shows the relations between Nickel, Testing temperature for Charpy Toughness and Charpy Toughness by **GRNN**. The graph gives the information about how these two, Nickel and Testing temperature for Charpy Toughness control the Charpy Toughness from 25J to 100J.

Figure 4.12.1. CT (z) - Mn (y) - C (x) 3D plot.

Figure 4.12.1. shows the maximum Charpy Toughness values 90 J and more than 90 J at the combination of wt% C less than 0,02% and wt% Mn in range of 0.08% to 1.3%. The decrease in Charpy Toughness is observed with an increase in wt% C and broadening the range of wt% Mn. (ie. Charpy Toughness contour from 90 J to 70 J).

Higher wt% of C in the range of 0.14% to 0.2% and Mn in the range of 1.04% to 2.4%, increases the Charpy Toughness from 70 J to more than 80 J in the top right corner of the plot.

The upper middle to the upper left corner portion of the graph shows that decrease in Charpy Toughness from 60 J to less than 50 J. In this region wt% Mn is the higher side and wt% C is spread maximum up to 0.162% C.

From centre portion to right bottom corner of the graph shows decrease in Charpy Toughness from 60 J to less than 30 J. This is the region where wt% C is increasing from 0.054% to highest 0.2 % and wt% Mn is decreasing from 0.78% to 0.0%.

Wt% C and wt% Mn both have a good control over the Charpy Toughness within the range of given weld deposits data.

The variations are observed in the Charpy Toughness is because of microstructural changes happened in the Ferritic Steel Welds.

The microstructural changes are very complex in Ferritic Steel Welds. And due to this the Charpy Toughness values are also vary nonlinearly.

Figure 4.12.2. CT(z) - Ni(y) - Mn(x) 3D plot.

Figure 4.12.2. shows the decrease in the Charpy Toughness from 75 J to 12.5 J with increase in the concentration of both Manganese and Nickel. Higher value of Charpy Toughness is observed in the contour of 75 J where wt% of Mn is 1.2% and wt% of Ni is 7.2. Increase in Nickel content is not improved the Charpy Toughness and it must be managed with content of Manganese. The General trend of the Charpy toughness for Manganese indicates a reduction with an increase in wt% Mn.

Figure 4.12.3. CT (z) - IPT (y) - Mn (x) 3D plot.

Figure 4.12.3. shows the increase of the Charpy Toughness with the increase in the Interpass Temperature. The Manganese concentrations have less effect comparatively on the Charpy Toughness. The Charpy Toughness values from 75 J to 150 J and more is observed with increase in the Interpass Temperature in the range of 200 C to 400 C. Below the Interpass Temperature 200 C, the Charpy Toughness values are observed between 50 J to 75 J for the wide range of Mn concentrations. The lower Charpy Toughness values of 50 J and less appears at very low wt% of Mn and higher wt% Mn.

Figure 4.12.4. CT (z) - IPT (y) - Ni (x) 3D plot.

Figure 4.12.4. In the plot from the upper left to middle portion shows the Charpy Toughness contours from 150 J to 75 J. The bottom right corner to the bottom middle portion of the plot gives the Charpy toughness values from more than 100 J to 75 J. These higher values of Charpy Toughness are observed above 200 C to 400 C Interpass temperature with wt% of Nickel up to 6.6% and also below the Interpass Temperature 100 C and Ni wt% in the range of 2.8% to 12%. The pattern of decrease in the Charpy Toughness from 50 J to below 25 J appears at upper right corner to middle right where Wt% Ni is in the range of 7.8% to 12% and the Interpass Temperature in between 130 C to 400 C. Lower values below 50 J of the Charpy Toughness are also observed at very low wt% of Ni 0.4% and the Interpass Temperature below 80 C. The relation of the Nickel concentrations and Interpass Temperature are complex.

Figure 4.12.5. CT (z) - IPT (y) - Cr (x) 3D plot.

Figure 4.12.5. shows the increase in the Charpy Toughness from 75 J to more than 150 J in the upper left to middle left portion which is covered by contour of 75 J. Interpass Temperature in this portion is in the range from 170 C to 400 C and wt% Cr from 0% to 10%. Below 100 C Interpass Temperatures and in a range of wt% Cr between 1.6% to 11% gives the Charpy Toughness 75 J to more than 75 J. The area between the contours 75 J and 50 J has stable values of the Charpy Toughness for different wt% Cr and Interpass Temperature. More than 8.8% to 14% Cr and from 0 C to 400 C Interpass Temperature, the Charpy Toughness is in a range of 50 J to less than 25 J at the right side of the Plot.

Figure 4.12.6. CT (z) - IPT (y) – Heat Input (x) 3D plot.

Figure 4.12. 6. shows the increase in the Charpy Toughness from 75 J to more than 175 J in the middle left to upper left corner portion which is covered by contour of 75 J. Interpass temperature in this region in the range from 200 C to 400 C and Heat input in the range between 0 kJ mm⁻¹ to 4.2 kJ mm⁻¹. Below 160 Interpass Temperature and in the range Heat Input from 2.1 kJ mm⁻¹ to 7 kJ mm⁻¹ increases the Charpy Toughness from 75 J to more than 175 J at bottom middle to right middle and right corner of the plot. Both opposite sides, bottom left and upper right corners of the plot indicates the Charpy Toughness values 50 J and less than 50 J. Right upper area has both Heat Input and Interpass Temperature in higher values and Left bottom area has both Heat Input and Interpass Temperature in lower values. The centre area of the plot has the Charpy toughness between 50 J to 75 J, more stable effect of both the independent variables. Both the Variables have a strong effect on the Charpy Toughness of the Ferritic Steel Welds.

Figure 4.12.7. CT (z) - Si (y) – C (x) 3D plot.

Figure 4.12.7. shows the increase in the Charpy Toughness from 75 J to more than 150 J mainly in right side of the plot in the area covered by the contour of 75 J. This area has the Silicon from 0.14% to 1.8% and the Carbon below 0.068%. The area between the 50 J and 75 J in bottom middle to centre of the plot is more stable range of the Charpy Toughness. Higher concentration of both the elements reduces the Charpy Toughness from 50 J to less than 25 J. But in right bottom corner, an area covered by the 75 J contour has 75 J and more than 75 J with higher Carbon in the range from 0.14% to 0.20% and Silicon below 0.32%. Both the variables have a complex relationship with the Charpy Toughness.

Figure 4.12.8. CT (z) - Cr (y) – Ni (x) 3D plot.

Figure 4.12.8. shows a decrease in the Charpy Toughness from more than 87.5 J to 12.5 J in left side near middle, to bottom towards the centre of the plot. More than 87.5 J is obtained with 0.4 % of Ni and 2.8% to 5.7% Cr. Increase in % Ni and decrease in % Cr and vice versa decreases in the

Charpy Toughness General trend of the Charpy Toughness decrease with the increase in both % Ni and % Cr as illustrated by contours from 62.5 J to 12.5 J. Below 10% of both the Ni and Cr

gives 50 J and more than 50 J a sufficient Charpy Toughness. For more than 75 J Charpy Toughness, the role of Chromium is very significant compare to the Nickel. This is also a very important finding. Because traditionally in alloy design it is given that the Nickel improve the Charpy Toughness of weld alloys.

Figure 4.12.9. CT (z) - V (y) – Mo (x) 3D plot.

Figure 4.12.9. shows an increase in the Charpy Toughness from 25 J to more than 175 J with an increase in the Molybdenum in the range of 0% to 1.8% and decrease in Vanadium in the range of 0% to 0.4%. The higher Charpy Toughness, more than 175 J is obtained with less than 0.05 % V and more than 1.72% Mo. The relationship of both variables is straight forward for the Charpy Toughness.

Figure 4.12.10. CT (z) - O (y) – Cu (x) 3D plot.

Figure 4.12.10. shows the Charpy Toughness 75 J and more than 75 J, the left side of plot with 430ppm to 580 ppm Oxygen and 0.06% Cu and the right side of plot with 2.34% Cu and 130 ppm to 260 ppm. Both the variables have the very good control on the Charpy Toughness values between the left and right contour of 75 J, and central contour and bottom contour of 50J. The Charpy Toughness is more sensitive to Oxygen concentration in Ferritic Steel Welds.

Figure 4.12.11. CT (z) - Ti (y) – O (x) 3D plot.

Figure 4.12.11. shows the Charpy Toughness 70 J and more than 70 J with Oxygen in the range from 240 ppm to 700 ppm and Titanium in the range from 0 ppm to 420 ppm . If the concentration of Oxygen is more or less and the concentration of Titanium more than as mentioned above reduces the Charpy Toughness from 70 J to less than 10 J. The selection of these independent variables is also very critical for the design of the Weld deposits.

Figure 4.12.12. CT (z) - B (y) – N (x) 3D plot.

Figure 4.12.12. shows the Charpy Toughness 50 J and more than 70 J at the left side of the plot where the Boron in the range from 0 ppm to 220 ppm and the Nitrogen in the range from 0 ppm to 600 ppm. The increase in the Nitrogen concentration reduces the Charpy Toughness from 50 J

to 10 J. To design, high Charpy Toughness, the concentrations of both B and N are critical. Boron is more effective at lower ppm and higher ppm with combinations of lower Nitrogen ppm for higher values of the Charpy Toughness.

Figure 4.12.13. CT (z) - HI (y) – Nb (x) 3D plot.

Figure 4.12.13. shows the Charpy Toughness 80 J and more than 100 J at the bottom area of the plot where the Heat Input less than 1 kJ mm⁻¹ and the Niobium in the range from 180 ppm to 1900 ppm. The increase in the Heat Input reduces the Charpy Toughness from 70 J to 10 J with constant value of Nb ppm is observed in the plot. For the design of the wide range of the Charpy Toughness in the Ferritic Steel Welds maintain the Niobium 800 ppm for the Heat Input range up to 3 kJ mm⁻¹.

Figure 4.12.14. CT (z) - PWHTT (y) – PWHTt (x) 3D plot.

Figure 4.12.14. The Charpy Toughness contours 25 J, 50 J and 75 J show the curve shapes which indicate that at initially with low Post Weld Heat treatment Time and higher Post weld Heat treatment Temperature is required but for higher PWHTt there is reduction in PWHTT. For the Charpy Toughness contours 100 J, 125 J, 150 J 175 J and 200 J show with an increase in the PWHTT decrease the PWHTt. The response of the both the independent variables on the Charpy Toughness is not complex. It can be easily understood for the design of the Ferritic Steel Welds.

Figure 4.12.15. CT (z) - TTCT (y) – IPT (x) 3D plot.

Figure 4.12.15. shows the Charpy Toughness increases from 25 J to more than 175 J with the increase in the Testing Temperature of Charpy Toughness and the Interpass Temperature remains constant as given in the plot. More than 175J Charpy Toughness is observed with Interpass temperature in the range from 260 C to 400 C and Testing Temperature for Charpy Toughness in the range from 425 K to 450 K. Testing Temperature for Charpy Toughness is more effective compare to the Interpass Temperature of the Ferritic Steel welds. Both the independent variables have a different relationship to the Charpy Toughness.

Figure 4.12.16. CT (z) - TTCT (y) – Ni (x) 3D plot.

Figure 4.12.16. Shows the Charpy Toughness decreases from more than 100 J to 25 J with an increase in the increase in Nickel content from 0% to 12% and decrease in the Testing Temperature for Charpy Toughness from 450 K to 50 K. The higher Charpy Toughness more than 100 J is observed with Nickel in the range between 0% to 2.6% and Testing Temperature for Charpy Toughness from 280 K to 450 K. The Charpy Toughness is a very sensitive to %Ni and TTCT.

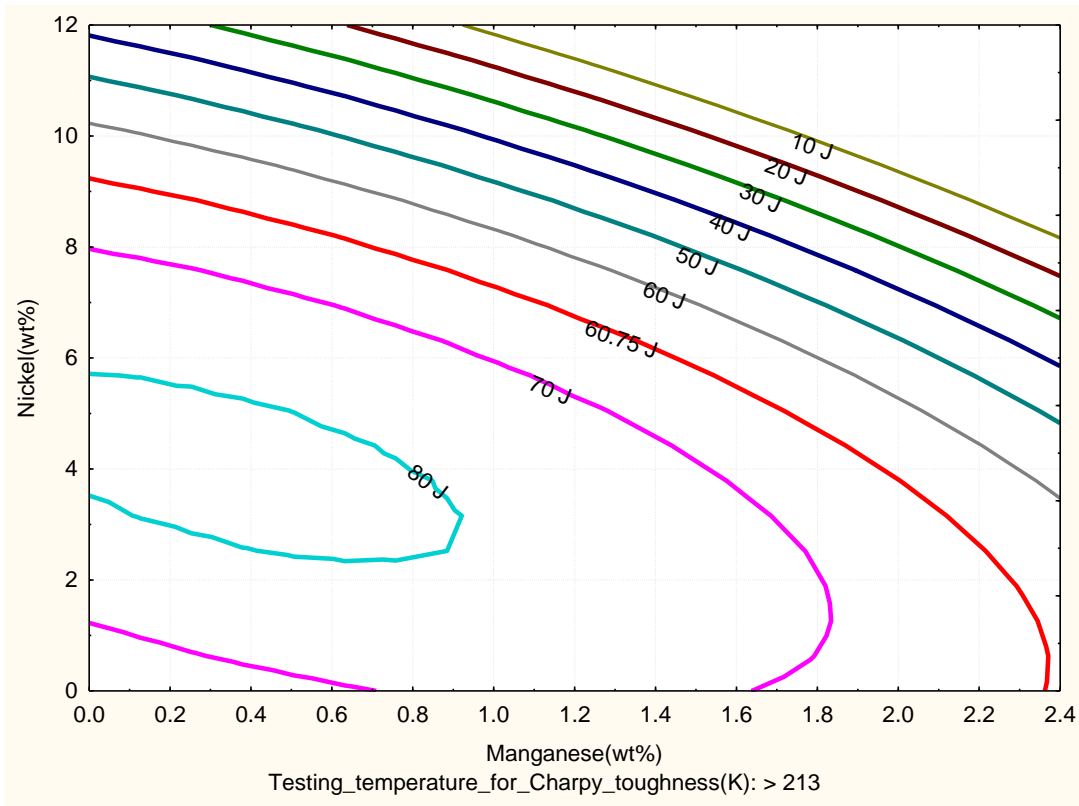


Figure. 4.12.17 3D Contour Plot of Charpy Toughness, Nickel Manganese and Testing Temperature for Charpy toughness > 213K (-60C) (GRNN)

3D contour Plot gives the relations between the three input variables and one output variable. Figure. 4.12.17 shows the relations between Nickel, Manganese and Testing Temperature for Charpy toughness > 213K (-60C) and Charpy Toughness by GRNN. Graph gives the information about how these three Nickel, Manganese and Testing Temperature for Charpy toughness > 213K control the Charpy Toughness from 10J to 80J. Traditionally in alloy design it is known that increase in the Nickel increases the Toughness. In Figure. 4.12.7, it is very critical to maintain the toughness with Nickel, Manganese and Testing Temperature for Charpy toughness > 213K. To achieve a 80J and more, the compositions of Nickel must be maintained in range of 3.5 to 5.8 wt% and Manganese must be maintained maximum 0.9 wt%. In literature, to these values are 6 to 10.8 wt% Nickel and 0.6 wt% Manganese.(BNN)

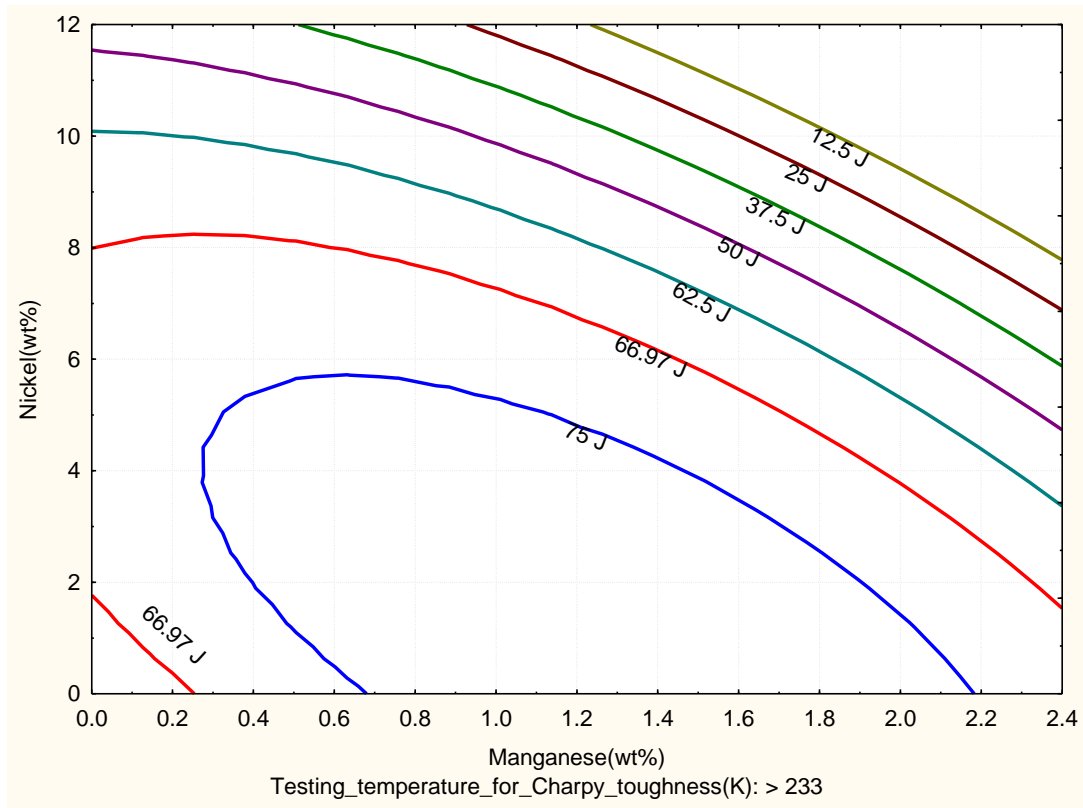


Figure. 4.12.18 3D Contour Plot of Charpy Toughness, Nickel Manganese and Testing Temperature for Charpy toughness > 233K (-40C) (GRNN)

3D contour Plot gives the relations between the three input variables and one output variable. Figure. 4.12.18 shows the relations between Nickel, Manganese and Testing Temperature for Charpy toughness > 233K (-40C) and Charpy Toughness by GRNN. Graph gives the information about how these three Nickel, Manganese and Testing Temperature for Charpy toughness > 233K control the Charpy Toughness from 10J to 80J. Traditionally in alloy design it is known that increase the Nickel increase the Toughness. In Figure 4.12.8, it is very critical to maintain the toughness with Nickel, Manganese and Testing Temperature for Charpy toughness > 233K. To achieve a 75J and more, the compositions of Nickel must be maintained less than 5.8 wt% and Manganese must be maintained in range of 0.7 to 2.1 wt%. In literature, to these values are 6 to 8 wt% Nickel and 0.8 wt% Manganese.(BNN)

4.4.4 Ternary Categorized Plots of Charpy Toughness GRNN Model

The effect in combination of any three input variables (Independent variables) and one variable as a categorical from Carbon, Silicon, Manganese, Sulphur, Phosphorus, Nickel, Chromium, Molybdenum, Vanadium, Copper, Oxygen, Titanium, Nitrogen, Boron, Niobium, Heat_input, Interpass_temperature, Post-weld heat treatment temperature, Post-weld heat treatment time and Testing Temperature Charpy Toughness on the Charpy Toughness of Ferritic Steel Welds can be studied in form of Ternary Categorized Plots.

The effect in the combination of Manganese, Nickel, Chromium with Heat Input as a categorical variable on the Charpy Toughness is presented in form of Ternary Categorized Plots in Figure. 4.13.1, Figure. 4.13.2, Figure.4.13.3, and Figure. 4.13.4.

Table 4.10 contains the scale of the Ternary Categorized Plot in Normalized values between 0 to 1. The Normalized values related to exact Actual values of all input variables are given.

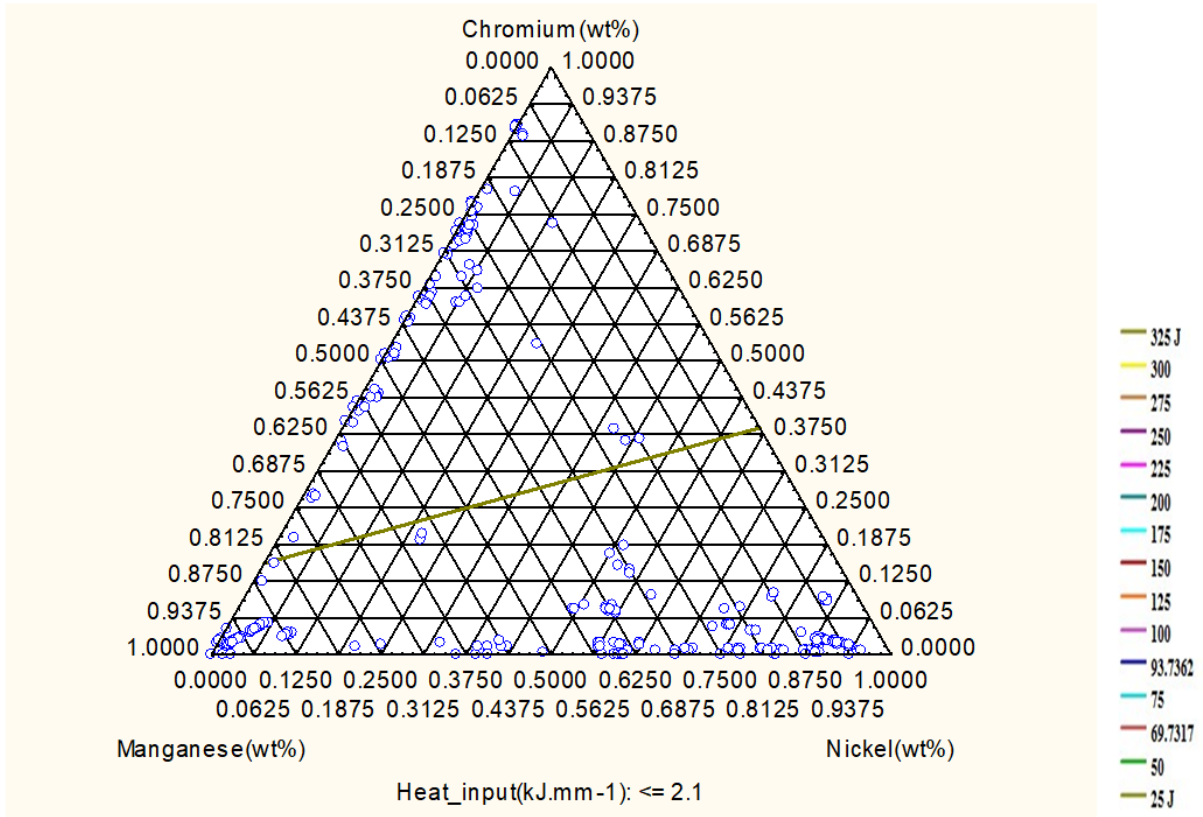


Figure.4.13.1 Ternary Categorized Graph of Chromium, Manganese, Nickel, **Heat Input** and Charpy Toughness shows 25 J line with Heat input ≤ 2.1 (wt% Mn range from 0 to 2.31, wt% Ni range from 0 to 10.8, wt% Cr range from 0 to 11.8)

	A	B	C	D	E	F	G	H	I	J	K	L	M	N	O	P	Q	R
1	Variables	0	0.0625	0.125	0.1875	0.25	0.313	0.38	0.4375	0.5	0.5625	0.625	0.6875	0.75	0.8125	0.875	0.9375	1
2	C	0	0.0119	0.0238	0.0356	0.05	0.059	0.07	0.0831	0.1	0.1069	0.119	0.1306	0.14	0.1544	0.166	0.1781	0.19
3	Si	0	0.1019	0.2038	0.3056	0.41	0.509	0.61	0.7131	0.82	0.9169	1.019	1.1206	1.22	1.3244	1.426	1.5281	1.63
4	Mn	0	0.1444	0.2887	0.4331	0.58	0.722	0.87	1.0106	1.15	1.2994	1.444	1.5881	1.73	1.8769	2.021	2.1656	2.31
5	S	0	0.0088	0.0175	0.0263	0.04	0.044	0.05	0.0613	0.07	0.0788	0.088	0.0963	0.11	0.1138	0.123	0.1313	0.14
6	P	0	0.0156	0.0313	0.0469	0.06	0.078	0.09	0.1094	0.13	0.1406	0.156	0.1719	0.19	0.2031	0.219	0.2344	0.25
7	Ni	0	0.675	1.35	2.025	2.7	3.375	4.05	4.725	5.4	6.075	6.75	7.425	8.1	8.775	9.45	10.125	10.8
8	Cr	0	0.7362	1.4725	2.2087	2.94	3.681	4.42	5.1537	5.89	6.6262	7.362	8.0987	8.83	9.5712	10.31	11.044	11.8
9	Mo	0	0.0963	0.1925	0.2888	0.39	0.481	0.58	0.6738	0.77	0.8663	0.963	1.0588	1.16	1.2513	1.348	1.4438	1.54
10	V	0	0.0331	0.0663	0.0994	0.13	0.166	0.2	0.2319	0.27	0.2981	0.331	0.3644	0.4	0.4306	0.464	0.4969	0.53
11	Cu	0	0.1363	0.2725	0.4088	0.55	0.681	0.82	0.9538	1.09	1.2263	1.363	1.4988	1.64	1.7713	1.908	2.0438	2.18
12	O	0	95.938	191.88	287.81	384	479.7	576	671.56	768	863.44	959.4	1055.3	1151	1247.2	1343	1439.1	1535
13	Ti	0	48.125	96.25	144.38	193	240.6	289	336.88	385	433.13	481.3	529.38	578	625.63	673.8	721.88	770
14	N	0	61.188	122.38	183.56	245	305.9	367	428.31	490	550.69	611.9	673.06	734	795.44	856.6	917.81	979
15	B	0	12.5	25	37.5	50	62.5	75	87.5	100	112.5	125	137.5	150	162.5	175	187.5	200
16	Nb	0	110.63	221.25	331.88	443	553.1	664	774.38	885	995.63	1106	1216.9	1328	1438.1	1549	1659.4	1770
17	HI	0	0.4125	0.825	1.2375	1.65	2.062	2.47	2.8875	3.3	3.7125	4.125	4.5375	4.95	5.3625	5.775	6.1875	6.6
18	IPT	0	21.875	43.75	65.625	87.5	109.4	131	153.13	175	196.88	218.8	240.63	263	284.38	306.3	328.13	350
19	PWHTT	0	47.5	95	142.5	190	237.5	285	332.5	380	427.5	475	522.5	570	617.5	665	712.5	760
20	PWHTT	0	6.25	12.5	18.75	25	31.25	37.5	43.75	50	56.25	62.5	68.75	75	81.25	87.5	93.75	100
21	TTCT	0	25.563	51.125	76.688	102	127.8	153	178.94	205	230.06	255.6	281.19	307	332.31	357.9	383.44	409
22	CharTou / J	0	18.75	37.5	56.25	75	93.75	113	131.25	150	168.75	187.5	206.25	225	243.75	262.5	281.25	300

Table 4.10 The normalized scale of Ternary Plot 0 to 1 First row red colour converted to Actual scale of variables

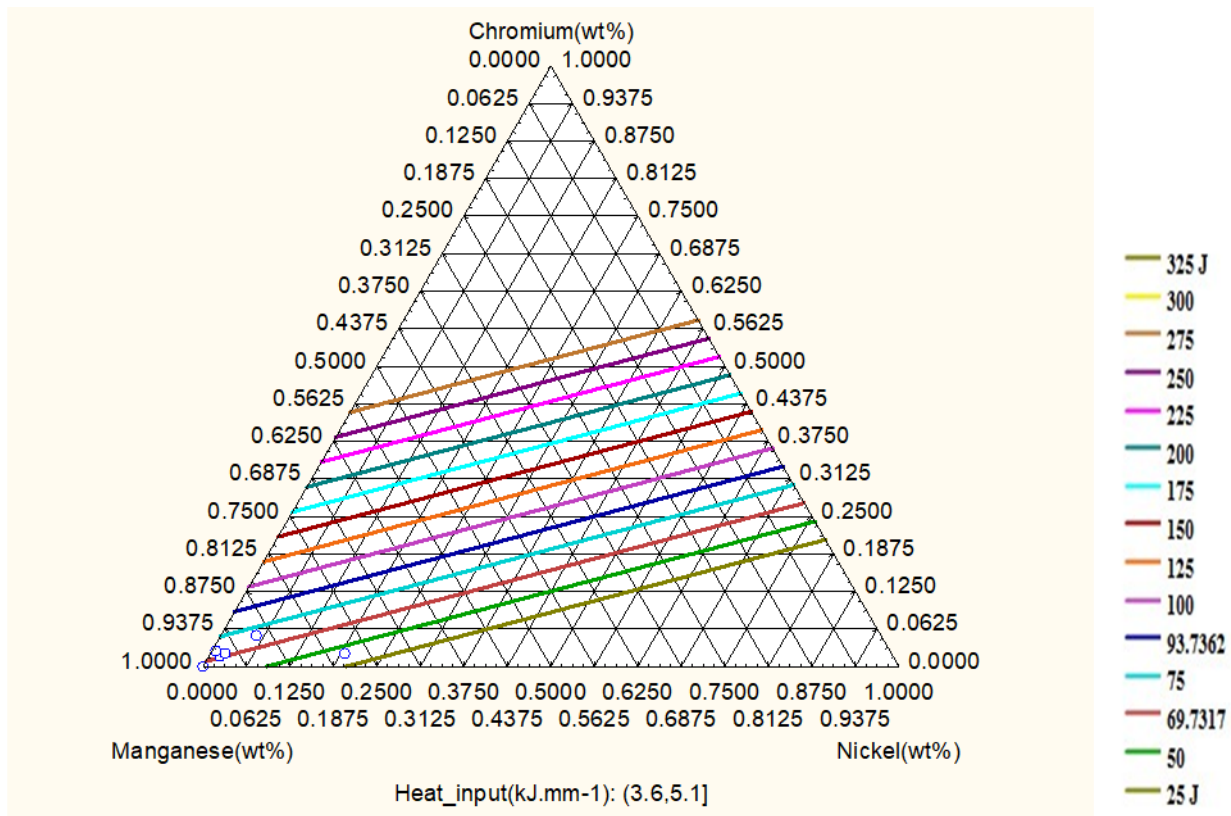


Figure.4.13.2 Ternary Categorized Graph of Chromium, Manganese, Nickel, **Heat Input** and Charpy Toughness shows 25 J to 275 J lines with Heat input in range 3.6 to 5.1 1 (wt% Mn range from 0 to 2.31, wt% Ni range from 0 to 10.8, wt% Cr range from 0 to 11.8)

Ternary Categorized Graph gives the relations between the four input variables and one output variable. Figure.4.13.2 , Figure. 4.13.3 and Figure. 4.13.4 show the relations between Chromium, Manganese, Nickel, Heat Input and Charpy Toughness by GRNN. Graphs gives the information about how these four Chromium, Manganese, Nickel, and Heat Input control the Charpy Toughness from 25J to 325J. Figure. 4.13.2, and Figure. 4.13.3 indicate the criticality to maintain the toughness with Chromium, Manganese, Nickel, and Heat Input. In Figure. 4.13.2 and Figure. 4.13.3 with Heat Input value ≤ 2.1 kJ mm⁻¹,the toughness is achieved 25J and Heat Input 3.6 to 5.1 kJ mm⁻¹ gives Toughness 25J to 275J. In Figure.4.12.10 shows that to increase the toughness, increase Chromium, decrease in Manganese and decrease in Nickel. There are number of combinations of alloying elements available for one value of Toughness. Figure. 4.13.3 gives more flexibility for alloy design or weld deposit design for high Heat Inputs.

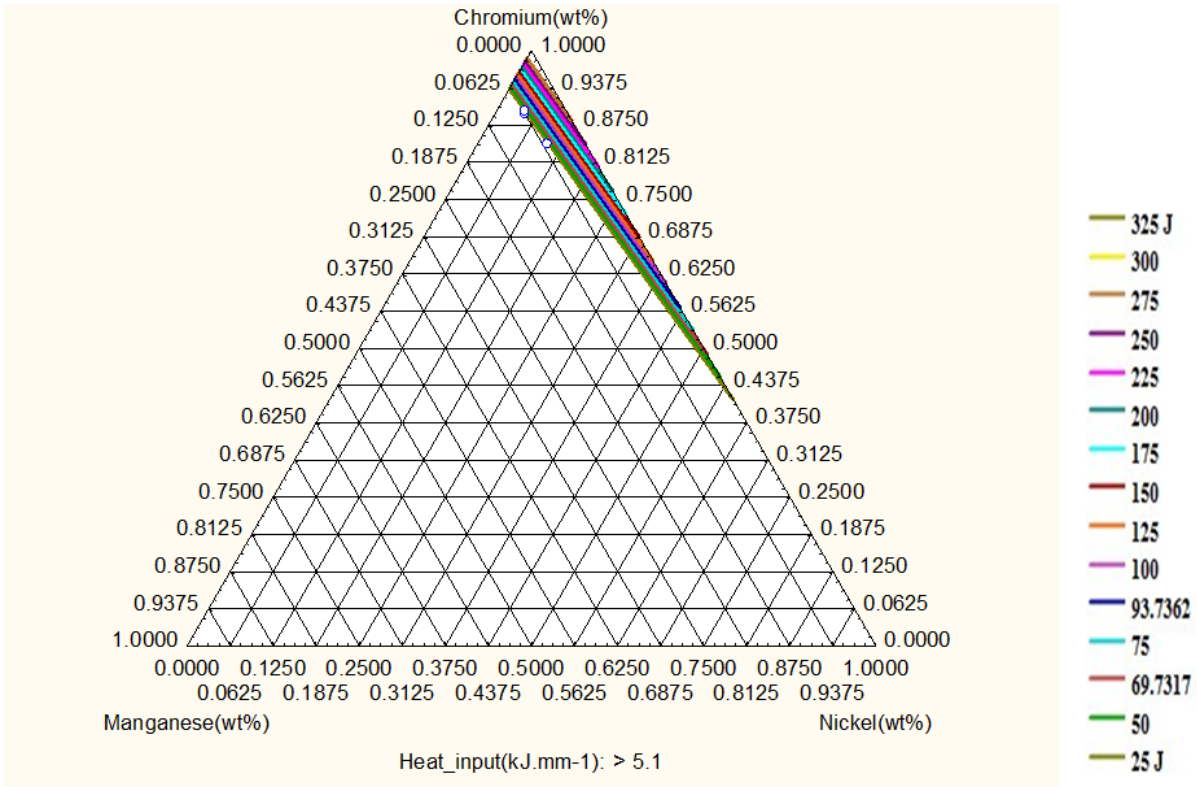


Figure. 4.13.3 Ternary Categorized Graph of Chromium, Manganese, Nickel, **Heat Input** and Charpy Toughness shows 25 J to 300 J lines with Heat input > 5.1 (wt% Mn range from 0 to 2.31, wt% Ni range from 0 to 10.8, wt% Cr range from 0 to 11.8)

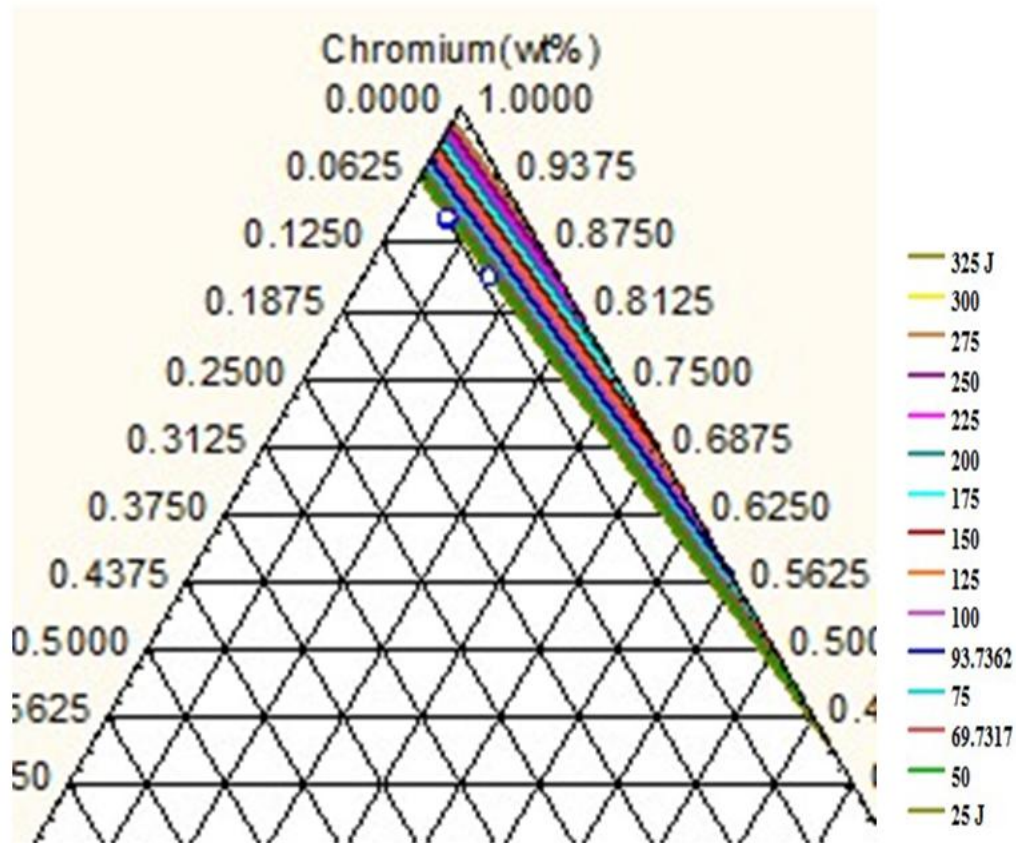


Figure. 4.13.4 Ternary Categorized Graph of Chromium, Manganese, Nickel, Heat Input and Charpy Toughness (Enlarged view of Figure. 4.13.3 near the Chromium.) (wt% Mn range from 0 to 2.31, wt% Ni range from 0 to 10.8, wt% Cr range from 0 to 11.8)

Figure. 4.13.4 show the relations between Chromium, Manganese, Nickel, Heat Input and Charpy Toughness by GRNN. Graphs gives the information about how these four Chromium, Manganese, Nickel, and Heat Input control the Charpy Toughness from 25J to 300J. At High Heat Input $> 5.1 \text{ kJ mm}^{-1}$ can give wide range of Toughness, 25J to 300J. The alloying elements require for higher toughness more than 275J, Manganese less than 0.14 wt%, Chromium 9.0 to 11.78 wt% and Nickel less than 1.35 wt%. This finding is totally new that with increase in the Chromium content and decreasing both Manganese and Nickel, increases the Charpy Toughness at higher input value greater than 5.1 kJ mm^{-1} . Figure.4.12.11 indicates more convenience for alloy design or weld deposit design because very small region available for input variables selection. This region also mentions that control of three alloying elements must be controlled very precisely for the desired Charpy Toughness.

4.4.5 Application of Trained Best Neural Network Models

4.4.5.1 Prediction of The Charpy Toughness on unseen data by BNN Model

The BNN model has good accuracy in prediction of Charpy Toughness of ferritic steel welds on unseen data which is excellent for the design of welds. (Table. 4.11) The predicted Charpy Toughness of the unseen data of three weld alloys are compared with measured values of Charpy Toughness shows the prediction capacity of the BNN model. This BNN model can be used for practical applications, research and development of ferritic steel alloys.

Table 4.11 Predicted Charpy Toughness by BNN model for unseen data of three ferritic weld deposits

Variable	Weld alloy 1	Weld alloy 2	Weld alloy 3
Carbon(wt%)	0.037	0.033	0.03
Silicon(wt%)	0.3	0.3	0.04
Manganese(wt%)	0.65	2.17	0.61
Sulphur(wt%)	0.009	0.008	0.009
Phosphorus(wt%)	0.011	0.012	0.01
Nickel(wt%)	3.5	6.54	6.11
Chromium(wt%)	0.03	0.44	0.16
Molybdenum(wt%)	0.005	0.62	0.38
Vanadium(wt%)	0.012	0.021	0.018
Copper(wt%)	0.03	0.02	0.02
Oxygen(ppm)	440	320	340
Titanium(ppm)	55	0.0	0.0
Nitrogen(ppm)	69	139	129
Boron(ppm)	2.0	1.0	1.0
Niobium(ppm)	20	10	10
Heat_input(kJ.mm-1)	1.0	1.3	1.3
Interpass_temperature(C)	200	200	200
Postweld_heat_treatment_temperature(C)	580	0.0	0.0
Post-weld_heat_treatment_time(h)	2.0	0.0	0.0
Testing Temperature CT (K)	210	293	293
Measured CT (J)	100	41.5	123
Predicted CT (J)	83.11	42.49	114.43

4.4.5.2 Prediction of The Charpy Toughness on unseen data by GRNN Model

The GRNN model has good accuracy in prediction of Charpy Toughness of ferritic steel welds on unseen data which is excellent for the design of welds. (Table. 4.12) The predicted Charpy Toughness of the unseen data of three weld alloys are compared with measured values of

Charpy Toughness shows the prediction capacity of the GRNN model. This GRNN model can be used for practical applications, research and development of ferritic steel alloys.

Table 4.12 Predicted Charpy Toughness by GRNN model for unseen data of three ferritic weld deposits

Variable	Weld alloy 1	Weld alloy 2	Weld alloy 3
Carbon(wt%)	0.037	0.033	0.03
Silicon(wt%)	0.3	0.3	0.04
Manganese(wt%)	0.65	2.17	0.61
Sulphur(wt%)	0.009	0.008	0.009
Phosphorus(wt%)	0.011	0.012	0.01
Nickel(wt%)	3.5	6.54	6.11
Chromium(wt%)	0.03	0.44	0.16
Molybdenum(wt%)	0.005	0.62	0.38
Vanadium(wt%)	0.012	0.021	0.018
Copper(wt%)	0.03	0.02	0.02
Oxygen(ppm)	440	320	340
Titanium(ppm)	55	0.0	0.0
Nitrogen(ppm)	69	139	129
Boron(ppm)	2.0	1.0	1.0
Niobium(ppm)	20	10	10
Heat_input(kJ.mm-1)	1.0	1.3	1.3
Interpass_temperature(C)	200	200	200
Postweld_heat_treatment_temperature(C)	580	0.0	0.0
Post-weld_heat_treatment_time(h)	2.0	0.0	0.0
Testing Temperature CT (K)	210	293	293
Measured CT (J)	100	41.5	123
Predicted CT (J)	100	39	113.5

Prediction of The Charpy Toughness for new data of input variables can be achieved accurately with best trained models by BNN and GRNN as given in above Table 4.11 and Table 4.12. These Models have capacity for changing any individual input variable, any combination of more than one input variables or all input variables to predict the Charpy Toughness of Ferritic Steel Welds. These are only possible with the BNN and GRNN Models which are impossible practically. By simply running these Models the various design of the Ferritic Steel Welds are possible which save money, time and labor during Research and Development of the Ferritic Steel Welds.

4.4.6 Genetic Algorithms and applications to the yield strength of Ferritic Steel Welds

4.4.6.1 Target Charpy Toughness of 100J and High value of Charpy Toughness 350J

The first simulation is made to check the behavior of the genetic algorithm. The target value of Charpy toughness is set to -0.7 which correspond to an unnormalised value of 100 J. The dataset provides such values of Charpy toughness and the aim of this simulation is to check the results of the genetic algorithm. The 20 parameters (input variables) are allowed to vary, in between -1 and + 1 during the genetic algorithm process. After 3000 generations, the best results obtained are shown Table 4.13.

The second simulation is made to check the genetic algorithm for high value of the Charpy toughness. The target value of Charpy toughness is set to 0.2 which correspond to an unnormalised value of 350J. The dataset does not provide such value of Charpy toughness and the aim of this simulation is to check the results of the genetic algorithm. The 20 parameters (input variables) are allowed to vary, in between -1 and + 1 during the genetic algorithm process. After 3000 generations, the best results obtained are shown Table 4.13.

According to Table 4.13, the genetic algorithm has managed to reach the target after 3000 generations. Moreover, the associated error obtained is very reasonable.

To check if the given input variables correspond to Ferritic Steel Weld, compare with the actual data of Charpy toughness.

Table 4.13 Predicted Input variables by NN-GA model for two targeted Charpy Toughness of ferritic weld deposits

Variable	Weld 1	Weld 1	Weld 2
	Result GA	Data	Result GA
Carbon(wt%)	0.04	0.037	0.09
Silicon(wt%)	0.28	0.3	0.24
Manganese(wt%)	0.65	0.65	0.65
Sulphur(wt%)	0.006	0.009	0.005
Phosphorus(wt%)	0.005	0.011	0.006
Nickel(wt%)	3.8	3.5	0.19
Chromium(wt%)	0.01	0.03	3.76
Molybdenum(wt%)	0.004	0.005	0.12
Vanadium(wt%)	0.011	0.012	0
Copper(wt%)	0.023	0.03	0.32
Oxygen(ppm)	453	440	190
Titanium(ppm)	52	55	0
Nitrogen(ppm)	71	69	119
Boron(ppm)	1.0	2.0	0
Niobium(ppm)	16	20	0
Heat_input(kJ.mm-1)	1.2	1.0	2.5
Interpass_temperature(C)	210	200	250
Postweld_heat_treatment_temperature(C)	569	580	690
Post-weld_heat_treatment_time(h)	2.5	2.0	10
Testing Temperature CT (K)	220	210	293
GA calculated CT (J)	98	---	342
Targeted CT (J)	100	---	350
Error	32	---	51
Measured CT (J)	---	100	---

The NNGA models have good accuracy in predicting 20 input variables of the Charpy toughness of ferritic steel welds, which is excellent for weld design.(Table.4.13) The predicted results of the targeted values of the two weld deposits are very close. The results of Genetic Algorithms are match with trends of measured data and fundamental of metallurgy. The output results show the predictive capacity of the NNGA model.This NNGA model can be used in practical applications, research and development of ferritic steel alloys. [Appendix-B]

4.4.7 Summary

The Neural Network and Genetic algorithms Methods have been used for efficient design of the Charpy Toughness of Ferritic Steel Welds. From the Modeling works and Results and Discussion of this Chapter some useful conclusions can be drawn:

The distribution of the Data of the Charpy Toughness of Ferritic Steel Welds is uniform for some Input variables and non-uniform for some Input variables. The distribution is clearly observed in Scatter plots.

In this case, of Bayesian Neural Network method, all the response graphs show error bars when the concentration of Nickel and Chromium is respectively below 8 and 6 wt%, the prediction can be reliable. But above those limits (7 wt% for Ni and 6 wt% for Cr), the model can no more be trusted and this is inferred by the large error bars. Similarly it is applicable to other graphs where larger error bars are present. More experiments with concentrations in this range of values need to be carried out to improve the model. Uncertainty because of a lack of data is one of the limitations of a neural network. The error bars and output variable (Charpy Toughness) sometimes showing unphysical (negative) values, this is because of the empirical equation in Neural Network modeling. This error bars feature of Bayesian Neural Network is excellent guideline for research and Development.

In the case of General Regression Neural Network method, there are no problems of noisy data. It can handle noises in the Inputs. The Response graphs of the GRNN show more define about the non linearity or complexity between the Input variables and the Charpy Toughness of Ferritic Steel Welds.

The Response Graphs show about the individual relationship between the input variables and Output variable (Charpy Toughness). The 3D contour plots show the relationship between the two Input variables with Output variable (Charpy Toughness).

These trends are confirmed in the present analysis as illustrated in both the types of the Graphs Figure 4.10 (a to t) and Figure 4.11 (a to t). They are impossible to reproduce in practice. They give a clear understanding of the relationship between the Input variables and the Charpy Toughness of Ferritic Steel Welds. These pieces of information are very valuable for design, as

well as understanding the existing theory and also guiding about new research and new finding for the Ferritic steel Welds.

The 3D contour plots show the relationship between the two Input variables with Charpy Toughness. There is a total combination of 190 3D contour plots formed by 20 Input variables with the Charpy Toughness. The Ternary Categorical plots show the relationship between the four Input variables with Charpy Toughness. There is a total combination of (three input variables) 1140 Ternary plots formed by 20 Input variables with the Charpy Toughness. In the present work, 18 3D contour plots and 4 Ternary Categorized plots are given with their important relationship with the Charpy Toughness. These 3D contour plots show some hidden complex behavior of the input variables with the Charpy Toughness which is also not available and well understood. Some innovative theoretical relations can be established by the proper interpretation of these 3D contour plots which become the new knowledge base for the future work on Ferritic Steel Welds. The Input variables show complex trends because during welding, there are formation of various types of the microstructures in Ferritic Steel Welds, qualitatively and quantitatively.

The Ternary Categorized plots show the relations between Chromium, Manganese, Nickel, Heat Input and Charpy Toughness by GRNN model. Graphs give the information about how these four Chromium, Manganese, Nickel, and Heat Input control the Charpy Toughness from 25J to 300J. At High Heat Input $> 5.1 \text{ kJ mm}^{-1}$ can give wide range of Toughness, 25J to 300J. The alloying elements require for higher toughness more than 275J, Manganese less than 0.14 wt%, Chromium 9.0 to 11.78 wt% and Nickel less than 1.35 wt%. This finding is totally new that with increase in the Chromium content and decreasing both Manganese and Nickel, increases the Charpy Toughness at higher input value greater than 5.1 kJ mm^{-1} (i.e. Chromium has a significant role in increase the Charpy Toughness of Ferritic Steel Welds). Figure.4.13.4 indicates more convenience for alloy design or weld deposit design because very small region available for input variable selection. This region also mentions that control of three alloying elements must be controlled very precisely for the desired Charpy Toughness. This region also mentions that control of three alloying elements must be done very precisely for the desired Charpy Toughness

The trained BNN and GRNN models give the accurate predictions of unseen data which is useful in designing the Ferritic Steel Welds for the welding electrodes industries. With simply change the quantity of Input variables in model and run it, the predicted Charpy Toughness is obtained in the seconds.

The Genetic Algorithms method gives the prediction of the Input Variables for the Targeted Charpy Toughness value. It also predicted Input variables for the Targeted Charpy Toughness value which is beyond the range of data. The results are excellent.